Synthesis and Characterization of Periodic Mesoporous Organosilica Materials

A thesis submitted

by

Alufelwi Maxwell Tshavhungwe

to

the Faculty of Science, University of the Witwatersrand, Johannesburg, in fulfilment of the requirements for the degree of Doctor of Philosophy.

Supervisors: Prof Neil J. Coville
Prof Marcus Layh

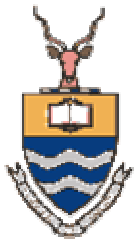

Johannesburg, 2005

Declaration

I, *Alufelwi Maxwell Tshavhungwe*, declare that this thesis is my own, unaided work. It is being submitted for the degree of Doctor of Philosophy at the University of the Witwatersrand, Johannesburg. It has not been submitted before for any degree or examination at any other University.

_____

Signature of Candidate

14th day of March 2005

Abstract

Periodic mesoporous organosilica (PMO) materials (consisting of ethane groups in the framework) and bifunctional periodic mesoporous organosilica materials (consisting of ethane groups in the framework and either glycidoxypropyl groups or aminopropyl groups in the channels) were synthesized by the sol-gel method under basic conditions. Ethanesilica materials were synthesized by condensation of 1,2-bistrimethoxysilylethane (BTME) and by co-condensation of BTME with tetraethylorthosilicate (TEOS). Bifunctional periodic mesoporous organosilica materials were synthesized by the co-condensation of BTME with either 3-glycidoxypropyltriethoxysilane (GPTS) or 3-aminopropyltriethoxysilane (APTS). Cetyltrimethylammonium bromide was used as the structure-directing template. Cobalt ion incorporated ethanesilica and modified ethanesilica materials were synthesized *in situ* by adding cobalt nitrate to the reaction mixture. Cobalt was also supported on ethanesilica materials and APTS-modified materials by using the incipient wetness impregnation method.

Raman spectroscopy and diffuse reflectance infrared spectroscopy (DRIFTS) results confirmed the formation of organosilica materials and showed that the surfactant was removed by solvent extraction. Thermogravimetric analysis (TGA) and differential thermal analysis (DTA) showed that the ethane portion of the materials (originating from the bridging ethane group in BTME) only decomposed at temperatures > 400 ^{o}C. These techniques also showed that the surfactant is removed by solvent extraction. Cobalt ion incorporation was confirmed by Raman spectroscopy and UV-vis diffuse reflectance spectroscopy.

Powder powder X-ray diffraction (XRD) and nitrogen adsorption data indicated that the mesophase and textural properties of the materials are dependent on the reaction conditions (i.e. ageing duration, ageing temperature, amount of silica precursor(s), amount of water and amount of base (NH_4OH)). The periodicity of the materials was indicated by the presence of low angle diffraction peaks in

powder X-ray diffraction patterns. Cubic and hexagonal mesophases were identified using powder X-ray diffraction. When solvent extraction is prolonged, the BET surface area and the pore volume increase, while the average pore diameter decreases. Materials with more dominant XRD structural features and larger d values, higher surface areas, lower pore volumes and average pore diameters are obtained when low ageing temperatures are used.

For samples prepared from a mixture of BTME and TEOS at a given temperature, the surface area was found to increase with increasing amount of TEOS added. This trend was observed for materials with and without cobalt. Type IV isotherms, typical of mesoporous materials, were obtained for ethanesilica and modified ethanesilica materials prepared without cobalt.

For cobalt incorporated periodic mesoporous ethanesilica materials, the XRD lattice parameter (d_{100}) increased whereas surface area and pore volume decreased with increasing cobalt loading.

Nitrogen gas adsorption on samples with varying ratios of BTME:GPTS or BTME:APTS revealed that increasing the amount of GPTS or APTS affects pore size, surface area and pore volume as well as shapes of the isotherms and hysteresis loops. The hysteresis loops of the Type IV isotherms obtained for GPTS-modified ethane silica materials (without cobalt) change from Type H3 to Type H4. There is a tendency for pore sizes to change from mesopore to micropore when the amount of GPTS is increased. Isotherms of cobalt incorporated GPTS-modified ethane silica materials changed from Type IV to Type I. The surface area, pore volume and pore diameter decreased with increasing loading of GPTS or APTS as well as after cobalt incorporation.

Dedication

To my mother, Phophi Tshavhungwe

Acknowledgements

I wish to extend my sincerest gratitude and thanks to Prof. Neil J. Coville and Dr Marcus Layh, my research directors, for their expert guidance and assistance during the entire research.

Special thanks to my wife (Tshifhiwa), my two sons (Phathutshedzo and Vhutali) and my three daughters (Vhuhwavho, Khwathiso and Ndivho), my mother (Vho-Phophi) and other members of the family for their encouragement and unwavering moral support.

The financial support provided by the following organizations and institutions is highly appreciated: Mellon Foundation, DAAD, National Research Foundation (NRF), Sastech, and the University of the Witwatersrand. I thank my employer, the University of Venda, for granting me leave of absence for the duration of my studies.

I would like to thank Rudolph Erasmus and George Amolo of the Department of Physics for recording Raman and UV-Vis diffuse reflectance spectra, respectively. Linda Linganiso, who prepared some BTME samples as part of her BSc (Honours) project, also deserves a pat on the back.

Finally I would like to thank staff members in the Department of Chemistry, and other members of the CATOMCER group for making my stay at Wits a memorable one. Your contributions by showing me how to operate various instruments is highly appreciated. I miss those Friday afternoon meetings!

Publications emanating from this work

1. A. M. Tshavhungwe, M. Layh, and N. J. Coville, "Cobalt ion incorporation into periodic mesoporous organosilica materials synthesized by co-condensation of 1,2-bistrimethoxysilylethane with 3-glycidoxypropyltriethoxysilane," Journal of Sol-Gel Science and Technology 29 (2004), 167–177.

2. A. M. Tshavhungwe, and N. J. Coville, "*In situ* and post reaction cobalt incorporation into periodic mesoporous ethanesilica materials," Journal of Sol-Gel Science and Technology 31 (2004) 161 - 164.

3. A. M. Tshavhungwe, and N. J. Coville, "*In situ* and post reaction cobalt-incorporation into aminopropyl-modified periodic mesoporous ethanesilica materials," Accepted. Journal of Ethiopian Chemical Society.

Oral Presentations

1. December 08 – 11, 2003: 2nd African Materials Research Society Conference, Johannesburg. Synthesis and characterization of inorganic-organic hybrid silica materials (by AMT).

2. November 09 – 12, 2003: CATSA/SACI (Catalysis South Africa/South African Chemical Institute) 2003 Conference, Durban. Cobalt-incorporation into periodic mesoporous organosilica materials synthesized by co-condensation of 1,2-bistrimethoxysilylethane with 3-glycidoxypropyltriethoxysilane (by NJC).

3. August 24 – 29, 2003: XIIth International Conference on Sol-Gel Chemistry, Sydney, Australia. Synthesis and study of hybrid catalysts supports containing cobalt (by NJC).

Poster Presentations

1. July 11 – 16, 2004, 13th International Congress on Catalysis, Paris, France.
Periodic Mesoporous Organosilica Materials Synthesized in the Presence of Cobalt Ions (by NJC).

2. November 13 – 18, 2003: 3rd IPCAT-3 & TSCRE-2003 Conference, Taipei, Taiwan. Synthesis and Characterisation of Cobalt-incorporated Periodic Mesoporous Organosilica Materials (by AMT).

3. November 10 – 13, 2002: CATSA/SACI 2002 Conference, Cape Town.
Metal Incorporated Functionalized Periodic Mesoporous Organosilica Materials (by AMT).

4. November 04 – 08, 2001: CATSA/SACI 2001 Conference, Pilanesberg.
Synthesis and Characterisation of Periodic Mesoporous Organosilica Materials (by AMT).

Table of Contents

Topic	Page
Title	i
Declaration	ii
Abstract	iii
Dedication	v
Acknowledgements	vi
Publications emanating from this work	vii
Oral Presentations	viii
Poster Presentations	ix
Table of Contents	x
List of Tables	xviii
List of Schemes	xx
List of Figures	xxi
Abbreviations and Symbols	xxviii
Notation used to identify samples	xxix
Aims and Objectives	1
Chapter 1 Sol-gel Processing of Hybrid Organic-Inorganic Mesoporous Silica Materials	**3**
1.1 Introduction	3
1.2 Sol-gel processing of alkoxysilanes	3
1.2.1 Monomers	3
1.2.2 Sol-gel synthesis and processing of xerogels from alkoxysilanes and bridged polysilsequioxanes	5
1.3 Silica and hybrid silica materials	10
1.3.1 Background	10
1.3.2 Ordered mesoporous inorganic materials	10
1.4 Organic-inorganic hybrid materials	15
1.4.1 Organically modified mesoporous silicas	17

1.4.2 Organic-inorganic hybrid materials with organosilica frameworks (Organo-bridged polysilsesquioxanes)…….. 20
1.4.3 Periodic mesoporous organosilica materials……21
1.5 Conclusions……21
1.6 References…….. 22

Chapter 2 Periodic mesoporous organosilica materials: a review……..26
2.1 Introduction……26
2.2 Synthesis…….. 26
2.3 Properties and advantages of PMO…… 31
2.4 PMOs with short chain bridging organic functional groups…… 32
2.4.1 Ionic surfactants……32
2.4.2 Non-ionic surfactants…… 34
2.5 Aromatic Periodic Mesoporous Organosilica Materials…… 36
2.6 PMOs functionalised by co-condensation with organosilanes…… 37
2.7 Metal incorporation and applications of PMOs…… 40
2.8 Conclusions …… 42
2.9 References……54

Chapter 3 Experimental Section……60
3.1 Introduction……60
3.2 Reagents and Chemicals…….62
3.3 Synthesis of mesoporous materials……65
3.3.1 Mesoporous materials from a single silica precursor…….. 65
3.3.1.1 Synthesis…….. 65
3.3.1.2 Surfactant extraction……65
3.3.1.3 Calcination……65
3.3.2 Mesoporous materials from co-condensation of silica precursors……66
3.3.3 Cobalt incorporated mesoporous materials…….. 66
3.3.3.1 In situ cobalt incorporation……66
3.3.3.2 Post reaction cobalt incorporation…… 66

3.4 Characterization……66
3.4.1 Background ……67
3.4.1.1 Powder X-Ray Diffraction……67
3.4.1.2 Nitrogen sorption……69
3.4.2 Measurements……..75
3.4.2.1 Powder X-Ray Diffraction……75
3.4.2.2 Nitrogen sorption……..75
3.4.2.3 Thermogravimetric Analysis…… 75
3.4.2.4 Differential Thermal Analysis……..75
3.4.2.5 Differential Scanning Calorimetry……75
3.4.2.6 Infrared spectroscopy ……..76
3.4.2.7 Raman Spectroscopy ……76
3.4.2.8 Scanning Electron Microscopy ……76
3.4.2.9 ^{1}H NMR spectroscopy…….. 76
3.4.10 UV-Vis Diffuse Reflectance Spectroscopy……77
3.5 References……77

Chapter 4 A systematic study of factors governing the condensation of 1,2-bistrimethoxysilylethane and tetraethylorthosilicate……..... 79
4.1 Introduction…… 79
4.2 Experimental Section……..80
4.2.1 Reagents and Chemicals……..80
4.2.2 Synthesis……80
4.2.2.1 As-synthesized PMOs……...80
4.2.2.2 Solvent extraction……..81
4.2.2.3 Influence of ageing temperature on textural properties of ethanesilica materials……81
4.2.2.4 Influence of ageing length on textural properties of periodic mesoporous silica……81
4.2.2.5 Influence of the amount of BTME on textural properties of periodic mesoporous ethanesilica materials…..82
4.2.2.6 Influence of pH on textural properties of

periodic mesoporous ethanesilica materials…….. 82
4.2.2.7 Influence of the amount of water on textural properties of periodic mesoporous ethanesilica materials…..82
4.2.3 Nomenclature……83
4.2.4 Characterization……83
4.3 Results and discussion…… 83
4.3.1 Synthesis……..83
4.3.2 Diffuse Reflectance Fourier Transform Infrared Spectroscopy and Raman Spectroscopy…… 86
4.3.2.1 Diffuse Reflectance Fourier Transform Infrared Spectroscopy…… 86
4.3.2.2 Raman spectroscopy…… 87
4.3.3 Thermal analysis……. 92
4.3.4 Effect of solvent extraction time on Powder X-ray Diffraction patterns and nitrogen adsorption data of MCM-41……. 96
4.3.4.1 Powder X-ray Diffraction…….. 96
4.3.4.2 Nitrogen adsorption/desorption…… 99
4.3.5 Effect of ageing temperature on powder X-ray diffraction patterns and nitrogen adsorption data of ethanesilica materials synthesized from BTME…… 102
4.3.5.1 Powder X-ray diffraction……... 102
4.3.5.2 Nitrogen adsorption/desorption.…… 105.
4.3.6 Effect of the amount of BTME on powder X-ray diffraction patterns and nitrogen adsorption data of ethanesilica materials……109
4.3.6.1 Powder X-ray diffraction……109
4.3.6.2 Nitrogen adsorption/desorption……..112
4.3.7 Effect of pH on Powder X-Ray diffraction patterns and nitrogen adsorption data of ethanesilica materials……112
4.3.7.1 Powder X-Ray diffraction……112
4.3.7.2 Nitrogen adsoption……115
4.3.8 Scanning electron microscopy (SEM)…… 118
4.4 Conclusions……120

4.5 References……120

Chapter 5 In situ and post reaction cobalt ion incorporation into periodic mesoporous ethanesilica materials……..124

5.1 Introduction……124

5.2 Experimental Section……..125

5.2.1 Chemicals……125

5.2.2 Synthesis…….. 125

5.2.2.1 In situ cobalt incorporation…… 125

5.2.2.2 Post reaction cobalt incorporation……..125

5.2.3 Characterization……126

5.3 Results and Discussion……126

5.3.1 Synthesis…….. 126

5.3.2 Raman spectroscopy……. 126

5.3.3 Powder X-Ray Diffraction……129

5.3.4 Thermal analysis……129

5.3.5 Nitrogen sorption…….. 137

5.4 Conclusions……..141

5.5 References……141

Chapter 6 A systematic study of factors governing the condensation of 1,2-bistrimethoxysilylethane and tetraethylorthosilicate…….143

6.1 Introduction……143

6.2 Experimental Section……..144

6.2.1 Reagents and Chemicals……144

6.2.2 Synthesis……144

6.2.2.1 Co-condensation of BTME with TEOS…….144

6.2.2.2 Typical synthesis……147

6.2.2.3 Solvent extraction…….. 147

6.2.3 Nomenclature……147

6.3 Results and discussion…… 148

6.3.1 Synthesis…….. 148

6.3.2 Raman Spectroscopy……148
6.3.3 Thermal analysis……151
6.3.4 Powder X-ray diffraction……151
6.3.4.1 Influence of the BTME:TEOS ratio and cobalt incorporation……151
6.3.4.2 Influence of the ratio of precursors and the ageing temperature……161
6.3.5 Nitrogen adsorption……164
6.3.5.1 Influence of the BTME:TEOS ratio and cobalt incorporation……164
6.3.6 Pore size distributions obtained from non-local density functional theory (DFT)……171
6.4 Conclusions……173
6.5 References……173

Chapter 7 Cobalt ion incorporation into periodic mesoporous organosilica materials synthesized by co-condensation of 1,2-bistrimethoxysilylethane with 3-glycidoxypropyltriethoxysilane.....176
7.1 Introduction……176
7.2 Experimental Section……178
7.2.1 Chemicals……178
7.2.2 Synthesis……179
7.2.2.1 GPTS-functionalized ethanesilica and cobalt ion incorporated GPTS-functionalized ethanesilica……179
7.2.2.2 Surfactant extraction……179
7.2.2.3 Nomenclature……179
7.2.3 Characterization……182
7.3 Results and Discussion……182
7.3.1 Synthesis……182
7.3.2 Powder X-ray Diffraction……184
7.3.2.1 GPTS modified ethane silica……184
7.3.2.2 Cobalt ion incorporated GPTS-modified

ethanesilica……184
7.3.3 Nitrogen sorption……189
7.3.3.1 GPTS modified ethane silica……189
7.3.3.2 Cobalt ion incorporated GPTS-modified ethanesilica……193
7.3.4 Thermal analysis……196
7.3.4.1 GPTS-modified ethanesilica……196
7.3.4.2 Cobalt ion incorporated GPTS-modified ethanesilica……197
7.3.5 Raman spectroscopy……202
7.3.5.1 GPTS-modified ethanesilica……202
7.3.5.2 Cobalt ion incorporated GPTS-modified ethanesilica……202
7.4 Conclusions……204
7.5 References……204

Chapter 8 In situ and post reaction cobalt-incorporation into aminopropyl-modified periodic mesoporous ethanesilica materials….. 208
8.1 Introduction……208
8.2 Experimental Section……211
8.2.1 Chemicals……211
8.2.2 Synthesis……211
8.2.2.1 APTS-functionalized ethanesilica……211.
8.2.2.2 Surfactant extraction……211
8.2.2.3 *In situ* cobalt incorporated APTS-functionalized ethanesilica……212
8.2.2.4 Post reaction cobalt incorporated APTS-functionalized ehanesilica……212
8.2.2.5 Nomenclature……212
8.2.3 Characterization……213
8.3 Results and Discussion……213
8.3.1 Synthesis……213

8.3.2 Powder X-ray Diffraction……. 214
8.3.2.1 APTS-modified ethanesilica……. 214
8.3.2.2 Co-incorporated APTS-modified ethanesilica…….. 215.
8.3.3 Nitrogen sorption……. 218
8.3.3.1 APTS-modified ethanesilica…….. 218
8.3.3.2 Co-incorporated APTS-modified ethanesilica……218
8.3.4 Thermogravimetric analysis…….224
8.3.4.1 APTS-modified ethanesilica…….. 224
8.3.4.2 Co-incorporated APTS-modified ethanesilica……224
8.3.5 Raman spectroscopy…… 229
8.3.5.1 APTS-modified ethanesilica…….. 229
8.3.5.2 Co-incorporated APTS-modified ethanesilica……232
8.3.6 UV-Vis diffuse reflectance spectroscopy…… 232
8.3.6.1 Co-incorporated APTS-modified ethanesilica……232
8.3.7 Scanning Electron Microscopy (SEM)…… 234
8.3.7.1 APTS-modified ethanesilica…….. 234
8.3.7.2 Co-incorporated APTS-modified ethanesilica……234
8.4 Conclusions…….236
8.5 References……236

Chapter 9. Concluding Remarks and Suggested Future Work…… 240
9.1 Conclusion…….. 240
9.2 Suggested Future Work…….. 241

List of Tables

Chapter 2

Table 2.1 Abbreviations and Acronyms……27

Table 2.2 Examples of bridged silicon precursors……28

Table 2.3 Summary of an overview of PMO literature ……43

Chapter 3

Table 3.1 Molecular structures of silica precursors and surfactant molecule……63

Chapter 4

Table 4.1 Raman and Infrared band locations and assignments for periodic mesoporous ethanesilica…….....88

Table 4.2 TGA results of a PMO material prepared from BTME…… 93

Table 4.3 Surface properties of silica materials prepared from TEOS……. 97

Table 4.4 Surface properties of PMOs synthesized from BTME and TEOS.....107

Table 4.5 BJH diameters obtained from adsorption and desorption isotherms for materials aged at 80 ^{o}C…….108

Table 4.6 Surface properties of materials synthesized with various amounts of NH_4OH……116

Table 4.7 Surface properties of ethanesilica materials synthesized with various amounts of water……117

Chapter 5

Table 5.1 Surface properties of cobalt incorporated ethanesilica materials..130

Table 5.2 TGA results of a PMO material prepared from BTME……133

Table 5.3 TGA results of a PMO material prepared from BTME in the presence of 0.2 g cobalt nitrate…….. 134

Chapter 6

Table 6.1 Molecular structures of silica sources and surfactant molecule… 145

Table 6.2 Amounts of silica precursors used……146

Table 6.3 Surface properties of PMOs synthesized from BTME and TEOS……..155

Table 6.4 DFT and BJH pore diameters obtained from adsorption and desorption isotherms…….. 156

Chapter 7

Table 7.1 Amounts of silica sources used in the reaction mixture……181

Table 7.2 d_{100} Spacings and their positions……..185

Table 7.3 Structural properties of the organosilica materials…….. 191

Table 7.4 TGA results of a PMO material prepared from BTME…….. 198

Table 7.5 Total mass losses obtained by TGA for GPTS-modified ethane silica materials…… 199

Chapter 8

Table 8.1 Structural properties of organosilica materials……..216

Table 8.2 TGA results of as-synthesized and solvent-extracted APTS-modified ethanesilica materials prepared from a mixture with BTME:APTS = 1:1…… 226

Table 8.3 Raman band locations and assignments for APTS-modified ethane silica……230

List of Schemes

Chapter 2

Scheme 2.1 Formation of a periodic mesoporous organosilica material……30

Chapter 3

Scheme 3.1 Reaction scheme showing the synthesis of periodic mesoporous organosilica materials…… 64

Chapter 4

Scheme 4.1 Reaction scheme showing the formation of periodic mesoporous ethane silica. Note that the framework is made of units of $O_3SiCH_2CH_2SiO_3$…….. 85

Chapter 7

Scheme 7.1 Reaction scheme showing the formation of periodic mesoporous glycidoxypropyl-modified ethane silica. Note that the framework is made up of units $(CH_2OCH_2)CH_2OCH_2CH_2CH_2SiO_3$ and $O_3SiCH_2CH_2SiO_3$…….183

Chapter 8

Scheme 8.1 Reaction scheme showing the formation of periodic mesoporous aminopropyl-modified ethane silica. Note that the framework is made up of units of $H_2NCH_2CH_2CH_2SiO_3$ and $O_3SiCH_2CH_2SiO_3$……210

List of Figures

Chapter 1

Figure 1.1 Sol-gel process and their products……..9

Figure 1.2 Three structure types observed for silica-surfactant mesophases: (a) MCM-41 (hexagonal, 1-dimensional); (b) MCM-48 (cubic, bicontinuous, 3-D); (c) MCM-50 (lamellar, 2-D)…….13

Figure 1.3 Liquid-crystal templating mechanism proposed by Beck et. al. showing two pathways for the formation of MCM-41: (1) liquid-crystal-initiated and (2) silicate-initiated……14

Figure 1.4 General strategies for the design of functional ybrids……16

Figure 1.5 Organic modification of the mesoporous silicate. (a) post-synthesis grafting, (b) co-condensation……19

Chapter 3

Figure 3.1 XRD patterns of hexagonal MCM41 (a), cubic MCM48 (b), and lamella MCM50 mesophases…….....68

Figure 3.2 IUPAC classification of isotherms……..73

Figure 3.3 IUPAC classification of hysteresis loops……74

Chapter 4

Figure 4.1 DRIFTS spectra of an as synthesized (BA80) and a solvent extracted (BE80) ethanesilica material……..89

Figure 4.2 DRIFTS spectra of "as synthesized" periodic ethane silica heated at different temperatures. (120, 200, 250, 300, 350, 400, 450, 500, 550 and 600 ^{o}C)……. 90

Figure 4.3 Raman spectra of (a) hexadecyltrimethylammonium bromide (CTAB), (b) liquid 1,2-Bistrimethoxysilylethane (BTME), (c) ethanesilica prepared without surfactant, and (d) solvent extracted ethane silica……91

Figure 4.4 TGA and DTA curves of an as synthesized (BA80) and an extracted (BE80) periodic ethane silica material. A = TGA, extracted; B = TGA, as-synthesized; C = DTA, extracted; D = DTA, as-synthesized…94

Figure 4.5 TGA curve of as synthesized and solvent extracted samples prepared with various amounts of BTME. A = derivative TGA curve, 14.3 mmol BTME, as-synthesized; B = 7.14 mmol BTME, extracted; C = 14.3 mmol BTME, extracted; and D = 14.3 mmol BTME, as synthesized…… 95

Figure 4.6 Powder XRD patterns of MCM-41 materials extracted for different times…… 98

Figure 4.7 The N_2 adsorption–desorption isotherms of ordered silica material calcined at 600 ^oC for 6 hours……. 100

Figure 4.8 Effect of surfactant removal time on BET surface area and pore volume of MCM-41…… 101

Figure 4.9 XRD patterns of as synthesized ethane silica materials aged at different temperatures. Ageing temperatures: A = 0 ^oC, B = 25 ^oC, C = 55 ^oC and D = 80 ^oC……103

Figure 4.10 XRD patterns of solvent extracted ethane silica materials aged at different temperatures. Ageing temperatures: A = 0 ^oC, B = 25 ^oC, C = 55 ^oC and D = 80 ^oC……104

Figure 4.11 Nitrogen adsorption desorption isotherms and adsorption PSDs of ethane silica materials aged at different temperatures. Ageing temperatures: A = 0 ^oC, B = 25 ^oC, C = 55 ^oC, and D = 80 ^oC…….106

Figure 4.12 XRD patterns of as synthesized ethane silica materials synthesized with different amounts of BTME. Amount BTME: A = 7.14 mmol, B = 10.7 mmol and C = 14.3 mmol……110

Figure 4.13 XRD patterns of solvent extracted ethane silica materials synrthesized with different amounts of BTME. Amount BTME (mmol): A = 3.57, B = 7.14, C = 10.7 and D = 14.3……..111

Figure 4.14 XRD patterns of as synthesized ethane silica materials prepared with different amounts of ammonium hydroxide. Volumes ammonium hydroxide (ml): A = 7 and B = 28……..113

Figure 4.15 XRD patterns of as synthesized ethane silica materials prepared with different amounts of water. Volume water (ml): A = 14, B = 28 and C = 56……..114
Figure 4.16 SEM image of extracted ethanesilica (BE80)……119

Chapter 5

Figure 5.1 Raman spectra of solvent extracted ethanesilica and cobalt-incorporated ethanesilica (insert) prepared in the presence of 0.1 g cobalt nitrate……128
Figure 5.2 (a) Powder XRD patterns of cobalt incorporated organosilica materials prepared from BTME. (b) Variation of lattice parameter (d) with amount of cobalt added……..131
Figure 5.3 Powder XRD patterns of cobalt incorporated silica materials prepared from. TEOS……132
Figure 5.4 TGA curves of as synthesized (a) and solvent extracted (b) cobalt-incorporated (0.2 g) periodic ethane silica materials…….135
Figure 5.5 DSC curve of as synthesized cobalt-incorporated (0.1 g) periodic ethane silica……..136
Figure 5.6 Nitrogen adsorption desorption isotherm and adsorption PSD (insert) of an ethanesilica material (a) and cobalt incorporated ethanesilica material (b) synthesized in the presence of 0.1 g cobalt nitrate…….138
Figure 5.7 Variation of BET surface area or pore volume with amount of cobalt nitrate for cobalt impregnated ethanesilica materials…….139
Figure 5.8 Nitrogen adsorption desorption isotherms (a) and BJH pore size distributions derived from adsorption isotherms (b) of MCM-41 silica and cobalt incorporated MCM-41 silica materials…….140

Chapter 6

Figure 6.1 Raman spectra of (a) solvent extracted ethanesilica synthesized from BTME (BT0E80), and (b) solvent extracted ethanesilica material prepared by co-condensation of TEOS with BTME (BT20E80)……150

Figure 6.2 TGA and derivative TGA curves of extracted cobalt-incorporated periodic ethane silica materials. (a) CoBT20E80 and (b) CoBT67E80……154
Figure 6.3 Powder XRD pattern of as synthesized (BT20A80) and solvent extracted (BT20E80) ethanesilica PMO materials containing 20 % TEOS……157
Figure 6.4 Powder XRD patterns of organosilica materials prepared from TEOS and BTME and aged at 80 ^{o}C……..158
Figure 6.5 Powder XRD patterns of extracted cobalt incorporated ethanesilica materials synthesized from BTME and TEOS and aged at 80 ^{o}C……159
Figure 6.6 Variation in lattice parameter as a function of the amount of TEOS in the reaction mixture for ethanesilica (A) and cobalt-incorporated ethanesilica (B) materials……160
Figure 6.7 Powder XRD patterns of extracted cobalt incorporated ethanesilica materials synthesized from BTME and TEOS and aged at 55 ^{o}C……162
Figure 6.8 Powder XRD pattern of an extracted cobalt incorporated ethanesilica materials synthesized from BTME and TEOS (CoBT20E27) and aged at room temperatures…….. 163
Figure 6.9 Nitrogen adsorption isotherm of an ethanesilica material containing 20 % TEOS (BT20E80)……165
Figure 6.10 Nitrogen adsorption isotherm (main) and adsorption (A) and desorption (B) pore size distributions (insert) of an ethanesilica material containing 67 % TEOS (BT67E80)……166
Figure 6.11 Nitrogen adsorption-desorption isotherms for extracted cobalt-incorporated mesoporous ethanesilica materials containing variable amounts of TEOS and aged at various temperatures……169

Figure 6.12 BJH Pore size distributions derived from adsorption (bold lines and square points) and desorption (dotted lines and open circular points) isotherms for extracted cobalt-incorporated mesoporous ethanesilica materials containing variable amounts of TEOS and aged at various temperatures……170
Figure 6.13 DFT plots for cobalt incorporated ethanesilica materials aged at 80 ^{o}C……172

Chapter 7

Figure 7.1 XRD patterns for solvent extracted glycidoxypropyl-functionalized ethane silicas……186
Figure 7.2 XRD patterns for solvent extracted glycidoxypropyl-functionalized ethane silicas……187
Figure 7.3 Variation of lattice parameter (d) with amount of GPTS for extracted (A) and as synthesized (B) GPTS-modified ethane silica materials……188
Figure 7.4 N_2 adsorption isotherms and BJH pore size distributions derived from adsorption and desorption isotherms for GPTS-modified ethane silica materials: A, B and C are isotherms of GB53E, GB21E and GB0E, respectively; D, E and F are BJH adsorption pore size distributions of GB53E, GB21E and GB0E, respectively; G, H and I are BJH desorption pore size distributions of GB53E, GB21E and GB0E, respectively……..192
Figure 7.5 N_2 adsorption isotherms and BJH pore size distributions derived from adsorption and desorption isotherms for cobalt ion incorporated GPTS-modified ethane silica materials: A, B C and D are isotherms for GBCo53E, GBCo36E, GBCo21E and GB0E, respectively; E is the BJH adsorption pore size distribution of GB0E; F, G, H and I are BJH desorption pore size distributions of GBCo53E, GBCo36E, GBCo21E and GB0E, respectively……..194

Figure 7.6 Variation of surface area and pore volume with amount of GPTS. A = Surface area vs Amount GPTS for GPTS-modified ethane silica; B = Pore volume versus Amount of GPTS for GPTS-modified ethane silica; C = Surface area vs Amount GPTS for cobalt ion incorporated GPTS-modified ethane silica; D = Pore volume versus Amount of GPTS for cobalt ion incorporated GPTS-modified ethane silica…….195

Figure 7.7 TGA and DTA curves of an as synthesized (GB0A) and extracted (GB0E) periodic ethane silica material. A = TGA, extracted; B = TGA, as-synthesized; C = DTA, extracted; D = DTA, as-synthesized.. 200

Figure 7.8 TGA curve of as synthesized GPTS silica (GB100)……201

Figure 7.9 Raman spectra for solvent extracted ethane silica (A) and GPTS modified ethane silica prepared with 21 and 36 % GPTS (B and C, respectively)……203

Chapter 8

Figure 8.1. XRD patterns for aminopropyl-functionalized ethanesilicas. A = extracted APTS-modified ethane silica (BTME:APTS = 1:0.5); B = extracted APTS-modified ethane silica (BTME:APTS = 1:0.5) prepared in the presence of 0.1 g cobalt nitrate; C and D = extracted and as-synthesized APTS-modified ethane (BTME:APTS = 1:1), respectively. Insert: APTS-modified ethane silica (BTME:APTS = 1:1) impregnated with 0.1 g cobalt nitrate…….....217

Figure 8.2. N_2 adsorption desorption isotherms and BJH pore size distributions derived from desorption isotherms for APTS-modified ethane silica and Co-incorporated APTS-modified ethane silica materials. A, B and C are isotherms of APTS-modified ethane silica with BTME:APTS mole ratios of 1:0.5, 1:0.7, and 1:1, respectively. D and E are BJH desorption PSDs for BAE1:1 and BAE(1:0.5), respectively…….220

Figure 8.3. Variation of surface area (SA) and pore volume (PV) with amount of APTS loading for APTS-modified ethane silicas. (A = PV vs volume APTS; B = SA vs volume APTS)……...221

Figure 8.4. N_2 adsorption desorption isotherms and BJH pore size distributions derived from desorption isotherms for Co-incorporated APTS-modified ethane silica materials. A and B are isotherms of APTS-modified ethane silica with BTME:APTS mole ratio of 1:1 impregnated with 6.7 % and 13.5 % cobalt, respectively. C and D are BJH desorption PSDs for 6.7CoBAE(1:1)-*imp* and 13.5CoBAE(1:1)-*imp*, respectively……222
Figure 8.5. Variation of surface area and pore volume (insert) with amount of cobalt loading for APTS-modified ethane silicas obtained using the impregnation method……. 223
Figure 8.6. TGA curves and derivative thermograms for APTS-modified ethanesilica materials. A = derivative TGA curve of BAE(1:1); B, C, D and E are TGA curves of BAE(1:0.5), BAE(1:1), BAE(1:0.7) and BAA(1:1), respectively…… 227
Figure 8.7. TGA curves for solvent extracted APTS-modified ethanesilica materials impregnated with cobalt nitrate. A = 6.7CoBAE(1:1) and B = 13.5CoBAE(1:1)…… 228
Figure 8.8. Raman spectra for solvent extracted ethanesilca (BE) and APTS-modified ethanesilica [BAE(1:0.5) and BAE(1:0.7) materials……...231
Figure 8.9. UV-VIS diffuse reflectance spectra of unsupported cobalt nitrate and supported cobalt nitrate……233
Figure 8.10. SEM micrographs of ethanesilica, APTS-modified ethanesilica and cobalt incorporated APTS-modified ethanesilica materials. A = ethanesilica (BE), B = In situ Co incorporated ethanesilica [6.7CoBAE(1:1)- *in situ*], C = APTS-modified ethanesilica [BAE(1:0.7)], D = cobalt impregnated APTS-modified silica [6.7CoBAE(1:1) - *imp*], and E = Cobalt impregnated APTS-modified ethanesilica [13.4CoBAE(1:1) - *imp*]…… 235

Abbreviations, Acronyms and Symbols

Abbreviation/acronym/symbol	Name
APTS	3-Aminopropyltriethoxysilane
BET	Brunauer-Emmett-Teller
BJH	Barrett-Joyner-Halenda
BTME	1,2-bistrimethoxysilylethane
CTAB	cetyltrimethylammonium bromide
d	XRD lattice spacing
DFT	Density functional theory
DRIFTS	Diffuse reflectance infrared fourier transform spectroscopy
DSC	Differential scanning calorimetry
DTA	Differential thermal analysis
GPTS	3-Glycidoxypropyltrimethoxysilane
IUPAC	International Union of Pure and Applied Chemistry
MCM	Mobil Composition of Matter, Mobil Catalytic Material
^{1}H NMR	Proton Nuclear Magnetic Resonance
PMO	Periodic Mesoporous Organosilica
PSD	Pore Size Distribution
PV	Pore volume
SA	Surface area
SEM	Scanning electron microscopy
TEOS	Tetraethylorthosilicate
TGA	Thermogravimetric analysis
XRD	X-ray diffraction

Notation used to identify samples[1,2]

Notation	Description
BAE(1:1)	an extracted (*E*) sample synthesized from APTS (*A*) and BTME (*B*) in which the ratio of BTME to APTS is 1:1.
BAE(1:0.7)	an extracted (*E*) sample synthesized from APTS (*A*) and BTME (*B*) in which the ratio of BTME to APTS is 1:0.7.
BAE(1:0.5)	an extracted (*E*) sample synthesized from APTS (*A*) and BTME (*B*) in which the ratio of BTME to APTS is 1:0.5.
BE	an extracted (*E*) sample synthesized from 7.14 moles BTME (*B)* and aged at 80 ^{o}C.
0.5BE80	an extracted (*E*) material synthesized from 3.57 mol (i.e. half of 7.14 moles) of BTME (B) and aged at 80 ^{o}C.
BE80	an extracted (*E*) sample synthesized from 7.14 moles BTME (*B)* and aged at 80 ^{o}C.
1.5BE80	an extracted (*E*) sample synthesized from 10.7 moles BTME (*B)* and aged at 80 ^{o}C.

1 The notation used to identify the samples is as follows: A = APTS, B = BTME, G = GPTS, T = TEOS, Co = cobalt, A = as synthesized, and E = extracted. The method used to incorporate cobalt is identified by *imp* (impregnated) or *in situ* after the name.

2 Note that as-synthesized materials corresponding to extracted materials listed herein are named by replacing letter E with letter A. For example, BAA(1:1) is an as synthesized (A) sample synthesized from APTS (*A*) and BTME (*B*) in which the ratio of BTME to APTS is 1:1.

Notation	Description
2BE80	an extracted (*E*) sample synthesized from 14.3 moles BTME (*B)* and aged at 80 ^{o}C.
BT67E80	an extracted (*E*) sample synthesized from TEOS (*T*) and BTME (*B*). The amount of TEOS in the reaction mixture is 20 % by moles of Si atoms (20). The material was aged at 80 ^{o}C.
BT100E80	an extracted (*E*) sample synthesized from TEOS (100 %). The material was aged at 80 ^{o}C.
6.7CoBAE(1:1)-*imp.*	an extracted (*E*) material synthesized from APTS (*A*) and BTME (*B*) in a 1:1 ratio in which cobalt (6.7 %) was supported by impregnation (*imp*).
6.7CoBAE(1:1)-*in situ*	an extracted (*E*) material synthesized from APTS (*A*) and BTME (*B*) in a 1:1 ratio in which cobalt (6.7 %) was incorporated *in-situ.* The material was aged at 80 ^{o}C.
13.5CoBAE(1:1)-*imp*	An extracted material synthesized from APTS (*A*) and BTME (*B*) in a 1:1 ratio in which cobalt (13.5 %) was supported by impregnation (*imp*).
0.05CoBE(*in situ*)	an extracted (*E*) sample synthesized from BTME (*B*) in the presence of 0.05 g (*0.05*) cobalt nitrate (*Co*). The material was aged at 80 ^{o}C.
0.1CoBE(*in situ*)	an extracted (*E*) sample synthesized from BTME (*B*) in the presence of 0.1 g (*0.1*) cobalt nitrate (*Co*). The

Notation	Description
	material was aged at 80 ^{o}C.
0.2CoBE(*in situ*)	an extracted (*E*) sample synthesized from BTME (*B*) in the presence of 0.2 g (*0.2*) cobalt nitrate (*Co*). The material was aged at 80 ^{o}C.
0.05CoBE(Imp.)	an extracted (*E*) sample synthesized from BTME (*B)* and aged at 80 ^{o}C. 0.05 g Cobalt was supported by impregnation (*imp*).
0.1CoBE(Imp.)	an extracted (*E*) sample synthesized from BTME (*B)* and aged at 80 ^{o}C. 0.1 g Cobalt was supported by impregnation (*imp*).
6.7CoBE - *in situ*	an extracted (*E*) material synthesized from BTME (*B)* in which cobalt (6.7 %) was incorporated *in-situ*. The material was aged at 80 ^{o}C.
CoBT20E80	an extracted (*E*) sample synthesized from TEOS (*T*) and BTME (*B*) in the presence of cobalt nitrate (*Co*). The amount of TEOS in the reaction mixture is 20 % by moles of Si atoms (20). The material was aged at 80 ^{o}C.
CoBT50E55	an extracted (*E*) sample synthesized from TEOS (*T*) and BTME (*B*) in the presence of cobalt nitrate (*Co*). The amount of TEOS in the reaction mixture is 50 % by moles of Si atoms (50). The material was aged at 55 ^{o}C.
CoBT50E80	an extracted (*E*) sample synthesized from TEOS (*T*) and BTME (*B*) in the presence of cobalt nitrate (*Co*). The

Notation	Description
	amount of TEOS in the reaction mixture is 50 % by moles of Si atoms (50). The material was aged at 80 ^{o}C.
CoBT67E27	an extracted (*E*) sample synthesized from TEOS (*T*) and BTME (*B*) in the presence of cobalt nitrate (*Co*). The amount of TEOS in the reaction mixture is 67 % by moles of Si atoms (67). The material was aged at 27 ^{o}C.
CoBT67E55	an extracted (*E*) sample synthesized from TEOS (*T*) and BTME (*B*) in the presence of cobalt nitrate (*Co*). The amount of TEOS in the reaction mixture is 67 % by moles of Si atoms (67). The material was aged at 55 ^{o}C.
CoBT67E80	an extracted (*E*) sample synthesized from TEOS (*T*) and BTME (*B*) in the presence of cobalt nitrate (*Co*). The amount of TEOS in the reaction mixture is 67 % by moles of Si atoms (67). The material was aged at 80 ^{o}C.
GB0E	an extracted (*E*) sample synthesized from BTME (*B*) and aged at 80 ^{o}C.
GB21E	an extracted (*E*) sample synthesized from GPTS (*G*) and BTME (*B*) and aged at 80 ^{o}C. The amount of GPTS in the reaction mixture is 21% by moles of Si atoms.
GB36E	an extracted (*E*) sample synthesized from GPTS (*G*) and BTME (*B*) and aged at 80 ^{o}C. The amount of GPTS in the reaction mixture is 36% by moles of Si atoms.
GB53E	an extracted (*E*) sample synthesized from GPTS (*G*) and BTME (*B*) and aged at 80 ^{o}C. The amount of GPTS in

Notation	Description
	the reaction mixture is 53% by moles of Si atoms.
GBCo0E	an extracted (*E*) sample synthesized from BTME (*B*) in the presence of cobalt nitrate (*Co*) and aged at 80 ^{o}C.
GBCo21E	an extracted (*E*) sample synthesized from GPTS (*G*) and BTME (*B*) in the presence of cobalt nitrate (*Co*) and aged at 80 ^{o}C. The amount of GPTS in the reaction mixture is 21% by moles of Si atoms.
GBCo36E	an extracted (*E*) sample synthesized from GPTS (*G*) and BTME (*B*) in the presence of cobalt nitrate (*Co*) and aged at 80 ^{o}C. The amount of GPTS in the reaction mixture is 36% by moles of Si atoms.
GBCo53E	an extracted (*E*) sample synthesized from GPTS (*G*) and BTME (*B*) in the presence of cobalt nitrate (*Co*) and aged at 80 ^{o}C. The amount of GPTS in the reaction mixture is 53% by moles of Si atoms.

Aims and Objectives

The overall aim of this project is to synthesise and characterise ordered hybrid organic inorganic silica materials (called periodic mesoporous organosilica materials, PMOs). Periodic mesoporous organosilicas are characterised by high surface areas and uniform pore sizes. Initial reports on the synthesis of PMOs were published in 1999. This is an emerging area of science and consequently much information is still to be obtained on these materials.

In this research study, periodic mesoporous inorganic silica and periodic mesoporous organosilica materials were synthesized by using the base-catalysed surfactant templated sol-gel method. Cobalt was incorporated into the periodic mesoporous materials by using *in situ* and post-reaction (impregnation) procedures. Mesoporous silica materials prepared were characterised using thermogravimetric analysis (TGA), differential thermal analysis (DTA), differential scanning calorimetry (DSC), nitrogen adsorption, powder X-ray diffraction (XRD), diffuse reflectance UV-Vis spectroscopy, Raman spectroscopy, diffuse reflectance infrared spectroscopy (DRIFTS), proton NMR spectroscopy and scanning electron microscopy (SEM).

Background information on the sol-gel process as it relates to silicon alkoxide-based sol gel materials is presented in Chapter 1. The synthesis of periodic mesoporous silica materials and hybrid silica materials is also described in this chapter. A review of periodic mesoporous organosilica materials, introduced in Chapter 1, is given in Chapter 2. General preparation methods and characterisation techniques of mesoporous silica materials used in this study are described in Chapter 3.

Periodic mesoporous ethanesilica prepared by condensation of 1,2-bistrimethoxysilylethane (BTME) and by co-condensation of BTME with tetraethylorthosilicate (TEOS) are described in Chapter 4 – 6. Chapters 7 and 8

focus on the preparation of bifunctional periodic mesoporous organosilica materials synthesized by co-condensation of 1,2-bistrimethoxysilylethane (BTME) with 3-glycidoxypropyltrimethoxysilane (GPTS) and 3-aminopropyltriethoxysilane (APTS). The ageing duration, ageing temperature, concentration of BTME, amount of water and amount of NH_4OH were varied systematically in order to study their effect on the mesophase formed and on the surface properties of the materials synthesised. Results are compared with literature reports for other BTME synthesised materials. The effect of cobalt ion incorporation into PMO materials is described in Chapter 5 – 8.

Concluding remarks and suggestions for future work are presented in Chapter 9.

CHAPTER ONE

Sol-gel processing of hybrid organic-inorganic mesoporous silica materials

1.1 Introduction

In this chapter background information about the sol-gel process as it relates to silicon alkoxide-based sol gel materials precedes a description of templated mesoporous silica materials. This is followed by a description of the preparation of hybrid organic-inorganic silica materials.

1.2 Sol-gel processing of alkoxysilanes

The sol-gel process [1 – 3] involves a series of stages in which an alkoxysilane monomer is converted into a hyper-cross-linked siloxane network. These stages are: hydrolysis and condensation, gelation, aging, and drying. A siloxane network consists of a series of silicon-oxygen-silicon bonds arranged in 3-D (three dimension). The term sol-gel describes the transition of a solution (liquid) into a gel phase (solid).

1.2.1 Monomers

Metal alkoxides, $M(OR)_n$, (where M is the desired metal with oxidation number n, and R is an alkyl group) are widely used as sol-gel precursors [1 – 3]. For silicon based metal alkoxides, tetraethylorthosilicate (TEOS, $Si(OC_2H_5)_4$), is the most common example. Sol-gel processing of TEOS results in the formation of a purely inorganic silica material.

Organosilanes of type $R_{4-n}SiX_n$ (n = 1, 2 or 3) where R is an alkyl or substituted alkyl group and X is a hydrolyzable group such as a halogen (mostly chlorine) or an alkoxy group, are commonly used to form organically-modified silica surfaces. The alkyl group imparts various chemical properties to the surface of the polymerised material. Alkoxysilanes (and alkylalkoxysilanes) are more stable, less reactive and easier to handle than chlorosilanes (and alkylchlorosilanes). The byproducts of silanization reactions when silylating reagents are alkoxysilanes are alcohols, which are less harmful when compared to the corrosive HCl produced when silylating agents are chlorosilanes.

Examples of organosilanes of type $R_{4-n}SiX_n$ include 3-aminopropyltriethoxysilane (APTS) and 3-glycidoxypropyltrimethoxysilane (GPTS); reagents that will be used in this study.

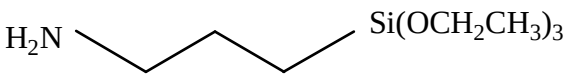

3-aminopropyltriethoxysilane

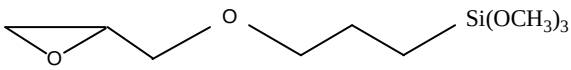

3-glycidoxypropyltrimethoxysilane

Nanocomposites and nanostructured hybrid organic-inorganic materials in which organic spacers are inserted into the siloxane network are prepared through the sol-gel processing of compounds with organobridged trifunctional silyl groups, $X_3Si\text{-}R\text{-}SiX_3$ (where X is an alkoxy group and R is an alkyl group) [3]. Preparation methods for precursors are available in the literature [4 – 9]. There are three approaches commonly used to prepare monomers for bridged polysilsesquioxanes from readily available starting materials [9]:

(1) *Metallation.* Metallation of aryl, alkyl, and alkynyl precursors followed by reaction with a tetrafunctional silane.

(2) *Hydrosilylation.* Hydrosilylation of dienes (or polyenes) or, less commonly, diynes is an efficient reaction for preparing bridged monomers in high yields from chemicals bearing two or more terminal olefins.
(3) *Functionalisation of an organotrialkoxysilane*. An electrophillic substituent on the organotrialkoxysilane can be reacted with any organic molecule with two or more nucleophilic groups. For example, isocyanates react readily with amines to give urea linkages.

1.2.2 Sol-gel synthesis and processing of xerogels from alkoxysilanes and bridged polysilsequioxanes

Sol-gel polymerisation and processing of bis(trialkoxysilyl) monomers parallel, in almost all respects, those of the purely inorganic precursors such as TEOS [1 – 3]. The sol-gel reaction is generally divided into two steps: hydrolysis of metal alkoxides to produce hydroxyl groups, followed by polycondensation of the hydroxyl groups and residual alkoxy groups to form a three dimensional network. A summary of the key steps in the sol-gel polymerisation of alkoxysilanes, which will be represented as ≡ Si – OR (where R is an alkyl group, C_nH_{2x+1}) is shown in Equations 1 – 3 and 4 – 6 for acid and base catalysed reactions, respectively. Equations 7 – 9 (acid catalysed) as well as 10 – 12 (base catalysed) are the corresponding reactions for bis(trialkoxysilyl) monomers.
Trialkoxysilanes (Equations 1 – 6) or bis(trialkoxysilyl) (Equations 7 – 12) monomers are hydrolysed and condensed under relatively mild conditions that are typical for sol-gel polymerisation reactions. Monomers are dissolved in a mutual solvent (e.g ethanol, tetrahydrofuran, etc) and the polymerisation reactions are initiated by addition of an aqueous catalyst (acidic, basic or fluoridic). Because water and alkoxysilanes are immiscible, a mutual solvent such as an alcohol is normally used as a homogenizing agent. An excess of water is employed (> $3H_2O$ per Si atom).

Acid catalysed hydrolysis of trialkoxysilanes:

$$\equiv Si - OR + H_2O/H^+ \rightarrow \equiv Si - OH + ROH \qquad (1)$$

Acid catalysed homo-condensation/Water condensation of trialkoxysilanes:

$$\equiv Si - OH + \equiv Si - OH + H_2O/H^+ \rightarrow \equiv Si - O - Si \equiv + H_2O \quad (2)$$

Acid catalysed hetero-condensation/Alcohol condensation of trialkoxysilanes:

$$\equiv Si - OH + \equiv Si - OR + H_2O/H^+ \rightarrow \equiv Si - O - Si \equiv + ROH \quad (3)$$

Base catalysed hydrolysis of trialkoxysilanes:

$$\equiv Si - OR + H_2O/OH^- \rightarrow \equiv Si - OH + ROH \quad (4)$$

Base catalysed homo-condensation of trialkoxysilanes:

$$\equiv Si - OH + \equiv Si - OH + H_2O/OH^- \rightarrow \equiv Si - O - Si \equiv + H_2O \quad (5)$$

Base catalysed hetero-condensation of trialkoxysilanes:

$$\equiv Si - OH + \equiv Si - OR + H_2O/OH^- \rightarrow \equiv Si - O - Si \equiv + ROH \quad (6)$$

Acid catalysed hydrolysis of bistrialkoxysilylalkanes:

$$(RO)_3Si\text{-}R\text{-}Si(OR)_3 + H_2O/H^+ \rightarrow (HO)_m(RO)_{3-m}Si\text{-}R\text{-}Si(OR)_{3-m'}(OH)_{m'} + ROH \quad (7)$$

Acid catalysed homo-condensation of bistrialkoxysilylalkanes:

$$(HO)_m(RO)_{3-m}Si\text{-}R\text{-}Si(OR)_{3-m'}(OH)_{m'} + (HO)_m(RO)_{3-m}Si\text{-}R\text{-}Si(OR)_{3-m'}(OH)_{m'} + H_2O/H^+ \rightarrow Network + H_2O \quad (8)$$

An organosilica network formed by homo-condensation can be represented as shown below:

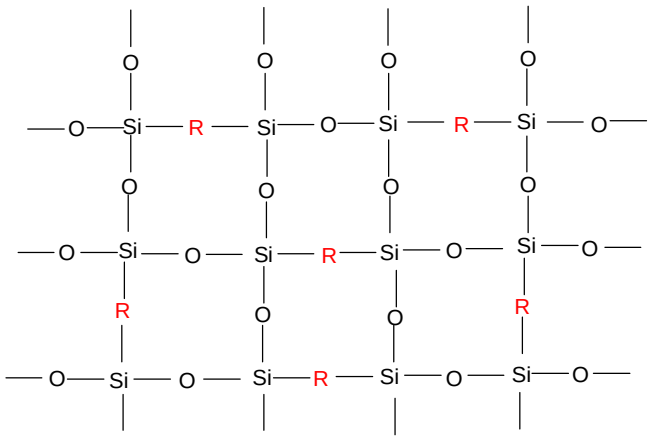

Acid catalysed hetero-condensation of bistrialkoxysilylalkanes:

$(HO)_m(RO)_{3-m}Si\text{-}R\text{-}Si(OR)_{3-m'}(OH)_{m'} + \equiv Si - OR' + H_2O/H^+ \rightarrow Network + ROH$ (9)

An organosilica network formed by hetero-condensation contains terminal alkyl groups (R') and it can be represented as shown below:

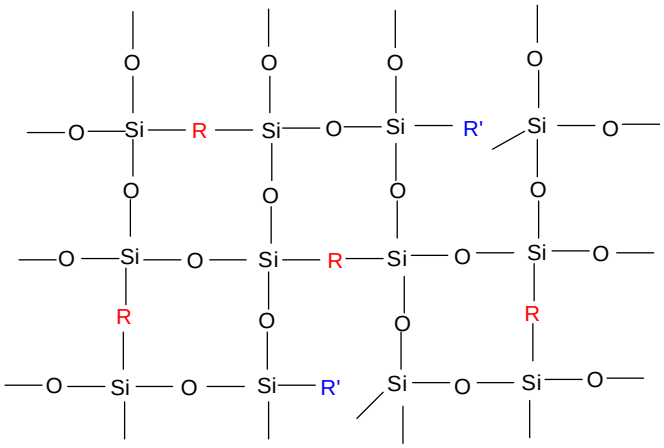

Base catalysed hydrolysis of bistrialkoxysilylalkanes:

$(RO)_3Si\text{-}R\text{-}Si(OR)_3 + H_2O/OH^- \rightarrow (O^-)_m(RO)_{3-m}Si\text{-}R\text{-}Si(OR)_{3-m'}(O^-)_{m'} + ROH$ (10)

Acid catalysed homo-condensation of bistrialkoxysilylalkanes:

$(HO)_m(RO)_{3-m}Si\text{-}R\text{-}Si(OR)_{3-m'}(OH)_{m'} + (HO)_m(RO)_{3-m}Si\text{-}R\text{-}Si(OR)_{3-m'}(OH)_{m'} + H_2O/OH^- \rightarrow Network + H_2O$ (11)

Acid catalysed hetero-condensation of bistrialkoxysilylalkanes:

$(HO)_m(RO)_{3-m}Si\text{-}R\text{-}Si(OR)_{3-m'}(OH)m' + \equiv Si - OR' + H_2O/OH^- \rightarrow Network + ROH$ (12)

Alkoxide groups on the silicon atoms are hydrolysed to silanols that subsequently condense with each other (homocondensation) or with alkoxysilanes (heterocondensation) to give rise to siloxane (Si-O-Si) bonds. As hydrolysis and condensation reactions continue, viscosity increases until the 'sol' ceases to flow and forms the 'gel'.

Further processing of the sol enables one to make ceramic materials in different forms. The detailed sol-gel process is illustrated in Figure 1.1. Prior to gelation, the sol containing the growing polymers can be cast as thin films (by spin-coating or dip-coating) or drawn into fibres. When the sol is cast into a mold, a wet gel will form. After gelation the solvent can be removed, to leave a three-dimensional network that resembles to some degree, the original polymeric structure. The gels are aged for a period of time before drying to form xerogels (dry gels) or aerogels (air gels).

Depending on the drying conditions, sol-gel derived oxides can be termed xerogels or aerogels. Xerogels are gels that have been air-dried. A xerogel undergoes considerable shrinkage during the drying process. Aerogels are gels that have been dried under supercritical conditions resulting in a highly porous and extremely low density material. With further drying and heat treatment, the gel is converted into dense ceramic or glass particles. Ultra-fine and uniform ceramic powders are formed by precipitation, spray pyrolysis, or emulsion techniques.

There are a certain number of synthesis parameters which have an effect on the final properties of oxide materials. These are: (i) reaction pH, (ii) alkyl groups, (iii) the activity of metallic precursors, (iv) water-to-alkoxide mole ratio (called water ratio), (v) solvent effects, (vi) reaction time, and (vii) reaction temperature [10]. By varying these processing parameters, materials with different microstructure and surface chemistry can be obtained.

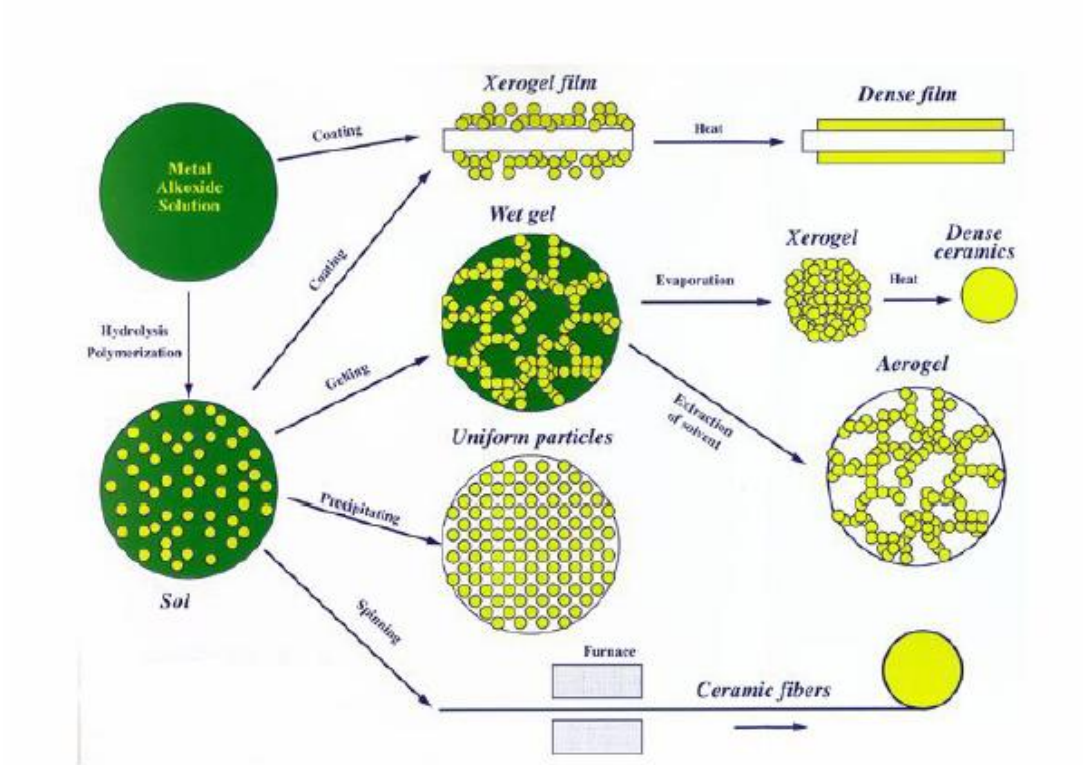

Figure 1.1 Sol-gel process and their products [11].

1.3 Silica and hybrid silica materials

1.3.1 Background

Porous materials are used as adsorbents and industrial catalyst supports owing to their high surface area and large pore volume. These materials are classified by IUPAC according to their types of predominant pore size as: (a) micropores with diameters less than 2.0 nm, (b) mesopores with diameters between 2.0 and 50 nm, and (c) macropores with diameters greater than 50 nm [12]. The expression 'nanopore' is used to encompass both micropores and mesopores.

Silica is a commonly found material and is used as a starting complex in many applications. Interestingly, this common material can be synthesized in many different forms and it is this ability to make materials with different surface areas and porosity that gives silica some of its unique properties [1 – 3]. Further, it is possible to replace some of the Si atoms by other elements (e.g. Al) in the structure of the SiO_2 to produce materials (e.g. aluminosilicates) with varying properties such as acidity [2]. Thus, control of the material structure leads to control of the properties that can be tailored for use in chemical reactions.

Synthetic silicates prepared by the sol-gel processing of alkoxysilanes – most commonly tetramethylorthosilicate (TMOS) or tetraethylorthosilicate (TEOS) - allow for the preparation of amorphous (xerogels) and ordered materials that are precursors for high purity glasses, ceramics, coatings and fibres [1,2]. Silica formed from the aqueous polymerisation of alkoxysilanes in the absence of surfactants is amorphous with irregular shaped particles and broad distribution in pore size.

1.3.2 Ordered mesoporous inorganic materials

The synthesis of the first surfactant templated silica material, called MCM41, was reported in 1992 [13, 14]. Mesoporous silica materials prepared using a surfactant

have a periodic structure with tunable uniform pore sizes ranging from 1.5 nm to more than 10 nm. They also show high thermal and hydrothermal stability, and have large surface areas. These materials have the potential to be used in separation science, catalysis, nanoelectronics, and environmental remediation [2, 3, 15]. Because of their larger and well-defined pores, mesoporous materials can be used in applications where microprous materials (e.g. zeolites) are limited by their relatively small size.

Over the past decade, since the discovery of the two-dimensionally ordered hexagonal mesoporous silica MCM-41, a great deal of research has been undertaken to examine the synthesis, characterisation and potential applications of this solid [16 – 18]. In this period M41S mesophases, namely, MCM-41 (hexagonal, *p6mm*), MCM-48 (cubic, *Ia3d*), and MCM-50 (lamellar), were synthesized under basic conditions in the presence of alkyltrimethylammonium surfactants as supramolecular templates (Figure 1.2). Removal of the surfactants by calcination gave mesoporous oxide structures. A wide range of surfactant types have been similarly used to generate a range of mesoporous oxide structures. This led to the discovery of other mesophases including (i) SBA-15 (Santa Barbara-15), which possesses the same symmetry (*p6mm*) as MCM41, but is prepared using non-ionic, rather than cationic, surfactants [19], (ii) SBA-1 and the similar SBA-6 (*Pm3n*) [20 – 23], (iii) SBA-2 and the similar SBA-12 ($p6_3mmc$ and intergrowth structures) [24 – 25], and SBA-16 (*Im3m*) [19], SBA-11(*Pm3m*) [19], MSU-V [26], and KIT-1 [27] and disordered HMS [28].

A liquid-crystal templating (LCT) mechanism was proposed by Beck et. al. [14] to explain the formation mechanism of MCM-41 (Figure 1.3). The mechanism centers around long-chain quartenary ammonium surfactants which minimise their energy in solution by assembling into micelles. Under certain conditions these micelles can adopt a rod-like shape and even organise into long-range hexagonal arrays (with rod diameters in the mesopore range 2.0 to 4.0 nm). In the arrangements the charged head groups point toward the solution and the long hydrocarbon chains (hydrophobic) point toward the centre of the micelles. The

formation of the micellar rods and their organisation into hexagonal arrays is strongly dependent on the surfactant alkyl chain length, concentration, the nature of the halide counter-ion, and the temperature of the solution [29 - 31].

Upon addition of a silicate precursor, the negatively charged silica species (I^-) condense and polymerise on the surface of the positively charged micelles (S^+), giving rise to the corresponding hexagonal S^+I^- organic-inorganic complex. Calcination of the complex has revealed the solid framework of this particular mesoporous molecular sieve (denoted MCM-41).

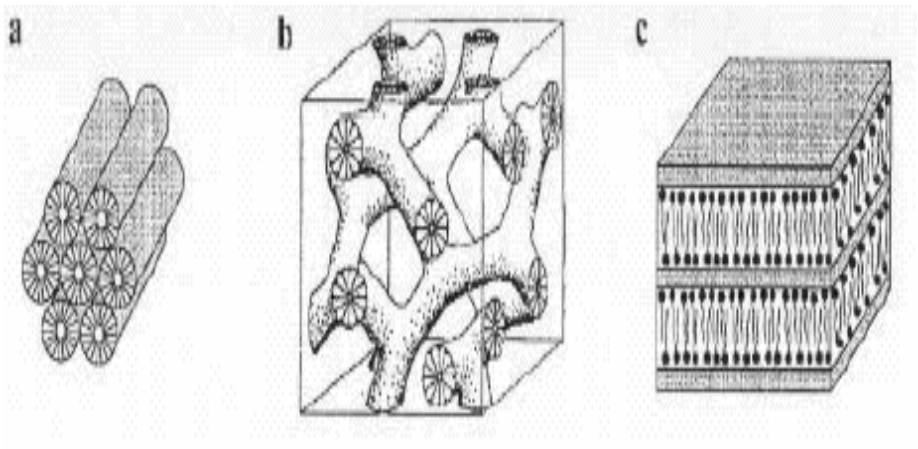

Figure 1.2 Three structure types observed for silica-surfactant mesophases: (a) MCM-41 (hexagonal, 1-dimensional); (b) MCM-48 (cubic, bicontinuous, 3-D); (c) MCM-50 (lamellar, 2-D) [13].

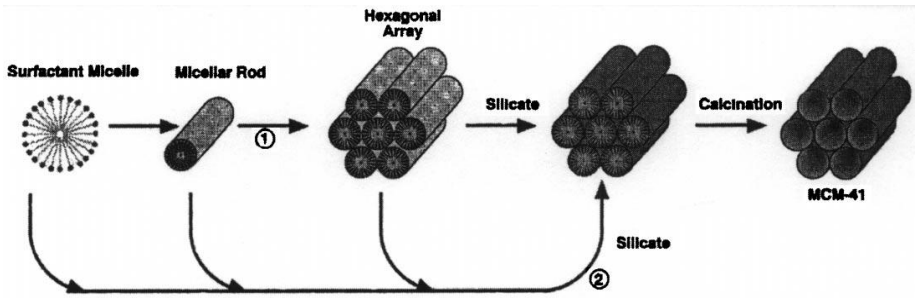

Figure 1.3 Liquid-crystal templating mechanism proposed by Beck et. al. [14]. showing two pathways for the formation of MCM-41: (1) liquid-crystal-initiated and (2) silicate-initiated.

1.4 Organic-inorganic hybrid materials

In order to impart new properties to the silica surface, organic groups have been incorporated on the surfaces of ordered mesoporous silicas. Hybrid organic-inorganic compounds where both organic and inorganic components are bonded through strong covalent bonds are termed ceramers (ceramic polymers), ormosils (organically modified silicates) or ormocers (organically modified ceramics) [3].
The study of organic-inorganic hybrid materials is a field of growing interest [3]. They are an attractive target achievable by the sol-gel process. Organic-inorganic composites include materials with silica frameworks and organic groups on the pore surface [32 – 34], and materials with organosilica frameworks, [3, 6 – 8, 35] whose surface can be covered by organic groups [3, 35].

Using the sol-gel route, it is possible to introduce a large variety of organic moieties into inorganic matrices, so leading to the possibility to tailor physicochemical properties. The synthesis of hybrid mesoporous silica materials with controlled functionality and hydrophobicity could open up new avenues for organometallic chemistry, catalysis, and organic-inorganic host-guest chemistry [3, 35].

Most of the organic-inorganic hybrid materials have sizes in the nanometer domain (typically 1 – 100 nm) – and are hence nanocomposite materials. Traditional macroscale composites have domain sizes in the millimetre and even micrometer scales. General strategies for the design of functional hybrids are shown in Figure 1.4 [9]. Path A corresponds to conventional sol-gel chemistry. Hybrid networks are obtained through hydrolysis of organically modified metal alkoxides or metal halides condensed with or without metallic oxides. Periodic mesostructured hybrid materials are prepared by using organic templates as structure directing agents (Route B and D). Route C shows the assembling of well-defined nanobuilding blocks to form mesostructured nanobuilding block-based hybrids.

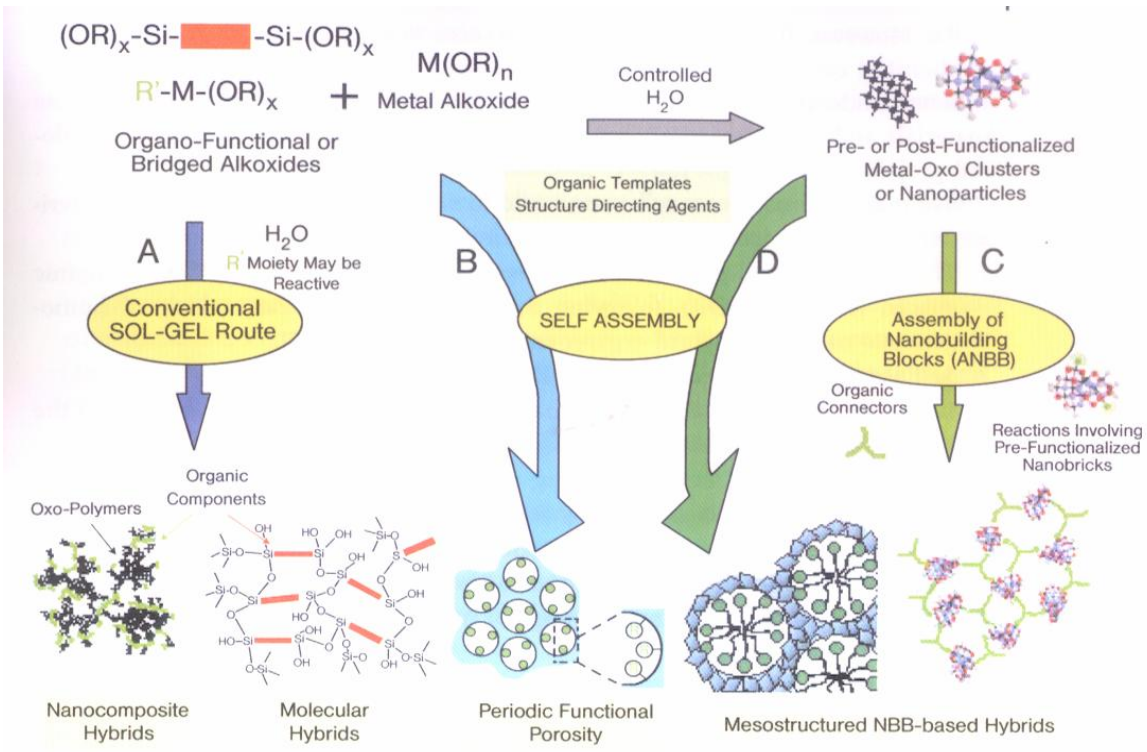

Figure 1.4 General strategies for the design of functional hybrids [3].

1.4.1 Organically modified mesoporous silicas

The discovery of ordered mesoporous silicas in the early nineties opened up remarkably broad opportunities in the synthesis of ordered mesoporous organic-inorganic composites [38, 39]. Considerable attention has been focused on tailoring the chemical composition of MCM-41 type ordered mesoporous materials in order to increase their potential for electrical, optical, structural, and related properties. Organic functionalization of silicates permits precise control over the surface properties, modification of the hydrophilic/hydrophobic character of the surface, alteration of the surface reactivity, protection of the surface from attack, modification of the bulk properties of the materials and at the same time the ability to stabilize the materials towards hydrolysis.

Chemical modification of periodic mesoporous silicas via covalent bonding of organic molecules has been achieved using two general strategies: a postsynthesis procedure and a co-condensation (one-pot) procedure (Figure 1.4) [38 – 41]. In the postsynthesis procedure organic groups are grafted onto silanol-containing surface using a trichloro- or trialkoxy organosilane [42 - 44]. The tethering is done by covalently attaching an organosilane to a surface silicon atom through the silicon (surface) – oxygen – silicon (external) – carbon bond in the organosilane [Figure 1.5(a)].

In materials prepared by co-condensation of siloxane and organosiloxane precursors, an organic moiety is covalently linked via a nonhydrolyzable Si-C bond to a siloxane species, which hydrolyzes to form a silica network. Many kinds of organic grafted mesoporous materials have been synthesised through the hydrolysis and condensation of organically modified silanes, R_1-Si$(OR_2)_3$, (where R_1 = C_8H_{17} [45], C_6H_5 [45], $C_3H_7NH_2$ [42], C_2H_5 [46], C_3H_7SH [47] etc., and R_2 = CH_3, C_2H_5) with alkoxysilane, Si$(OR_2)_4$ compounds in the presence of a surfactant. These organic-grafted mesoporous materials have a heterogeneous structure composed of an inorganic main framework with an organic layer grafted onto the framework.

For catalytic applications, aminopropyl-functionalised amorphous and mesoporous (ordered) silicas have been the most widely studied organic-inorganic hybrid solids [48]. These organic-inorganic hybrids have been used as catalysts for the Knoevenagel condensation of various aldehydes and ketones with ethyl cyanoacetate [49 – 51] as well as for base-catalysed reactions such as the nitroaldol condensation and Michael addition reactions [52, 53].

3-Glycidoxypropyltrimethoxysilane (GPTS) has been used as a coupling agent in transparent abrasion-resistant hybrid coatings for polymers [54] and metals [55] and for gas separation membranes [56]. GPTS is an attractive candidate for further functionalization of silica materials because the epoxy ring can be opened using amines (e.g. 3-aminopropyltriethoxysilane) [57, 58] to afford other functional groups [59, 60].

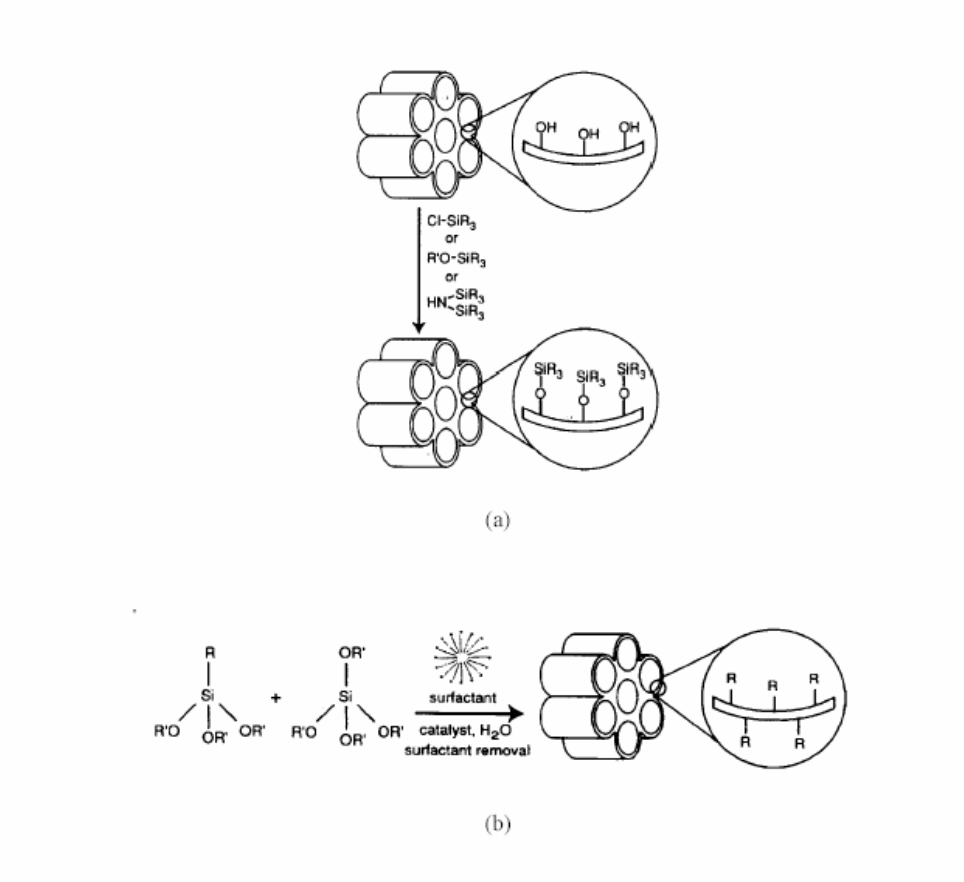

Figure 1.5 Organic modification of the mesoporous silicate. (a) post-synthesis grafting, (b) co-condensation.

1.4.2 Organic-inorganic hybrid materials with organosilica frameworks (Organo-bridged polysilsesquioxanes)

While the area of ordered mesoporous silicas was growing, a steady research effort has also been devoted to the synthesis of amorphous porous organosilica xerogels by heterolytic polycondensation of bridged silsesquioxane $(R'O)_3SiRSi(OR')_3$ (*where R' is an alkyl group, commonly methyl or ethyl, and R is an organic group)* [4 – 9, 61 - 63]. The advantages of using a double trialkoxysilyl precursor are that bonding is already established between the organic and inorganic phases and the stoichiometry between silicon and carbon in the framework is assured. The organic bridging group provides added functionality and opportunities for manipulating properties such as hydrophobicity, refractive index, chemical durability, or dielectric constant.

The idea of tailoring the internal structures of organosilicate xerogels by inserting organic spacers into the siloxane network through the sol-gel processing of compounds with organobridged trifunctional silyl groups, $X_3Si\text{-}R\text{-}SiX_3$ (where X is an alkoxy group and R is an alkyl group), was originally reported in 1989 by Shea [6]. The sol-gel method allows the preparation of both nanocomposites and nanostructured hybrid organic-inorganic materials under mild conditions [7]. The sol-gel derived hybrid organic-inorganic materials exhibit properties associated with both the organic moieties and the inorganic framework. The sol-gel technology provides an opportunity to produce an almost infinite variety of silicate-like structures by the introduction of organic spacers at regular intervals in the silicate framework. The organic group, covalently attached to the trifunctional silicon groups through Si-C bonds can be varied in length, rigidity, geometry of substitution, and functionality. Because the organic group remains an integral component of the material, this variability provides an opportunity to modulate bulk properties such as porosity, thermal stability, refractive index, optical clarity, chemical resistance, hydrophobicity, and dielectric constant.

The organic groups in the building blocks range from rigid arylenic, acetylinic, and olefinic bridging groups to flexible alkylenes ranging from 1 to 14 methylene groups in length [9]. They also include a variety of functionalised groups such as amines, ethers, sulfides, phosphines, amides, ureas, carbamates, and carbonates. In addition, bridging groups have included organometallics in which the metal is part of the bridge or pendant to the bridge.

The textural properties (i.e. specific surface area, porosity, pore size, density, etc) of the xerogel depends on the kinetic parameters involved during the hydrolytic polycondensation [8] of the molecular precursor. These parameters that can be varied include the organic moiety [64, 65], leaving group [67], solvent [67], catalyst [68], concentration [66], temperature [67, 68] and aging conditions [64]. By varying these processing parameters, materials with different microstructure and surface chemistry can be obtained.

1.4.3 Periodic mesoporous organosilica materials

In 1999 a new class of hybrid mesoporous materials that incorporate organic components within a silica framework have been synthesized by combining the self-assembly approach for making ordered mesoporous silica and the use of bridged silsequioxanes. $((R'O)_3SiRSi(OR')_3)$ [15, 35, 69 – 71]. These organic-inorganic hybrid materials, called periodic mesoporous organosilica materials (PMOs), are prepared through the surfactant-templated hydrolytic polycondensation of bifunctional organosiloxane precursors [15, 35]. A detailed review of PMOs, the theme of this thesis, can be found in Chapter 2.

1.5 Conclusions

Precursors that integrate organic and inorganic groups at molecular length scales are used to synthesise hybrid organic-inorganic silica materials by using the sol-gel process. Hybrid organic-inorganic silica materials can be synthesised in a variety of forms that range from nonporous films to high surface area monolithic

structures. Properties of these materials can be tailored by varying kinetic parameters involved during hydrolytic polycondensation of the molecular precursor. These materials have found a variety of applications, for example in optics and nanoelectronics, and as coatings and catalyst supports.

1.6 References

1. R. K. Iler, The Chemistry of Silica, John Wiley & Sons, New York (1979).

2. C. J. Brinkner and G. W. Scherer, Sol-Gel Science. The Physics and Chemistry of Sol-Gel Processing, Academic Press, San Diego (1990).

3. P. Gomez-Romero and C. Sanchez, Eds., Functional Hybrid Materials, Wiley-VCH, Weinheim (2004).

4. E. Lindner, A. Enderle and A. Baumann, J. Organomet. Chem. **558**, 235 (1998).

5. J. Blumel, Inorg. Chem. **33**, 5050 (1994).

6. K. J. Shea and D.A. Loy, Chem. Mater. **1,** 572 (1989).

7. G. Cerveau, R. J. P. Corriu and E. Framery, J. Mater. Chem. **11**, 713 (2001) and references therein.

8. G. Cerveau, R. J. P. Corriu and C. Fischmeister-Lepeytre, J. Mater. Chem. **9**, 1149 (1999).

9. K. J. Shea, J. Moreau, D. A. Loy, R. J. P. Corriu, and B. Boury. In Functional Hybrid Materials, P. Gomez-Romero and C. Sanchez, Eds., Wiley-VCH, Weinheim (2004).

10. R. D. Gonzalez, T. Lopez, and R. Gomez, Catalysis Today **35**, 293 (1997).

11. http://www.solgel.com.

12. K. S. W. Sing, D. H. Everett, R. A. W. Haul, L. Moscou, R. A. Pierotti, J. Rouquerol, T. Siemieniewska, Pure Appl. Chem. **57**, 603 (1985).

13. C. T. Kresge, M. E. Leonowicz, W. J. Roth, J. C. Vartuli and J. S. Beck, Nature **359**, 710 (1992).

14. J. S. Beck, J. C. Vartuli, W. J. Roth, M. E. Leonowicz, C. T. Kresge, K. D. Schmitt, C. T-W. Chu, D. H. Olson, E. W. Sheppard, S. McCullen, J. B. Higgins and J. L. Schlenker. J. Am. Chem. Soc. **114**, 10834 (1992).

15. T. Asefa, M. J. MacLachlan, H. Grondey, N. Coombs and G. A. Ozin, Angew. Chem. Int. Ed. **39**, 1808 (2000) and references therein.

16. A. Corma, Chem. Rev. **97**, 2373 (1996).

17. J. M. Thomas, Angew. Chem., Int. Ed. **38**, 3589 (1999).

18. U. Ciesla and F. Schuth, Micropor. Mesopor. Mater. **27**, 131 (1999).

19. D. Zhao, Q. Huo, J. Feng, B. F. Chmelka and G. D. Stucky, J. Am. Chem. Soc. **120**, 6024 (1998).

20. Q. Huo, D. Margolese and G. D. Stucky, Chem. Mater. **8**, 1147 (1997).

21. M. J. Kim and R. Ryoo, Chem. Mater. **11**, 487 (1999).

22. S. Che, Y. Sakamoto, O. Terasaki and T. Tatsumi, Chem. Mater. **13**, 2237 (2001).

23. W. Zhou, H. M. A. Hunter, P. A. Wright, Q. Ge and J. M. Thomas, J. Phys. Chem. B **102**, 6934 (1998).

24. H. M. A. Hunter, A. E. Garcia-Bennett, I. J. Shannon, W. Zhou and P. A. Wright, J. Mater. Chem. **12**, 20 (2002).

25. M. Kruk, M. Jaroniec, R. Ryoo and J. M. Kim, Chem. Mater. **11**, 2568 (1999).

26. S. S. Kim, W. Zheng, and T. J. Pinnavia, Science **282**, 1302 (1998).

27. R. Ryoo, J. M. Kim, C. H. Shin, and J. Y. Lee, Stud. Surf. Sci. Catal. **105A**, 45 (1996).

28. P. T. Tanev, and T. J. Pinnavia, Science **267**, 865 (1995).

29. N.K Raman, M. T. Anderson, and C.J. Brinker, Chem. Mater. **8**, 1682 (1996).

30. A. Sayari and P. Liu, Microporous Mater. **12**, 149 (1997).

31. J. Y. Ying, C. P. Mehnert and M. S. Wong, Angew. Chem., Int. Ed. Engl. **38**, 56 (1999).

32. T.Yanagisawa, T. Shimizu, K. Kuroda and C. Kato, Bull. Chem. Soc. Jpn. **63**, 1535 (1990).

33. S. L. Burkett, S. D. Sims and S. Mann, Chem. Commun. 1367 (1997).

34. D. J. Macquarrie, Chem. Commun. 1961 (1996).

35. T. Asefa, M. Kruk, M . J. MacLachlan, N. Coombs, H. Grondey, M. Jaroniec, and G. A. Ozin; J. Am. Chem. Soc. **123**, 8520 (2001).

36. U. Schubert, N. Husing and N. Lorenz, Chem. Mater. **7**, 2010 (1995).

37. J. Wen and G. L. Wilkes, Chem. Mater. **8**, 1667 (1996).

38. A. Stein, B. J. Melde and R. C. Schroden, Adv. Mater. **12**, 147 (2000).

39. A. Sayari and S. Hamoudi, Chem. Mater. **13**, 3151 (2001).

40. M. S.Morey, A. Davidson and G. D. Stucky, J. Porous. Mater **5**, 195 (1998).

41. V. Alfredsson and M. W. Anderson, Chem. Mater. **8**, 1141 (1996).

42. A. M. Tshavhungwe, Master of Science Thesis, Eastern Illinois (1996).

43. J. H. Clark, and D. J. Macqquarrie, Chem. Commun. 853 (1998)

44. K. Moller, and T. Bein, Chem. Mater. **10**, 2950 (1998).

45. S. L. Burkett, S. D. Sims, and S. Mann, Chem. Commun. 1362 (1996).

46. M. H. Lim, C. F. Blanford, and A. Stein, J. Am. Chem. Soc. **119**, 4090, (1997).

47. C. E. Fowler, S. L. Burkett, and S. Mann, Chem. Commun. 1769 (1997).

48. A. P. Wight, and M. E. Davis, Chem. Rev. **102**, 3589 (2002).

49. D. J. Macquarrie, J. H. Clark, A. Lambert, J. E. G. Mdoe, and A. Priest, React. Funct.. Polm. **35**, 153 (1997).

50. E. Angeletti, C. Canepa, C. Martinetti, and P. Venturello, Tetrahedron Lett. **29**, 2261 (1988).

51. M. Lasperas, T. Llorett, L. Chaves, I. Rodriguez, A. Cauvel, and D. Brunel, Stud. Surf. Sci. Catal. **108**, 75 (1997).

52. F. Bigi, S. Carloni, R. Maggi, A. Mazzacani, and G. Sartori, Stud. Surf. Sci. Catal. **130**, 3501 (2000).

53. D. Demicheli, R. Maggi, A. Mazzacani, P. Righi, G. Sartori, and F. Bigi, Tetrahedron Lett. **42**, 2401 (2001).

54. C. A. Glotfelter, and R. P. Ryan, US Patent 5120811 (1992).

55. H. Schmidt, B. Seiferling, G. Phillip, and K. Deichmann, in Processing of Advanced Ceramics, Wiley, New York, 651 (1988).

56. M. Pilz, and H. Romich, J. Sol-Gel Sci. Technol. **8**, 1071 (1997).

57. S. R. Davis, A. R. Brough, and A. Atkinson, J. Non-Crystalline Solids **315**, 197 (2003).

58. P. Cardiano, S. Sergi, M. Lazzari, and P. Piraino, Polymer **43**, 6635 (2002).

59. M. Templin, U. Wiesner, and H. W. Spiess, Adv. Mater. **9**, 814 (1997).

60. P. Innocenzi, A. Sassi, G. Brusatin, M. Guglielmi, D. Favretto, R. Bertani, A. Venzo, and F. Babonneau, Chem. Mater. **13**, 3635 (2001).

61. H. W. Oviatt, Jr., K. J. Shea and J. H. Small, Chem. Mater. **5**, 943 (1993).

62. R. J. P. Corriu, J. Moreau, P. Thepot, M. Wong Chi Man, Chem. Mater. **4**, 1217 (1992).

63. E. Lindner, T. Schneller, F. Auer, P. Wegner and H. A. Mayer, Chem. Eur. J. **3**, 1833 (1997).

64. G. Cerveau, R. J. P. Corriu, C. Lepeytre and P. H. Mutin, J. Mater. Chem. **8**, 2707 (1998).

65. G. Cerveau, R. J. P. Corriu and C. Lepeytre, J. Organomet. Chem. **548**, 99 (1997).

66. G. Cerveau, R. J. P. Corriu and E. Framery, Polyhedron **19**, 307 (2000).

67. G. Cerveau, R. J. P. Corriu and E. Framery, Chem. Commun. 2080 (1999).

68. G. Cerveau, R. J. P. Corriu and E. Framery, J. Mater. Chem.**10**, 1617 (2000).

69. S. Inagaki, S. Guan, Y. Fukushima, T. Ohsuna, and O. Terasaki, J. Am. Chem. Soc. **121**, 9611 (1999).

70. T. Asefa, M. J MacLachlan, N. Coombs and G. A. Ozin, Nature **402**, 867 (1999).

71. B. J. Melde, B. T. Holland, C. F. Blanford, and A. Stein, Chem. Mater. **11**, 3302 (1999).

CHAPTER TWO

Periodic Mesoporous Organosilica Materials: A Review

2.1 Introduction

Since the inception of surfactant-templated, mesoporous silica science in 1992, [1,2] significant research efforts have been devoted to the preparation and study of the properties of hybrid organic-inorganic silica materials because of their potential applications in catalysis, ion-exchange, encapsulation of transition metal complexes or semiconductor clusters, chemical sensors and nanomaterial fabrication [3,4]. Selected topics concerning organic-inorganic composites can be found in a recent book [4], a special issue of Chemistry of Materials [5] as well as in conference and symposia proceedings and reviews [6-11]. Acronyms used in this chapter are listed in Table 2.1.

2.2 Synthesis

Periodic mesoporous organosilica (PMO) materials, in which the organic component occupies framework positions in the walls rather than in the voids of the hexagonal channels, are organic-inorganic hybrid materials prepared through the surfactant-templated hydrolytic polycondensation of bifunctional organosiloxane precursors, $R'O)_3SiRSi(OR')_3$:

$$(R'O)_3SiRSi(OR')_3 + H_2O + surfactant + catalyst \rightarrow [O_{1.5}Si]_2R$$

where R' is an alkyl group, commonly methyl or ethyl, and R is an organic group [3, 6 – 91]. Examples of bifunctional organosilane precursors are listed in Table 2.2.

Table 2.1 Abbreviations and Acronyms

Abbreviation/Acronym	Name
brij 76	polyoxyethylene (10) stearyl ether oligomer $C_{18}H_{37}(OCH_2CH_2)_{10}OH$
BTEE	1,2-bis(triethoxysilyl)ethane
BTEM	bis(triethoxysilyl)methane
CP/MAS NMR	Cross Polarization Magic Angle Nuclear Magnetic Resonance
CTAB	cetyltrimethylammonium bromide
CTAC	cetyltrimethylammonium chloride
CTMA	Cetyltrimethylammonium
LGE76	triblock copolymer $EO_{43}(L_{23}G_6)EO_{43}$
MCM	Mobil Catalytic Material
ODTMA	Octadecyltrimethylammonium
PEO	poly(ethylene oxide)
PLGA	poly(DL-lactic acid-co-glycolic acid)
Pluronic P123	$H(OCH_2CH_2)_{20}(OCH(CH_3)CH_2)_{70}(OCH_2CH_2)OH$
PMO	Periodic Mesoporous Organosilica
SBA	Santa Barbara
TEOS	Tetraethylorthosilicate

Table 2.2 Examples of bridged silicon precursors.

Precursors	**Bridging organic group**
bis(trimethoxysilyl)methane	$-CH_2-$
1,2-bis(triethoxysilyl)ethane (BTEE) 1,2-bis(trimethoxysilyl)ethane (BTME)	$-CH_2CH_2-$
1,2-bis(triethoxysilyl)ethylene	-CH=CH-
bis[(3-trimethoxysilyl)propyl]amine	$-(CH_2)_3\ N(CH_2)_3-$
1,3- bis(triethoxysilyl)propaneterasulfide	$-(CH_2)_3\ S_4(CH_2)_3-$
2,5- bis(triethoxysilyl)-p-xylene	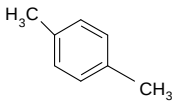
2,5- bis(triethoxysilyl)-1,4-dimethoxybenzene	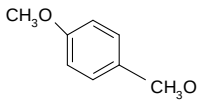
4,4'- bis(triethoxysilyl)biphenyl	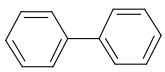
Silylated bipyridine	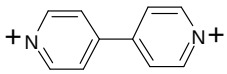

Successful syntheses of PMOs incorporating various organic groups have been reported to take place under a wide range of pHs from highly basic to strongly acidic conditions using cationic, anionic and neutral surfactants and a variety of commercially available block copolymers. See Table 2.3 (pages 43 – 53) for a summary of the PMOs produced to date. Precursors, surfactants and catalysts used to synthesize PMOs as well as the mesophases formed are listed. Organic groups which have been incorporated into the PMOs include ethane, ethylene, methylene, ferrocene, thiophene, bithiophene, acetylene, phenylene, and vinylene [Tables 2.2 and 2.3]. Further, other functional groups have been incorporated by co-condensation of bridged silsequioxanes with organoalkoxysilanes and by chemical conversion of organic groups, resulting in materials with different physical and chemical properties.

The formation of a PMO material is schematically illustrated in Scheme 2.1. Supramolecular assemblies of surfactants are used as structure directing agents to engineer the porosity of these materials using a templating method. The micellar assemblies, which are first formed in solution, are encapsulated by the polymerization of silsesquioxane precursors containing alkoxysilyl groups. This polymerization results in the formation of nanoscopic composites that precipitate out of solution. Subsequent extraction of the surfactants gives porous organosilicas.

Structural rigidity of the bridged polysilsequioxane precursor is an essential characteristic in order to form PMOs. The lack of structural rigidity (i.e. too much flexibility) will result in a material that does not hold its shape once the surfactant templates are removed. Because of their rigidity, short chain organic functional groups (e.g. methane, ethane, ethene) and aromatic functional groups (e.g. benzene) are commonly used for the synthesis of PMOs.

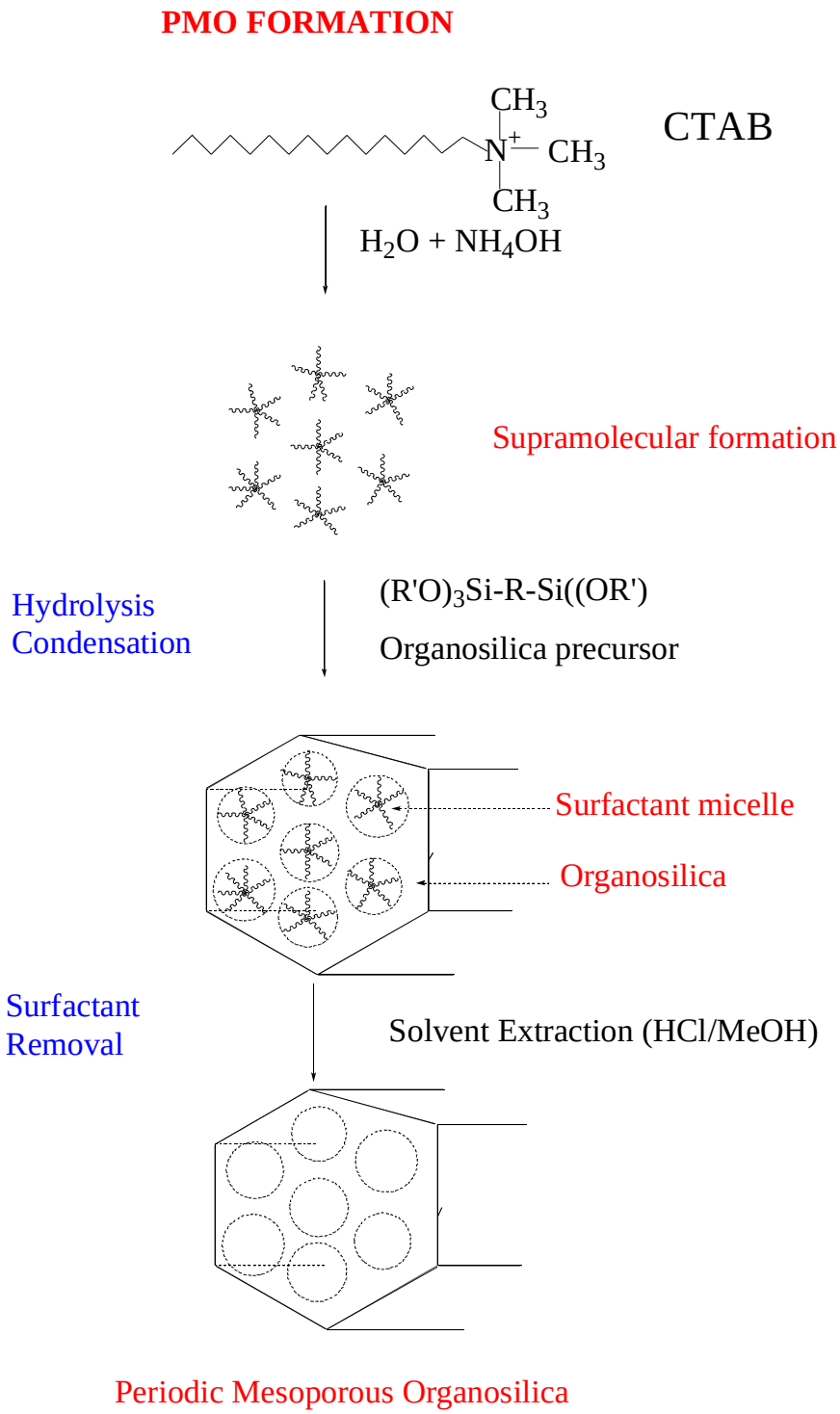

Scheme 2.1 Formation of a periodic mesoporous organosilica material.

2.3 Properties and advantages of PMOs

The surfactant templating sol-gel method ensures a homogeneous distribution of bridging organic groups inside the channel walls and permits populations of up to 100 % organosilica sites. The presence of uniform mesopores in the PMOs distinguishes them from traditional hybrid organic-inorganic materials prepared without surfactants. The ordered pore structures formed by this process allow ready access of diffusing molecules to the large internal surface areas and organic groups. With both structural rigidity and organic functionality, PMOs possess structural properties of ordered mesoporous materials (i.e. well ordered pores, crystalline mesoporosity, Ångstrom precise pore dimensions, high surface areas, and narrow pore size distributions) with the chemical properties of both the silica and the organic bridging group.

The porous structure, surface and framework properties of PMO materials can be finely tuned by changing the bridging organic groups incorporated and the synthesis conditions employed. Depending on the amphiphile templating material used and on the synthesis conditions, several PMO mesophases have been obtained. These include a 2-D hexagonal structure (*p6mm*) similar to MCM-41 or SBA-15, a cubic structure (*Pm3n*) akin to SBA-1 and a 3-D hexagonal mesophase [Table 2.3]. New mesostructures such as mesoporous benzene-silica with crystal-like pores were also synthesized [Table 2.3].

Advantages of these new PMO materials include: (i) the organic groups are incorporated within the silica framework (i.e. on the perimeter of the channels), not blocking or occupying pore volume; (ii) the properties of the framework may be modified by simply changing the bridging group; (iii) the physical and mechanical properties of the mesoporous framework may be modified by chemical reactions with the bridging organic group; (iv) a greater fraction of the organic species can be kept in the framework before loss of mesostructure; (v) the organic groups are homogeneously distributed in the materials; (vi) the amount of organic groups in the framework can be controlled by co-condensation with

tetraethylorthosilicate (TEOS); (vii) other functional groups can be introduced into PMOs by co-condensation of bifunctional organosiloxane precursors with trialkoxyorganosilanes; and (viii) potential catalysts can be synthesized by incorporating ligands, which can coordinate with metals thereby binding them directly into the silica framework.

2.4 PMOs with short chain bridging organic functional groups

2.4.1 Ionic surfactants

In 1999 three groups (Inagaki et. al., Ozin et. al. and Stein et. al.) independently described the synthesis of hybrid organic-inorganic silica materials incorporating organic groups in the silica framework [12 -14]. Inagaki et al. [12] reported the synthesis of highly ordered ethane-bridged PMOs synthesized from the 1,2-bis(trimethoxysilyl)ethane (BTME) as the silica source and octadecyltrimethylammonium (ODTMA) as template under basic conditions. The PMOs had two-dimensional (2-D) and three dimensional (3-D) hexagonal pore structure symmetries and well-defined morphologies with pore sizes of 3.1 and 2.7 nm respectively. The structure control was achieved by adjusting the synthesis temperature and the molar ratios of components of the synthesis gel. The surfactant template was removed by solvent extraction, thus opening uniform pores of large specific surface area. The successful synthesis of PMOs with methylene, phenylene, and vinylene groups in the framework was also mentioned in this initial report, but no synthetic and structural details were provided. ^{29}Si and ^{13}C CP/MAS NMR (Cross Polarization Magic Angle Nuclear Magnetic Resonance) spectroscopy was used to verify the presence of Si-C bonds and of the ethane bridge. TGA results showed that the organic groups were stable up to 400 ^{o}C. Detailed gas adsorption and thermogravimetric characterization of these 2-D and 3-D hexagonal materials was also reported [15].

Stein et al [13] reported PMOs (designated unified organically functionalized mesoporous network, UOFMN) with ethane and ethylene groups synthesized

using 1,2-bis(triethoxysilyl)ethane (BTEE) and 1,2-bis(triethoxysilyl)ethylene organosilane precursors in the presence of hexadecyltrimethylammonium ion surfactant. The resulting materials had a disordered structure with uniform channels, which were accessible after surfactant removal via solvent extraction. The PMO with ethylene groups was reactive toward bromine and the brominated material was reactive as a bromine source. Fourier transform Raman (FT-Raman) and ^{13}C and ^{29}Si CP/MAS NMR spectroscopy were used to confirm the presence of ethylene moieties and the Si-C bonds.

Ozin et al. [14] reported 2-D hexagonally ordered PMOs with ethylene groups (synthesized using BTEE and hexadecyltrimethylammonium ion) and a range of ordered materials with a framework composition intermediate between those of pure silica and pure ethylene PMO (synthesized using BTEE, TEOS and hexadecyltrimethylammonium ion surfactant). Solvent extraction and ion exchange were found to be suitable for surfactant removal. This ethylene PMO was reactive toward bromine in solution, and the reaction resulted in the unit-cell size increase and was accompanied by reaction with solvent, which led to formation of ethane bridges.

Since the publication of the initial reports, journals have been flooded with reports on the synthesis of PMOs. Ozin et al. reported the synthesis and characterisation of a two dimensional hexagonal methylene PMO [3]. Bis(triethoxysilyl)methane (BTEM) was co-condensed with TEOS in the presence of CTAB. The order in the materials decreased as the ratio of BTEM to TEOS was increased.

Amongst the PMO materials, periodic mesoporous ethanesilica has been widely studied [Table 2.3]. Periodic mesoporous ethanesilica materials have been synthesized from 1,2-bistrialkoxysilylethane precursors (alkoxy = ethoxy or methoxy) in the presence of long alkylammonium, triblock , non-ionic polymeric, and non-ionic oligomeric surfactants [Table 2.3]. A highly ordered cubic PMO with crystal-like morphology of decaoctahedron and uniform particle sizes of 5 μm was prepared using BTME and hexadecyltrimethylammonium surfactants [16,

17]. Such well-defined particle morphology has only rarely been observed for ordered mesoporous materials [92].

Brinker et. al. [19 – 21] used an evaporation-induced self-assembly procedure to prepare poly-bridged silsesquioxane films and spherical nanoparticles under acidic conditions. 2-D hexagonal, cubic, and multilamellar vesicular mesophases were obtained. Suo and co-workers [22] reported the synthesis of PMOs using BTEE as the precursor and cetylpyridinium bromide as the structure-directing species via the $S^+X^-I^+$ route under acidic conditions. Compared to the synthesis via the S^+X^- route, the synthesis temperature and concentration of surfactant of the $S^+X^-I^+$ route are lower. The synthesis time of the latter is also shorter, and the surfactant can be easily removed by solvent extraction. Park and co-workers [23 – 25] synthesized PMOs with a range of morphologies based on rope and gyroid shapes using ODTMA as a templating surfactant and BTME as the Si-C bonding source.

2.4.2 Non-ionic surfactants

Other than using alkyltrimethylammonium cationic surfactants of different chain lengths PMOs have also been synthesized using other amphiphilic species such as block copolymers, poly(oxyethylene) alkyl ethers and primary amine surfactants. Advantages presented by non-ionic oligomeric surfactants are that they are inexpensive, biodegradable, nontoxic and have excellent interfacial stabilization properties [26]. Materials formed by using these surfactants had larger pores (> 5 nm) compared to those formed with alkylammonium surfactants (< 5 nm).

Among the non-ionic surfactant family, triblock copolymers such as pluronic P123 or F127 copolymers as well as poly(ethylene oxide) (PEO-PLGA-PEO) were used under acidic conditions and yielded materials with large pores (up to 10 nm) and rather poor structural ordering [29 - 31]. Furthermore synthesis under neutral conditions in the presence of alkylphenylpolyethylene oxide surfactants provided materials in the super-microporous domain [28]. Char et al [29]

described the synthesis of mesoporous organosilicas from the co-condensation of TEOS and BTME by using PEO-containing triblock copolymer templates such as F127 (EO_{106}-PO_{70}-PO_{106}) and poly(ethylene oxide) (PEO-PLGA-PEO). They concluded that the more hydrophobic PEO-PLGA-PEO triblock copolymer is more effective in incorporating organosilicate precursors into the mesoporous silica materials than the PEO-PPO-PEO triblock template. Froba et al. [30] used neutral Pluronic P123 ($EO_{20}PO_{70}EO_{20}$) triblock copolymer as structure-directing agent and BTME as the organosilica source under acidic conditions. Their material exhibited hexagonal symmetry akin to SBA-15 silica with large pores (6.5 nm) and high surface area (900 m^2/g). Markowitz et. al. [31] used the same triblock copolymer in addition to a trimethylbenzene micelle-swelling agent under acidic conditions in the presence of BTEE to synthesize a series of PMOs with pore sizes ranging from 6 to 20 nm. Recent results have shown that PMOs have better hydrothermal and mechanical stability than ordered mesoporous silicas [32].

High quality large pore PMOs were synthesized in the presence of polymer surfactants as supramolecular template. A well-ordered organosilicate with large cagelike pores whose diameter was ca. 12 nm was prepared using BTEE and B50-6600($EO_{39}BO_{47}EO_{39}$) poly(butylenes oxide) containing triblock copolymer under acidic conditions [33]. The structure of this material was similar to that of FDU-1 silica prepared under similar conditions using tetraethylorthosilicate instead of BTEE. [34] Another report dealing with highly ordered large pore organosilicate used a lyotropic liquid crystal Pluronic P123 triblock copolymer as template [35]. The pore sizes of the obtained PMOs were adjustable within the range 5.8 to 7.7 nm.

Highly ordered large-pore ethanesilica materials were synthesized using bistrialkoxysilylethane (BTEE or BTME) as the silica source and nonionic oligomeric alkylethylene oxide surfactants as the structure-directing agent [36, 37]. Sayari and Yang [36] synthesized highly ordered large-pore ethanesilica with 2-D hexagonal symmetry using BTEE as the silica source and Brij 76

[polyoxyethylene(10) stearyl ether oligomer] as the structure-directing agent at 50 ^{o}C. The material had a pore size, surface area and pore volume equal to 5.5 nm, 1024 m^2/g and 1.01 cm^3/g, respectively. The synthesis of a highly ordered PMO with 2-D hexagonal symmetry using BTME and Brij 56 (nominal chemical structure $CH_3(CH_2)(OCH_2CH_2)_{10}OH$) was also reported ($d_{100}$ = 58.8, a_o = 6.79 nm, pore volume = 1.32 cm^3/g); SA = 1190 m^2/g, wall thickness = 2.3 Å) [37].

2.5 Aromatic periodic mesoporous organosilica materials

Aromatic periodic mesoporous organosilica materials have also been synthesized. PMOs containing phenylene-bridged mesoporous organosilica having periodically ordered pore-wall structure, and introduction of sulfo groups therein have recently been reviewed [6].

Ozin et. al. reported the successful synthesis of 2-D hexagonal PMOs with benzene and thiophene under initially acidic and then neutral synthesis conditions using cetylpyridinium surfactant and addition of ammonium fluoride (NH_4F) [38]. An ordered mesoporous benzene-silica hybrid material with a crystal-like wall structure was reported by Inagaki et. al.[39] This material had an hexagonal array of mesopores with a lattice constant of 5.2 nm, and crystal-like pore walls that exhibit structural periodicity with a spacing of 7.6 nm along the channel direction. The periodic pore surface structure results from alternating hydrophilic and hydrophobic layers, composed of silica and benzene, respectively. Inagaki and Goto [40] reported the synthesis of large-pore (6.0 – 7.4 nm) phenylene-bridged mesoporous silica materials having a well-defined hexagonal rod morphology and high thermal stability up to 823 K in air. The materials were synthesized from 1,4-bis(triethoxysilyl)benzene precursor in the presence of poly(ethylene oxide)-poly(propylene oxide)-poly(ethylene oxide) triblock template (Pluronic P123). The degree of periodicity of the benzene silicas prepared in the presence of Pluronic P123 was significantly lower than that of phenylene-bridged materials prepared using alkyltrimethyl-ammonium surfactant under basic conditions [39]

Ozin et. al. [41] reported the synthesis of an aromatic periodic mesoporous organosilica material containing benzene functional groups that are symmetrically integrated with three silicon atoms (1,3,5-substituted benzene) in an organosilica mesoporous framework. The material had a high surface area, well-ordered mesoporous structure and thermally stable framework aromatic groups. The functional aromatic moieties were observed to undergo sequential thermal transformation from a three to two and then to a one point attachment within the framework upon continuous thermolysis under air before eventually being converted to periodic mesoporous silica devoid of aromatic groups at high temperatures and longer pyrolysis times. Hexagonal aromatic PMOs with thick arylsilica walls consisting of tolyl, xylyl and dimethoxyphenyl groups were also synthesized by Ozin's group [42].

The effect of the precursor on the ordering of cetyltrimethylammonium bromide templated and acid catalysed benzenesilica materials was demonstrated by Goletto et. al. [43]. A 2-dimensional hexagonal (*p6m*) phase was formed from 1,3-bis(triethoxysilyl)benzene, whereas 1,4-bis(triethoxysilyl)benzene lead to a cubic *Pm3n* phase.

Froba et. al. [44] used 1,4-bis(triethoxysilyl)benzene and triblock copolymer Pluronic P123 as structure directing agent to synthesize a benzenesilica material with exceptional thick pore walls (7.2 nm). 4,4'-Bis(triethoxysilyl)biphenyl was used to synthesize an ordered mesoporous biphenylene-bridged silsesquioxane with crystal-like pore walls [45].

2.6 PMOs functionalised by co-condensation with organosilanes

The lack of structural rigidity in the organic portion of the silsesquioxane precursor and the number of available silsesquioxane precursors limit the number of PMOs that can be synthesized by the templating method. Too much flexibility will result in a material (similar to an organic polymer) that does not hold its shape once the surfactant templates are extracted. An attractive alternative for

functionalizing polysilsesquioxanes is the co-condensation of trialkoxy organosilanes with silsesquioxane precursors during material formation.

Further functionalization of PMOs has been achieved by co-condensation of 1,2-bistrialkoxysilylalkane precursors with various trialkoxyorganosilanes. Organic-inorganic hybrid bifunctional PMOs containing both bridging organic functional moieties in the framework and terminal organic functional groups protruding into the channel pores were first reported by Ozin et. al. [46]. The materials were synthesized by using bistriethoxysilylethylene as the source of the bridging group and triethoxyvinylsilane as the source of the terminal organic group. It was also mentioned in the report that bifunctional PMOs incorporating ethylene/methyl and methylene/vinyl, as well as trifunctional PMOs incorporating ethylene/methylene/methyl organic functional groups were also synthesized. According to the report, bifunctional samples prepared with cetylpyridinium chloride surfactant also resulted in structurally well ordered materials.

Periodic ethanesilica, by far the most widely studied PMO, has been modified by co-condensation of 1,2-bistrialkoxysilylethane precursors with various trialkoxyorganosilanes in the presence of surfactants [Table 2.3]. Properties of the ethanesilica matrix that make it suitable as a support for functionalized mesoporous materials are: (i) unlike TEOS, BTEE mixes very well with many trialkoxyorganosilanes, and (ii) with its ethylene bridges, BTEE can co-condense with organosilanes without noticeable decrease in the surface area and porosity of the materials [50]. Many organosilanes can disrupt the silica matrix, which contains only relatively short siloxane bridges between silicon atoms, resulting in a noticeable decrease in the surface area and porosity of the materials.

Organosilane precursors co-condensed with bistrialkoxysilylethane include 3-cyanopropyltriethoxysilane [$NC\text{-}(CH_2)_3\text{-}Si(OCH_2CH_3)_3$] [47], N-(2-aminoethyl)-3-aminopropyltrimethoxysilane [$H_2N\text{-}(CH_2)_2\text{-}NH\text{-}(CH_2)_3\text{-}Si(OCH_3)_3$] [50], N-[3-(trimethoxysilyl)propyl]ethylenediamine [51], mercaptopropyltrimethoxysilane [$HS\text{-}(CH_2)_3\text{-}Si(OCH_3)_3$] [50, 52, 53, 55, 56], bis[(3-trimethoxysilyl)propyl]amine

$[(H_3CO)_3Si\text{-}(CH_2)_3\text{-}NH(CH_2)_3\text{-}Si(OCH_3)_3]$ [60] and 1,3-bis(triethoxysilylpropanetetrasulfide) $[(CH_3CH_2O)_3Si\text{-}(CH_2)_3\text{-}S\text{-}S\text{-}S\text{-}S\text{-}(CH_2)_3\text{-}Si(OCH_2CH_3)_3]$ [56].

PMOs containing different amounts of sulfonic acid bearing groups were synthesized using bis(trimethoxysilyl)ethane (BTME) and mercaptopropyltrimethoxysilane as framework precursors under basic [52] or acidic conditions [53]. Pluronic P123 or polyoxyethylene (Brij-56) were used as surfactants for acidic synthesis [53] while cetyltrimethylammonium chloride (CTAC) [52] or octadecyltrimethylammonium chloride [55] were used as surfactants for basic synthesis. Conversion of the mercaptopropyl groups into sulfonic acid moieties was achieved via oxidation using hydrogen peroxide [52]. Ordered hexagonal [53] or cubic-like [52] mesostructures with high surface areas and narrow pore size distributions were obtained. Periodic sulfuric acid-functionalized mesoporous benzene-silicas were derived from mesoporous benzene-silica possesing mercaptopropyl groups by the oxidative transformation of –SH into $–SO_3H$ [57].

PMO materials containing "nitrogen-bearing" functional groups (e.g. cyano- (CN) [47], amines (NH) [48 – 51, 58], etc) have also received some attention. Asefa et. al. prepared periodic mesoporous aminosilicas that contain amine functional groups in the framework of a mesoporous network via thermal ammonolysis of periodic mesoporous organosilicas (PMOs) under a flow of ammonia gas [58]. Markowitz and co-workers described the preparation of a porous organosilica by co-condensation of bistriethoxysilylethane and N-(2-aminoethyl)-3-aminopropyltrimethoxysilane or N-[3-(trimethoxysilyl)propyl] ethylenediamine or Cu(II)-complexed N,N'-bis[3-(trimethoxysilyl)propyl]ethylenediamine under acidic and basic conditions [48 – 51]. Cetyltrimethylammonium chloride was used as the surfactant. The materials synthesized under acidic conditions did not form ordered pore structures. Triblock copolymers have also been used to synthesize highly ordered large mesopore organosilicas functionalized by co-condensation of bistriethoxysilylethane with Cu(II)-complexed N,N'-bis[3-

(trimethoxysilyl)propyl]ethylenediamine [54]. Cu(II) can then be removed by acid leaching after surfactant extration.

2.7 Metal incorporation and applications of PMOs

PMOs have already found use as novel catalysts [18, 55, 57], adsorbents [51] and hosts for nanocluster syntheses [27]. Periodic mesoporous organosilicas functionalized with sulfonic acid groups were found to exhibit much higher catalytic activity than ZSM-5 zeolite and higher catalytic stability than MCM-41 functionalized with the same group for the synthesis and alkylation of phenol [55].

The adsorption of phenolic compounds (4-nitrophenol, 4-chlorophenol, 4-methylphenol) by arylene- and ethylene-bridged polysilsesquioxane materials was investigated by Markowitz et. al. [61]. The arylene-bridged material exhibited a much greater affinity for all three phenols. Mercier et. al investigated the adsorption of metal ions such as Cu^{2+}, Ni^{2+} and Zn^{2+} by PMOs [62]. Results were compared with that of ethylenediamine functionalized nanoporous adsorbents.

Porous materials based on silica are widely used as supports for monolayer-type catalysts in the field of heterogeneous catalysis. Loading a catalyst on an inert but high surface area silica support, by impregnation with an aqueous catalyst precursor, by vapour deposition [94] or by solid/solid wetting [95], improves the accessibility of the active phase [94]. In recent years highly ordered mesoporous silicas, such as MCM41, have shown excellent performance as a support for metal catalysts, resulting in several cases in significant improvement when compared to conventional and commercial catalysts [96, 97]. This improvement has been attributed to the high surface areas and the superior dispersion of the active metals on the support.

Metals such as aluminium (Al), gold (Au), titanium (Ti) and zirconium (Zr) have been incorporated within the framework of hybrid organic-inorganic silica

materials. Aluminum was successfully incorporated within the frameworks of periodic mesoporous organosilicas (Al-PMO) by co-condensation of bis(triethoxysilyl)ethane and dibutoxyaluminotriethoxysilane [70]. The Al-PMO materials exhibited highly ordered 2-D hexagonal structures, high surface areas, and narrow pore size distribution in the mesoporous range. The Al-PMO catalysts resulted in excellent catalytic activity and selectivity for the etherification reaction between 2-naphthol and ethanol, which is comparable with those of beta zeolite. Aluminium-containing. periodic mesoporous organosilicas with hexagonal symmetry have also been synthesized by varying the source and concentration of aluminium [71]. Unlike MCM-41, all Al species used in this study, except aluminum hydroxide, were exclusively incorporated into the tetrahedral site of framework of PMO synthesized under the optimized reaction condition.

Titanium-containing ethane-bridged hybrid mesoporous materials with uniform hexagonal arrangement were prepared by Inagaki et. al. [72]. The materials were highly hydrophobic and selectively epoxidize α-pinene to α-pinene oxide (with >99% selectivity) and displayed high hydrogen peroxide efficiencies. Inagaki et. al reported the ammoximation of bulky ketones catalyzed by titanium-containing ethanebridged hybrid mesoporous silsesquioxane [73]. The reaction was highly selective to oximes. Thermally stable mesoporous silicon oxynitrides were synthesized by direct nitridation of periodic ethane-bridged mesoporous silica with nitrogen [74].

Haruta et al. supported gold nanoparticles inside titanium incorporated periodic mesoporous ethanesilica materials via a wet impregnation methodology [18]. The catalyst was used for the vapour-phase epoxidation of propene using hydrogen and oxygen. The formation of gold nanoparticles with size less than 5 nm inside mesoporous materials (hexagonal mesoporous silica (HMS), Michigan State University silica (MSU), and PMO) were prepared by Dai et. al. by employing co-synthesis sol–gel process [76]. Bis(triethoxysilyl)ethane and tetrachloroaurate(III) trihydrate were used as silica and gold sources, respectively. The effects of post-

treatments, such as calcination and reduction, on pore structures and nanoparticle size distributions were also investigated.

Hybrid organic-inorganic xerogels possessing zirconium in the inorganic framework have been synthesized from $Zr[OSi(OtBu)_3]_4$ and bis(triethoxysilyl)methane or 1,2-bis(triethoxysilyl)ethane or bis(triethoxysilyl)-1,4-phenylene [77].

2.8 Conclusions

In summary, a variety of bridged organoalkoxysilanes can be used as silicon precursors when synthesizing periodic mesoporous organosilica materials. This has been achieved by condensation reactions of silicon precursors in the presence of long alkyammonium, triblock, non-ionic polymeric and non-ionic oligomeric surfactants. Further functionalization has been achieved by co-condensation of bridged organoalkoxysilanes with alkoxysianes or by chemical conversion of functional groups. Properties of periodic mesoporous organosilica materials are dependent on the nature of the silicon precursor, the surfactant and reaction conditions. Catalysts are obtained by incorporating metals into PMOs.

Table 2.3 Summary of an overview of PMO literature

Mesophase and comments	**Precursor(s)**	**Surfactant**	**Catalyst**	**Author, year and reference number**
Hexagonal	bis(triethoxysilyl)**methane** tetraethylorthosilicate	CTAB	NH_4OH	Ozin 2000 [3]
2-D and 3-D hexagonal	1,2-bis(trimethoxysilyl)**ethane**	ODTMA CTMA	NaOH	Inagaki 1999 [12]
Hexagonal	1,2-bis(triethoxysilyl)**ethane** 1,2-bis(triethoxysilyl)**ethylene**	CTAB	H_2SO_4:NaOH	Stein 1999 [13]
Cubic	1,2-bis(trimethoxysilyl)**ethane**	CTAB	NaOH	Inagaki [16]
2D hexagonal	1,2-bis(trimethoxysilyl)**ethane**	CTAC	NaOH	Inagaki 2002 [18]
Gold catalysis Ti incorporated	Titanium butoxide			
Cubic	1,2-bis(triethoxysilyl)**ethane** (and others)	CTAB Brij 56	HCl	Brinker 1999, 2000, 2001 [19 – 21]

Mesophase and comments	**Precursor(s)**	**Surfactant**	**Catalyst**	**Author, year and reference number**
	1,2-bis(triethoxysilyl)**ethane**	Cetylpyridinium bromide	HCl	Suo 2002 [22]
2-D and 3-D hexagonal	1,2-bis(trimethoxysilyl)**ethane**	ODTMA CTMA	NaOH	Park 2001 [23 - 25]
Pt-Rh/HMM1 catalyst	**Ethane**silica			Fukuoka 2001 [27]
Worm-hole motif Lamellar	1,2-bis(triethoxysilyl)**ethane**	Alkylamines	Octylamine Dodecylamine Triton X100)	Mercier 2001 [28]
	Bis-**urea** silylated precursor			
Cubic Co-condensation	1,2-bis(trimethoxysilyl)**ethane** Tetraethylorthosilicate	Pluronic F127 LGE76	HCl	Char 2001 [29]
	1,2-bis(trimethoxysilyl)**ethane**	Pluronic P123	HCl	Froba 2001 [30]
Wormhole, hexagonal	1,2-bis(triethoxysilyl)**ethane**	Pluronic P123	HCl	Markowitz 2001 [31]

Mesophase and comments	**Precursor(s)**	**Surfactant**	**Catalyst**	**Author, year and reference number**
Mechanical and hydrothermal treatment	1,2-bis(trimethoxysilyl)**methane** 1,2-bis(triethoxysilyl)**ethane** 1,2-bis(trimethoxysilyl)**benzene**	Brij 76	HCl	Markowitz [32]
Cagelike	1,2-bis(triethoxysilyl)**ethane**	Triblock copolymer (EO_{39}-BO_{47}-EO_{39})		Jaroniec 2002 [33]
2-D hexagonal	1,2-bis(triethoxysilyl)**ethane**	Pluronic P123	HCl	Roziere 2001 [35]
2-D and 3-D hexagonal	1,2-bis(trimethoxysilyl)**ethane**	ODTMA CTMA	NaOH	Sayari 2000 [36]
Hexagonal	1,2-bis(trimethoxysilyl)**ethane**	Brij 56	HCl	Kaliaguine 2002 [37]
Hexagonal	1,4- bis(triethoxysilyl)**benzene** 2,5- bis(triethoxysilyl)**thiophene** 1,1'- bis(triethoxysilyl)**ferrocene** bis(triethoxysilyl)**bithiophene** bis(triethoxysilyl)**acetylene**	CTAB CPCl	NH_4OH HCl	Ozin 1999 [38]

Mesophase and comments	**Precursor(s)**	**Surfactant**	**Catalyst**	**Author, year and reference number**
2-D hexagonal	1,4-bis(triethoxysilyl)**benzene**	Pluronic P123	HCl	Inagaki 2002 [40]
2-D hexagonal	1,3,5- tris(triethoxysilyl) **benzene**	CTAB	NH_4OH	Ozin 2002 [41]
	1,3- bis(triethoxysilyl) **benzene**	CPCl	HCl	
hexagonal	2,5- bis(triethoxysilyl)**toluene**	CPCl	HCl	Ozin 2001 [42])
	2,5- bis(triethoxysilyl)-**p-xylene**			
	2,5- bis(triethoxysilyl**)-1,4-dimethoxybenzene**			
Lamella	4,4'-bis(triethoxysilyl)**biphenyl**	ODTMA	NaOH	Inagaki 2003 [45]
2-D hexagonal	1,2-bis(triethoxysilyl)**ethylene**	CTAB	NH_4OH	Ozin 2001 [46]
Hydroboration	Triethoxyvinylsilane			
Cyanopropyl-modified	1,2-bis(trimethoxysilyl)**ethane**	CTAB	ammonia	Ha 2004 [47]
	3-cyanopropyltriethoxysilane			

Mesophase and comments	**Precursor(s)**	**Surfactant**	**Catalyst**	**Author, year and reference number**
Acid catalyzed: disordered	1,2-bis(triethoxysilyl)**ethane** N-(2-aminoethyl)-3-aminopropyltrimethoxysilane	CTAC :	HCl NaOH	Markowitz2001 [48]
Hexagonal	1,2-bis(triethoxysilyl)**ethane** N-(2-aminoethyl)-3-aminopropyltrimethoxysilane	CTAC :	NaOH	Markowitz 2001 [49]
Co-condensation	1,2-bis(triethoxysilyl)**ethane** various organosilicas*	CTAC	NaOH	Markowitz 2001 [50]
Cubic	1,2-bis(trimethoxysilyl)**ethane**	CTAC	NaOH	Kaliaguine 2003 [52]
Wormhole	1,2-bis(trimethoxysilyl)**ethane** 2-(4-chlorosulfonylphenyl)ethyltrimethoxysilane 3-mercaptopropyltrimethoxysilane	Pluronic P123 Brij 56	HCl	Kaliaguine 2004 [55]
Co-condensation	1,3- bis(triethoxysilyl)**propanetetrasulfide**	Pluronic P123	HCl	Zhang 2003 [56]

Mesophase and comments	**Precursor(s)**	**Surfactant**	**Catalyst**	**Author, year and reference number**
Lamella	4,4- bis(triethoxysilyl)**biphenyl**	CTAC	NaOH	Inagaki 2002 [57]
2-D hexagonal cubic periodic aminosilica	1,2-bis(trimethoxysilyl)**methane** 1,2-bis(trimethoxysilyl)**ethylene**	CTAB	NH_4OH	Ozin 2003 [58]
Bifunctional PMO	1,2-bis(triethoxysilyl)**ethane** N,N'-bis[3-trimethoxysilylpropyl]ethylenediamine	Pluronic P123		Zhu 2002 [59]
Hexagonal	1,2-bis(triethoxysilyl)**ethane** bis[(3-trimethoxysilyl)**propyl]amine**	CTAB	ammonia	Ha 2004 [60]
2-D hexagonal Aluminium organophosphonate	**Methylene diphosphonic** acid	ODTMA	Tetramethyl ammonium hydroxide	Kimura 2003 [64]

Mesophase and comments	**Precursor(s)**	**Surfactant**	**Catalyst**	**Author, year and reference number**
Hexagonal	1,2-bis(triethoxysilyl)**ethylene**	Brij 56 Brij 76 Brij 78 Pluronic P123	HCl	Sayari 2004 [65]
2-D hexagonal Platinum nanowires	**Ethane** bridged $H_2PtCl_6.6H_2O$			Ichikawa 2004 [67]
2-D and 3-D hexagonal	1,2-bis(trimethoxysilyl)**ethane** 1,2-bis(triethoxysilyl)**ethane**	CTAB Divalent surfactant	NaOH	Anwander 2004 [68]
2-D hexagonal microporous and mesoporous silicas	1,2-bis(trimethoxysilyl)**ethane**	trialkylammoium chlorides	NaOH	Sayari 2001 [69]
2-D hexagonal	1,3-bis(triethoxysilyl)**benzene**	ODTMA	NaOH	Inagaki 2003 [75]

Mesophase and comments	**Precursor(s)**	**Surfactant**	**Catalyst**	**Author, year and reference number**
2-D and 3-D hexagonal Cubic	1,2-bis(trimethoxysilyl)**ethane** 1,2-bis(triethoxysilyl)**ethane**	CTAC ODTMA	NaOH	Sayari 2000 [78]
Hexagonal Salt added	1,2-bis(trimethoxysilyl)**ethane**	Pluronic P123	HCl	Ha 2003 [79]
Hexagonal	1,2-bis(triethoxysilyl)**ethane**	1-hexadecane-2,3-dimethylimidazolium bromide and 1-hexadecane-3-dimethylimidazolium bromide		Lee 2004 [82]
Multifunctional PMO	**Phenylene** and **ethylene**-bridged	Brij 76	HCl	Markowitz 2004 [80]
	Silylated 4,4'-**bipyridine**	CTAB	ammonia	Garcia 2001 [81]

Mesophase and comments	**Precursor(s)**	**Surfactant**	**Catalyst**	**Author, year and reference number**
Hexagonal	1,2-bis(triethoxysilyl)**ethane**	1-hexadecane-2,3-dimethylimidazolium bromide and 1-hexadecane-3-dimethylimidazolium bromide		Lee 2004 [82]
2-D hexagonal	1,4-bis(triethoxysilyl)**benzene**	Brij 56 Brij 76	HCl	Sayari 2003 [83]
Hexagonal Titanium incorporated	1,2-bis(triethoxysilyl)**ethane** titanium isopropoxide	CTAB	NaOH	Ha 2004 [84]

Mesophase and comments	**Precursor(s)**	**Surfactant**	**Catalyst**	**Author, year and reference number**
Bimodal PMOs	1,2-bis(triethoxysilyl)**ethylene** TEOS Methyltriethoxysilane	CTAB	2,2',2"-nitrotrithanol	Amoros 2002 [85]
3-D cubic salts added	1,2-bis(trimethoxysilyl)**ethane**	Pluronic F127	HCl	Ha 2003 [86]
Hexagonal Al-PMO Alkylation catalyst	1,2-bis(trimethoxysilyl)**ethane** Aluminium isopropoxide	CTAC	NaOH	Yang 2004 [87]
2-D hexagonal	1,2-bis(trimethoxysilyl)**ethane** 1,2-bis(triethoxysilyl)**ethane**	Triblock copolymers	HCl	Char 2004 [88]
2-D hexagonal	1,2-bis(triethoxysilyl)**ethane**	Brij56 Brij 76 CTAC	HCl	Markowitz 2002 [89]

Mesophase and comments	**Precursor(s)**	**Surfactant**	**Catalyst**	**Author, year and reference number**
Chiral PMOs	Silylated **biphenyl** and **cyclohexadiyl** precursors, TEOS	CTAB	Ammonia	Garcia 2004 [90]
Hexagonal	1,2-bis(triethoxysilyl)**methane**	Eicosyldiethyl-methylammonium bromide	ammonia	Froba 2004 [91]
	1,2-bis**(4-pyridyl)ethylene** TEOS	CTAB	NH_4OH	Garcia 2002 [92]

* R'Si(OR)*$_4$ = 3-aminopropyltrimethoxysilane, 3-aminopropyltriethoxysilane, N-(2-aminoethyl)-3-aminopropyltrimethoxysilane, 2-(trimethoxysilylethyl)pyridine, N-(triethoxysilylpropyl)-4,5-dihydroimidazole, 3-mercaptopropyltrimethoxysilane, 3-mercaptopropyltriethoxysilane, benzyltriethoxysilane, phenethyltrimethoxysilane

2.9 References

1. C. T. Kresge, M. E. Leonowicz, W. J. Roth, J. C. Vartuli, and J. S. Beck, Nature **359**, 710 (1992).

2. J. S. Beck, J. C. Vartuli, W. J. Roth, M. E. Leonowicz, C. T. Kresge, K. D. Schmitt, C. T-W. Chu, D. H. Olson, E. W. Sheppard, S. McCullen, J. B. Higgins, and J. L. Schlenker. J. Am. Chem. Soc. **114**, 10834 (1992).

3. T. Asefa, M. J. MacLachlan, H. Grondey, N. Coombs, and G. A. Ozin, Angew. Chem. Int. Ed. **39**, 1808 (2000) and references therein.

4. P. Gomez-Romero, and C. Sanchez, Eds., Functional Hybrid Materials, Wiley-VCH, Weinheim (2004).

5. Chem. Mater. **13**, (2001).

6. S. Inagaki, and O. Terasaki, Kagaku to Kogyo (Tokyo, Japan) **56**, 239 (2003).

7. T. Asefa, G. A. Ozin, H. Grondey, M. Kruk, and M. Jaroniec, Studies in Surface Science and Catalysis, **141** (Nanoporous Materials III), 1 (2002).

8. T. Asefa, N. Coombs, H. Grondey, M. Jaroniec, M. Kruk, M. J. MacLachlan, and G. A. Ozin, Materials Research Society Symposium Proceedings **711** (Advanced Biomaterials: Characterization, Tissue Engineering and Complexity), 347 (2002).

9. . T. Asefa, N. Coombs, H. Grondey, M. Jaroniec, M. Kruk, M. J. MacLachlan, and G. A. Ozin, Materials Research Society Symposium Proceedings **707** (Self-Assembly Processes in Materials), 93 (2002).

10. M. J. MacLachlan, T. Asefa, and G. A. Ozin, Chemistry-A European Journal **6**(14), 2507 (2000).

11. A. Sayari, S. Hamoudi, Y. Yang, I. Moudrakovski, and J. R. Ripmeester, Chem Mater. **12**, 3857 (2000).

12. S. Inagaki, S. Guan, Y. Fukushima, T. Ohsuna, and O. Terasaki, J. Am. Chem. Soc. **121**, 9611 (1999).

13. B. J. Melde, B. T. Holland, C. F. Blanford, and A. Stein, Chem. Mater. **11**, 3302 (1999).

14. T. Asefa, M. J MacLachlan, N. Coombs, and G. A. Ozin, Nature **402**, 867 (1999).

15. M. Kruk, M. Jaroniec, S. Guan, and S. Inagaki, J. Phys. Chem. B **105**, 681 (2001).

16. S. Guan, S. Inagaki, T. Ohsuna, and O. Terasaki, J. Am. Chem. Soc. **122**, 5660 (2000).

17. S. Guan, S. Inagaki, T. Ohsuna, and O. Terasaki, Micropor. Mesopor. Mater. **44 – 45**, 165 (2001).

18. M.P. Kapoor, A.K. Sinha, S. Seelan, S. Inagaki, S. Tsubota, H. Yoshida, and M. Haruta. Chem. Commun. 2902 (2002).

19. Y. Lu, H. Fan, N. Doke, D. A. Loy, R. A. Assink, D. A. LaVan, and C. J. Brinker, J. Am. Chem. Soc. **122**, 5258 (2000).

20. H. Fan, Y. Lu, A. Stump, S. T. Reed, T. Baer, R. Schunk, V. Perez-Luna, G. P. López, and C. J. Brinker, Nature **405**, 56 (2000).

21. H. Fan, S. Reed, I. Baer, R. Schunk, G. P. López, and C. J. Brinker, Micropor. Mesopor. Mater. **44-45**, 625 (2001).

22. T. Ren, X. Zhang, and J. Suo, Micropor. Mesopor. Mater. **54**, 139 (2002).

23. S. S. Park, C. H. Lee, J. H. Cheon, and D. H. Park, J. Mater. Chem. **11**, 3397 (2001).

24. S. S. Park, C. H. Lee, J. H. Cheon, S. J. Choe, and D. H. Park, Bull. Korean Chem. Soc. **22**, 948 ((2001).

25. C. H. Lee, S. S. Park, S. J. Choe, and D. H. Park, Micropor. Mesopor. Mater. **46**, 257 (2002).

26. D. Zhao, Q. Huo, J. Feng, B. F. Chmelka, and G. D. Stucky, J. Am. Chem. Soc. **120**, 6024 (1998).

27. A. Fukuoka, Y. Sakamoto, S. Guan, S. Inagaki, N. Sugimoto, Y. Fukushima, K. Hirahara, S. Iijima, and M. Ichikawa, J. Am. Chem. Soc. **123**, 3373 (2001).

28. M. D. McInall, J. Scott, L. Mercier, and P. J. Kooyman, Chem. Commun. 2282, (2001).

29. E-B. Cho, K-W. Kwon, and K. Char, Chem Mater. **13**, 3837 (2001).

30. O. Muth, C. Schellbach, and M. Froba, Chem. Commun. 2032 (2001).

31. M. C. Burleigh, M. A. Markowitz, E. M. Wong, J-S. Lin, and B. P. Gaber, Chem. Mater. **13**, 4411 (2001).

32. M. C. Burleigh, M. A. Markowitz, S.Jasasundera, M. S. Spector, C. W. Thomas, and G. B. Gaber, J. Phys Chem B **107**, 12628 (2003).

33. J. R. Matos, M. Kruk, L. P. Mercuri, M. Jaroniec, T. Asefa, N. Coombs, G. A. Ozin, T. Kamiyama, and O. Terasaki, Chem. Mater. **14**, 1903 (2002).

34. C. Yu, Y. Yu, and D. Zhao, Chem. Commun. 275 (2000).

35. H. Zhu, D. J. Jones, J. Zajac, J. Rozière, and R. Dutartre, Chem. Commun. 2568 (2001).

36. A. Sayari, and Q. Yang, Chem. Commun. **21**, 2582 (2002).

37. S. Hamoudi, and S. Kaliaguine, Chem. Comm. 2118 (2002).

38. C. Yoshina-Ishii, T. Asefa, N. Coombs, M. J. MacLachlan, and G. A. Ozin, Chem. Commun. 2539 (1999),

39. S. Inagaki, S. Guan, T. Ohsuna, and O. Terasaki, Nature **416**, 304 (2000).

40. Y. Goto, and S. Inagaki, Chem. Commun. 2410 (2002).

41. M. Kuroki, T. Asefa, W. Whitnal, M. Kruk, C. Yoshina-Ishii, M. Jaroniec, and G. A. Ozin, J. Am. Chem. Soc. **124**, 13886 (2002).

42. G. Temtsin, T. Asefa, S. Bittner, and G. A. Ozin. J. Mater. Chem. **11**, 3202 (2001).

43. V. Goletto, A. Bled, G. Trimmel, M. Man, W. C. Michel, H. Woo, D. Durand, and F. Babonneau, Materials Research Society Symposium Proceedings **726** (Organic/Inorganic Hybrid Materials), 123. (2002).

44. V. Rebbin, O. Muth, and M. Froba, Materials Research Society Symposium Proceedings **726** (Organic/Inorganic Hybrid Materials), 263, (2002).

45. M. P. Kapoor, Q. Yang, and S. Inagaki, J. Am. Chem. Soc. **124**, 15176 (2003).

46 T. Asefa, M. Kruk, M . J. MacLachlan, N. Coombs, H. Grondey, M. Jaroniec, and G. A. Ozin, J. Am. Chem. Soc. **123**, 8520 (2001).

47. M. A. Wahab, I. Kim, and C-S. Ha, Micropor. and Mesopor. Mater. **69**, 19 (2004).

48. M. C. Burleigh, M. A. Markowitz, M. S. Spector, and B. P. Gaber, Langmuir **17**, 7923 (2001).

49. M C. Burleigh, M. A. Markowitz, M. S. Spector, and B. P. Gaber, Chem. Mater. **13**, 4760 (2001).

50. M. C. Burleigh, M. A. Markowitz, M. S. Spector, and B. P. Gaber, J. Phys. Chem. B **105**, 9935 (2001).

51. M. C. Burleigh, S. Dai, and E. W. Hagaman, Chem. Mater. **13**, 2537, (2001).

52. S. Hamoudi, and S. Kaliaguine, Micropor. and Mesopor. Mater. **59**, 195 (2003).

53. S. Hamoudi, and S. Kaliaguine, Stud. Surf. Sci. Catal. **146**, 473, (2003).

54. X. Yuan, H. I. Lee, J. W. Kim, J. E. Yie, and J. M. Kim, Stud. Surf. Sci. Catal. **146**, 477 (2003).

55. X. Yuan, H. I. Lee, J. W. Kim, J. E. Yie, and J. M. Kim, Chem. Lett. **32** (2003) 650.

56. L. Zhang, W. Zhang, J. Shi, Z. Hua, Y. Li, and J. Yan, Chem. Commun. 210 (2003)

57. Q. Yang, M. P. Kapoor, and S. Inagaki, J. Am. Chem. Soc. **124**, 9694 (2002).

58. T. Asefa, M. Kruk, N. Coombs, H. Grondey, M. J. MacLachlan, M. Jaroniec, and G. A. Ozin, J. Am. Chem. Soc. **125**, 11662 (2003).

59. H. Zhu, D. Jones, J. Zajac, R. Dutartre, M. Rhomari, and J. Roziere, Chem. Mater. **14**, 4886 (2002).

60. M. A. Wahab, I. Kim, and C-S. Ha, J. Solid State Chem. **177** 3439 (2004).

61. M. C. Burleigh, M. A. Markowitz, M. S. Spector, and B. P. Gaber, Environ. Science Technol. **36**, 2515 (2002).

62. K. Hossain, Z. Kazi, and L. Mercier, Adv. Mater. **14**, 1053 (2002).

63. M. P. Kapoor, and S. Inagaki, Chem. Mater. **14**, 3509 (2002).

64. T. Kimura, Chem. Mater. **15**, 3743 (2003).

65. W. Wang, S. Xie, W. Zhou, and A. Sayari, Chem. Mater. **16**, 1756 (2004).

66. B. Toury, and F. Babonneau, J. European Ceramic Soc. **25**, 265 (2005).

67. Y. Sakamoto, A. Fukuoka, T. Higuchi, N. Shomomura, S. Inagaki, and M. Ichikawa, J. Phys. Chem. B **108**, 853 (2004).

68. Y. Liang, and R. Anwander, Micop. Mesopor. Mater. **72**, 153 (2004).

69. S. Hamoudi, Y. Yang, I. L.. Moudrakovski, S. Lang, and A. Sayari, J. Phys. Chem. B **105**, 9118 (2001).

70. J. Kim, H. I. Lee, J. M. Kim, X. Yuan, and J. E. Yie, Studies in Surface Science and Catalysis **146** (Nanotechnology in Mesostructured Materials), 665 (2003).

71. S. S. Park, J. H. Cheon, and D. H Park, Studies in Surface Science and Catalysis, **146** (Nanotechnology in Mesostructured Materials), 481 (2003).

72. M. P. Kapoor, A. Bhaumik, S. Inagaki, K. Kuraoka, and T. Yazawa, J. Mater. Chem. **12**, 3078 (2002).

73. A. Bhaumik, M. P. Kapoor, and S. Inagaki, Chem. Commun. **4**, 470 (2003).

74. M. P. Kapoor, and S. Inagaki, Chem. Lett. **32**, 94 (2003).

75. M. P. Kapoor, Q. Yang, and S. Inagaki, Chem. Mater. **16**, 1209 (2004).

76. B. Lee, H. Zhu, Z. Zhang, S. H. Overbury, and S. Dai, Micropor. Mesopor. Mater. **70**, 71 (2004)

77. A. M. Tshavhungwe, M. Layh, and N. J. Coville, J. Sol-Gel Science and Technol. **29**, 167 (2004).

78. A. Sayari, S. Hamoudi, Y. Yang, I. I. Moudrakovski, and J. R. Ripmeester, Chem Mater. **12**, 3857 (2000).

79. W. Guo, J. Park, M. Oh, H. Jeong, W. Cho, I. Kim, and C. Ha, Chem. Mat. **15**, 2295 (2003).

80. M. C. Burleigh, S. Jayasundera, M. S. Spector, C. W. Thomas, M. A. Markowitz, and G. B. Gaber, Chem. Mater. **16**, 3 (2004).

81. M. Alvaro, B. Ferrer, B. Fornes, and H. Garcia, Chem. Commun. 2546 (2001)

82. B. Lee, H. Luo, C. Y. Yuan, J. S. Lin, and S. Dai, Chem. Commun. 240 (2004).

83. W. Wang, W. Zhou, and A. Sayari, Chem. Mater. **15**, 4886 (2003).

84. W. Cho, J. Park, and C. Ha, Mater. Lett. **58**, 3551 (2004).

85. J. E. Haskouri, D. O. de Zarate, C. Guillem, A. Beltran-Porter, M. Caldes, M. D. Maros, D. Beltran-Porter, J. Latorre and P. Amoros, Chem. Mater. **14**, 4502 (2002).

86. W. Guo, J. Kim, and C. Ha, Chem. Commun. 2692 (2003)

87. Q. Yang, Y. Li, L. Zhang, J. Yang, J. Liu and C. Li, J. Phys. Chem. B **108**, 7935 (2004).

88. E. Cho and K. Char, Chem. Mater. **16**, 271 (2004).

89. M. C. Burleigh, M. A. Markowitz, M. S. Spector, and G. B. Gaber, J. Phys. Chem. **106**, 9712 (2002).

90. M. Alvaro, M. Benitez, D. Das, B. Ferrer, and H. Garcia, Chem. Mater. **16**, 2222 (2004).

91. V. Rebbin, M. Jakubowski, S. Potz, and M. Froba, Microp. Mesopor. Mater. **72**, 99 (2004).

92. M. Alvaro, B. Ferrer, H. Garcia, and F. Rey, Chem. Commun. 2012 (2002).

93. J. M. Kim; S. K. Kim, and R. Ryoo. Chem. Commun. 259, (1998).

94. G. J. K. Acres, A. J. Bird, J. W. Jenkins, and F. King, in: Preparation of Catalysts II, edited by B. Delmon, P. A. Jacobs, and G. Poncelet, (Elsevier, Amsterdam, 1979), 1.

95. H. Knozinger, Mater. Sci. Forum **25 – 26**, 233 (1988).

96. C. Song, and K. M. Reddy, Appl. Catal. *A* **176**, 1 (1999).

97. F. Schuth, A. Wingen, and J. Sauer, Micropor. Mesopor. Mater. **44 – 45**, 465 (2001).

CHAPTER THREE

Experimental Section

3.1 Introduction

Periodic mesoporous organosilica materials (PMOs) are prepared through the surfactant-templated hydrolytic polycondensation of bifunctional organosiloxane precursors, $(R'O)_3SiRSi(OR')_3$ (See Scheme 3.1) [1, 2]. In a typical sol-gel experiment, a molecular precursor in which trifunctional silicon atoms (SiX_3) are attached to the organic moiety ($X_3Si\text{-}R\text{-}SiX_3$) is hydrolytically polycondensed in the presence of a surfactant.

$$(R'O)_3SiRSi(OR')_3 + H_2O + surfactant + catalyst \rightarrow [O_{1.5}Si]_2R$$

After aging, the product is filtered, washed thoroughly with water, and air-dried under ambient conditions. The surfactant is removed by either solvent extraction (the solution is stirred in a solution of HCl and methanol) or ion exchange (the solution is stirred in a refluxing solution of NaCl and ethanol).

It is to be noted that calcination, the most commonly used method for template removal in surfactant-templated mesoporous silica materials, cannot be used in order to retain the chemical integrity of the organic groups in the hybrid matrix.

Periodic mesoporous organosilica materials prepared using surfactants have high thermal and hydrothermal stability, large surface area, and tunable pore size. The properties of sol-gel processed materials are strongly dependent on factors such as organic groups in the precursor, templates, catalyst (acidic or basic), time (stirring, aging, drying), and aging conditions (length and temperature).

Porous materials based on silica are widely used as supports for monolayer-type catalysts in the field of heterogeneous catalysis. Loading a catalyst on an inert but high surface area silica support, by impregnation with an aqueous catalyst precursor, by vapour deposition [3] or by solid/solid wetting [4], improves the

accessibility of the active phase [3]. In this study cobalt, which is used as a Fischer-Tropsch catalyst, was incorporated into PMO materials using the *in situ* and impregnation methods [5].

Characterization studies of porous solids include collecting information relating to microstructure, morphology, physical properties, crystal structure and surface features of the material. For a full description of the properties of a material, it is necessary to use information obtained from different characterization techniques.

Reliable characterization of the porous hexagonal structure requires the use of three independent techniques [6, 7]: X-ray diffraction (XRD), transmission electron microscopy (TEM) and adsorption analysis. The discovery of ordered mesoporous silicas such as MCM-41 [8, 9] allowed an independent determination of the pore width of these materials by means of powder X-ray diffraction and transmission electron microscopy. Periodic mesoporous silica materials exhibit XRD patterns dominated by low-angle peaks. TEM is used to support the XRD data regarding the mesophase symmetry and the pore sizes. TEM in combination with electron diffraction is used to elucidate the structure of hybrid materials. The technique provides direct evidence of the location of tethers bearing functional groups in hybrid materials prepared by co-condensation. Scanning electron microscopy (SEM) is used to obtain information about particle morphology.

Molecular spectroscopy techniques (e.g. diffuse reflectance infrared fourier transform spectroscopy (DRIFTS), Raman spectroscopy, solid-state nuclear magnetic resonance spectroscopy, etc.) are used to determine the identities, surrounding environments, and concentrations of the chemical bonds that are present [2]. These techniques are especially important in identifying organic groups in hybrid organic-inorganic silica materials.

The thermal stability of mesoporous materials as well as the hydrophobic or hydrophilic character is obtained from temperature programmed techniques (i.e. thermogravimetric analysis (TGA), differential thermal analysis (DTA),

differential scanning calorimetry (DSC) and temperature programmed reduction/oxidation (TPR or TPO)). UV-Vis diffuse reflectance spectroscopy is a technique that determines the oxidation state of metal oxides. Surface area, pore volume and pore diameter are obtained from nitrogen sorption.

In this study characterization of the samples was carried out by powder X-ray diffraction (XRD), nitrogen sorption, diffuse reflectance fourier transform infrared spectroscopy (DRIFTS), fourier transform infrared spectroscopy (FTIR), Raman spectroscopy, thermogravimetric analysis (TGA), differential thermal analysis (DTA), differential scanning calorimetry (DSC), scanning electron microscopy (SEM), proton NMR spectroscopy (^{1}H NMR) and UV-Vis diffuse reflectance spectroscopy.

General preparation methods and characterisation techniques of mesoporous silica materials used in this study are described in this chapter. Specific preparation methods are described in the relevant chapters. Relevant background information about gas sorption measurement and powder X-ray diffraction is also provided.

3.2 Reagents and Chemicals

1,2-Bistrimethoxysilylethane (BTME), hexadecyltrimethylammonium bromide (CTAB) and cobalt nitrate hexahydrate were obtained from Aldrich; 3-glycidoxypropyltrimethoxysilane (GPTS), and 3-aminopropyltriethoxysilane (APTS) were obtained from ABCR (Germany); tetraethylorthosilicate (TEOS), ammonium hydroxide and hydrochloric acid were obtained from Fluka. All chemicals were used as received. Deionised water was used in the synthesis. The molecular structures and abbreviations of the silica precursors and the surfactant used are shown in Table 3.1.

Table 3.1 Molecular structures of silica precursors and surfactant molecule

Molecular Structure	Name and abbreviation
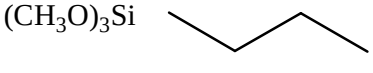	1,2-Bistrimethoxysilylethane (BTME)
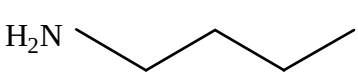	3-Aminopropyltriethoxysilane (APTS)
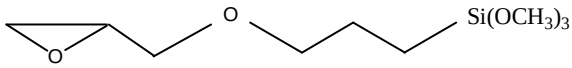	3-Glycidoxypropyltrimethoxysilane (GPTS)
$Si(OCH_2CH_3)_4$	Tetraethylorthosilicate (TEOS)
	Hexadecyltrimethylammonium bromide (cetyltrimethylammonium bromide) (CTAB)

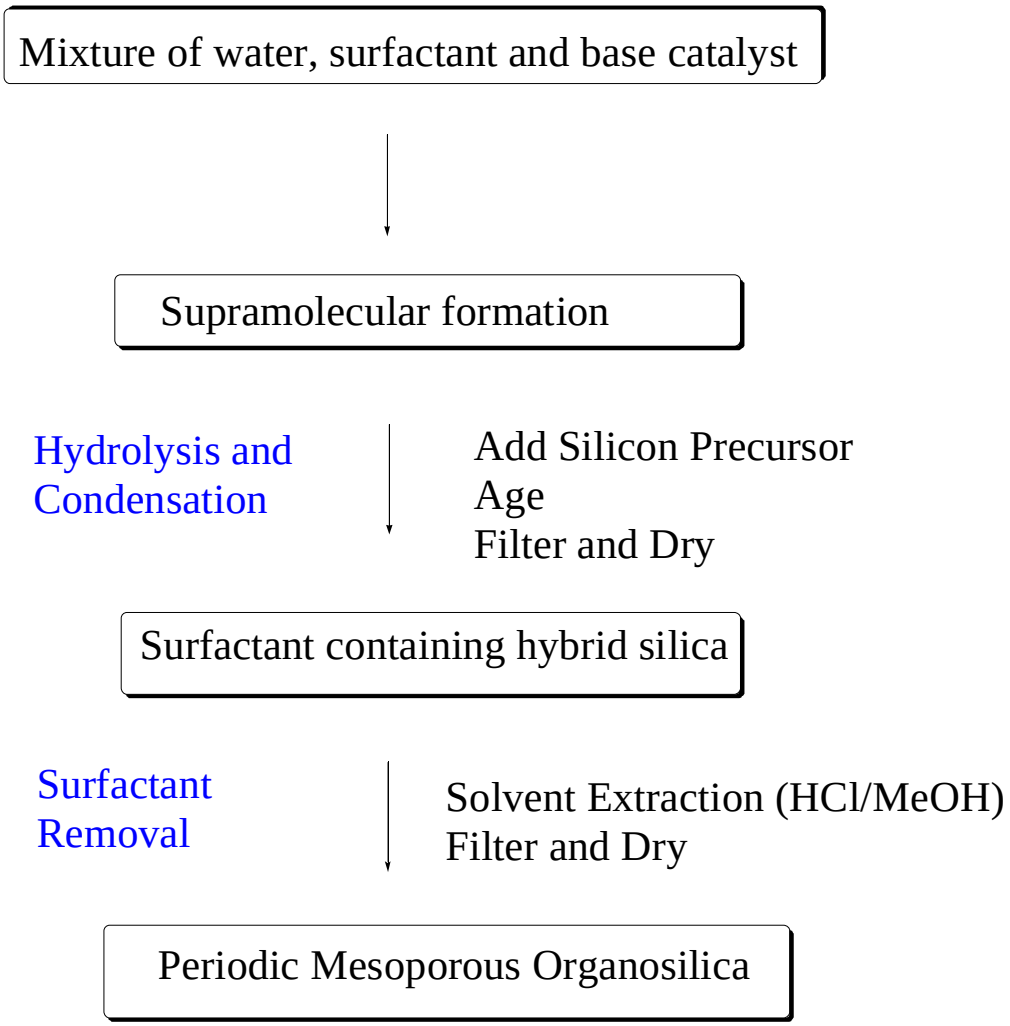

Scheme 3.1 Reaction scheme showing the synthesis of periodic mesoporous organosilica materials.

3.3 Synthesis of mesoporous materials

3.3.1 Mesoporous materials from a single silica precursor

Mesoporous silica materials and periodic mesoporous organosilica materials were prepared using a modified method based on that reported by Ozin and co-workers [10]. Materials were prepared from a mixture consisting of the following reagents: Silicon precursor, CTAB, NH_4OH and H_2O (where the Silicon Precursor = TEOS, BTME, GPTS and APTS). Materials without either CTAB, NH_4OH or H_2O were also prepared. Studies were conducted to study the effect of the following variables on the textural properties: the precursor, the surfactant (CTAB), the base (NH_4OH), and the solvent (water).

3.3.1.1 Synthesis. In a typical synthesis, CTAB (0.36 g; 0.98 mmol) was dissolved in a solution consisting of water (14 ml) and 28 % ammonium hydroxide (8 ml; 0.058 mol). The mixture was stirred for 15 minutes. The pH of the solution was estimated by pH paper to be approximately 10. A silicon precursor [(e.g. BTME (0.9 ml, 3.57 mmol)] was added dropwise to the stirred mixture. Stirring was continued for a further 30 minutes, followed by ageing at various temperatures (0 ^oC, 25 ^oC, 55 ^oC and 80 ^oC) for 4 days. The solid was suction filtered in a Büchner funnel and washed with an excess of water. The solid was dried in air overnight. This material is referred to as the "as-synthesised" material.

3.3.1.2 Surfactant extraction. A portion of the as synthesized sample (0.5 g) was stirred in a solution of concentrated HCl (5 ml) in methanol (200 ml) at 50 ^oC for 2 days. The solid was suction filtered in a Büchner funnel, washed with water and finally with methanol (200 ml) and then dried in air. This material is referred to as the "solvent extracted" material.

3.3.1.3 Calcination. A portion of the as-synthesized silica sample prepared from TEOS was calcined in an oven at 600 ^oC for 6 hours.

3.3.2 Mesoporous materials from co-condensation of silica precursors

APTS-modified ethanesilica and GPTS-modified ethanesilica materials were prepared as described in Sections 3.3.1.1 and 3.3.1.2 above from a mixture consisting of the following reagents: Silicon precursor, CTAB, NH_4OH and H_2O (where the Silicon precursor is a mixture of BTME and either APTS or GPTS).
Materials with properties intermediate between those of pure mesoporous silica and ethanesilica were prepared from a mixture consisting of the following reagents: Silicon precursor, CTAB, NH_4OH and H_2O (where the Silicon precursor is a mixture of BTME and TEOS).

3.3.3 Cobalt incorporated mesoporous materials

3.3.3.1 ***In situ*** **cobalt incorporation.** Cobalt incorporated ethanesilica, APTS-modified ethanesilica, GPTS-modified ethanesilica and TEOS-modified ethanesilica materials were synthesized by adding different amounts of cobalt nitrate to a mixture of CTAB, water and ammonium hydroxide. A silicon precursor or a mixture of silicon precursors was then added dropwise to the stirred solution. The procedure was continued as described in Section 3.3.1.1 and 3.3.1.2.

3.3.3.2 Post reaction cobalt incorporation. Cobalt incorporated mesoporous silica, ethanesilica and APTS-modified ethanesilica materials were prepared using the incipient wetness impregnation of the materials. Different amounts of cobalt nitrate, $Co(NO_3)_2.6H_2O$, were dissolved in deionised water and impregnated into the support using incipient wetness to give materials with different percentages of cobalt. Materials were dried at 120 ^oC for 12 hours.

3.4 Characterization

Characterization of the samples was carried out by powder X-ray diffraction (XRD), nitrogen adsorption, diffuse reflectance fourier transform infrared spectroscopy (DRIFTS), fourier transform infrared spectroscopy (FTIR), Raman

spectroscopy, thermogravimetric analysis (TGA), differential thermal analysis (DTA), differential scanning calorimetry (DSC), scanning electron microscopy (SEM), proton NMR spectroscopy (^{1}H NMR) and UV-Vis diffuse reflectance spectroscopy.

3.4.1 Background

3.4.1.1 Powder X-Ray Diffraction. Diffraction is a technique that uses interference of short wavelength particles (such as neutrons or electrons) or photons (X or γ rays) reflected from planes of atoms in crystalline materials to yield three-dimensional structural information at the atomic level [11]. In XRD a collimated beam of X-rays, with $\lambda \sim 0.5 - 2$ Å, is incident on a specimen and is diffracted by the crystalline phases in the specimen according to Bragg's law ($n\lambda = 2d\sin\theta$, where d is the spacing between atomic planes in the crystalline phase, n is an integer, and θ is Bragg's angle). The intensity of the diffracted X-rays is measured as a function of the diffraction angle 2θ and the specimen's crystalline orientation. This diffraction pattern is used to measure the specimen's structural properties (e.g. crystallite orientation and size) and to identify crystalline phases.

The periodicity of mesoporous materials can be probed using powder XRD. Periodic mesoporous silica materials display a very high intensity peak at around $2\theta = 2^o$, together with low intensity peaks in the 2θ range $3 - 8^o$ [8, 9]. Different mesophases, e.g. hexagonal, cubic, lamella, etc. can be assigned from observation of XRD patterns (Figure 3.1).

The unit cell parameter can be calculated from the equation $a_o = 2d_{100}/(3)^{1/2}$ for a hexagonal and a lamella mesophase [8]. The difference between the unit cell parameter and the pore diameter (which can be obtained from nitrogen adsorption measurement) gives the wall thickness of the mesopores.

(a)

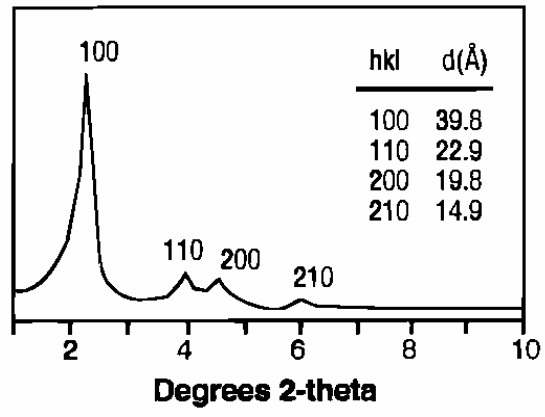

(b)

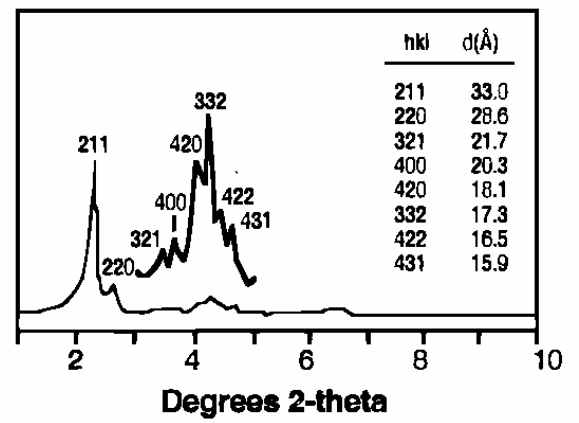

(c)

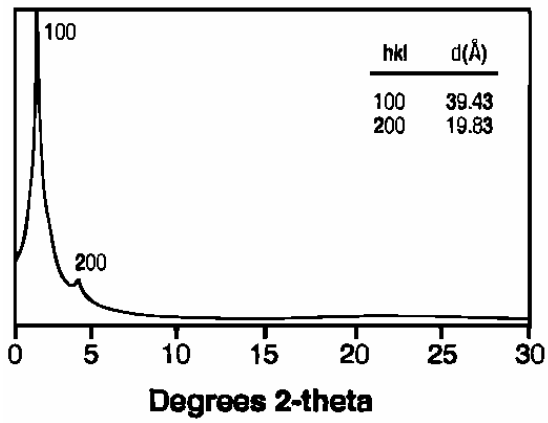

Figure 3.1 XRD patterns of hexagonal MCM41 (a), cubic MCM48 (b), and lamella MCM50 mesophases.

3.4.1.2 Nitrogen sorption According to the IUPAC recommendation, pores are classified on the basis of diameter as micropores (<2 nm), mesopores (2 – 50 nm) and macropores (>50 nm) [12, 13]. The expression 'nanopore' is used to encompass both micropores and mesopores. Ordered mesopores are referred to as primary mesopores, whereas other mesopores and macropores (up to about 200 nm) are referred to as secondary pores.

Gas sorption measurement (physisorption) is a nondestructive method used to analyze microporous and mesoporous materials. The method is used to determine the specific surface area, pore volume, and pore size distribution as well as to study surface properties. Ordered materials are associated with a well defined pore geometry and narrow pore size distribution (PSD), whereas disordered materials exhibit pores with a wide distribution of different shapes and widths. The specific surface area of macroporous solids is very small, that is why adsorption on this surface is usually neglected. The adsorption in micropores is a pore-filling process in which their volume is the main controlling factor.

A main source of information about adsorption and its mechanism is, besides the calorimetric measurements of adsorption heats, the adsorption isotherm. The adsorption isotherm is a plot of the amount of gas adsorbed as a function of the equilibrium gas pressure (or relative pressure) at a known temperature [usually liquid nitrogen temperature (–196 °C)]. The amount of the adsorbed gas is expressed in volume at standard temperature and pressure (STP) relative to the weight of the sample. During the measurement, the pressure of the gas increases from vacuum to saturation pressure, and then gradually decreases back to vacuum. Along with the pressure variation, two branches of the isotherm are obtained, namely adsorption branch and desorption branch. The term *adsorption* deals with the process in which molecules accumulate in the interfacial layer, but *desorption* denotes the converse process.

There are a variety of techniques used to determine specific surface area, pore volume and pore-size or pore-volume distribution [14].

Specific surface area. The Brunauer, Emmet, and Teller (BET) equation is commonly used for the determination of surface areas of porous solids [12, 13]. The BET equation reduces to the Langmuir equation in the area of low relative pressures and describes adsorption relatively well in the area of relative pressures of 0.05 – 0.35. The specific surface area, a_s(BET), is obtained from the equation

$$a_s(BET) = n_m^a xLxa_m$$

where L is Avogadro's number, n^a_m is the monolayer capacity (defined as the amount of the adsorbate required to form a complete monolayer on the surface of unit mass of the adsorbent), a_m is the molecular cross-sectional area (i.e. the average area occupied by the adsorbate molecule). For nitrogen, a_m (N_2) = 0.162 nm^2 at 77 K.

Pore size. The traditional method for analysing pore size distributions (PSDs) in the mesopore range is the Barrett-Joyner-Halenda (BJH) method [15] which is based on the Kelvin equation and, thus has a thermodynamic origin. In the BJH method, the derived mesopore size distribution is usually expressed in the graphical form $\Delta V_p / \Delta r_p$ versus r_p (or d_p) (where V_p is the mesopore volume and r_p is the pore radius for cylindrical pores, and d_p is the width for parallel sided slits). The mesopore volume is assumed to be completely filled at high relative pressure. The derived pore size distribution is dependent on whether the adsorption or desorption branch of the hysteresis loop is used for computation. However, compared with new methods that rely on more localized descriptions such as density functional theory (DFT) [6, 16, 17] and Monte Carlo simulation [6, 18], the thermodynamically based methods overestimate the relative pressure at desorption and therefore underestimate the calculated pore diameters by ca. 1.0 nm. The usefulness of DFT methods to characterize MCM-41 type materials has been reported [19].

IUPAC classification of isotherms According to the IUPAC classification six types of isotherms can be distinguished (Figure 3.2) [12, 13]. The shape of the isotherm depends on the solid's porous texture. Type I, Type II and Type IV

isotherms are characteristic of microporous, macroporous and mesoporous materials, respectively [6, 12 – 14]. Point B (see Figure 3.2) represents the stage at which monolayer coverage is complete and multilayer adsorption is beginning.
Type I isotherms exihibit prominent adsorption at low relative pressures and then level off. Type I reversible isotherms are typical in microporous solids with relatively small external surfaces. Monolayer adsorption occurs significantly at relatively low partial pressures < 0.5 P/P_0.
Type II reversible isotherms describe the gas sorption with a non-porous or macroporous solid in which multi-layer adsorption forms due to a strong interaction between adsorbed molecules. Type III reversible isotherms are convex towards the relative pressure axis. This type of isotherm originates from both non-porous and macroporous solids. These isotherms are characteristic of weak adsorbate-adsorbent interactions.
Adsorption on mesoporous solids proceeds via multilayer adsorption followed by capillary condensation (Type IV and Type V isotherms). The adsorption process is initially similar to that on macroporous solids, but at higher pressures the amount adsorbed rises very steeply due to capillary condensation in mesopores. After these pores are filled, the adsorption isotherm levels off. Capillary condensation and capillary evaporation often do not take place at the same pressure, which leads to the appearance of hysteresis loops. Type IV isotherms are associated with mesoporous solids. Type V isotherms are related to the Type III isotherms in that the adsorbate-adsorbent interactions are weak.
Type VI isotherms are stepwise, which represent multilayer adsorption on a uniform non-porous surface.

Adsorption hysteresis Adsorption hysteresis occurs when the adsorption and desorption curves deviate from one another. In such a case the isotherm possesses a hysteresis loop, the shape of which varies from one adsorption system to another. A Type IV isotherm shows a hysteresis loop attributed to capillary condensation and a plateau at high relative pressures. Hysteresis loops are classified into four types, designated Type H1, H2, H3 and H4 (Figure 3.3) [6, 12 – 14]. The Type H1 loop exhibits parallel and nearly vertical branches. Type H1

is representative of an adsorbent with a narrow distribution of relatively uniform mesopores. The Type H2 hysteresis loop has a triangular shape and a steep desorption branch. Type H2 is associated with a more complex pore structure in which network effects are important. A Type H2 loop indicates the presence of pores with narrow mouths (ink-bottle pores). The phenomenon is also observed for materials with relatively uniform channel-like pores when the desorption branch happened to be located at relative pressures in the proximity of a lower pressure limit (a relative pressure of about 0.4 for N_2 at 77 K) of adsorption-desorption hysteresis. Types H3 and H4 hysteresis loops do not exhibit any limiting adsorption at high relative pressure. Type H3 loops are often obtained with materials composed of aggregates of plate-like particles forming slit-like pores. Type H4 loops feature parallel and almost horizontal branches and their occurrence has been attributed to adsorption-desorption in narrow slit-shaped pores. Type IV hysteresis loops are also observed for materials with large mesopores embedded in a matrix with pores of much smaller size (e.g hollow spheres with walls composed of ordered mesoporous silica).

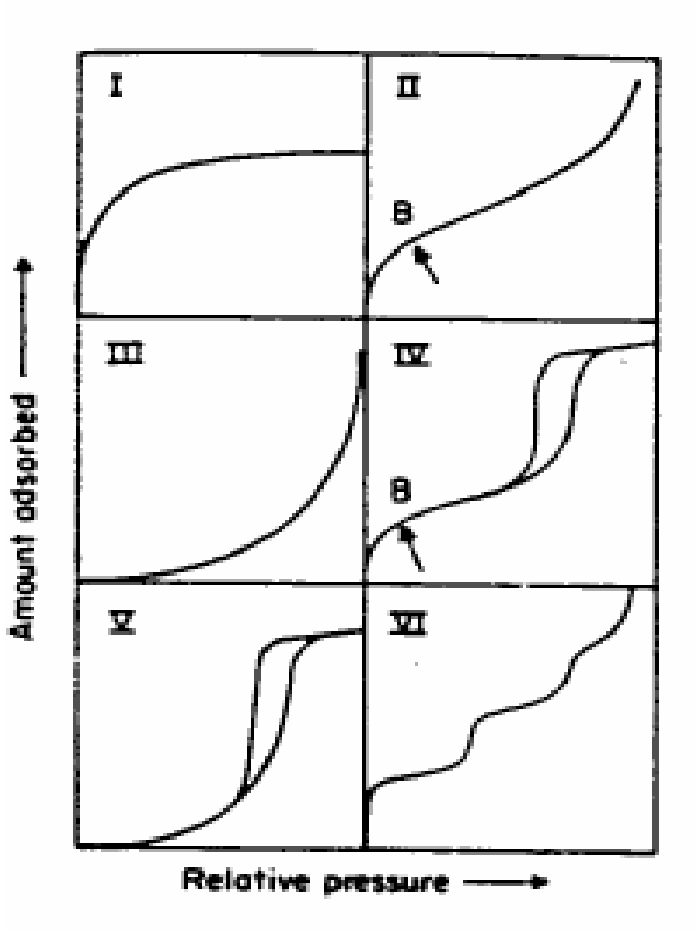

Figure 3.2 IUPAC classification of isotherms.

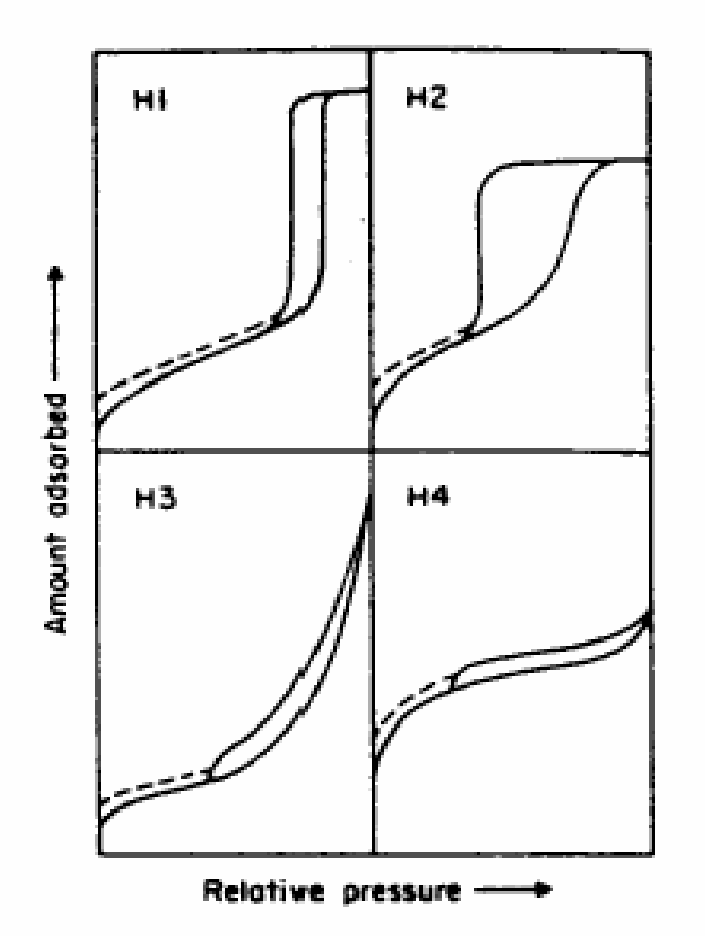

Figure 3.3 IUPAC classification of hysteresis loops.

3.4.2 Measurements

3.4.2.1 Powder X-Ray Diffraction Powder X-Ray diffraction measurements were made on a Phillips PW1710 diffractometer with Cu K-α radiation (λ = 1.5443 Å). Powdered disc samples were analysed at a scan speed of 5^o s^{-1} in the 1.5 – 10^o or 1.5 – 70^o 2θ range at a generator voltage of 40 kV and a generator current of 20 mA.

3.4.2.2 Nitrogen sorption The nitrogen adsorption and desorption isotherms were measured at –196 ^{o}C using a Micromeritics ASAP2010 instrument. Prior to adsorption measurements, all samples were degassed for 12 hours at 120^{o}C. The BET surface area was calculated from the adsorption isotherm in a relative pressure range from 0.00 to 0.20 [12]. The total pore volume was evaluated from the amount of nitrogen adsorbed at a relative pressure of 0.98. The average pore diameter was evaluated by the BET method (4V/A). The pore size distribution (PSD) was obtained from analysis of the adsorption and desorption branches of the isotherm using the Barrett-Joyner-Halenda (BJH) method [15]. Pore size distributions were also obtained using DFT-Plus software from Micromeritics.

3.4.2.3 Thermogravimetric Analysis Thermogravimetric analyses were performed with a Perkin Elmer Pyris 1 TGA Thermogravimetric analyser using nitrogen or air as the purge gas and a heating rate of 5 ^{o}C per minute.

3.4.2.4 Differential Thermal Analysis Measurements were performed using a Perkin Elmer DTA7 Differential Thermal Analyzer using nitrogen or air as the purge gas and a heating rate of 5 ^{o}C per minute.

3.4.2.5 Differential Scanning Calorimetry (DSC) Measurements were performed using a Du Pont 960 Differential Scanning Calorimeter using nitrogen or air as the purge gas and a heating rate of 5 ^{o}C per minute.

3.4.2.6 Infrared spectroscopy Diffuse reflectance spectra were recorded using a Bruker Tensor 27 Spectrometer equipped with a Thermo Spectra-Tech Collector II diffuse accessory and a high temperature chamber. Spectra were acquired at a nominal resolution of 4 cm^{-1} after signal averaging 4 scans. 5 % (w/w) dispersions of solid material in KBr were mixed. An Omega CN8501 Temperature and Pressure Controller regulated sample temperature, with a resolution of 1 ^{o}C.

Fourier transform infrared (FTIR) spectra were recorded on a Bruker Vector FTIR spectrometer, at a spectral resolution of 4 cm^{-1}, using 16 scans per spectrum. Samples were dissolved in chloroform ($CHCl_3$) and placed in a KBr cell holder that was then placed on the path of the IR beam.

3.4.2.7 Raman Spectroscopy Measurements were made using the micro-Raman attachment of a Jobin-Yvon T64000 Raman spectrometer, configured in single spectrograph mode. A grating with 600 grooves/mm was used to disperse the spectrum onto a charge coupled device (CCD) detector. The laser spot size on the sample was ~1.5 microns in diameter, and the excitation wavelength was 514.5 nm from an argon ion laser.

3.4.2.8 Scanning Electron Microscopy (SEM) Scanning electron microscopy images were recorded on a JSM 840 Scanning Electron Microscope with an acceleration voltage of 10 kV and a working distance of 15 mm. Prior to measurements, the samples were sprinkled on a disk smeared with carbon and then coated with gold.

3.4.2.9 ^{1}H NMR spectroscopy ^{1}H NMR spectra were recorded by a Bruker Avance 300 NMR spectrometer operating at 300 MHz. DMSO and TMS were used as a solvent and a standard, respectively.

3.4.2.10 UV-Vis Diffuse Reflectance Spectroscopy UV-Vis diffuse reflectance spectra were recorded with a Cary-5E Varian spectrometer equipped with a Praying–Mantis diffuse reflectance attachment. $BaSO_4$ was used as reference.

3.5 References

1. See Chapter 2 for a review of periodic mesoporous organosilica materials.

2. A. Sayari, and S. Hamoudi, Chem. Mater. **13**, 3151 (2001) and references therein.

3. G. J. K. Acres, A. J. Bird, J. W. Jenkins, and F. King, in: Preparation of Catalysts II, edited by B. Delmon, P. A. Jacobs, and G. Poncelet, Elsevier, Amsterdam, 1 (1979).

4. H. Knozinger, Mater. Sci. Forum **25 – 26**, 233 (1988).

5. A. M. Tshavhungwe, M. Layh, and N. J. Coville, J. Sol-Gel Science and Technology **29**, 167 (2004).

6. U. Ciesla, and F. Schüth, Micropor. Mesopor. Mater. **27**, 131 (1999).

7. U. Ciesla, M. Grün, T. Isajeva, A.A. Kurganov, A.V. Neimark, P. Ravikovitch, S. Schacht, F. Schüth, and K.K. Unger, in: T.J. Pinnavaia, M.F. Thorpe (Eds.), Access in Nanoporous Materials, Plenum Press, New York (1995).

8. J. S. Beck, J. C. Vartuli, W. J. Roth, M. E. Leonowicz, C. T. Kresge, K. D. Schmitt, C. T-W. Chu, D. H. Olson, E. W. Sheppard, S. McCullen, J. B. Higgins, and J. L. Schlenker, J. Am. Chem. Soc. **114**, 10834 (1992).

9. C. T. Kresge, M. E. Leonowicz, W. J. Roth, J. C. Vartuli, and J. S. Beck, Nature **359**, 710 (1992).

10. T. Asefa, M. Kruk, M . J. MacLachlan, N. Coombs, H. Grondey, M. Jaroniec, and G. A. Ozin, J. Am. Chem. Soc. **123**, 8520 (2001).

11. D. A. Skoog and J. J. Leary, Principles of Instrumental Analysis (5^{th} ed.), Saunders College Publishing, New York (1992).

12. S. J. Gregg, K. S. W. Sing, Adsorption Surface Area and Porosity, Academic Press, London (1984)

13. K. S. W. Sing, D. H. Everett, R. A. W. Haul, L. Moscou, R. A. Pierotti, J. Rouquerol, and T. Siemieniewska, Pure Appl. Chem. **57**, 603 (1985).

14. G. Leofanti, M. Padovan, G. Tozolla, and B. Venturelli, Catal. Today **41**, 207 (1998).

15. E. P. Barrett, L. G. Joyner, and P. P. Halenda, J. Am. Chem. Soc. **73**, 373 (1951).

16. P.I. Ravikovitch, D. Wei, W.T. Chueh, G.L. Haller, and A.V. Neimark. J. Phys. Chem. B **101**, 3671 (1997).

17. P.I. Ravikovitch, S.C. O'Domhnaill, A.V. Neimark, F. Schüth, and K.K. Unger. Langmuir **11**, 4765 (1995).

18. M.W. Maddox, J.P. Olivier, and K.E. Gubbins, Langmuir **13**, 1737 (1997).

19. P. I. Ravikovich, and A. V. Neimark, Langmuir **18**, 1550 (2000).

CHAPTER FOUR

A systematic study of factors governing the condensation of 1,2-bistrimethoxysilylethane and tetraethylorthosilicate

4.1 Introduction

Periodic mesoporous organosilica materials (PMOs), which possesses uniformly sized channel mesopores similar to those of MCM41-type silicas [1 – 36], have been the focus of much recent research because of their potential applications as catalysts, catalyst supports, adsorbents, and hosts for nanocluster syntheses [30, 33 – 36]. PMOs are prepared through the surfactant-templated hydrolytic polycondensation of bifunctional organosiloxane precursors, $(R'O)_3SiRSi(OR')_3$.

$$(R'O)_3SiRSi(OR')_3 + H_2O + \text{surfactant} + \text{catalyst} \rightarrow [O_{1.5}Si]_2R$$

Amongst the PMO materials, periodic mesoporous ethanesilica has been widely studied [6 – 25, 31, 33, 34]. It has been synthesized from 1,2-bistrialkoxysilylethane precursors (alkoxy = ethoxy or methoxy) in the presence of long alkylammonium [6 – 17, 33, 34], triblock [13, 14, 18 – 22], non-ionic polymeric, and non-ionic oligomeric [12 – 14, 23 – 25] surfactants.

Macroscopic data describing the texture (e.g. specific surface area, pore volume, pore diameter, etc.) of xerogels and periodic mesoporous organosilica materials synthesized from bridged silsesquioxane precursors are dependent on parameters governing the kinetics of polycondensation [37 – 42]. These parameters include organic moiety [37, 39], leaving group [39], solvent [39], catalyst [40], concentration [37], temperature [41, 42], and ageing conditions [38].

It is to be noted that previous studies of xerogels, unlike studies of PMOs, did not include X-ray diffraction analysis because the materials synthesized without surfactant molecules were amorphous. Inagaki et. al. [10] and Suo et. al. [23]

have shown the dependence of a mesophase formed on synthesis conditions (i.e. surfactant:precursor ratio, surfactant concentration and temperature) in basic and acidic conditions respectively. However, as the mesophase formed is also a function of the molar ratio of reactants, we have undertaken a study to evaluate the effects of different mole ratio of reactants and a catalyst from that used by Inagaki's group [10]. This study also provides the basis for providing comparative data for studies reported in later chapters of this thesis.

Herein we report on the synthesis of periodic mesoporous ethanesilica by condensation of 1,2-bistrimethoxysilylethane (BTME) and tetraethylorthosilicate (TEOS) in the presence of hexadecyltrimethylammonium bromide (CTAB) under basic conditions. The ageing duration, ageing temperature, concentration of BTME, amount of water and amount of NH_4OH were varied systematically in order to study their effect on the mesophase formed and on the surface properties of the materials synthesized. Results are compared with literature reports for other BTME synthesized materials.

4.2 Experimental Section

4.2.1 Reagents and Chemicals

1,2-Bistrimethoxysilylethane (BTME) and hexadecyltrimethylammonium bromide (CTAB) were obtained from Aldrich; tetraethylorthosilicate (TEOS), ammonium hydroxide (NH_4OH) and hydrochloric acid (HCl) were obtained from Fluka. All chemicals were used as received. Deionised water was used in the synthesis. The molecular structures of the silica precursor and the surfactant used are shown in Scheme 4.1.

4.2.2 Synthesis

4.2.2.1 As-synthesized PMOs. PMOs were prepared using a modified method based on that reported by Ozin and co-workers [26]. In a typical synthesis, a

mixture of CTAB (0.68 g; 1.86 mmol), water (28 ml) and 28 % ammonium hydroxide (8 ml; 0.058 mol) was stirred for 30 minutes. BTME was then added and stirring was continued for a further 30 minutes, followed by ageing at 80 ^{o}C for 4 days. The solid was suction filtered in a Büchner funnel, washed with an excess of water and dried in air overnight to give between 1 and 2 g of a white powder. These materials are referred to as "as-synthesized" materials. See Section 4.2.3 for notation.

4.2.2.2 Surfactant removal. A portion of the as-synthesized sample (0.5 g) was stirred in a solution of concentrated HCl (5 ml) in methanol (200 ml) at 50 ^{o}C for 2 days. The solid was suction filtered, washed with water and finally with methanol (200 ml) and then dried in air. Mass losses of between 20 and 40 % were observed after solvent extraction. These materials are referred to as "solvent extracted" materials. See Section 4.2.3 for notation.
For MCM41 silica, the surfactant was also removed by calcining a sample (3 g) in an oven for 6 hours at 600 ^{o}C.

4.2.2.3 Influence of ageing temperature on textural properties of periodic mesoporous ethanesilica materials. Ethanesilica materials were prepared as described above using a mixture with a mole ratio of BTME:CTAB:NH_4OH:H_2O = 1: 0.293: 8: 244. The materials were aged at 0 ^{o}C, room temperature (27 ^{o}C), 55 ^{o}C and 80 ^{o}C. The as-synthesized materials are designated as BA0, BA27, BA55 and BA80. The corresponding extracted materials are designated as BE0, BE27, BE55 and BE80. See Section 4.2.3 for notation.

4.2.2.4 Influence of ageing length on textural properties of periodic mesoporous silica. Ordered silica materials were prepared as described in Section 4.2.2.1 and 4.2.2.2 above using a mixture with a mole ratio of TEOS:CTAB:NH_4OH:H_2O = 1: 0.293: 8: 244. The materials were aged for 12, 24, 48 and 72 hours.

4.2.2.5 Influence of the amount of BTME on textural properties of ethanesilica materials. A series of periodic mesoporous ethanesilica materials containing variable amounts of ethane bridging groups was prepared starting with a mole ratio of BTME:CTAB:NH_4OH:H_2O = x : 0.293: 8: 244, (where x = 0.5, 1.0, 1.5 and 2.0). The as-synthesized materials are designated as 0.5BA80, BA80, 1.5BA80 and 2BA80. The corresponding extracted materials are designated as 0.5BE80, BE80, 1.5BE80 and 2BE80. See Section 4.2.3 for notation.

4.2.2.6 Influence of pH on textural properties of periodic mesoporous ethanesilica materials. Samples were prepared from a reaction mixture consisting of x ml NH_4OH, 28 ml H_2O, 0.68 g CTAB and 1.6 ml BTME (where x = 0, 7.0, 14 and 28 ml). The materials were aged at 80 ^oC.

4.2.2.7 Influence of the amount of water on textural properties of periodic mesoporous ethanesilica materials. Samples were prepared from a reaction mixture consisting of x ml H_2O, 14 ml NH_4OH, 0.68g CTAB and 1.6 ml BTME (where x =14, 28 and 56 ml). The materials were aged at 80 ^oC.

4.2.3 Nomenclature

The notation used to identify the samples is as follows: T = TEOS, B = BTME, A = as synthesized, and E = extracted. Numerical figures following the letter E refer to the ageing temperature. In experiments where the amount of BTME was varied, the relative moles of BTME in the sample containing 7.14 moles is taken to be 1. The moles of BTME in the other samples are divided by 7.14 moles and the value thus obtained precedes the letter B in the name of the sample. For example, 0.5BA27 refers to an as synthesized (A) material synthesized from 3.57 mol (i.e. half of 7.14 moles) of BTME (B). The material was aged at room temperature (27). BE55 refers to an extracted (E) material synthesized from 7.14 moles of BTME (B) and aged at 55 ^oC.

4.2.4 Characterization

Characterization of the samples was carried out by powder X-ray diffraction (XRD), nitrogen adsorption, Raman spectroscopy, diffuse reflectance infrared Fourier transform spectroscopy (DRIFTS), thermogravimetric analysis (TGA), and scanning electron microscopy (SEM) as described in Chapter 3.

4.3 Results and discussion

4.3.1 Synthesis

Periodic mesoporous organosilica materials were synthesized using 1,2-bistrimethoxysilyethane (BTME) as the silica source in the presence of water, a basic catalyst (NH_4OH) and a surfactant (CTAB). A blank ethanesilica material was prepared without addition of CTAB. A pure inorganic silica material (MCM41) was synthesized from TEOS. Depending on the aims and objectives of a particular experiment, each of the constituents of the reaction mixture (BTME, water, and ammonium hydroxide) was varied. The ageing temperature and length of ageing was also varied.

Addition of BTME to the mixture without CTAB gave a clear solution which gelled on ageing. The solvent was removed by evaporation at 80 ^{o}C to yield a glassy material. For other materials a white precipitate formed within 30 minutes after addition of the silica source to a mixture of CTAB, water and ammonium hydroxide. The amount of the precipitate formed generally increased with the amount of the silica source used.

The base catalysed surfactant templated formation of periodic mesoporous ethanesilica is proposed to form from micelles [43] as illustrated in Scheme 4.1. The quaternary ammonium surfactant molecules assemble into micelles. Micelles organize into long range hexagonal arrays with the charged head groups pointing towards the solution and the long hydrocarbon chains (hydrophobic) pointing

towards the centre of the micelles [43]. Upon the addition of the silica source, the negatively charged organosilica species (I^-) condense and polymerise on the surface of the positively charged micelles (S^+), giving rise to the S^+I^- organic inorganic complex. Solvent extraction of the complex reveals the hexagonal solid framework of the PMO material.

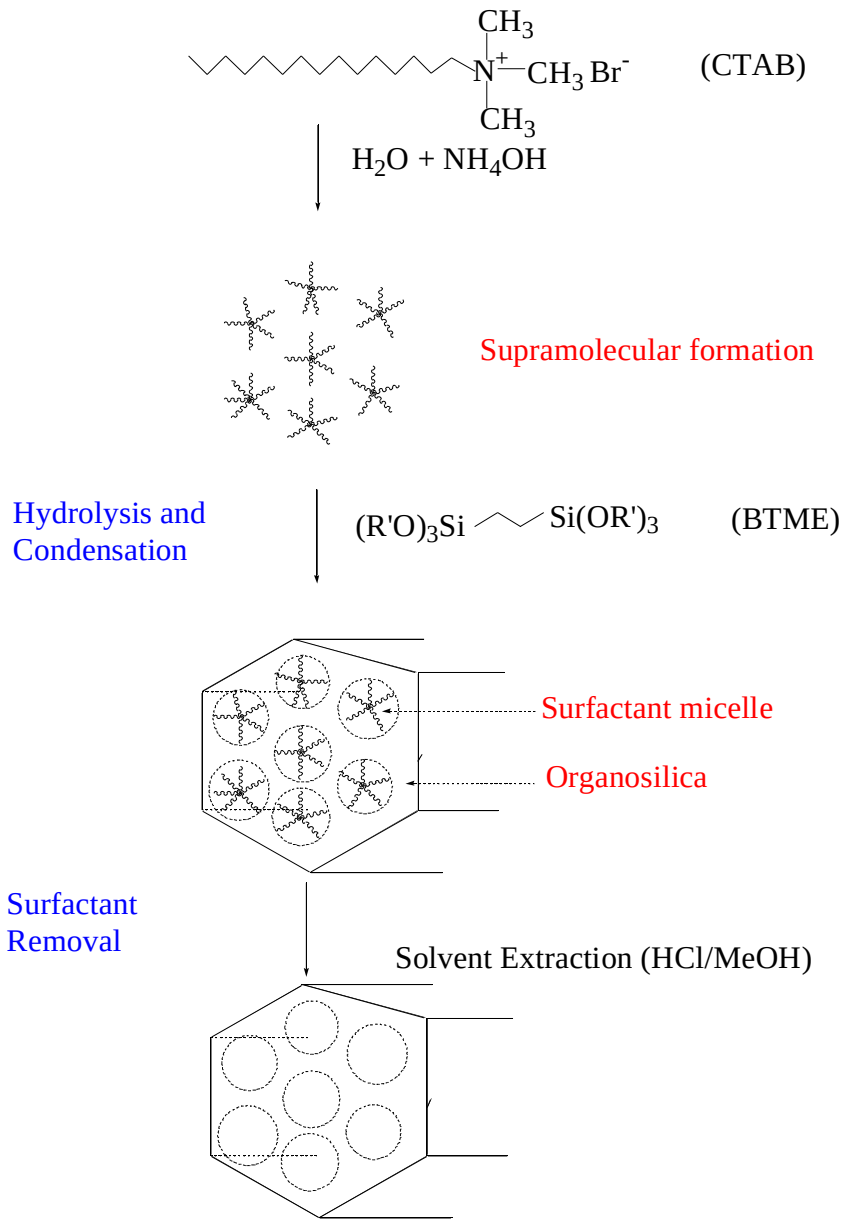

Scheme 4.1 Reaction scheme showing the formation of periodic mesoporous ethanesilica. Note that the framework is made of units of $O_3SiCH_2CH_2SiO_3$.

4.3.2 Diffuse Reflectance Fourier Transform Infrared Spectroscopy and Raman Spectroscopy

Raman spectroscopy and diffuse reflectance Fourier transform infrared spectroscopy (DRIFTS) were used to identify functional groups and to study the thermal stability of organic groups in the organosilica materials. Results confirm the formation of organosilica materials and show that the surfactant is removed by solvent extraction.

4.3.2.1 Diffuse Reflectance Fourier Transform Infrared Spectroscopy. DRIFTS spectra of an as synthesized [BA80] and a solvent extracted [BE80] ethanesilica material are shown in Figure 4.1. Band assignments for fundamental IR and Raman bands of ethanesilica are listed in Table 4.1. The vibrations observed at 1415 and 1467 cm^{-1} are assigned to $\delta(Si\text{-}CH_2)$ and $\delta(N\text{-}CH_2)$ or $\delta(C\text{-}CH_2)$ of the BTME and surfactant (CTAB) respectively. The broad band observed between 2800 and 3000 cm^{-1} is due to the CH stretching vibrations of both the BTME and the surfactant molecules [23, 29, 44 – 46]. The shoulder at ~2970 cm^{-1} originates from an alkyl stretching vibration associated with the surfactant and the bands at 2929 and 2862 cm^{-1} are caused by asymmetric and symmetric stretching vibrations of the $-CH_2CH_2-$ groups from the BTME molecule [23]. DRIFTS spectra revealed that, after removal of surfactant by the extraction process, the organic groups ($-CH_2CH_2-$) remained intact as indicated by the vibrations due to alkyl stretch (2897 cm^{-1}) and alkyl CH deformations (1410 cm^{-1}) [23, 46, 48]. Hydroxyl groups are evident in the DRIFTS spectra of some of the as synthesized and extracted spectra from a sharp band observed at 3726 cm^{-1} and a broad band centred near 3523 cm^{-1}. The absorption band at 3726 cm^{-1} is assigned to free SiOH groups while the broad band at 3430 cm^{-1} is ascribed to hydrogen bonded SiOH groups and hydrogen bonded water [46, 49]. The broad band observed between 950 and 1235 cm^{-1} is due to longitudinal optical (LO) and transverse optical (TO) siloxane (Si-O-Si) asymmetric stretching modes. The band due to Si-OH stretching is observed at 920 cm^{-1} [47, 49]. The vibrations due to symmetric Si-O-Si stretching appear at 800 cm^{-1} in liquid BTME [44]. The peak

shifts to lower cm^{-1} (773 cm^{-1}) in extracted ethanesilica. The shoulder observed at 703 cm^{-1} is due to the CH_2 rocking vibrations of Si-CH_2CH_2 groups [51].

To provide further information, DRIFTS spectra of the extracted periodic ethanesilica obtained at different temperatures are shown in Figure 4.2. The spectra showed that the bands due to alkyl stretching vibrations are still observed at temperatures above 500 ^oC. There is, however, a progressive reduction in the peaks assigned to CH over the 200 – 600 ^oC temperature interval. This provides further evidence that the mass losses observed between ~400 and 600 ^oC in thermogravimetric analysis curves of ethanesilica materials (discussed in Section 4.3) is due to decomposition of framework organic groups (-CH_2CH_2-). The broad band centred around 3542 cm^{-1}, assigned to SiOH stretching of surface silanols hydrogen-bonded to molecular water and O-H strectching of hydrogen bonded molecular water, disappears at higher temperature.

4.3.2.2 Raman spectroscopy. The Raman spectra of solid surfactant (CTAB), liquid BTME and an ethanesilica material prepared without surfactant are shown in Figure 4.3 (a) to (c). The Raman spectrum of a solvent extracted ethanesilica material prepared by condensation of BTME (BE80) is shown in Figure 4.3(d). Band assignments for fundamental IR and Raman bands of ethanesilica are listed in Table 4.1. The ethanesilica material prepared without surfactant has only one peak at 2887 cm^{-1}. This peak is observed in the same position in the Raman spectrum of liquid BTME and is assigned to CH stretching vibrations of BTME. Comparison of Figure 4.3(a) and 3(d) shows that vibrations due to the CH_2 and CH_3 groups in CTAB are not observed in spectra of solvent extracted materials indicating complete removal of the surfactant by solvent extraction. The absence of vibrations due to methoxy groups (observed in the spectrum of liquid BTME) in the Raman spectra of ethanesilica (Figures 4(c) and 4(d)) shows complete hydrolysis of the methoxy groups.

Table 4.1 Raman and Infrared band locations and assignments for periodic mesoporous ethanesilica.

Raman Band (cm^{-1})	**IR Band (cm^{-1})**	**Mode**	**Structural unit**
	3726	ν(O-H)	SiO-H
	3523	ν(O-H)	Hydrogen bonded SiO-H and H_2O
2887	2897	ν (C-H)	Methylene C-H
1460	1467	δ(N-CH_2) or δ(C-CH_2)	Surfactant C-H
1418	1415	δ (Si-CH_2)	BTME framework C-H
1260	1269	C-H_2 wag	BTME framework C-H
1147	1018 -1163	ν asymmetric Si-O	Longitudinal Optical (LO) mode
1078	1018 – 1163	ν asymmetric Si-O	Transverse Optical (TO) mode
956	920	ν asymmetric Si-O	Si-OH
798	773	ν symmetric Si-O	Si-O-Si
	703	CH_2 rock	Si-CH_2-CH_2

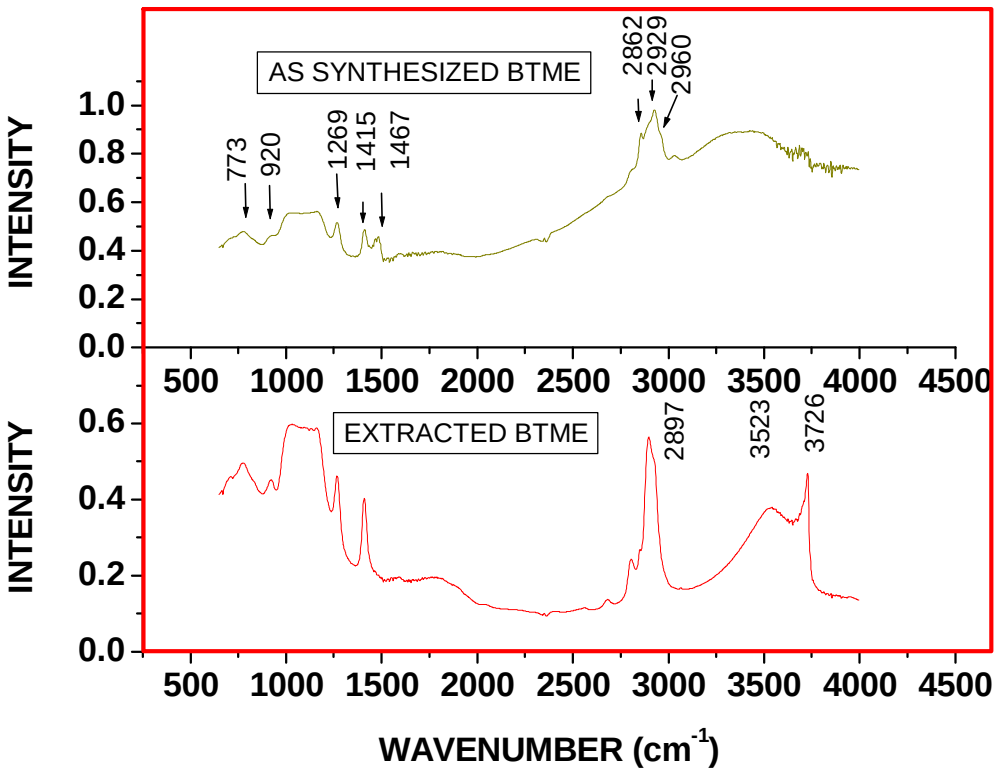

Figure 4.1 DRIFTS spectra of an as synthesized (BA80) and a solvent extracted (BE80) ethanesilica material.

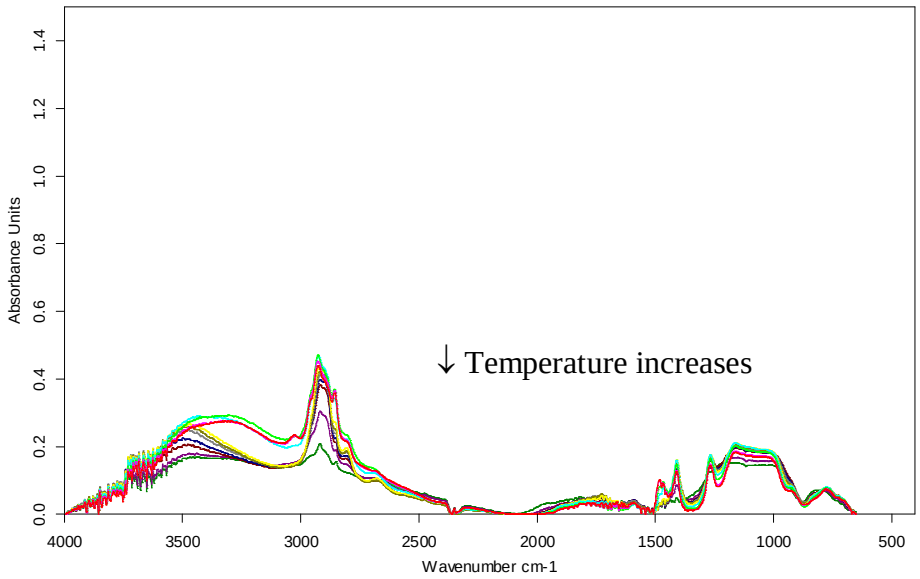

Figure 4.2 DRIFTS spectra of "as synthesized" periodic ethanesilica heated at different temperatures. (120, 150, 200, 250, 300, 350, 400, 450, 500, 550 and 600 ^{o}C).

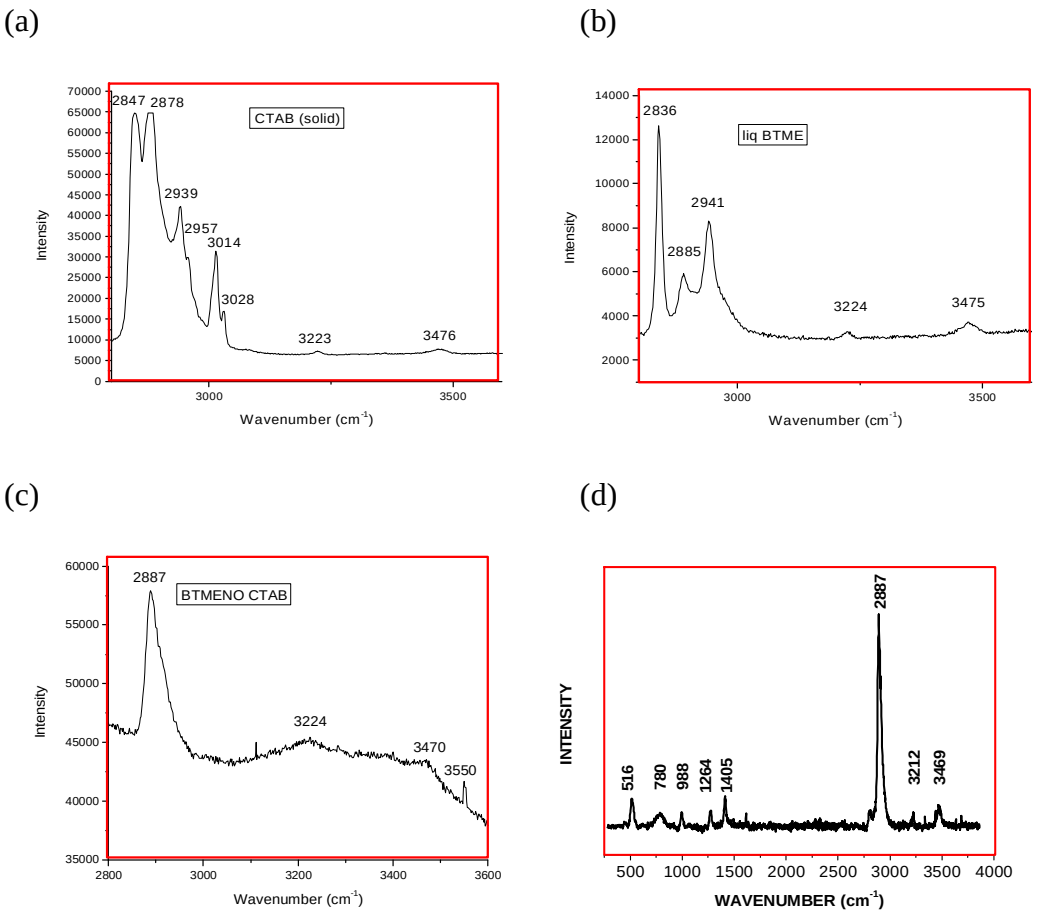

Figure 4.3 Raman spectra of (a) hexadecyltrimethylammonium bromide (CTAB), (b) liquid 1,2-bistrimethoxysilylethane (BTME), (c) ethanesilica prepared without surfactant, and (d) solvent extracted ethanesilica.

4.3.3 Thermal analysis

Samples were analysed before and after solvent extraction using thermogravimetric analysis (TGA) and differential thermal analysis (DTA). Analysis was conducted from room temperature to 800 ^{o}C or 1000 ^{o}C. Typical thermograms of the as synthesized PMO and the surfactant extracted PMO prepared from BTME (BA80 and BE80) are shown in Figures 4.4B and 4.4A, respectively. The corresponding DTA curves are presented in Figures 4.4D and 4.4C. Table 4.2 summarises the data obtained from the thermograms. The TGA curve of the as synthesized BTME sample exhibits a weight loss of about 5 % below 110 ^{o}C, accompanied by an endothermic DTA peak, attributed to the desorption of methanol and water. This is followed by a weight loss of approximately 20 % over the temperature range 108 – 262 ^{o}C with an endothermic DTA peak due to desorption of the surfactant. This mass loss is characterized by two overlapping peaks in the derivative of the thermogram (peaks 2 and 3 in Figure 4.5A). A 10 % mass loss attributed to matrix decomposition occurs in the range 440 – 727 ^{o}C. This mass loss appears as an exothermic DTA peak at 578 ^{o}C.

The thermogram of the solvent extracted BTME PMO shows a decrease in mass of about 2 % below 57 ^{o}C due to the loss of methanol. The sample shows no weight loss in the region where the surfactant is desorbed (108 – 262 ^{o}C) indicating that the surfactant was totally removed by solvent extraction. A 2 % mass loss, attributed to desorption of water formed from condensation of internal hydroxyl groups, occurs between 313 and 472 ^{o}C.

For samples prepared with variable amounts of BTME, an expected (small) increase in the total mass loss from the sample was observed (Figures 4.5B and 4.5C). The total mass loss for solvent extracted materials prepared from 7.14 mmol and 14.3 mmol BTME (BE80 and 2BE80 respectively) are 17.7 and 18.3 %, respectively.

Table 4.2 TGA results of a PMO material prepared from BTME.

Temperature range (^{o}C)	**% Mass loss of as synthesized material**	**% Mass loss of Solvent extracted material**	**Source of mass loss**
25 – 110	5 %	2 %	Desorption of methanol and water
110 – 265	30 %	-	Surfactant decomposition
310 – 440	17%	2 %	Surfactant decomposition and water from condensation of internal hydroxyls
440 – 780	10 %	10 %	Matrix decomposition

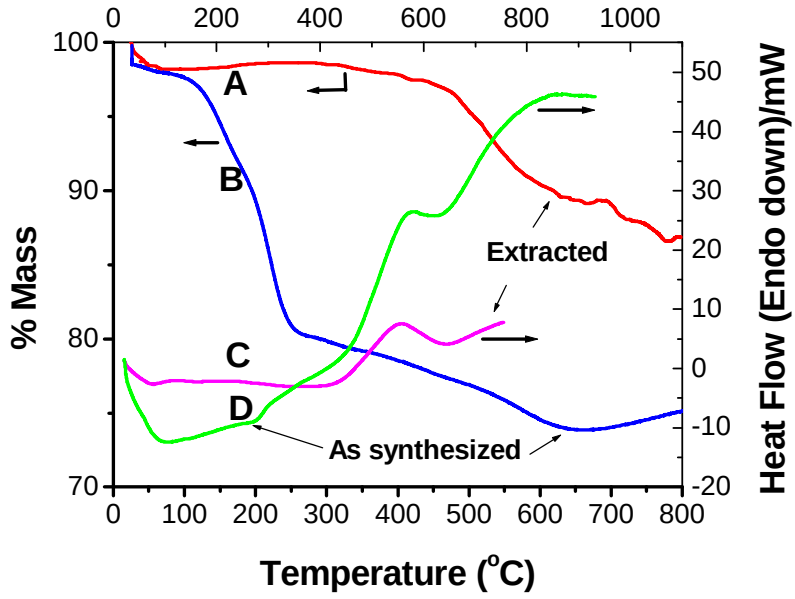

Figure 4.4 TGA and DTA curves of an as synthesized (BA80) and an extracted (BE80) periodic ethanesilica material. A = TGA, extracted; B = TGA, as-synthesized; C = DTA, extracted; D = DTA, as-synthesized.

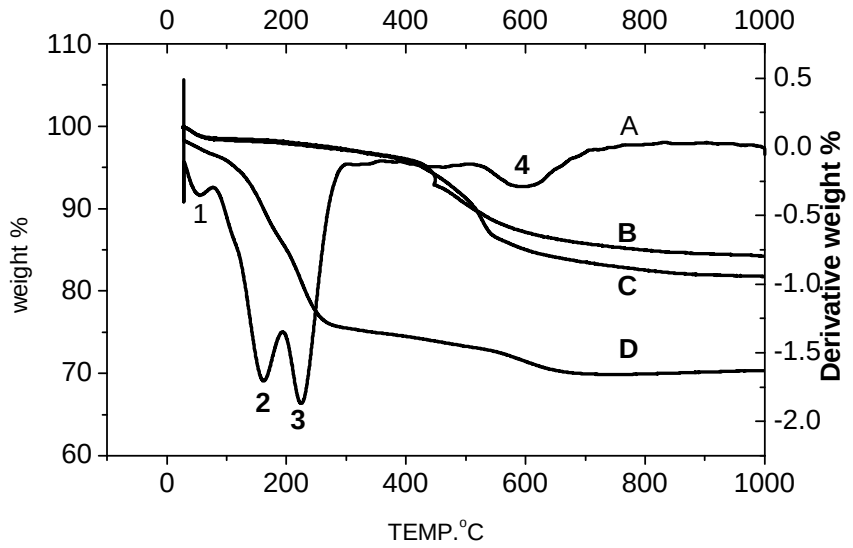

Figure 4.5 TGA curves of as synthesized and solvent extracted samples prepared with various amounts of BTME. A = derivative TGA curve, 14.3 mmol BTME, as-synthesized; B = 7.14 mmol BTME, extracted; C = 14.3 mmol BTME, extracted; and D = 14.3 mmol BTME, as synthesized.

4.3.4 Effect of solvent extraction time on Powder X-ray Diffraction patterns and nitrogen adsorption data of MCM-41

4.3.4.1 Powder X-ray Diffraction. The periodicity of mesoporous materials was probed using powder XRD. Periodic mesoporous materials synthesized using alkylammonium surfactants display a very high intensity peak at around $2\theta = 2^o$, together with low intensity peaks in the 2θ range $3 - 8^o$ [43, 52]. The pure inorganic silica material was synthesized from TEOS and used to study the effect of solvent extraction time on powder X-Ray diffraction data. The cationic surfactant species was removed by refluxing in an HCl/methanol mixture at 50 ^oC, varying the extraction time. Figure 4.6 shows the XRD patterns of the as synthesized and solvent extracted materials prepared using only TEOS as the silica precursor (100% TEOS). Table 4.3 summarizes surface properties of the silica materials. The XRD patterns show four clear diffraction peaks. This is the pattern expected for MCM-41 silica [43, 52]. The prominent low angle peak at approximately $2\theta = 2^o$ indicates the presence of uniformly sized pores for ordered materials. Lattice spacings of 3.99, 2.33, 2.00 and 1.52 were obtained for the sample extracted for 48 hours. They can be indexed as the d_{100}, d_{110}, d_{200} and d_{310} of a two dimensional hexagonal lattice with lattice constant a_o = 4.61 nm [where $a_o = 2d_{100}/(3)^{1/2}$].

The value of the lattice parameter (d_{100}) changes slightly from 4.1 nm to 4.0 nm on solvent extraction. The d_{100} value remains the same for solvent extracted samples regardless of the length of solvent extraction time. The unit cell parameters (a_o) for mesoporous silica (ranging from 4.62 to 4.64 nm) is similar to the value (4.57) of a sample calcined at 600 ^oC.

From the above observations it can be concluded that the ageing time (12 -72 h) has a negligible influence on the lattice parameter.

Table 4.3 Surface properties of silica materials prepared from TEOS.

Extraction Time (hrs)	**Surface Area (m^2/g)**	**Pore Volume (cm^3/g)**	**Average Pore Diameter (nm)**	**Lattice spacing, d_{100} (nm)**	**Unit cell parameter, a_o (nm)[a]**
0	91.0	0.08	3.67	4.10	4.73
12	385	0.37	3.70		
24	483	0.35	2.89	4.00	4.62
48	571	0.49	3.41	3.99	4.61
72	683	0.58	3.40	4.02	4.64
2 x 24	590	0.50	3.38	4.04	4.66
600 ^oC	796	0.67	3.38	3.96	4.57

[a]Unit cell parameter, $a_o = (2d_{100}/\sqrt{3})$ for hexagonal symmetry.

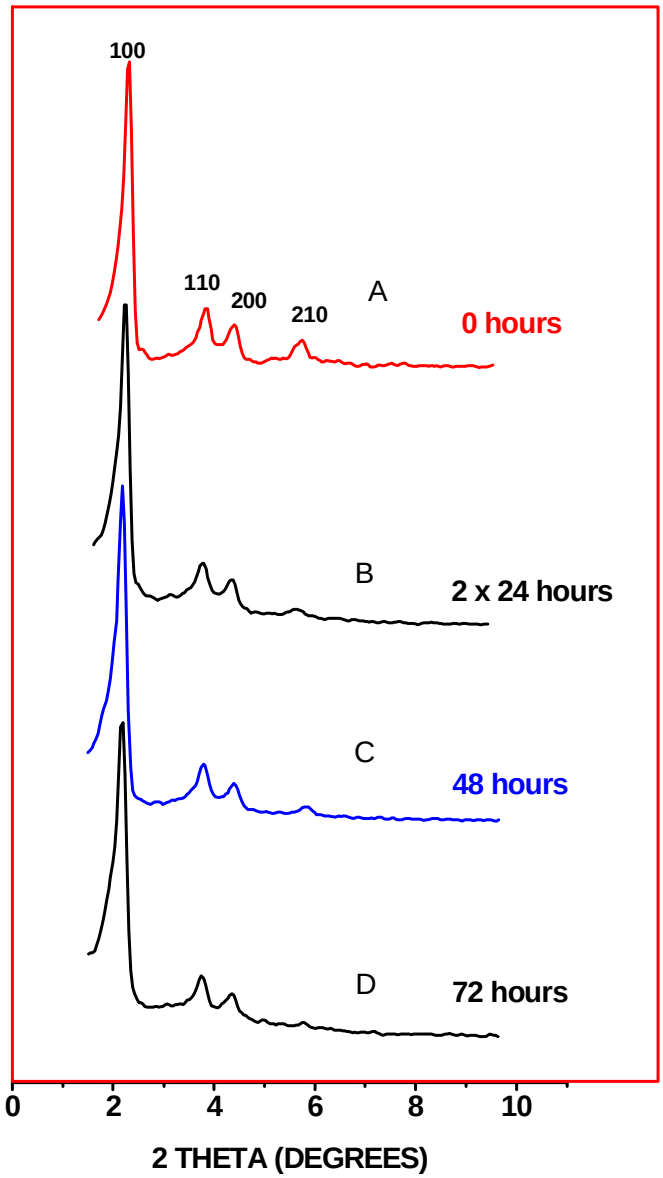

Figure 4.6 Powder XRD patterns of MCM-41 materials extracted for different times.

4.3.4.2 Nitrogen adsorption/desorption. The N_2 adsorption–desorption isotherms at 77 K of the MCM-41 silica material calcined at 600 ^oC for 6 hours, shown in Figure 4.7, is a completely reversible Type IV isotherm with an inflection in the low relative pressure range (p/p_0 = 0.20 – 0.3) [53]. This is a peculiar feature of MCM-41 materials due to the primary mesopore filling step [54]. A sharp inflection indicating capillary condensation within uniform mesophases, depends on the pore size and the sharpness of the capillary condensation step signifies a uniform pore size. As depicted in Figure 4.7 (inset), the BJH pore size distribution centered at 2.6 nm is very narrow, indicating an excellent textural uniformity of the silica material.

When solvent extraction is prolonged, the BET surface area and the pore volume increase, while the average pore diameter decreases (Table 4.3, Figure 4.8). Values of surface area (683 m^2/g) and pore volume (0.58 cm^3/g) for the material extracted for 72 hours are lower than that of the material calcined for 6 hours at 600 ^oC (796 m^2/g and 0.67 cm^3/g, respectively). However, these values of surface areas are substantially lower than literature values (>1000 m^2/g) reported for mesoporous silica [55]. Values of average pore diameters for samples solvent extracted for 48 and 72 hours respectively as well as the sample extracted twice for 24 h are the same (3.4 nm) and similar to the value of a material calcined at 600 ^oC.

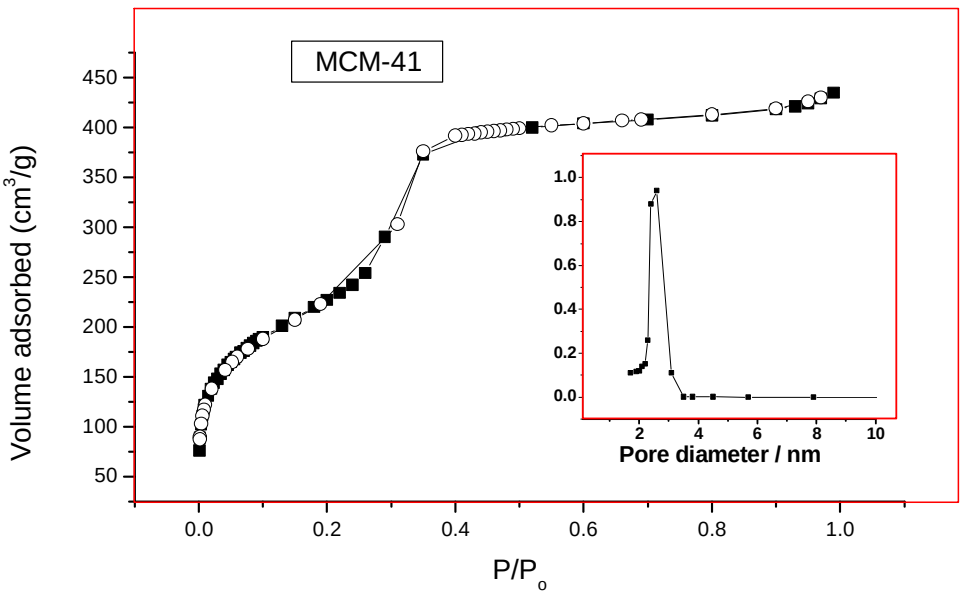

Figure 4.7 The N_2 adsorption–desorption isotherms of ordered silica material calcined at 600 ^{o}C for 6 hours.

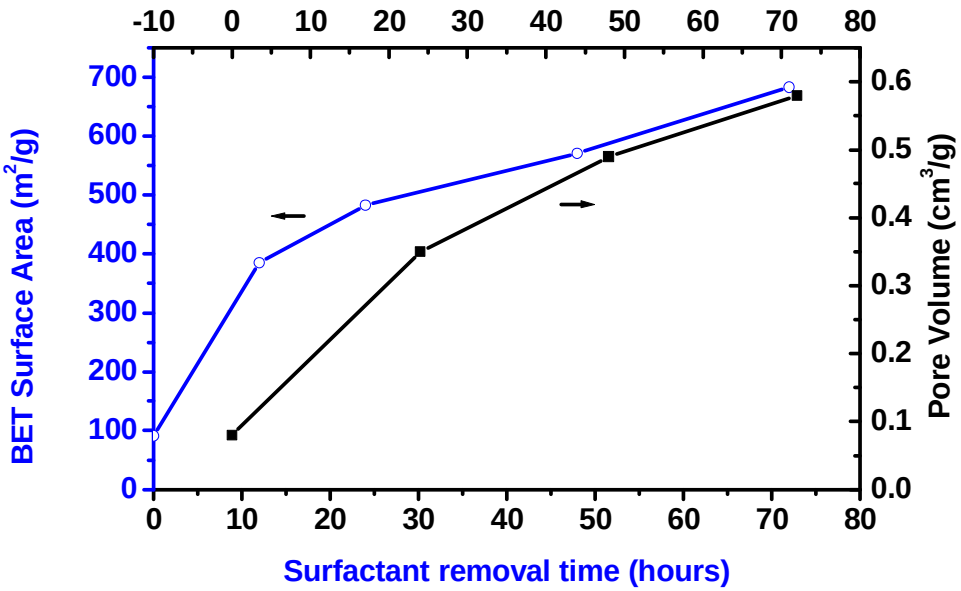

Figure 4.8 Effect of surfactant removal time on BET surface area and pore volume of MCM-41.

4.3.5 Effect of ageing temperature on powder X-ray diffraction patterns and nitrogen adsorption data of ethanesilica materials synthesized from BTME

4.3.5.1 Powder X-ray diffraction. The XRD patterns of as synthesized and solvent extracted ethanesilica samples aged at different temperatures are shown in Figures 4.9 and 4.10, respectively. The XRD patterns of solvent extracted ethanesilica show a better resolution of peaks as compared to patterns of as synthesized ethanesilica materials. The XRD pattern of the material synthesized at 80 ^{o}C (BE80) is similar to that observed for a cubic mesophase [10]. For materials aged at 0 ^{o}C, 25 ^{o}C and 55 ^{o}C a broad feature, with the best resolution obtained for BE25, is observed around $2\theta = 3.5^{o}$. XRD patterns with a similar feature were previously reported for periodic mesoporous organosilica materials [6]. Other researchers who investigated the influence of ageing temperature on XRD patterns also obtained materials with more dominant XRD structural features at low temperatures when compared to samples prepared at higher temperatures [23].

As the temperature increases the most prominent peak shifts to lower 2θ values, implying higher d values (Table 4.4). The peak shifts from 2.5 to 1.90^{o} for the materials aged at 0 ^{o}C (BE0) and 80 ^{o}C (BE80) respectively. This may be due to the fact that at higher temperature the condensation of BTME in the framework is accelerated, thereby resulting in some shrinkage of the BTME [23].

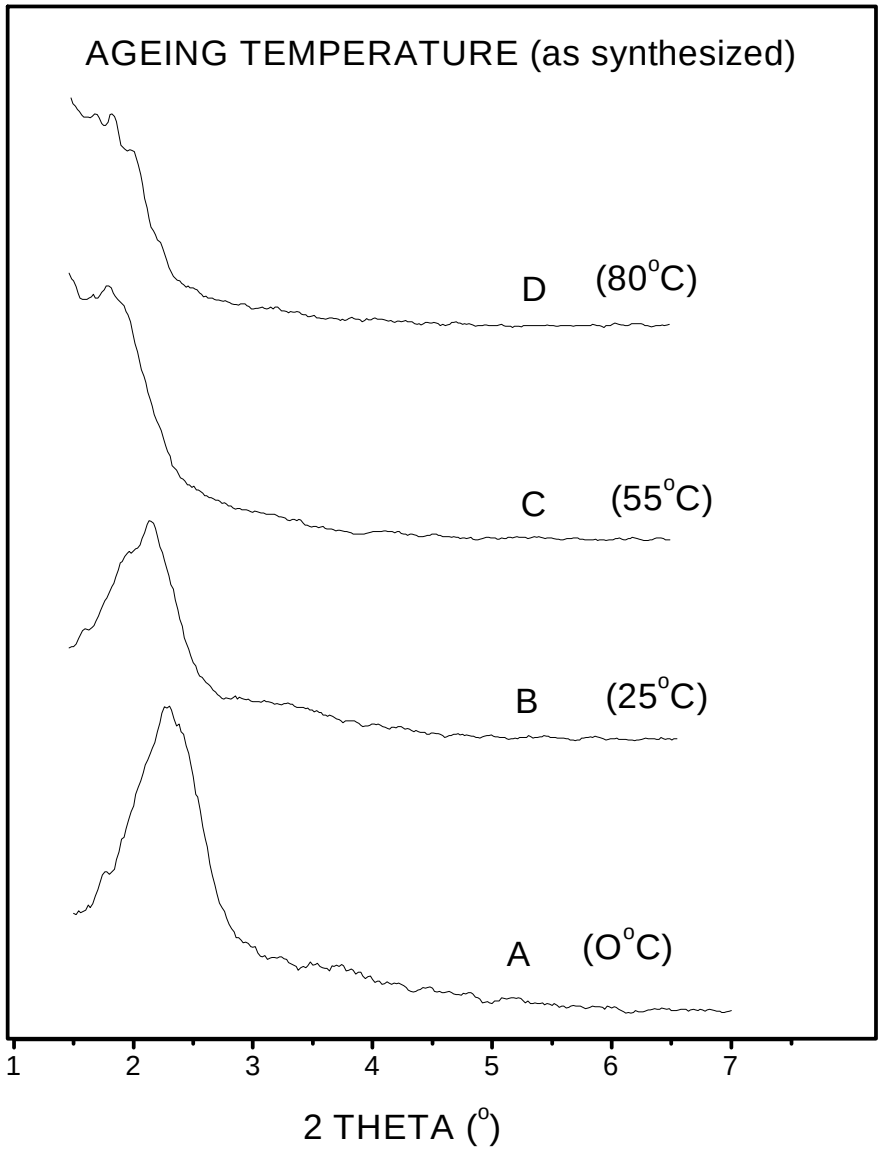

Figure 4.9 XRD patterns of as synthesized ethanesilica materials aged at different temperatures. Ageing temperatures: A = 0 ^{o}C, B = 25 ^{o}C, C = 55 ^{o}C and D = 80 ^{o}C.

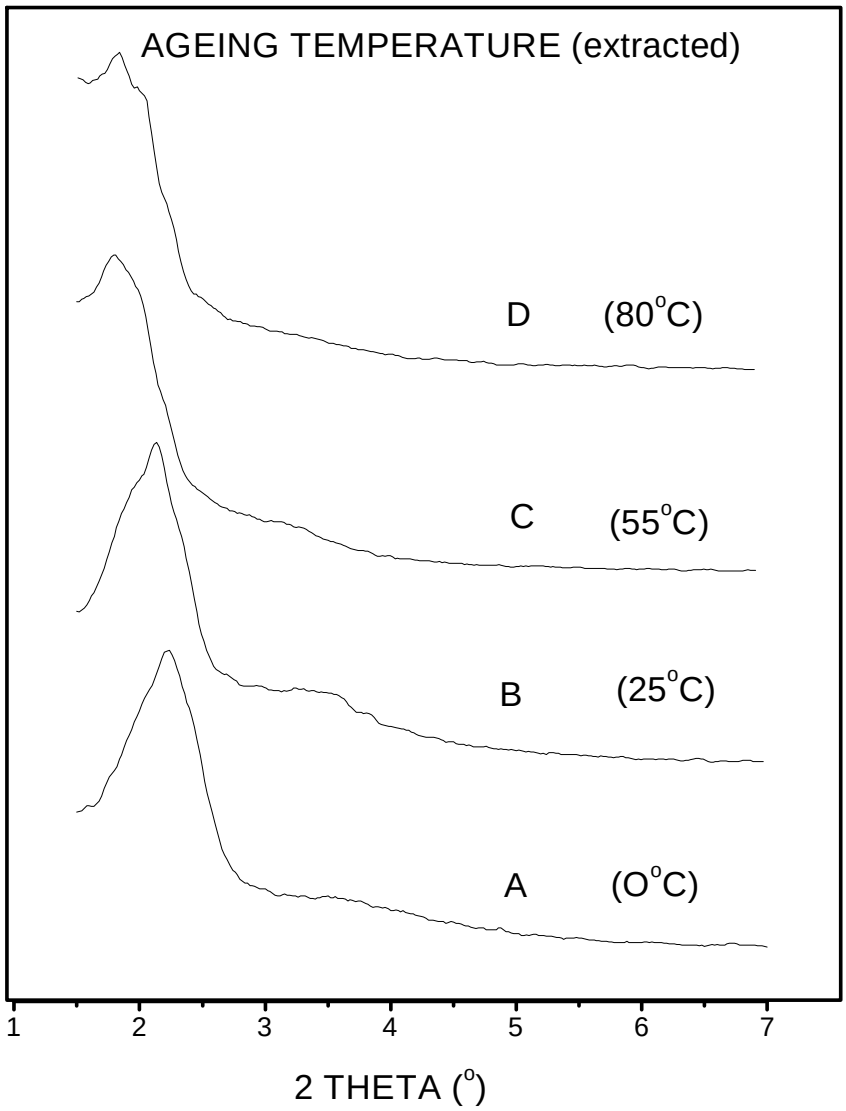

Figure 4.10 XRD patterns of solvent extracted ethanesilica materials aged at different temperatures. Ageing temperatures: A = 0 ^{o}C, B = 25 ^{o}C, C = 55 ^{o}C and D = 80 ^{o}C.

4.3.5.2 Nitrogen adsorption desorption. Nitrogen adsorption-desorption isotherms and BJH adsorption pore size distributions for extracted ethanesilica synthesized by condensation of BTME using CTAB as the structure-directing template are shown in Figure 4.11. The PMO materials were aged at 0 ^{o}C, room temperature (27 ^{o}C), 55 ^{o}C and 80 ^{o}C. The structural properties of these materials are listed in Tables 4.4 and 4.5. The PMO materials exhibit Type IV isotherms and narrow BJH adsorption pore size distributions characteristic of mesoporous materials [53]. A sharp inflection, indicating capillary condensation within uniform mesophases, is observed between relative pressure P/P_o = 0.25 and 0.4. The PMO aged at 0 ^{o}C exhibits an isotherm which is intermediate between Type IV and Type I. Type I isotherms are observed for microporous materials [53]. Extracted materials possess high specific surface areas. With the exception of the material aged at 0 ^{o}C whose surface area (977 m^2/g) is lower than that of the material aged at 25 ^{o}C (1049 m^2/g), the surface area decreases as ageing temperature increases (see Table 4.4). A similar trend was reported for xerogels synthesized from bridged alkoxysilanes in the absence of structure directing surfactants [56]. Higher pore volumes and average pore diameters are obtained at higher ageing temperatures. The pore volumes ranged from 0.54 to 0.94 cm^3/g, with the highest value being obtained for the material aged at 80 ^{o}C.

The hysteresis loops change from Type H4 to Type H3 with increasing ageing temperature (Figure 4.11). The ethanesilica material aged at 0 ^{o}C (BE0) has an almost reversible Type IV isotherm, with a reduced hysteresis loop. The ethanesilica material aged at room temperature (BE27) has a Type H4 hysteresis loop, which is often associated with narrow slit-like pores. The Type H3 hysteresis loops obtained for ethanesilica materials aged at 55 and 80 ^{o}C (BE55 and BE80) do not exhibit any limiting adsorption at high pressures. Type H3 hysteresis loops are observed with aggregates of plate-like particles giving rise to slit-shaped pores.

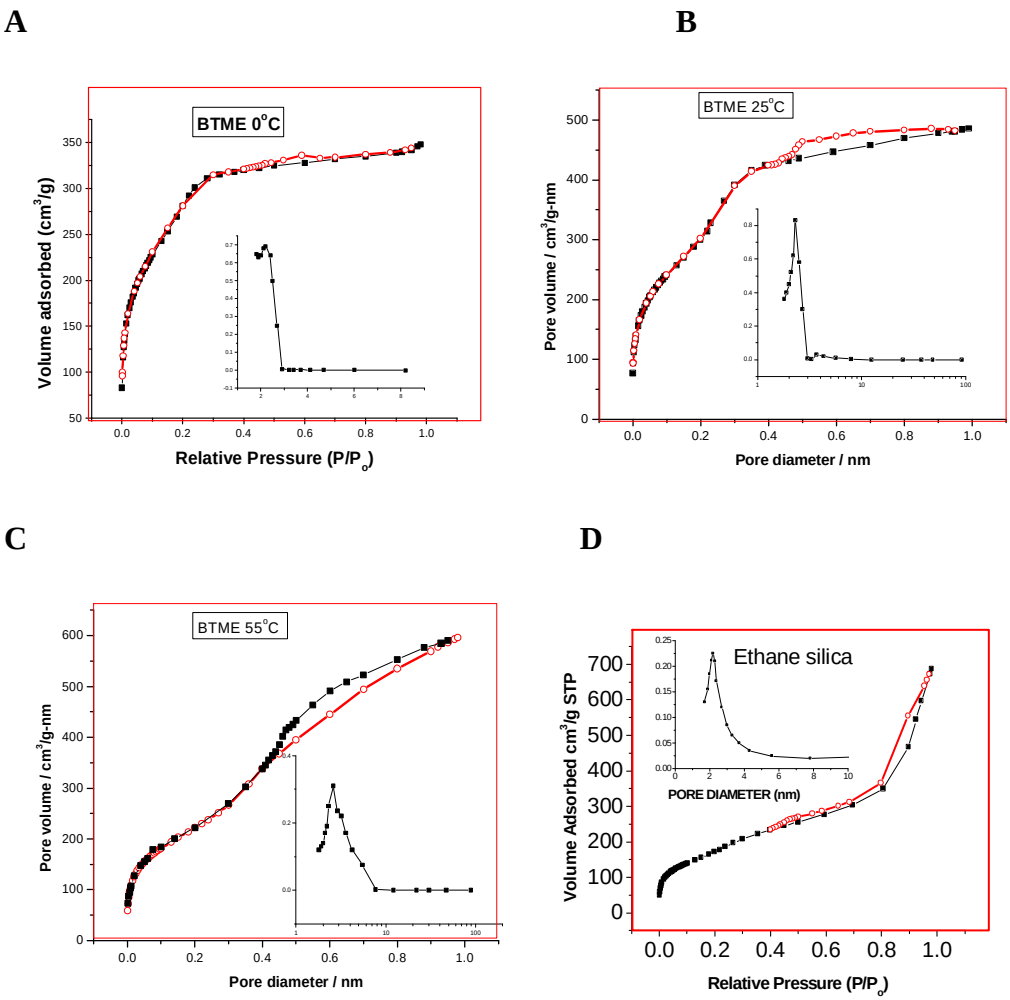

Figure 4.11 Nitrogen adsorption desorption isotherms and adsorption PSDs of ethanesilica materials aged at different temperatures. Ageing temperatures: A = 0 ^{o}C, B = 27 ^{o}C, C = 55 ^{o}C, and D = 80 ^{o}C.

Table 4.4 Surface properties of PMOs synthesized from BTME and TEOS.

Sample	**BTME (mmol)**	**Ageing Temperatute (°C)**	**Lattice Parameter, d (nm)**	**Surface Area (m^2/g)**	**Pore Volume (cm^3/g)**	**Average Pore Diameter (nm)**
BE0	7.14	0		977	0.54	2.2
BE27	7.14	25	4.72	1049	0.75	2.9
BE55	7.14	55	4.89	778	0.92	4.7
0.5BE80	3.57	80	5.64	697	0.92	5.3
BE80	7.14	80	4.81	686	0.92	5.3
1.5BE80	10.7	80	4.41	542	0.92	6.8
2BE80	14.3	80	4.39	617	1.18	7.7

Table 4.5 DFT and BJH diameters obtained from adsorption and desorption isotherms for materials aged at 80 ^{o}C.

	DFT		**BJH ADSORPTION PSD**		**BJH DESORPTION PSD**	
Sample	**Micropore diameter (nm)**	**Mesopore diameter (nm)**	**Pore diameter range (nm)**	**Average diameter (nm)**	**Pore diameter range (nm)**	**Average diameter (nm)**
BE0	1.2	2.7	2.3 - 2.2	2.2	4.0 - 3.6	3.6
BE27	1.3	3.0	2.4 - 2.2	2.3	3.4 - 3.3	3.3
BE55	1.4	3.4	2.8 - 2.4	2.6	3.3 - 3.2	3.2
BE80	1.4	3.4	2.4 - 2.3	2.3	3.2 - 3.1	3.2

4.3.6 Effect of the amount of BTME on powder X-ray diffraction patterns and nitrogen adsorption data of ethanesilica materials

4.3.6.1 Powder X-ray diffraction. XRD patterns of solvent extracted ethanesilica materials prepared with different concentrations of BTME and aged at 80 ^{o}C show a prominent low angle peak at approximately $2\theta = 2^{o}$ (Figures 4.12 and 4.13) typical of periodic mesoporous materials. Peaks are better resolved after solvent extraction. The XRD pattern of the material synthesized using 7.14 mmol BTME (BE80) is not observed in the material synthesized using 14.3 mmol of BTME (2BE). The XRD pattern of the former material has a broad peak and a shoulder, which is typical of cubic mesoporous materials [10]. The latter material may be assigned to a hexagonal symmetry [52]. The peak obtained for the sample synthesized from the smallest amount of BTME (3.57 mmol) is not well developed. This may be as a result of insufficient BTME molecules available to form siloxane bonds around the surfactant molecules. These results show that the structural order depends on the amount of BTME.

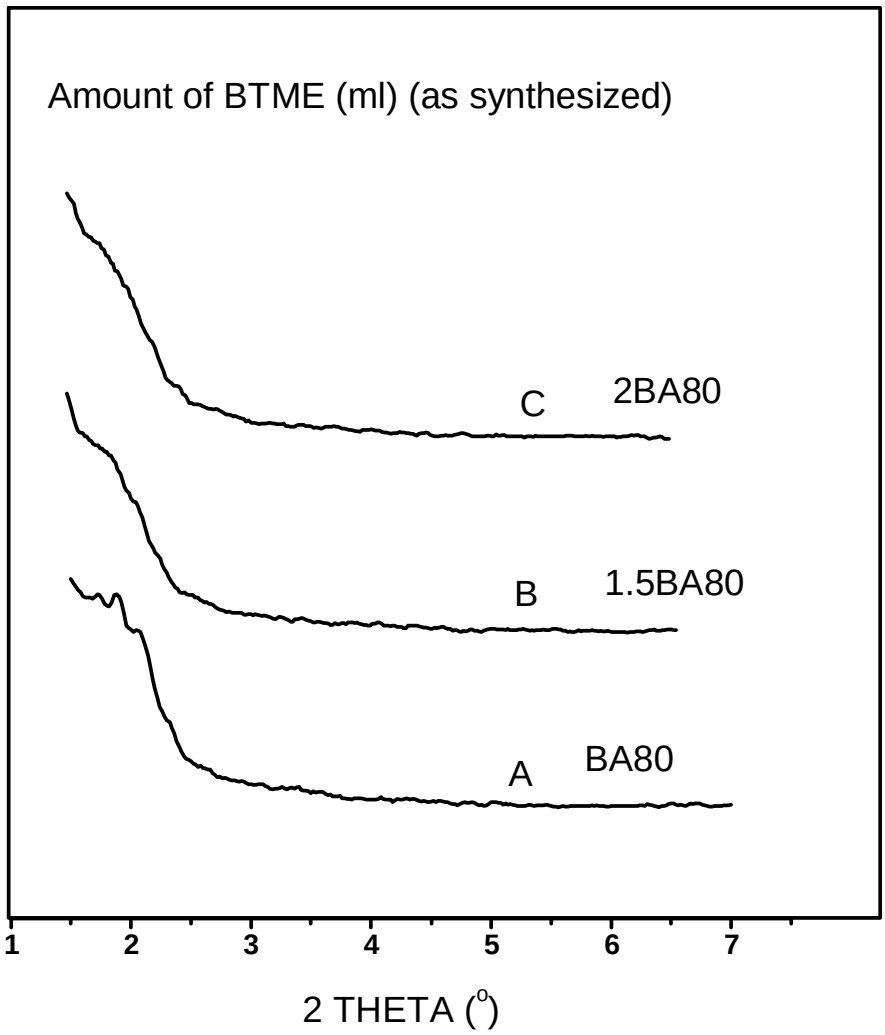

Figure 4.12 XRD patterns of as synthesized ethanesilica materials synthesized with different amounts of BTME. Amount BTME: A = 7.14 mmol, B = 10.7 mmol, and C = 14.3 mmol.

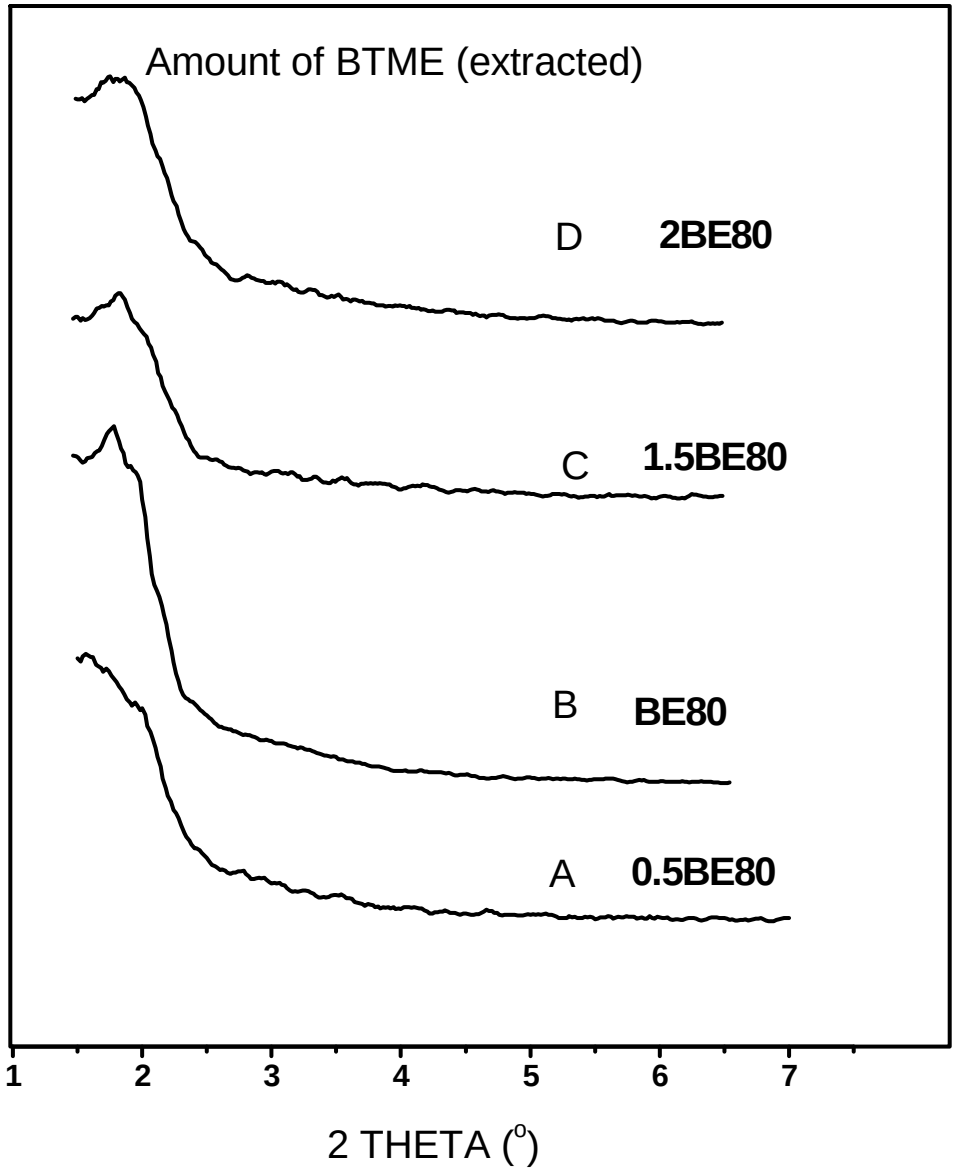

Figure 4.13 XRD patterns of solvent extracted ethanesilica materials synthesized with different amounts of BTME. Amount BTME (mmol): A = 3.57, B = 7.14, C = 10.7, and D = 14.3.

4.3.6.2 Nitrogen adsorption/desorption. The BET surface area (obtained from analysis of a 5-point adsorption curve) decreases from 697 to 617 m^2/g upon increasing the amount of BTME (Table 4.4). The same pore volume (0.92 cm^3/g) was obtained for 0.5BE80, BE80 and 1.5BE80. This value is lower than that obtained for 2BE80 (1.18 cm^3/g). The average pore diameter increases from 5.3 to 7.7 nm with increasing amount of BTME.

4.3.7 Effect of pH on Powder X-Ray diffraction patterns and nitrogen adsorption data of ethanesilica materials

4.3.7.1 Powder X-Ray diffraction. Figure 4.14 shows the effects of the amount of base on XRD patterns. The material synthesized without ammonium hydroxide (not shown) is amorphous as shown by the absence of XRD peaks. Patterns typical of hexagonal and cubic mesophases were obtained for materials synthesized in the presence of 7 and 14 ml of ammonium hydroxide, respectively [Figure 4.14]. Dilution of the base by doubling the amount of water (28 ml instead of 14 ml) added to 14 ml ammonium hydroxide yielded a cubic mesophase (Figure 4.15). Adding 56 ml of water yielded a hexagonal mesophase. These results show that low pH favours the formation of hexagonal mesophases whereas higher pH favours the formation of cubic mesophases.

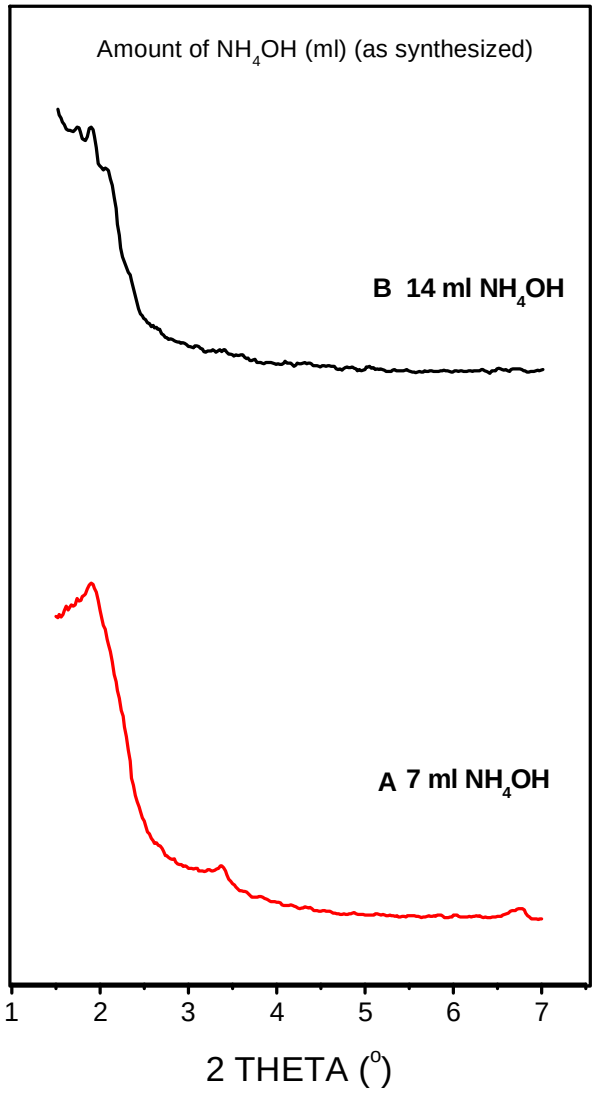

Figure 4.14 XRD patterns of as synthesized ethanesilica materials prepared with different amounts of ammonium hydroxide. Volume ammonium hydroxide (ml): A = 7 and B = 28.

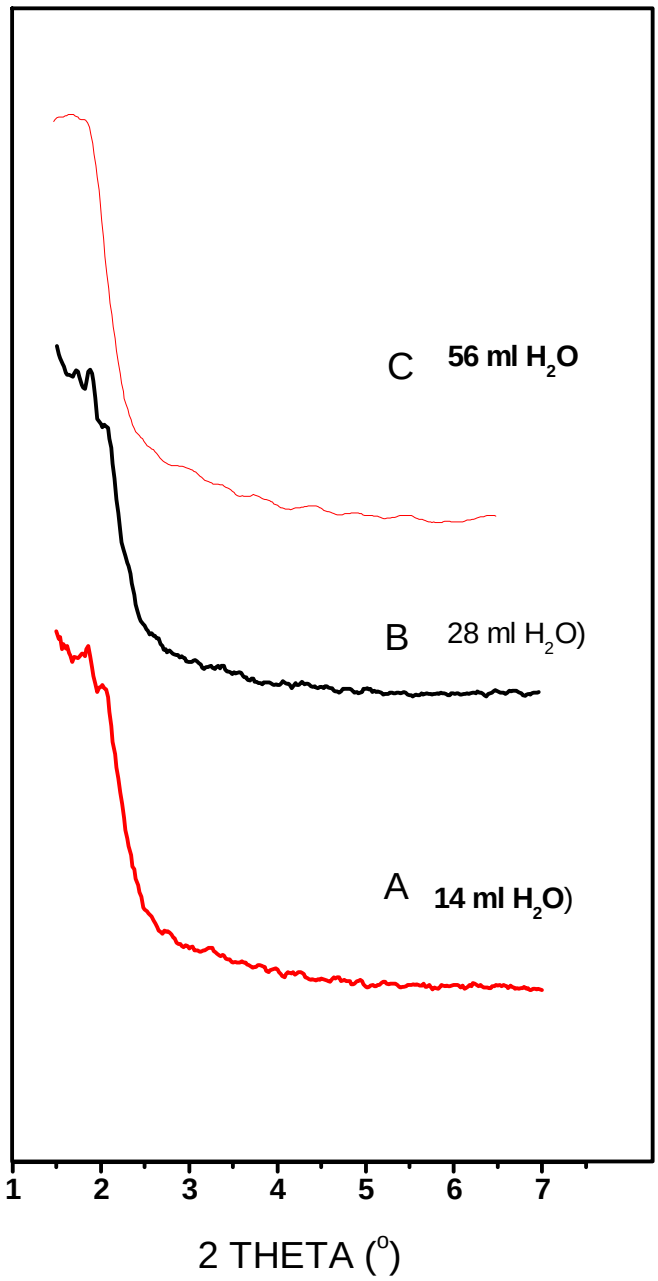

Figure 4.15 XRD patterns of as synthesized ethanesilica materials prepared with different amounts of water. Volume water (ml): A = 14, B = 28 and C = 56.

4.3.7.2 Nitrogen soption. An ethanesilica material synthesized without adding ammonium hydroxide has a lower surface area and a higher pore volume and average pore diameter as compared to materials prepared in the presence of ammonium hydroxide [Table 4.6]. For materials catalysed with ammonium hydroxide, the results show that an increase in the amount of ammonium hydroxide results in a reduction of the surface area and pore volume. The average pore diameter increases slightly from 4.6 nm to 5.3 nm. An increase in ammonium hydroxide from 14 ml to 28 ml has a negligible effect on the average pore diameter.

As shown in Table 4.7, the surface area, pore volume and average pore diameter of the material synthesized in the absence of water are higher than the corresponding values of the materials synthesized in the presence of water. For samples prepared in the presence of water the pore volume generally decreases, while the average pore diameter increases, with increasing amount of water.

Table 4.6 Surface properties of materials synthesized with various amounts of NH_4OH.*

Volume of NH_4OH (ml)	**Surface Area (m^2 / g)**	**Pore volume (cm^3 / g)**	**Average Pore Diameter (nm)**
0	324	1.24	15.3
7	726	1.18	4.6
14	697	0.92	5.3
28	653	0.85	5.2

* Samples were prepared from a reaction mixture consisting of x ml NH_4OH, 28 ml H_2O, 0.68 g CTAB and 1.6 ml BTME (where x =0, 7.0, 14 and 28 ml). The materials were aged at 80 ^oC.

Table 4.7 Surface properties of ethanesilica materials synthesized with various amounts of water.*

Volume of water (ml)	**Surface Area (m^2 / g)**	**Pore Volume (cm^3 / g)**	**Average Pore Diameter (nm)**
0	718	1.23	6.9
14	624	0.80	5.1
28	686	0.92	5.3
56	672	0.90	5.4

* Samples were prepared from a reaction mixture consisting of x ml H_2O, 14 ml NH_4OH, 0.68 g CTAB and 1.6 ml BTME (where x =14, 28 and 56). The materials were aged at 80 ^oC.

4.3.8 Scanning electron micrography (SEM)

Typical scanning electron microscopy (SEM) images of ethanesilica materials aged at 27 ^{o}C and 80 ^{o}C as well as the ethanesilica materials prepared without adding ammonium hydroxide and aged at 80 ^{o}C are shown in Figure 4.16. The SEM image of an ethanesilica sample aged at 80 ^{o}C displays spherical particles with diameters in the range 11.1 to 21.8 μm. There are however regions in which rod-like shapes and materials shaped like "peach-halves" are observed. The latter particles may be broken hollow spheres. Peach-half-like shapes as well as an elongated shape dominate in an ethanesilica material prepared from 3.2 ml BTME instead of 1.6 ml BTME (and aged at 80 ^{o}C). The SEM image of an ethanesilica sample aged at 27 ^{o}C displays predominantly spherical particles of different sizes. The largest diameter was about 2.7 μm. The material prepared without ammonium hydroxide was comprised of particles with different irregular shapes. From these observations it is clear that the morphology of the ethanesilica materials depends on the synthesis conditions.

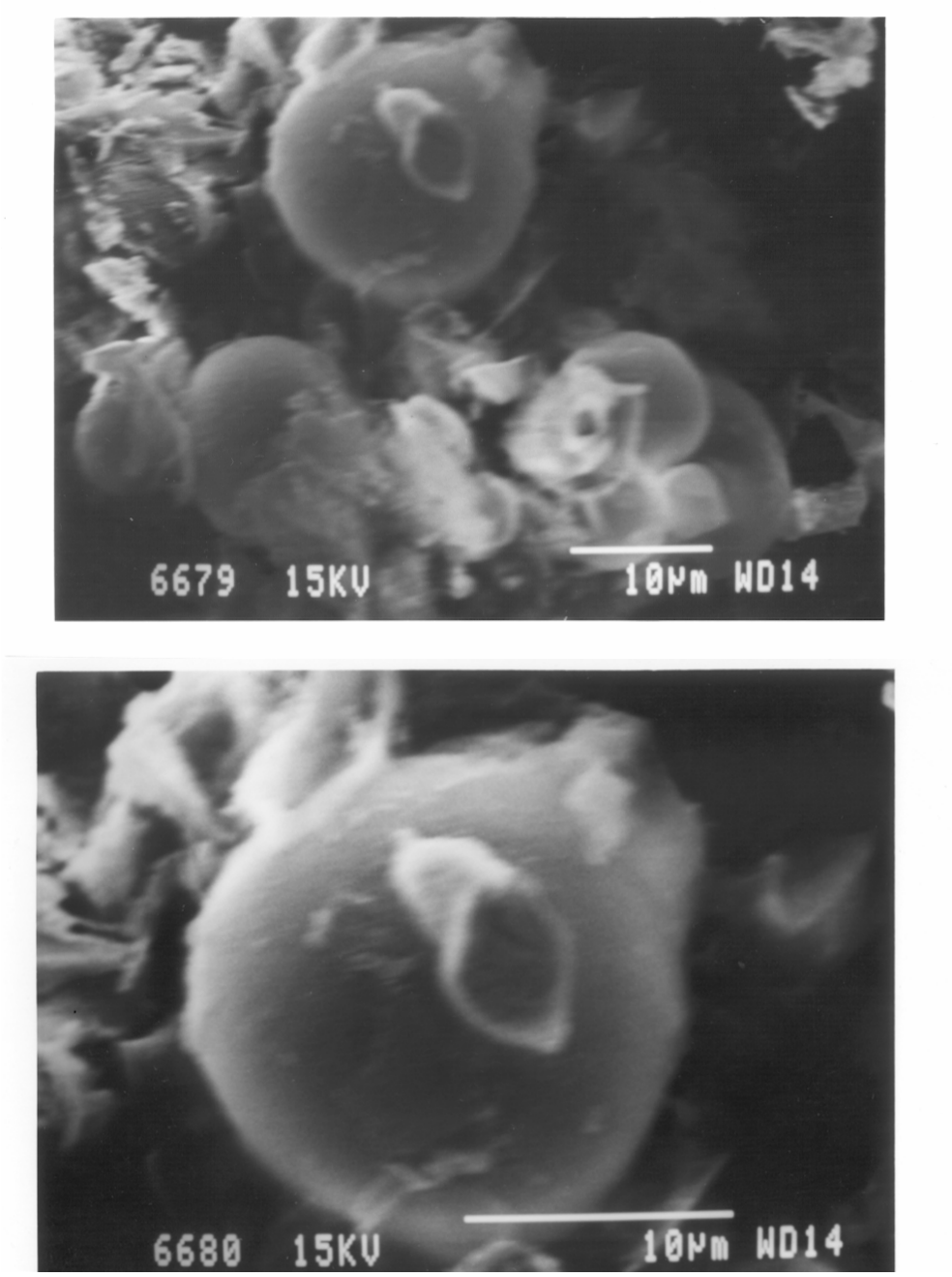

Figure 4.16 SEM image of extracted ethanesilica (BE80).

4.4 Conclusions

Periodic mesoporous organosilica materials (consisting of ethane groups in the framework) were synthesized. Raman spectroscopy and DRIFTS results confirmed the formation of organosilica materials and showed that the surfactant was removed by solvent extraction. TGA showed that the ethane portion of the material only decomposed at temperatures > 400 ^{o}C. The XRD and nitrogen adsorption data indicate that the mesophase and textural properties are dependent on the amount of BTME and ageing conditions. The ageing length has a negligible influence on the lattice parameter. When solvent extraction is prolonged, the BET surface area and the pore volume increase, while the average pore diameter decreases. Materials with more dominant XRD structural features and larger d values, higher surface areas, lower pore volumes and average pore diameters are obtained at lower ageing temperatures. The Type IV isotherms observed have hysteresis loops which change from Type H4 to Type H3 with increasing ageing temperature. An increase in the amount of BTME or pH results in an increase in average pore diameter and a reduction in the surface area and pore volume. These results show that the textural properties of ordered mesoporous silica can be tailored by choosing reaction conditions.

4.5 References

1. T. Asefa, M. J MacLachlan, N. Coombs, and G. A. Ozin, Nature **402**, 867 (1999).
2. T. Asefa, M. J. MacLachlan, H. Grondey, N. Coombs, and G. A. Ozin, Angew. Chem. Int. Ed. **39**, 1808 (2000).
3. T. Asefa, C. Yoshina-Ishii, M. J. MacLachlan, and G. A. Ozin, J. Mater. Chem. **10**, 1751 (2000).
4. C. Yoshina-Ishii, T. Asefa, N. Coombs, M. J. MacLachlan, and G. A. Ozin, Chem. Commun. 2539 (1999).
5. G. A. Ozin, Chem. Commun. 419 (2000).

6. J. Melde, B. T. Holland, C. F. Blanford, and A. Stein, Chem. Mater. **11**, 3302 (1999).
7. A. Sayari, S. Hamoudi, Y. Yang, I. Moudrakovski, and J. R. Ripmeester, Chem. Mater. **12**, 3857 (2000).
8. S. Guan, S. Inagaki, T. Ohsuna, and O. Terasaki, J. Am. Chem. Soc. **122**, 5660 (2000).
9. S. Inagaki, S. Guan, Y. Fukushima, T. Ohsuna, and O. Terasaki, J. Am. Chem. Soc. **121**, 9611 (1999).
10. S. Guan, S. Inagaki, T. Ohsuna, and O. Terasaki, Micropor. Mesopor. Mater. **44 – 45**, 165 (2001).
11. M. Kruk, M. Jaroniec, S. Guan, and S. Inagaki, J. Phys. Chem. B **105**, 681 (2001).
12. H. Fan, S. Reed, I. Baer, R. Schunk, G. P. López, and C. J. Brinker, Micropor. Mesopor. Mater. **44 – 45**, 625 (2001).
13. Y. Lu, H. Fan, N. Doke, D. A. Loy, R. A. Assink, D. A. LaVan, and C. J. Brinker, J. Am. Chem. Soc. **122**, 5258 (2000).
14. H. Fan, Y. Lu, A. Stump, S. T. Reed, T. Baer, R. Schunk, V. Perez-Luna, G. P. López, and C. J. Brinker, Nature **405**, 56 (2000).
15. S. S. Park, C. H. Lee, J. H. Cheon, and D. H. Park, J. Mater. Chem. **11**, 3397 (2001).
16. S. S. Park, C. H. Lee, J. H. Cheon, S. J. Choe, and D. H. Park, Bull. Korean Chem. Soc. **22**, 948 (2001).
17. C. H. Lee, S. S. Park, S. J. Choe, and D. H. Park, Micropor. Mesopor. Mater. **46**, 257 (2002).
18. O. Muth, C. Schellbach, and M. Froba, Chem. Commun. 2032 (2001).
19. E-B. Cho, K-W. Kwon, and K. Char, Chem. Mater. **13**, 3837 (2001).
20. H. Zhu, D. J. Jones, J. Zajac, J. Rozière, and R. Dutartre, Chem. Commun. 2568 (2001).
21. M. C. Burleigh, M. A. Markowitz, E. M. Wong, J-S. Lin, and B. P. Gaber, Chem. Mater. **13**, 4411 (2001).
22. J. R. Matos, M. Kruk, L. P. Mercuri, M. Jaroniec, T. Asefa, N. Coombs, G. A. Ozin, T. Kamiyama, and O. Terasaki, Chem. Mater. **14**, 1903 (2002).

23. T. Ren, X. Zhang, and J. Suo, Micropor. Mesopor. Mater. **54**, 139 (2002).
24. A. Sayari, and Y. Yang, Chem. Commun. **21**, 2582 (2002).
25. S. Hamoudi, and S. Kaliaguine, Chem. Comm. 2118 (2002).
26. T. Asefa, M. Kruk, M . J. MacLachlan, N. Coombs, H. Grondey, M. Jaroniec, and G. A. Ozin, J. Am. Chem. Soc. **123**, 8520 (2001).
27. M. C. Burleigh, M. A. Markowitz, M. S. Spector, and B. P. Gaber, Langmuir **17**, 7923 (2001).
28. M C. Burleigh, M. A. Markowitz, M. S. Spector, and B. P. Gaber, Chem. Mater. **13,** 4760 (2001).
29. M. C. Burleigh, M. A. Markowitz, M. S. Spector, and B. P. Gaber, J. Phys. Chem. B **105,** 9935 (2001).
30. M. C. Burleigh, S. Dai, and E. W. Hagaman, Chem. Mater. **13**, 2537 (2001).
31. E. Cho and K. Char, Chem. Mater. **16**, 271 (2004).
32. Q. Yang, M. P. Kapoor, and S. Inagaki, J. Am. Chem. Soc. **124**, 9694 (2002).
33. A. M. Tshavhungwe, M. Layh and N. J. Coville, J. Sol-Gel Sci.Technol. **29**, 167 (2004).
34. A. M. Tshavhungwe, and N. J. Coville, J. Sol-Gel Sci. and Technol. **31**, 161 (2004).
35. A. Fukuoka, Y. Sakamoto, S. Guan, S. Inagaki, N. Sugimoto, Y. Fukushima, K. Hirahara, S. Iijima, and M. Ichikawa, J. Am. Chem. Soc. **123**, 3373 (2001).
36. X. Yuan, H. I. Lee, J. W. Kim, J. E. Yie, and J. M. Kim, Chem. Lett. **32(7),** 6501 (2003).
37. G. Cerveau, R. J. P. Corriu, C. Lepeytre, and P. H. Mutin, J. Mater. Chem. **8**, 2707 (1998).
38. G. Cerveau, R. J. P. Corriu, and E. Framery, J. Mater. Chem. **11**, 713 (2001) and references therein.
39. G. Cerveau, R. J. P. Corriu, and C. Lepeytre, J. Organomet. Chem. **548**, 99 (1997).
40. G. Cerveau, R. J. P. Corriu, and E. Framery, Polyhedron **19**, 307 (2000).
41. G. Cerveau, R. J. P. Corriu, and E. Framery, Chem. Commun. 2080 (1999).
42. G. Cerveau, R. J. P. Corriu, and E. Framery, J. Mater. Chem. **10**, 1617 (2000).

43. J. S. Beck, J. C. Vartuli, W. J. Roth, M. E. Leonowicz, C. T. Kresge, K. D. Schmitt, C. T-W. Chu, D. H. Olson, E. W. Sheppard, S. McCullen, J. B. Higgins, and J. L. Schlenker, J. Am. Chem. Soc. **114**, 10834 (1992).
44. L. Bois, A. Bonhommé, A. Ribes, B. Pais, G. Raffin, and F. Tessier, Colloids and Surfaces A: Physicochem. Eng. Aspects **221**, 221 (2003).
45. N. B. Colthup, L. H. Daly, and S. E. Wiberley, Introduction to Infrared and Raman Spectroscopy. Academic Press (3rd Ed.) (1997).
46. X. S. Zhao, G. Q. Lu, A. K. Whittacker, and G. J. Millar, J. Phys. Chem. **101**, 60. (1997).
47. V. Rebbin, M. Jakubowski, S. Potz, and M. Froba, Micropor. Mesopor. Mater. **72**, 99 (2004).
48. O. Dag, and G. A. Ozin, Adv. Mater. **13**, 1182 (2001).
49. M. A. Wahab, I. Kim, and C. Ha, Micropor. and Mesopor. Mater. **69**, 19 (2004).
50. C. J. Brinkner and G. W. Scherer, Sol-Gel Science. The Physics and Chemistry of Sol-Gel Processing, Academic Press, San Diego (1990).
51. B. Lee, and Y. Kim, Micropor. Mesopor. Mater. **50**, 77 (2001)
52. C. T. Kresge, M. E. Leonowicz, W. J. Roth, J. C. Vartuli, and J. S. Beck, Nature **359**, 710 (1992).
53. S. J. Gregg, and K. S. W. Sing, Adsorption, Surface Area and Porosity, Academic Press, London (1982).
54. K. S. W. Sing, Adv. Colloid Interface Sci. **76 – 77**, 3 (1998).
55. D. Kumar, K. Schumacher, C. du Fresne von Hohenesche, M. Grun, and K.K. Unger, Colloids and Surfaces A : Physicochem. Eng. Aspects **187–188**, 109 (2001).
56. G. Cerveau, R. J. P. Corriu, and E. Framery, Chem. Mater. **13**, 3373 (2001).

CHAPTER FIVE

In situ and post reaction cobalt ion incorporation into periodic mesoporous ethanesilica materials[1]

5.1 Introduction

Silica materials, including ordered mesoporous silicas (MCM 41) have been used as supports for cobalt-based catalysts in the Fischer Tropsch (FT) synthesis [1–3]. Co/SiO_2 catalysts with a high degree of cobalt reduction and dispersion show high activity for FT synthesis and interactions between a cobalt precursor and a catalyst support can affect these properties [3]. Periodic mesoporous organosilicas (PMOs) synthesized from organosilanes, $(R'O)_3Si\text{-}R\text{-}Si(R'O)_3$ (R,R' = alkyl groups), via the surfactant-templated sol-gel method have structures with alternating hydrophobic organic groups and hydrophilic silica layers [4 – 8]. The FT process produces large quantities of water and the presence of a hydrophobic group in a Co/silica hybrid material is expected to react differently to a conventional Co/silica mesoporous material in the FT reaction.

Herein we report on the synthesis and characterization of cobalt-incorporated organosilica materials synthesized by condensation of 1,2-bistrimethoxysilylethane (BTME) in the presence of hexadecyltrimethylammonium bromide (CTAB) as the surfactant both in the presence and absence of cobalt. Cobalt catalysts synthesized by incipient wetness addition to ethanesilica and MCM41 silica are also described. This work is a continuation of our studies on Co supported FT catalysts [9 – 11]; catalytic studies will be reported elsewhere.

[1] Published. A. M. Tshavhungwe and N. J. Coville, Journal of Sol-Gel Science and Technology 31, 161–164, 2004.

5.2 Experimental Section

5.2.1 Chemicals

1,2-Bistrimethoxysilylethane (BTME), tetraethylorthosilicate (TEOS) hexadecyltrimethylammonium bromide (CTAB) and cobalt nitrate hexahydrate were obtained from Aldrich; ammonium hydroxide was obtained from Fluka. All chemicals were used as received.

5.2.2 Synthesis

5.2.2.1 *In situ* cobalt incorporation. Cobalt incorporated ethanesilica materials were synthesized by adding different amounts of cobalt nitrate (0.05 g, 0.1 g, 0.2g and 0.4 g) to a mixture of CTAB (0.68 g; 1.86 mmol), water (28 ml) and 28 % ammonium hydroxide (8 ml; 0.0576 mol). The mixture was stirred for 30 minutes. BTME was then added so that the initial mole ratio was BTME:CTAB:NH_4OH:H_2O:$Co(NO_3)_2$ = 1: 0.293: 36: 244 : x (where x = 0.027, 0.054, 0.108 and 0.216). See Table 5.1 for material nomenclature. Stirring was continued for a further 30 minutes, followed by ageing at 80 ^oC for 4 days. The solid was suction filtered in a Büchner funnel, washed with an excess of water and dried in air overnight to give between 1 and 2 g of a grey/black powder (1 – 5 % Co loading). A portion of the sample (0.5 g) was stirred in a solution of concentrated HCl (5 ml) in methanol (200 ml) at 50 ^oC for 2 days. The solid was suction filtered, washed with water and finally with methanol (200 ml) and then dried in air. Mass losses of between 20 and 40 % were observed after solvent extraction.

5.2.2.2 Post reaction cobalt incorporation. Ethanesilica was prepared as described above for cobalt incorporated ethanesilica materials using a mixture with a mole ratio of BTME:CTAB:NH_4OH:H_2O = 1: 0.293: 36: 244. Cobalt nitrate, $Co(NO_3)_2.6H_2O$, (0.1 g and 0.2g) was then added into the support (0.2 g) via the incipient wetness method to give materials with 5 % and 10 % cobalt

loadings. MCM41 silica was prepared as described above for ethanesilica materials using a mixture with a mole ratio of TEOS:CTAB:NH_4OH:H_2O = 1: 0.293: 36: 244. Cobalt nitrate, $Co(NO_3)_2.6H_2O$, was then added into the support (0.2 g) via the incipient wetness method to give materials with 1 %, 2.5 %, 5 % and 10 % cobalt loadings. Materials were dried at 120 ^oC for 12 hours.

5.2.3 Characterization

Powder X-Ray diffraction measurements, nitrogen adsorption, thermogravimetric analyses (TGA), differential scanning calorimetry (DSC) and Raman spectroscopy measurements were used as described in Chapter 3.

5.3 Results and Discussion

5.3.1 Synthesis

Addition of a mixture of BTME to a basic solution of hexadecyltrimethylammonium bromide forms white solid materials. Materials containing cobalt form grey/black samples. Cobalt is precipitated as cobalt hydroxide during synthesis, and this hydroxide is in equilibrium with aqueous cobalt ions in the synthesis gel [12]. The precipitated cobalt hydroxide precursors are incorporated into the mesoporous organosilica framework, while the aqueous cobalt ions remain dissolved in the aqueous phase.

5.3.2 Raman spectroscopy

Raman spectra were obtained on a range of samples. A typical spectrum (for 0.1 g Co sample) is shown in Figure 5.1. The presence of CTAB was clearly seen in the 'as synthesized' materials (not shown). After solvent extraction the peaks associated with CTAB had disappeared while those due to the C-H vibrations of the BTME ethane group (2885 cm^{-1}) are still to be seen (Figure 5.1). Addition of Co yielded a material that has peaks at 686 cm^{-1} and at 480 cm^{-1} (Figure 5.1,

insert), indicative of Co_3O_4 [9]. However, no evidence for the presence of Si-O-Co-O-Si species was evident. The Co impregnated samples give similar Raman spectra to those described above.

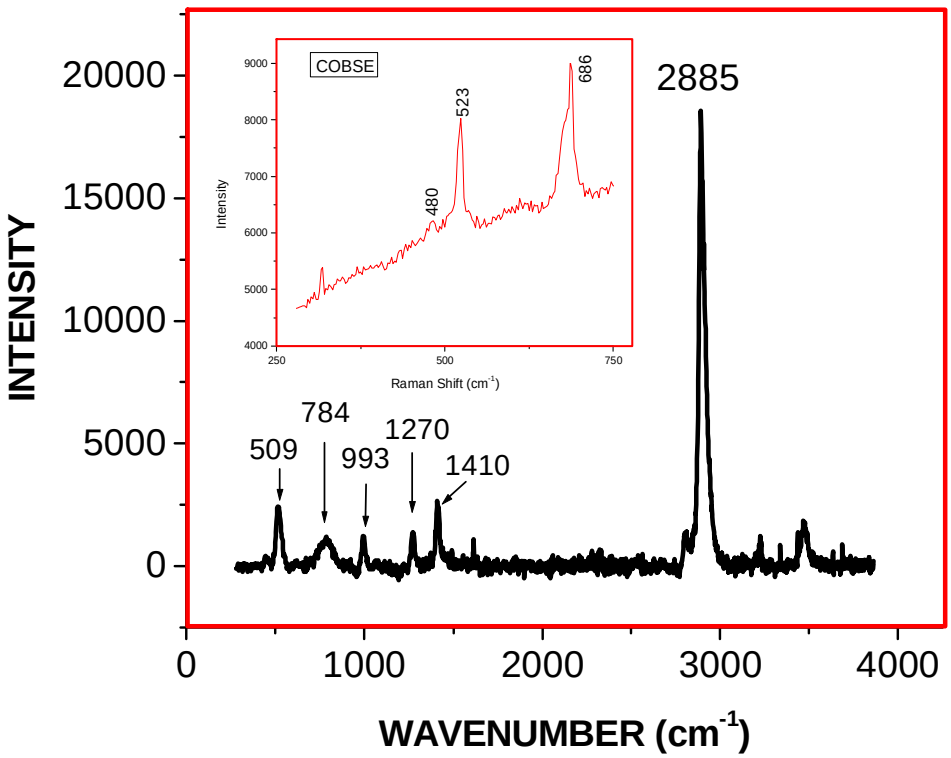

Figure 5.1 Raman spectra of solvent extracted ethanesilica and cobalt-incorporated ethanesilica (insert) prepared in the presence of 0.1 g cobalt nitrate.

5.3.3 Powder X-Ray Diffraction

The grey/black cobalt incorporated ethanesilica samples prepared in the presence of 0.05, 0.1 and 0.2 g cobalt nitrate exhibit a prominent low angle peak in the diffraction pattern at approximately $2\theta = 2^o$ (with d-spacings of 4.20, 4.45 and 4.96 nm, respectively), indicating the presence of uniformly sized mesopores in the materials [13, 14] (Figure 5.2a, Table 5.1). The sample with 0.1 g Co appears to have a major peak and a shoulder and the peaks lie in between the peaks recorded with lower and higher Co loadings. No low angle XRD peak was observed for a sample prepared in the presence of 0.4 g cobalt nitrate as well as for ethanesilica and MCM-41 silica materials impregnated with 10 % cobalt, suggesting loss of mesophase for these samples (Figure 5.3).

5.3.4 Thermal analysis

TGA (under N_2) was used to monitor the decomposition characteristics of the Co containing materials and some data are shown in Figure 5.4. The thermal decomposition of cobalt incorporated ethanesilica materials is similar to that of similar ethanesilica materials prepared without cobalt [11]. Tables 5.2 and 5.3 summarise the data obtained from the thermograms. Removal of the surfactant by solvent extraction results in the disappearance of the mass loss between 100 and 300 ^oC (Figure 5.4). The mass loss due to surfactant species also appears as an intense peak in the derivative plot (Figure 5.4) and as an exothermic peak in the differential scanning calorimetry (DSC) curve (Figure 5.5). The peak above 400 ^oC (6% mass loss) is thus attributed to the loss of the ethane groups and suggests that the material will be stable under the reducing Fischer-Tropsch reaction conditions. Similar results were obtained for the impregnated samples.

Table 5.1. Surface properties of cobalt incorporated ethanesilica materials.

Name[a]	**Description**	**SA** m^2/g	**PV** cm^3g^{-1}	**APD** nm	d_{100} nm
BE	No Co	672	0.71	0.34	4.75
0.05CoBE(in situ)	0.05 g $Co(NO_3)_2$, in situ	534	0.78	5.83	4.20
0.1CoBE(in situ)	0.1 g $Co(NO_3)_2$, in situ	438	0.48	4.34	4.45
0.2CoBE(in situ)	0.2 g $Co(NO_3)_2$, in situ				4.96
0.05CoBE(Imp.)	0.05 g $Co(NO_3)_2$, impregnated	263	0.53	8.06	
0.1CoBE(Imp.)	0.1 g $Co(NO_3)_2$, impregnated	190	0.32	6.64	

[a]Notation: B = BTME, E = extracted, Co = cobalt, the number preceding a name corresponds to the mass of $Co(NO_3)_2.6H_2O$ added.

(a)

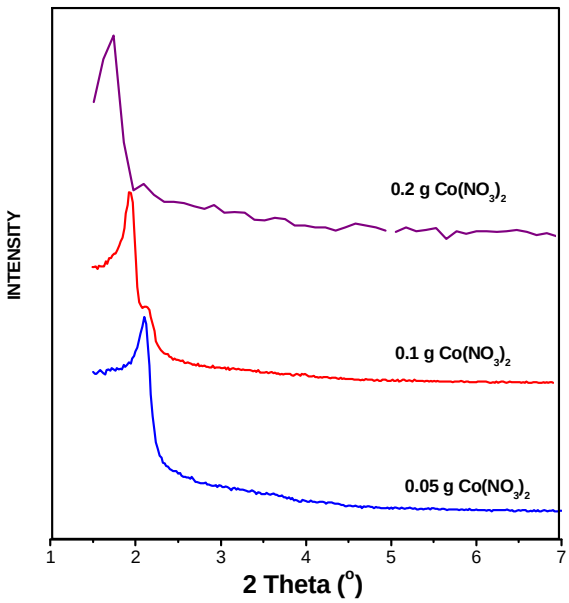

(b)

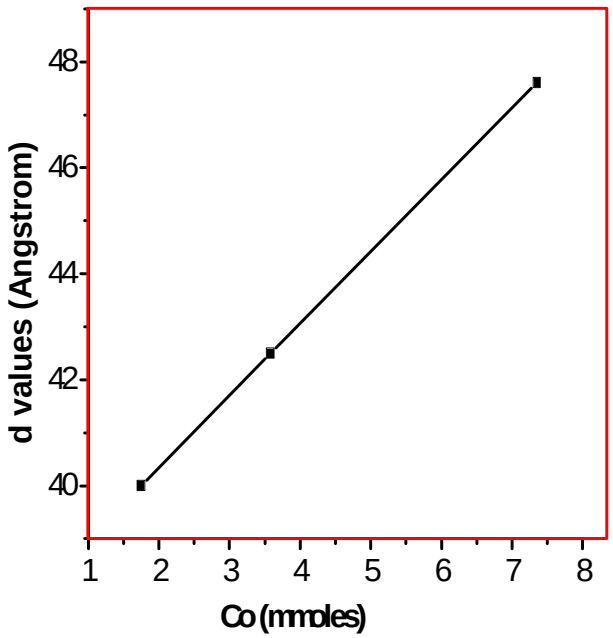

Figure 5.2 (a) Powder XRD patterns of cobalt incorporated organosilica materials prepared from BTME. (b) Variation of lattice parameter (d) with amount of cobalt added.

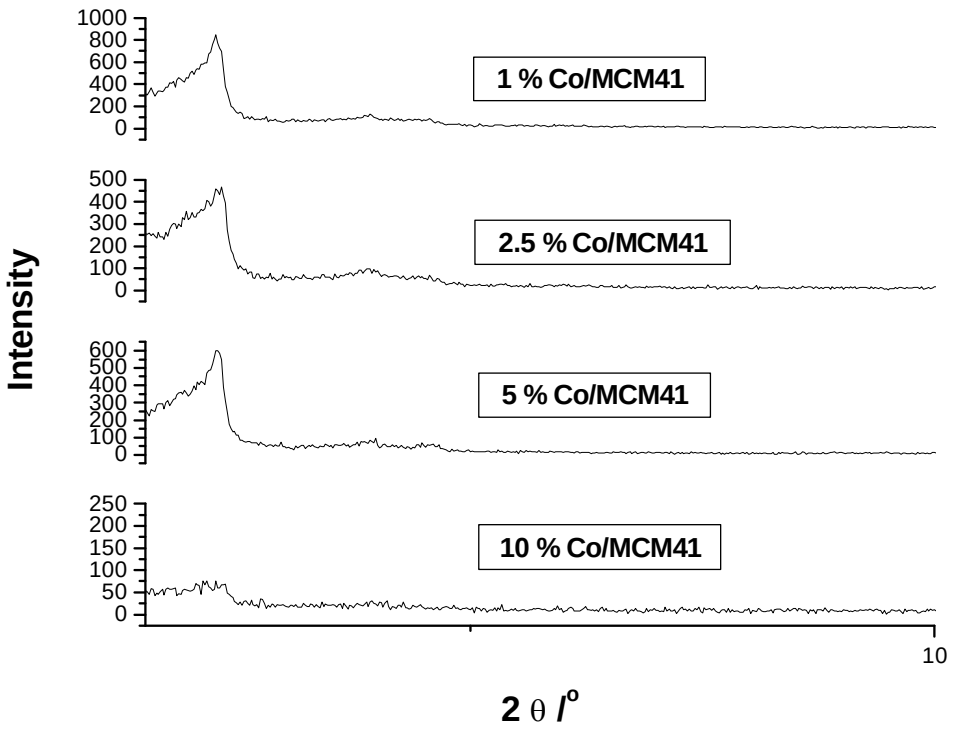

Figure 5.3 Powder XRD patterns of cobalt incorporated silica materials prepared from. TEOS.

Table 5.2 TGA results of a PMO material prepared from BTME .

Temperature range (^{o}C)	**% Mass loss of as synthesized material**	**% Mass loss of Solvent extracted material**	**Source of mass loss**
25 – 110	5 %	2 %	Desorption of methanol and water
110 – 265	30 %	-	Surfactant decomposition
310 – 440	17%	2 %	Surfactant decomposition and water from condensation of internal hydroxyls
440 – 780	10 %	10 %	Matrix decomposition

Table 5.3 TGA results of a PMO material prepared from BTME in the presence of 0.2 g cobalt nitrate.

Temperature range (^{o}C)	**% Mass loss of as synthesized material**	**% Mass loss of Solvent extracted material**	**Source of mass loss**
25 – 100	3	4	Desorption of methanol and water
100 – 400	12	2	Surfactant decomposition and Water from condensation of internal hydroxyls
400 – 800	6	6	Matrix decomposition

(a)

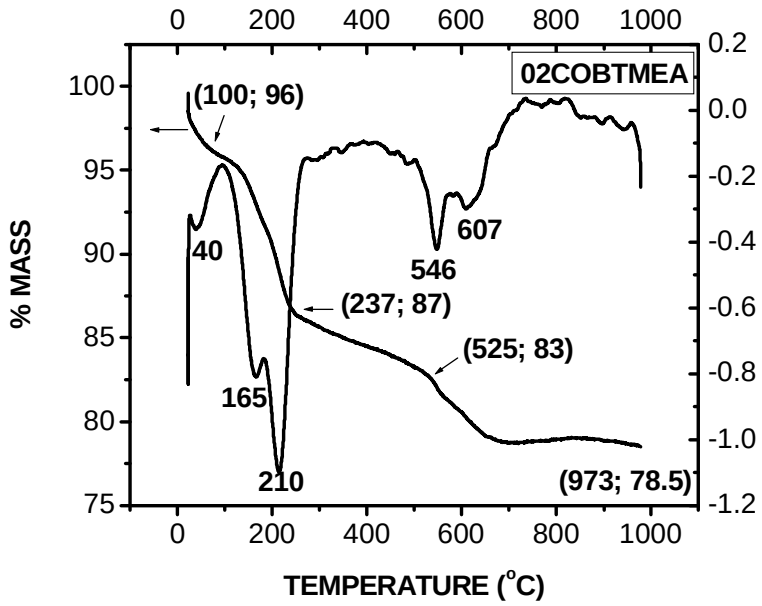

(b)

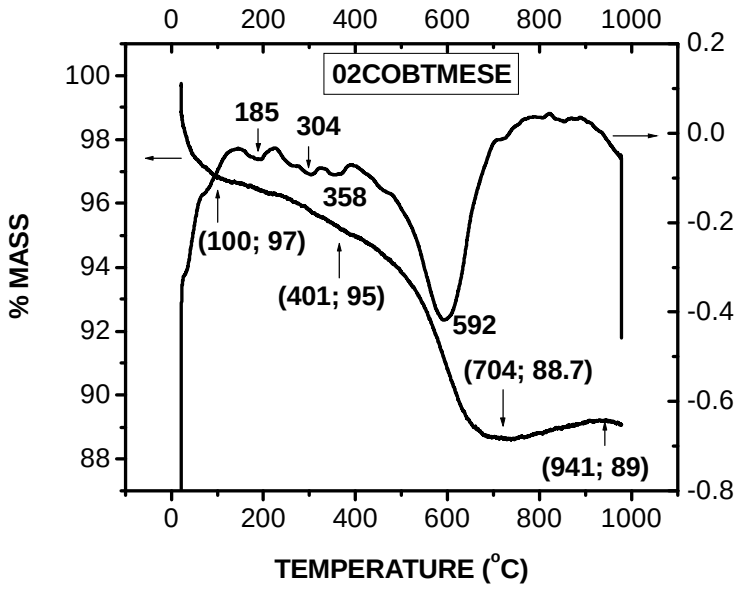

Figure 5.4 TGA curves of as synthesized (a) and solvent extracted (b) cobalt-incorporated (0.2 g) periodic ethanesilica materials.

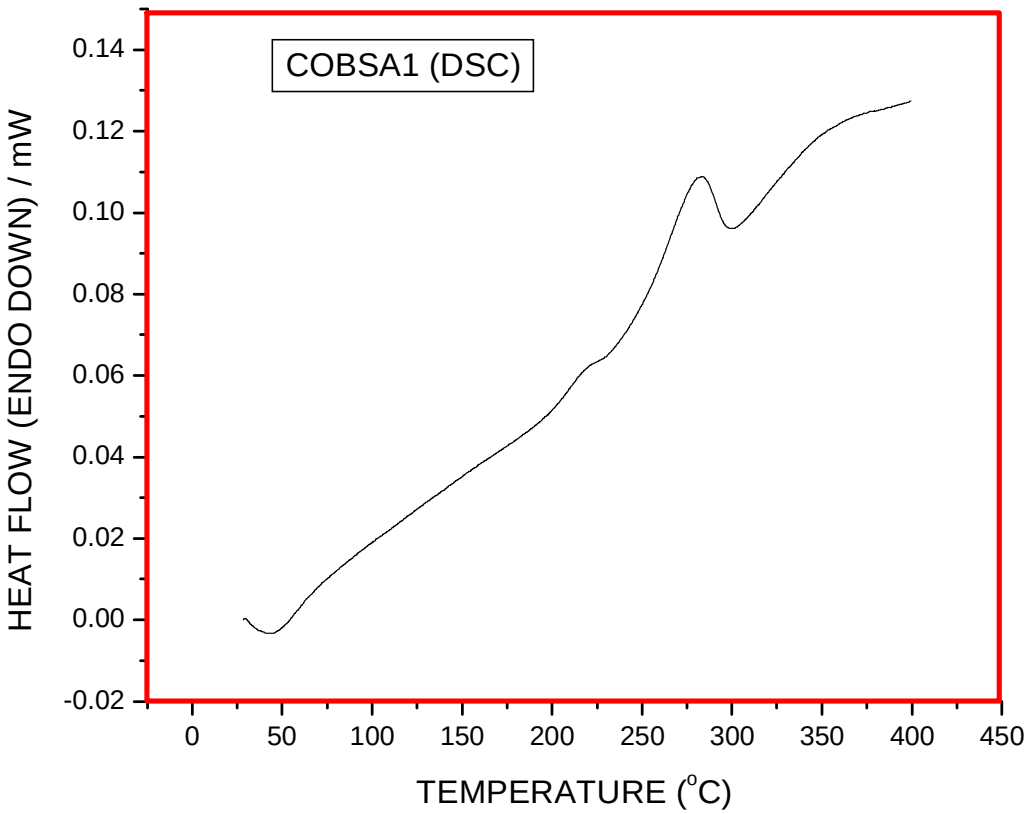

Figure 5.5 DSC curve of as synthesized cobalt-incorporated (0.1 g) periodic ethanesilica.

5.3.5 Nitrogen sorption

The nitrogen adsorption isotherm obtained for an ethanesilica material prepared in the presence of 0.1 g cobalt nitrate is similar to that obtained for ethanesilica (Figure 5.6). The materials exhibit a Type IV isotherm, characteristic of mesoporous materials, with a Type H3 hysteresis loop [15]. A narrow pore size distribution (PSD) with a maximum value at 2.2 nm is observed for both samples. The wall thicknesses, obtained by subtracting the pore size from the lattice parameter, $a_o = 2d/(3)^{1/2}$, are 3.3 and 2.9 nm, respectively.

Similar results were obtained for the Co containing materials prepared by incipient wetness. As expected, the surface area and pore volume decrease as the cobalt incorporation increases (Figure 5.7). Type IV isotherms with narrow pore size distributions are also obtained for MCM41 silica and cobalt incorporated MCM41(Figure 5.8). As shown in Figure 5.8(a), the shape of isotherms does not change after loading cobalt by the incipient wetness method.

The surface areas and pore volumes of the materials prepared by the impregnation method are lower than the corresponding values of the materials prepared by *in situ* procedure (Table 5.1). Presumably, in the impregnation method all the Co nitrate fills the pores while in the in situ method the Co is incorporated in the framework to form Co-O-Si bonds and hence the Co does not block the pores as effectively.

(a)

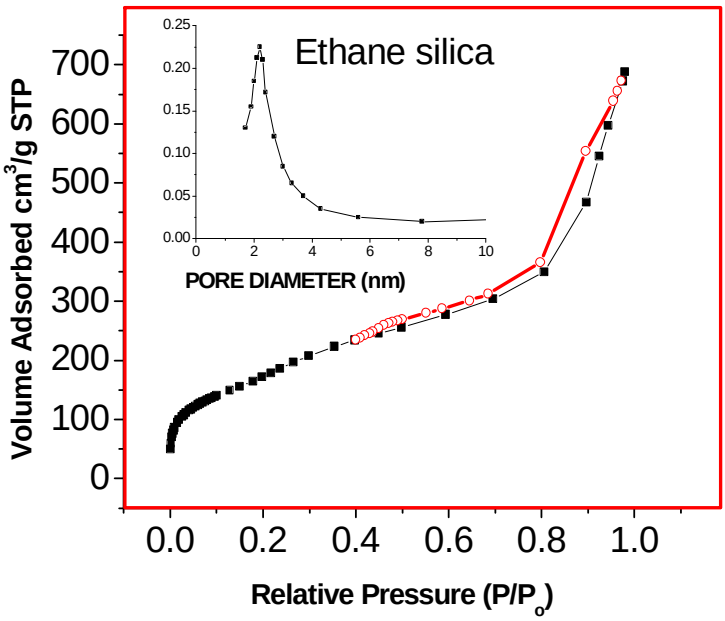

(b)

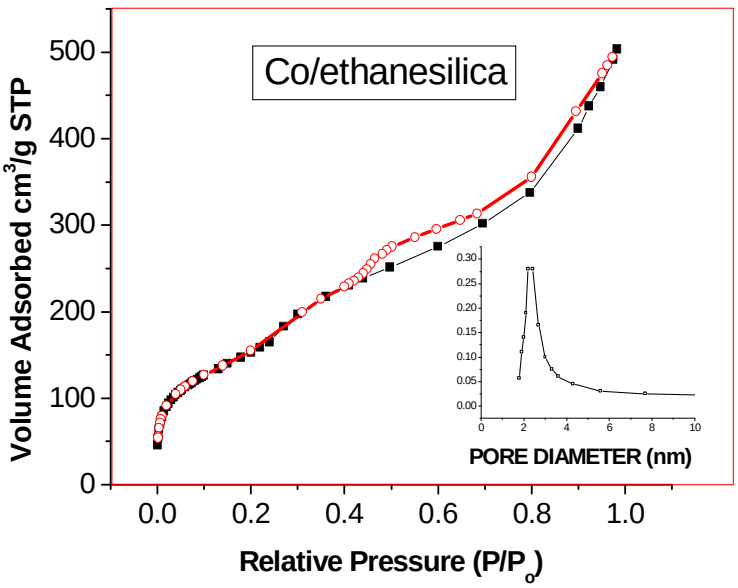

Figure 5.6 Nitrogen adsorption desorption isotherm and adsorption PSD (insert) of an ethanesilica material (a) and cobalt incorporated ethanesilica material (b) synthesized in the presence of 0.1 g cobalt nitrate.

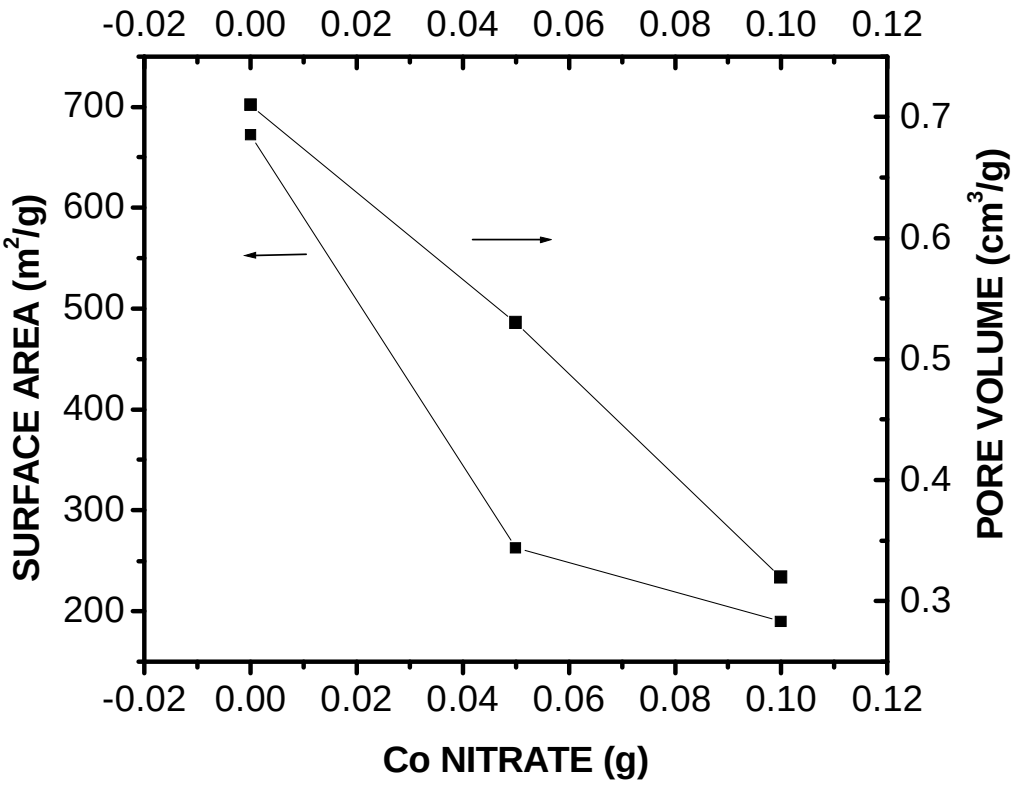

Figure 5.7 Variation of BET surface area or pore volume with amount of cobalt nitrate for cobalt impregnated ethanesilica materials.

(a)

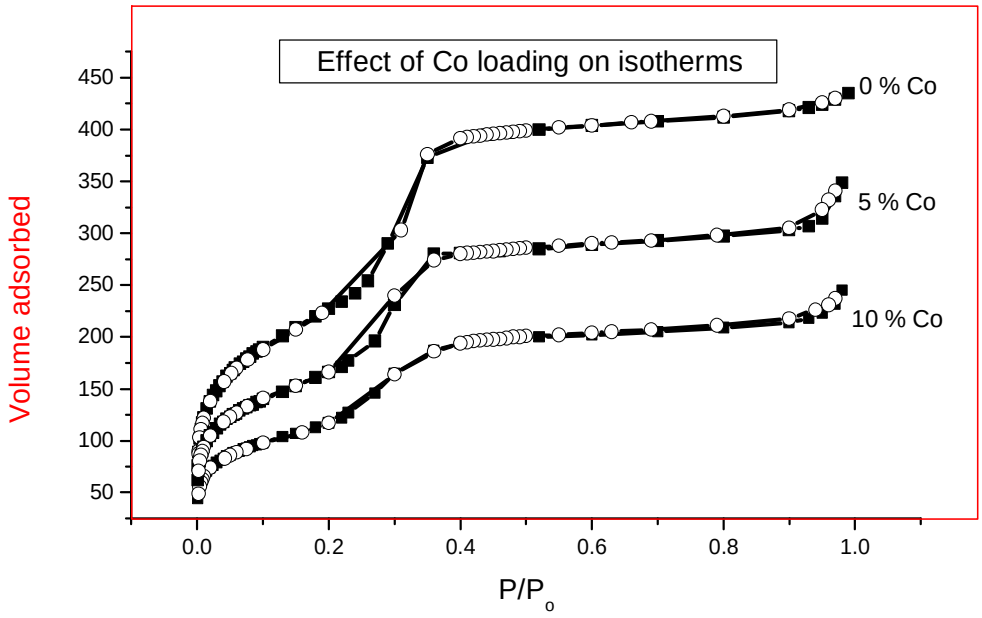

(b)

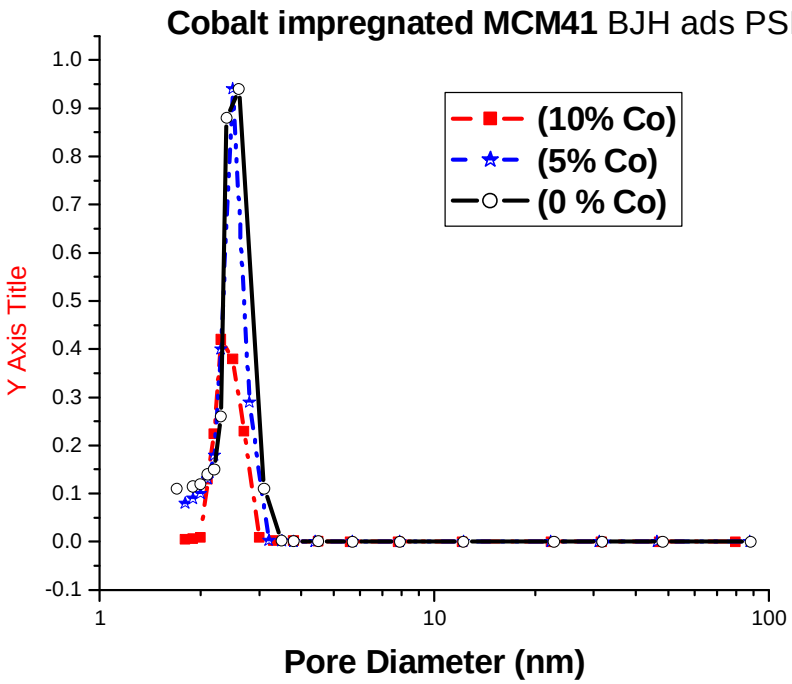

Figure 5.8 Nitrogen adsorption desorption isotherms (a) and BJH pore size distributions derived from adsorption isotherms (b) of MCM-41 silica and cobalt incorporated MCM-41 silica materials.

5.4 Conclusions

Periodic mesoporous organosilica materials (consisting of ethane groups in the framework) containing Co were synthesized. The XRD and pore volume data indicate that while the Co modifies the BTME containing material the essential mesoporous structure is maintained at the Co loadings studied (5% co-impregnated; 10% incipient wetness). Most significant was the finding that the ethane portion of the material only decomposed at temperatures > 400 ^{o}C. All the above data indicate that the new materials have potential in the FT reaction. It is apparent that both synthesis processes yield Co/SiO_2 materials with similar Raman and XRD characteristics but that differ in surface area and porosity.

5.5 References

1. Y. Ohtsuka, T. Arai, S. Takasaki, and N. Tsubouchi, Energy and Fuels **17**, 804 (2003).
2. A. Y. Khodakov, A. Griboval-Constant, R. Bechara, and F. Villain, J. Phys. Chem. B **105**, 9805 (2001).
3. G. Bian, T. Machizuki, N. Fujishita, H. Namoto, and M. Yamada, Energy and Fuels **17**, 8799 (2003).
4. S. Inagaki, S. Guan, Y. Fukushima, T. Ohsuna, and O. Terasaki, J. Am. Chem. Soc. **121**, 9611 (1999).
5. B. J. Melde, B. T. Holland, C. F. Blanford, and A. Stein, Chem. Mater. **11**, 3302 (1999).
6. T. Asefa, M. J. MacLachlan, N. Coombs, and G. A. Ozin, Nature **402**, 867 (1999).
7. A. Sayari, and S. Hamoudi, Chem. Mater. **13**, 3151 (2001).
8. W. Guo, J. Park, M. Oh, H. Jeong, W. Cho, I. Kim, and C. Ha, Chem. Mater. **15**, 2295 (2003).
9. J. Li, and N.J. Coville, Appl. Catal. A **181**, 201 (1999).
10. N. N. Madikizela, and N. J. Coville, J. Molec. Catal. A: General **181**, 129 (2002).

11. A. M. Tshavhungwe, M. Layh, and N. J. Coville, J. Sol-Gel Science and Technol. **29**, 167 (2004).
12. T. Vralstada, G. Øye, M. Rønning, W. R. Glomm, M. Stocker, and J. Sjoblom, Micropor. Mesopor. Mater. **80**, 291 (2005)
13. J. S. Beck, J. C. Vartuli, W. J. Roth, M. E. Leonowicz, C. T. Kresge, K. D. Schmitt, C. T-W. Chu, D. H. Olson, E. W. Sheppard, S. McCullen, J. B. Higgins, and J. L. Schlenker, J. Am. Chem. Soc. **114**, 10834 (1992).
14. C. T. Kresge, M. E. Leonowicz, W. J. Roth, J. C. Vartuli, and J. S. Beck, Nature **359**, 710 (1992).
15. S. J. Gregg, and K. S. W. Sing, Adsorption, Surface Area and Porosity (Academic Press, London, 1982).

CHAPTER SIX

A systematic study of factors governing the co-condensation of 1,2-bistrimethoxysilylethane and tetraethylorthosilicate

---

6.1 Introduction

Alkoxysilane (e.g. tetraethylorthosilicate) and silsequioxane precursors (e.g. 1,2-bistrialkoxysilylethane are commonly used to synthesize silica and hybrid organic-inorganic silica materials [1 – 3]. Periodic mesoporous silica [4, 5] and periodic mesoporous organosilica materials (PMOs) [6 – 21] are obtained from these monomers via the surfactant templated sol-gel method. PMOs possess high surface areas and uniformly sized channel mesopores similar to those of MCM41-type silicas.

Hybrid mesoporous materials with different proportions of organic groups in the framework in the channel walls can be synthesized from a mixture of a tetraalkoxysilane (e.g. tetraethylorthosilicate) and a precursor containing bridging organic groups (e.g. bridged silsesquioxanes such as 1,2-bistrialkoxysilylethane). Ordered materials with a framework composition intermediate between those of pure silica and pure organic PMO materials have previously been synthesized by co-condensation of tetraethylorthosilicate (TEOS) and bistriethoxysilylethane [8], TEOS and bistriethoxysilyl*m*ethane [18], as well as TEOS and bistrimethoxysilylethane (BTME) [19]. Ozin et. al. [8] reported 2-D hexagonally ordered PMOs with ethylene groups using hexadecyltrimethylammonium ions. Char et al [19] described the synthesis of mesoporous organosilicas from the co-condensation of TEOS and BTME by using polyethylene oxide-containing triblock copolymer templates.

Herein we report on the synthesis of periodic mesoporous ethanesilica by co-condensation of BTME and tetraethylorthosilicate (TEOS) in the presence of hexadecyltrimethylammonium bromide (CTAB) under basic conditions. For the purpose of developing catalysis applications, cobalt has been incorporated into the periodic mesoporous materials. The effect of cobalt incorporation on the porous structure of these materials is examined. The ageing temperature and ratio of BTME to TEOS were varied systematically in order to study their effect on the mesophase formed and on the surface properties of the synthesized materials.

6.2 Experimental Section

6.2.1 Reagents and Chemicals

1,2-Bistrimethoxysilylethane (BTME) and hexadecyltrimethylammonium bromide (CTAB) were obtained from Aldrich; Tetraethylorthosilicate (TEOS), ammonium hydroxide and hydrochloric acid were obtained from Fluka. All chemicals were used as received. Deionised water was used in the synthesis. The molecular structures and abbreviations of the silica precursors and the surfactant used are shown in Table 6.1.

6.2.2 Synthesis

6.2.2.1 Co-condensation of BTME with TEOS. PMOs were prepared using a modified method based on that reported by Ozin and co-workers [8, 18]. A series of materials was prepared starting with a mole ratio of BTME:TEOS:CTAB:NH_4OH:H_2O = 1: x : 0.293: 14: 244 (where x = 0, 0.5, 1.0, 2.0, and 4.0). Cobalt nitrate (0.1 g) was added to the reaction mixture when preparing *in situ* cobalt incorporated materials. Amounts of the silica precursors used as well as the notation employed to name the samples are given in Table 6.2. The synthesized materials were used to study the influence of the BTME:TEOS ratio, the ageing temperature, ageing length and cobalt incorporation on the textural properties of PMO materials.

Table 6.1 Molecular structures of silica sources and surfactant molecule

Molecular Structure	**Name and abbreviation**
$(CH_3O)_3Si$ 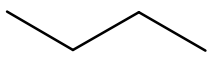 $Si(OCH_3)_3$	1,2-bistrimethoxysilylethane (BTME)
$Si(OCH_2CH_3)_4$	Tetraethylorthosilicate (TEOS)
 $N^+(CH_3)_3Br^-$	Hexadecyltrimethylammonium bromide (CTAB)

Table 6.2 Amounts of silica precursors used.

Sample[a]	**BTME/ mmol**	**TEOS/ mmol**	**BTME:TEOS (mole ratio)**	**% TEOS** [b]
BT100 and CoBT100	0	14.3		100
BT67 and CoBT67	7.14	28.6	1:4	67
BT50 and CoBT50	7.14	14.3	1:2	50
BT36 and CoBT36	7.14	8.07	1:1.1	36
BT20 and CoBT20	7.14	3.57	1:0.5	20
BT0 and CoBT0	7.14	0	1:0	0

[a]*Note that the letters A or E and the ageing temperature (as described in Section 6.2.3) are omitted from the sample names.*

[b]*% TEOS = mol TEOS/ [2(mol BTME) + mol TEOS]*

6.2.2.2 Typical synthesis. In a typical synthesis, CTAB (0.68 g; 1.86 mmol) was dissolved in a solution consisting of water (28 ml) and 28 % ammonium hydroxide (14 ml; 0.10 mol). Cobalt nitrate (0.1 g) was added to the reaction mixture when preparing *in situ* cobalt incorporated materials. The mixture was stirred for 30 minutes. BTME (1.8 ml; 7.14 mmol) and TEOS (varying amounts: 0 ml, 0.8 ml, 1.6 ml, 3.2 ml and 6.4 ml) were simultaneously added dropwise to the stirred mixture. Stirring was continued for a further 30 minutes, followed by ageing at 80 ^{o}C for 4 days. The solid was filtered and washed with copious amounts of water (> 5 L). The solid was dried in air overnight. This material is referred to as the "as-synthesized" material.

6.2.2.3 Solvent extraction. A portion of the as synthesized sample (1.5 g) was stirred in a solution of concentrated HCl (5 ml) in methanol (200 ml) at 50 ^{o}C for 2 days. The solid was filtered, washed with water (> 1.5 L) and finally with methanol (200 ml) and then dried in air. This material is referred to as the "solvent extracted" material.

6.2.3 Nomenclature

The amounts of BTME and TEOS as well as the percentage of TEOS in the reaction mixture are presented in Table 6.2. The percentage TEOS indicates the mole percentage of TEOS expressed per mole of silicon atoms in the BTME and TEOS silica precursors {% TEOS = [100 x (mol Si in TEOS)/(moles Si in BTME + mol Si in TEOS)] = [100 x (mol TEOS)/(2 x moles BTME) + mol TEOS]}. The moles of BTME are multiplied by 2 because each BTME molecule supplies two moles of Si whereas a TEOS molecule supplies one. The notation used to identify the samples is as follows: T = TEOS, B = BTME, Co = cobalt, A = as synthesized and E = extracted. Numerical figures preceding the letter *E* refer to the % TEOS in the reaction mixture. Numerical figures following the letter *E* refer to the ageing temperature. For example, CoBT20E80 refers to an extracted (*E*) sample synthesized from BTME (*B*) and TEOS (*T*) in the presence of cobalt

nitrate (*Co*). The amount of TEOS in the reaction mixture is 20 % by mole of Si atoms (20). The material was aged at 80 ^{o}C.

6.3 Results and discussion

6.3.1 Synthesis

Materials containing variable ratios of 1,2-bistrimethoxysilyethane (BTME) and tetraethylorthosilicate (TEOS) were synthesized by the surfactant-templated sol-gel co-condensation reaction of BTME with TEOS in basic conditions. The base catalysed surfactant templated formation of periodic mesoporous ethanesilica is proposed to form from micelles as described in Chapter 4. A pure inorganic silica material (MCM41) and a material containing 100 % BTME were synthesized from TEOS and BTME, respectively. Cobalt nitrate (0.1 g) was added to the reaction mixture when preparing *in situ* cobalt incorporated materials. For all the syntheses a white precipitate formed within 30 minutes after addition of the silica source to a mixture of CTAB, water and ammonium hydroxide. The amount of the precipitate formed generally increased with the amount of the silica source used.

To investigate if the amount of the silica source had any significant effect on XRD patterns and nitrogen adsorption data, the BTME to TEOS ratio was varied by increasing the amount of TEOS while keeping the amount of BTME constant. This is tantamount to increasing the ratio of silicon precursor to surfactant. This study was done using ethanesilicas prepared with and without addition of cobalt ions in the reaction mixture.

6.3.2 Raman Spectroscopy

The Raman spectrum of a solvent extracted ethanesilica material prepared by co-condensation of TEOS (20 %) with BTME (BT20E80), shown in Figure 6.1 (b), is similar to the Raman spectrum of ethanesilica prepared from BTME alone (Figure

6.1 (a). Band assignments for fundamental IR and Raman bands of ethanesilica were described in detail in Chapter 4. The peaks observed at 2887 cm^{-1} in the Raman spectra of solvent extracted materials are assigned to CH stretching vibrations of BTME. The presence of the peak at 517 cm^{-1} indicates that the Si-C bond is still intact [20 – 22].

(a)

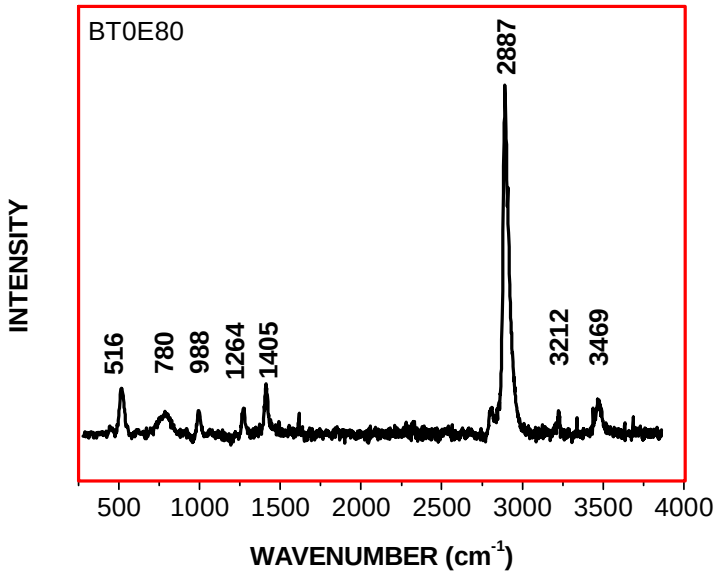

(b)

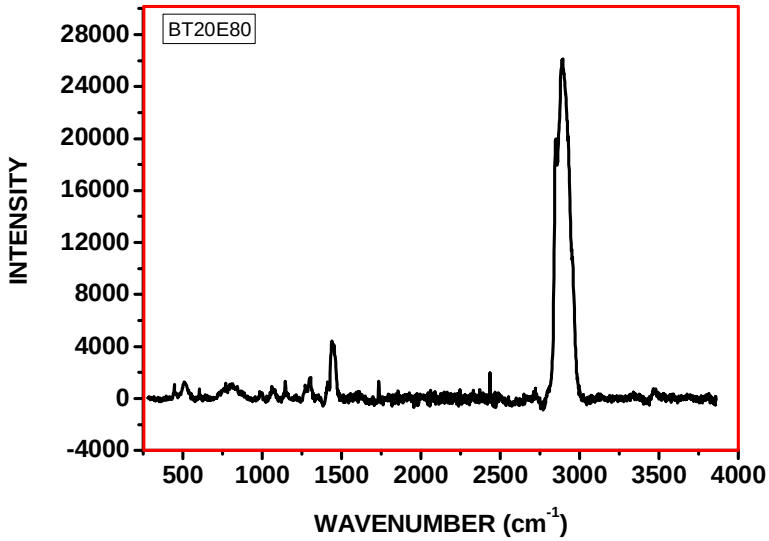

Figure 6.1 Raman spectra of (a) solvent extracted ethanesilica synthesized from BTME (BT0E80), and (b) solvent extracted ethanesilica material prepared by co-condensation of TEOS with BTME (BT20E80).

6.3.3 Thermal analysis

Samples were analysed before and after solvent extraction using thermogravimetric analysis (TGA). Analysis was conducted from room temperature to 1000 ^{o}C. Typical thermograms of the surfactant extracted PMO materials prepared from BTME and TEOS (20 % and 67%) in the presence of cobalt nitrate are shown in Figures 6.2 (a) and 6.2 (b), respectively. The mass loss observed between 400 and 600 ^{o}C is attributed to decomposition of ethane fragments [17]. The mass loss observed below 100 ^{o}C is due to adsorbed water and methanol.

6.3.4 Powder X-ray diffraction

6.3.4.1 Influence of the BTME:TEOS ratio and cobalt incorporation. Ethanesilica materials (BT20E80, BT50E80 and BT67E80) and cobalt incorporated ethanesilica materials (CoBT20E80, CoBT50E80 and CoBT67E80) synthesized by co-condensation of BTME with TEOS and aged at 80 ^{o}C were used to study the effect of the amount of TEOS and cobalt incorporation on XRD lattice parameters. All samples exhibit a prominent low angle peak in the diffraction pattern at approximately $2\theta = 2^{o}$, indicative of the periodicity of these materials (Figures 6.3 – 6.5) [23, 24]. Lattice spacings (d-values) of the most intense peak for PMO materials synthesized with and without cobalt are listed in Table 6.3

Ethanesilica. Figure 6.3 shows XRD patterns of an as synthesized and a solvent extracted ethanesilica material prepared with a BTME:TEOS mole ratio of 1:0.5 (samples BT20A80 and BT20E80, respectively). Low intensity peaks are better resolved after solvent extraction. The low angle diffraction pattern observed for BT20A80 and BT20E80 (Figure 6.3) differs from that observed for MCM41 (Figure 6.4D). Two well defined peaks and a shoulder appear in the 2θ range 1.5 – 2.5^{o} with d spacings of 4.93, 4.47 and 3.99 nm. In addition three poorly resolved peaks are also observed between 2 and 4^{o}. This pattern resembles that found for

SBA1 silica synthesized using an oligomeric alkyl-ethylene oxide surfactant [25]. Based on this similarity, the XRD pattern of BT20E80 can be indexed as a cubic mesophase belonging to the P*m*3*m* space group, with lattice parameters d_{210}, d_{211}, d_{300}, d_{310}, d_{411} and d_{331} [25]. The d values of the d_{210}, d_{211}, d_{300} and d_{310} inflections are 4.93, 4.47, 3.99 and 2.68 nm respectively.

The position of the d_{300} inflection coincides with the position of the d_{100} peak of MCM 41(see Figure 6.4A and 6.4D). The appearance of the d_{310}, d_{411} and d_{331} reflections indicate that the mesoporous material has a high degree of mesoscopic order**.** Hybrid ethane-siloxane mesoporous materials with cubic symmetry (Pm3n) have been reported [26]**.** The mesoporous methylene (-CH_2-) organosilica materials synthesized from TEOS and bistriethoxysilyl*me*thane using a method similar to the one we used were of 2-D hexagonal symmetry [18]**.**

The XRD pattern of BT50E80 has a broad peak whereas that of BT67E80 is relatively sharp (Figure 6.4C and D). The position of the main peak in BT67E80 is closer to the position of the peak observed in MCM41 (Figure 6.4D), although the intensity of the peak is reduced and the other peaks observed in the pattern of MCM41 are not well resolved in the pattern of BT67E80.

Cobalt incorporated ethanesilica. All cobalt incorporated samples, synthesized under the same conditions as the materials without cobalt, exhibit a prominent low angle peak in the diffraction pattern at approximately $2\theta = 2^o$ (Figure 6.5). The splitting pattern present in the XRD pattern of BT20E80 (Figure 6.3) is not observed in the XRD pattern of CoBT20E80. The XRD pattern of CoBT20E80 only has a broad peak and a shoulder, which may be indicative of the formation of a cubic or 3-D hexagonal mesophase. The low intensity peaks of cobalt-incorporated materials aged at 80 ^oC are not well resolved, if not absent, compared to the corresponding materials without cobalt (compare XRD patterns of BT20E80 and CoBT20E80), indicating the loss of long range order.

Lattice parameters (d-values) of the most intense peak for PMO materials synthesized with and without cobalt are listed in Table 6.3 and plotted in Figure 6.6. There is a shift to lower d values as the amount of TEOS in the reaction mixture increases.

From the observations above it can be concluded that increasing the amount of TEOS in the co-condensation sol-gel reaction of BTME and TEOS favours the formation of a hexagonal mesophase whereas materials containing no TEOS or low amounts of TEOS (i.e. more BTME) favour the formation of a cubic mesophase. By comparing d-values of materials with and without cobalt, it can be concluded that cobalt inclusion results in larger d values (Figure 6.6).

(a)

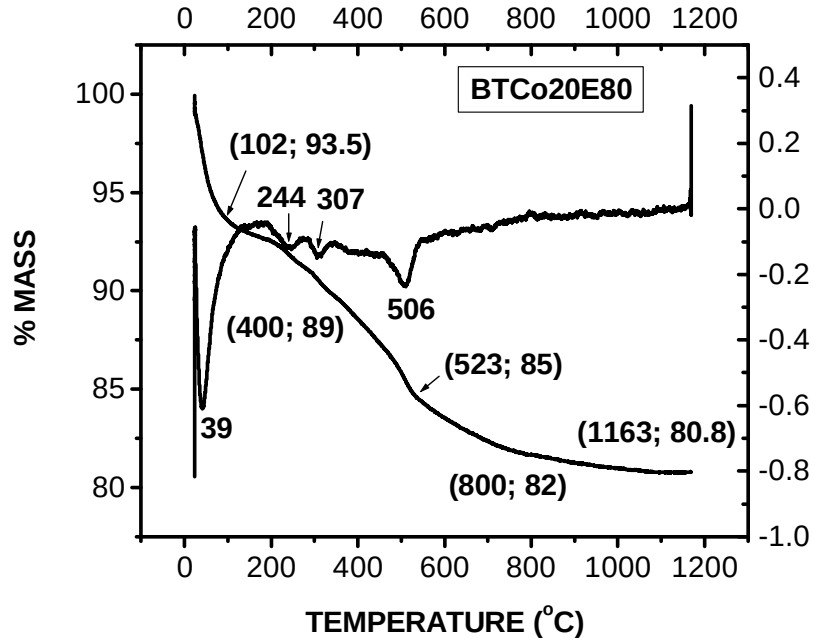

(b)

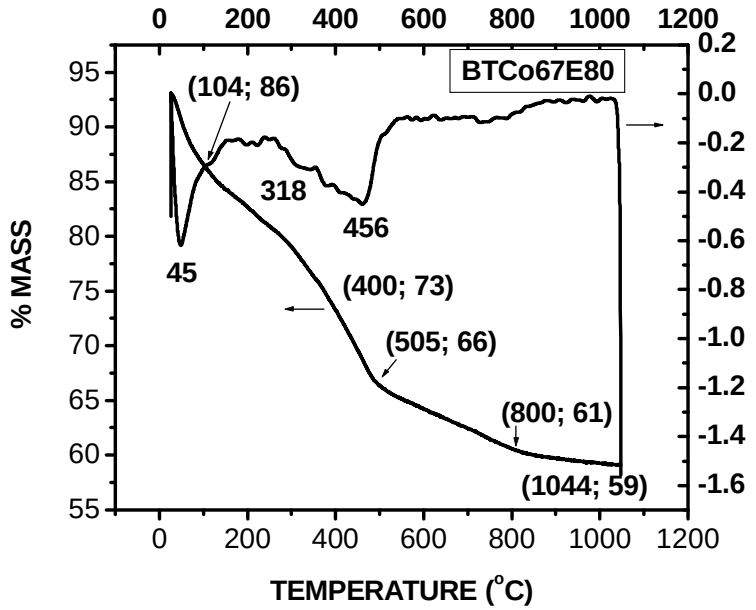

Figure 6.2 TGA and derivative TGA curves of extracted cobalt-incorporated periodic ethanesilica materials. (a) CoBT20E80 and (b) CoBT67E80.

Table 6.3 Surface properties of PMOs synthesized from BTME and TEOS.

Sample	**% TEOS**	**Ageing Temperatute (°C)**	**Lattice Parameter, d (nm)[a]**	**Surface Area (m^2/g)**	**Pore Volume (cm^3/g)**	**Average Pore Diameter (nm)**
BT0E80	0	80	4.23	686	0.92	5.3
BT20E80	20	80	4.93/4.47	25.8	0.12	18.3
BT50E80	50	80	4.76	*nd*	*nd*	*nd*
BT67E80	67	80	4.16	428	0.66	6.17
BT100E80	100	80	3.99	571	0.49	3.41
CoBT20E27	20	27	4.32	636	0.54	3.40
CoBT20E55	20	55	5.40/5.02	639	0.64	4.01
CoBT20E80	20	80	5.35/4.38	359	0.58	6.48
TBCo50E55	50	55	5.19	*nd*	*nd*	*nd*
CoBT50E80	50	80	4.92	399	0.61	6.13
CoBT67E27	67	27	4.88/4.41	858	0.71	3.30
CoBT67E55	67	55	4.45	582	0.75	5.14
CoBT67E80	67	80	4.76/4.41	483	0.53*	4.40

[a]Where a doublet or shoulder exist, two values are listed.

*Pore volume at $P/P_0 = 0.92$ instead of $P/P_0 = 0.98$ used for other values.

nd = values not determined.

Table 6.4 DFT and BJH pore diameters obtained from adsorption and desorption isotherms.

	DFT		**BJH ADSORPTION PSD**		**BJH DESORPTION PSD**	
Sample	**Micropore diameter (nm)**	**Mesopore diameter (nm)**	**Pore diameter range (nm)**	**Average diameter (nm)**	**Pore diameter range (nm)**	**Average diameter (nm)**
BT20E80	1.8	2.7 14.8				
CoBT0E80	1.4	2.9	2.4 – 2.2	2.2	3.3 – 3.2	3.3
CoBT20E27			2.5 – 2.4	2.5		
CoBT20E55			2.8 – 2.5	2.7		
CoBT20E80	1.3	3.2 9.3	2.8 – 2.5	2.7	2.6 – 2.3 3.3 – 3.2 10.4 – 6.1	2.4 3.2 7.2
CoBT50E80	1.3	3.2	2.5 – 2.4	2.4	2.9 – 2.6 3.4 – 3.3	2.8 3.3
CoBT67E27			2.4 – 2.3	2.3		
CoBT67E55			2.5 – 2.4	2.4		
CoBT67E80	1.3	2.9	2.5 – 2.4	2.4	2.5 – 2.3 3.2 – 2.7	2.4 2.9 sh.

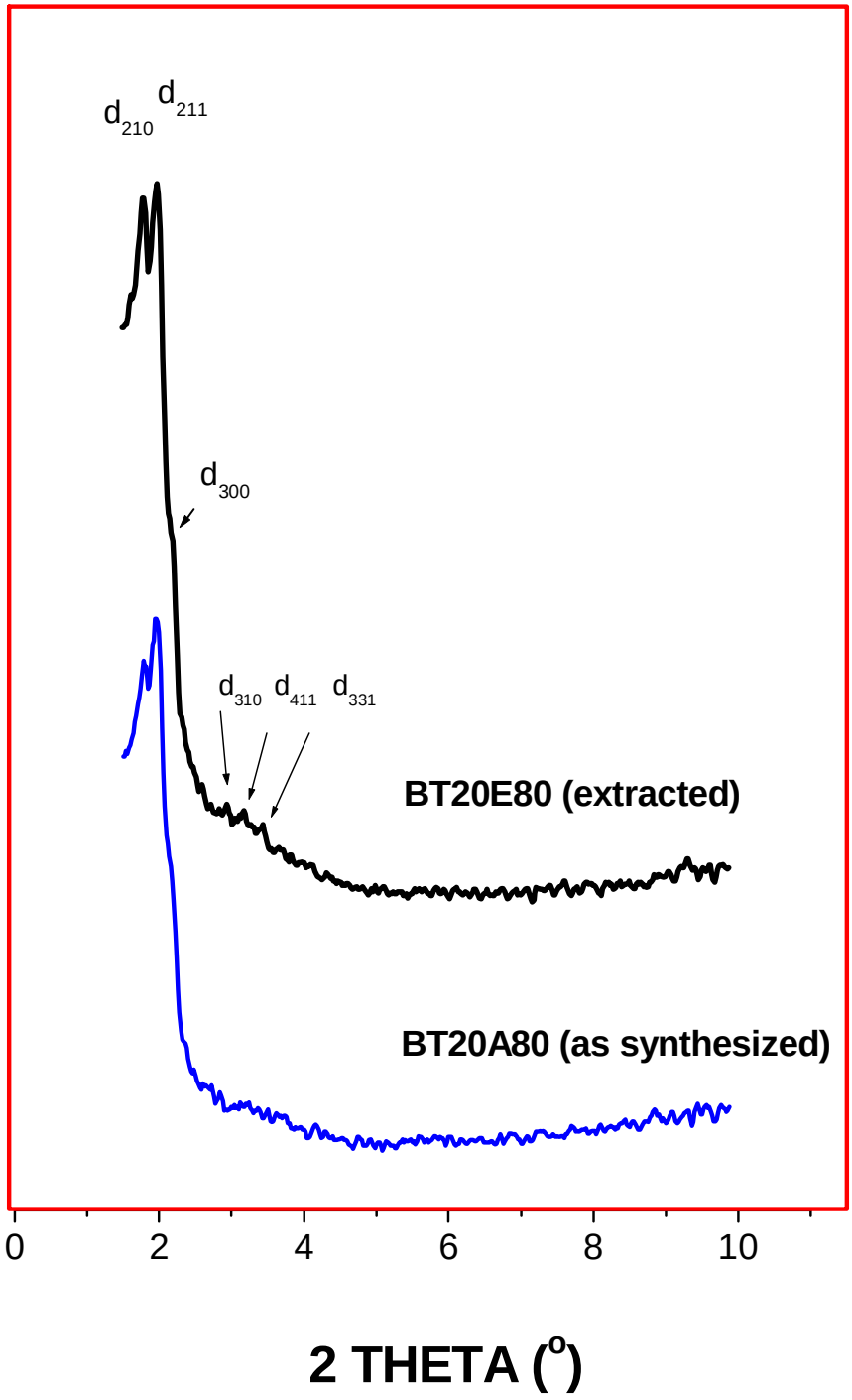

Figure 6.3 Powder XRD patterns of as synthesized (BT20A80) and solvent extracted (BT20E80) ethanesilica PMO materials containing 20 % TEOS.

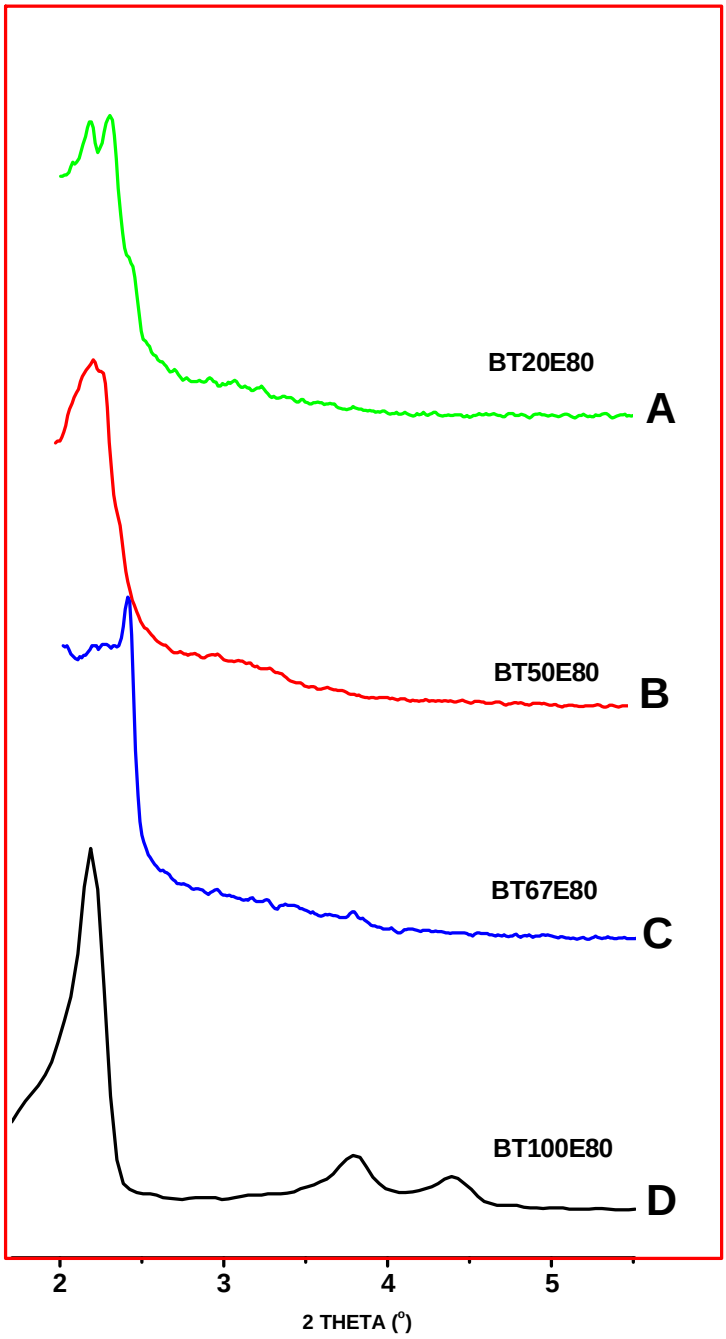

Figure 6.4 Powder XRD patterns of organosilica materials prepared from TEOS and BTME and aged at 80 °C.

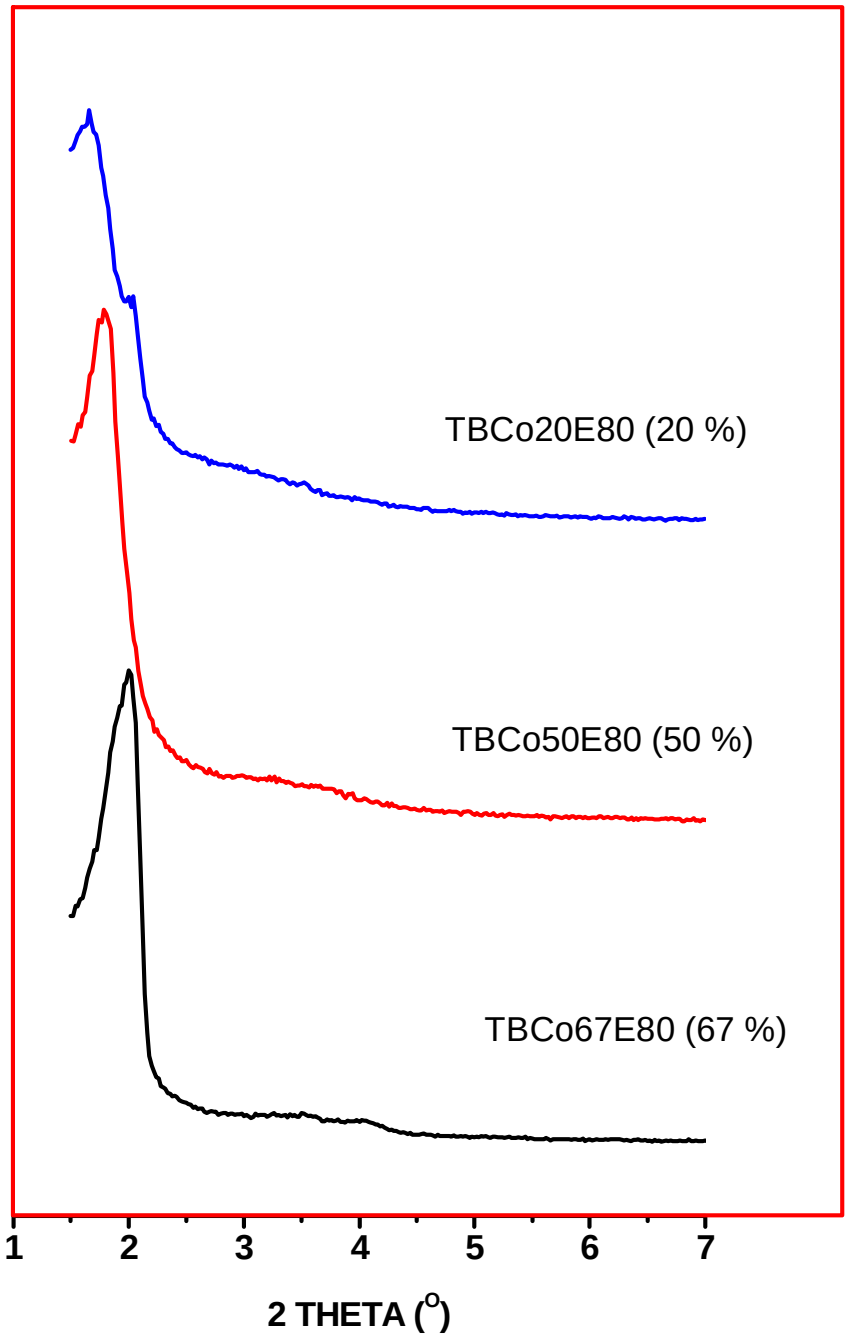

Figure 6.5 Powder XRD patterns of extracted cobalt incorporated ethanesilica materials synthesized from BTME and TEOS and aged at 80 ^{o}C.

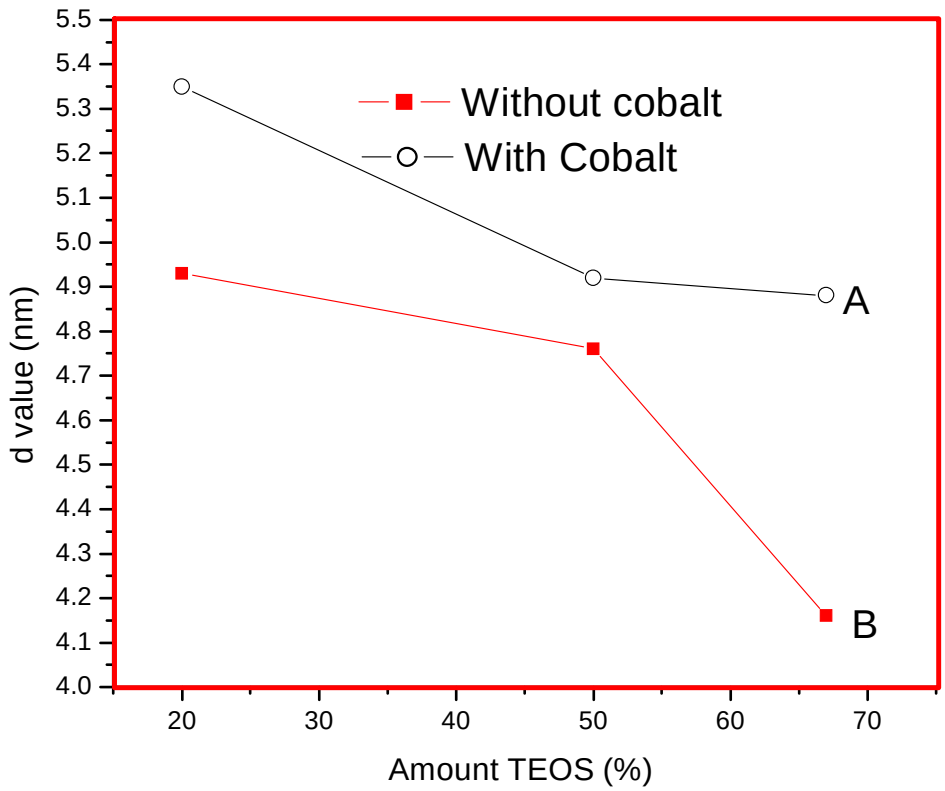

Figure 6.6 Variation in lattice parameter as a function of the amount of TEOS in the reaction mixture for ethanesilica (A) and cobalt-incorporated ethanesilica (B) materials.

6.3.4.2 Influence of the ratio of precursors and the ageing temperature. To study the effect of varying the BTME:TEOS ratio and the effect of ageing temperature, cobalt incorporated ethanesilica materials were prepared by co-condensation of BTME and TEOS and aged at 80 ^{o}C, 55 ^{o}C and room temperature (27 ^{o}C). The XRD patterns of extractedmaterials are shown in Figures 6.5, 6.7 and 6.8, respectively. Lattice parameters are listed in Table 6.3.

Ratio of precursors. The XRD patterns of materials with more TEOS (CoBT67E80 and CoBT50E80) have an XRD peak similar to that of the corresponding material prepared without cobalt (Figure 6.5). The material with 20% TEOS (CoBT20E80) has a shoulder (Figure 6.5) and this shoulder may be an indication that the mesophase is somewhat cubic. A cubic mesophase was obtained for the corresponding material prepared without cobalt (i.e. TB20E shown in Figure 6.3).

Ageing temperature. The low intensity peaksof cobalt-incorporated materials aged at lower temperatures, observed between 2.5 and 3.5^{o} (Figure 6.7), are better resolved when compared to the corresponding materials aged at 80 ^{o}C (Figure 6.5). The absence of low intensity peaks in materials aged at 80 ^{o}C indicates loss of long-range ordering. As shown in Figure 6.7, XRD patterns of materials aged at 55 ^{o}C (CoBT20E55 and CoBT50E55) display a broad secondary feature in the 2θ range 2.5 – 3.5 ^{o}. XRD patterns with this feature were also observed for other ethanesilica materials [9]. Two resolved low intensity peaks are observed for CoBT67E55, which can be indexed as the d_{110} and d_{200} peaks of a hexagonal mesophase [23, 24].

The XRD patterns of material aged at room temperature (CoB20E27), shown in Figure 6.8, is similar to that observed for hexagonally ordered mesosporous MCM-41 [23, 24].

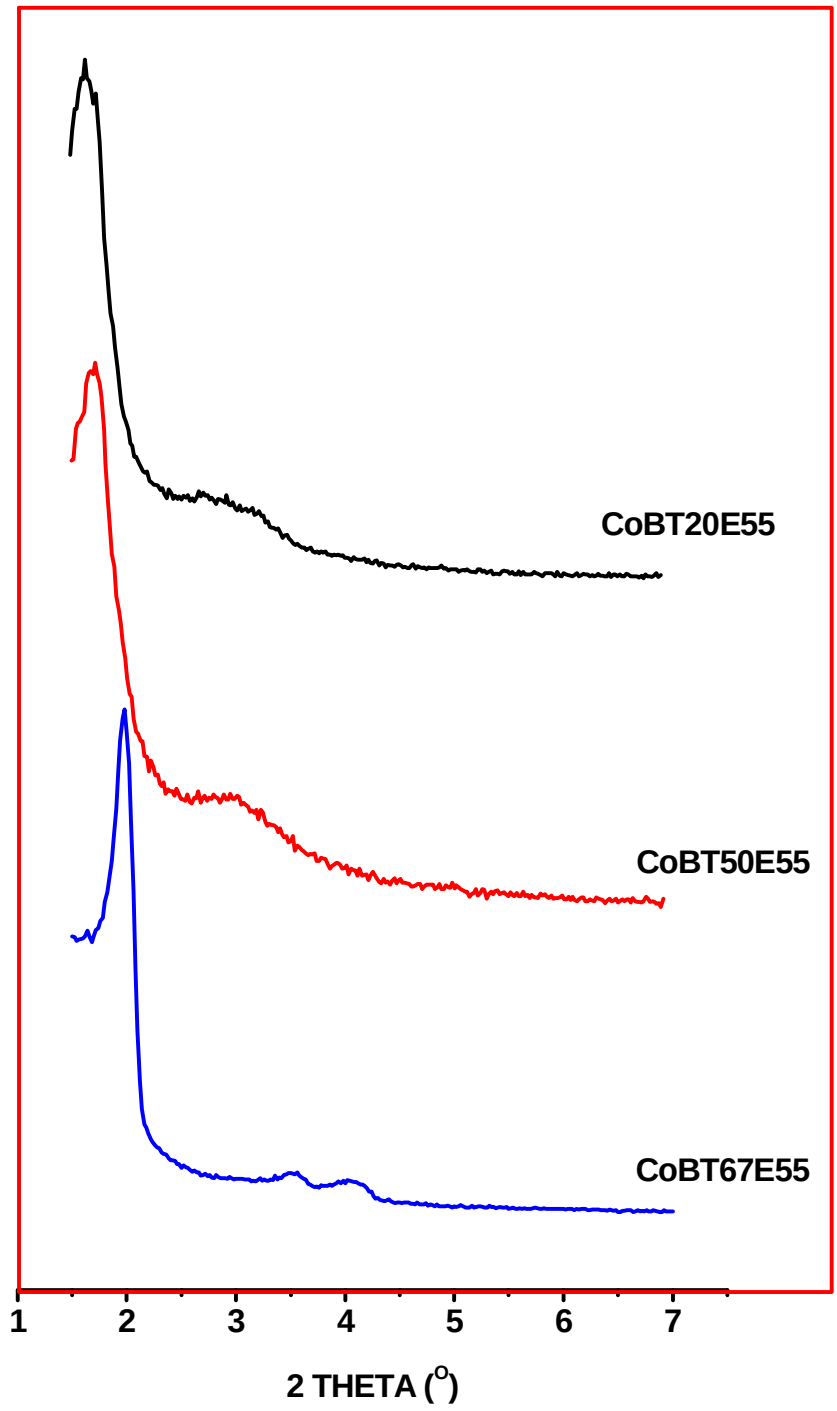

Figure 6.7 Powder XRD patterns of extracted cobalt incorporated ethanesilica materials synthesized from BTME and TEOS and aged at 55 ^{o}C.

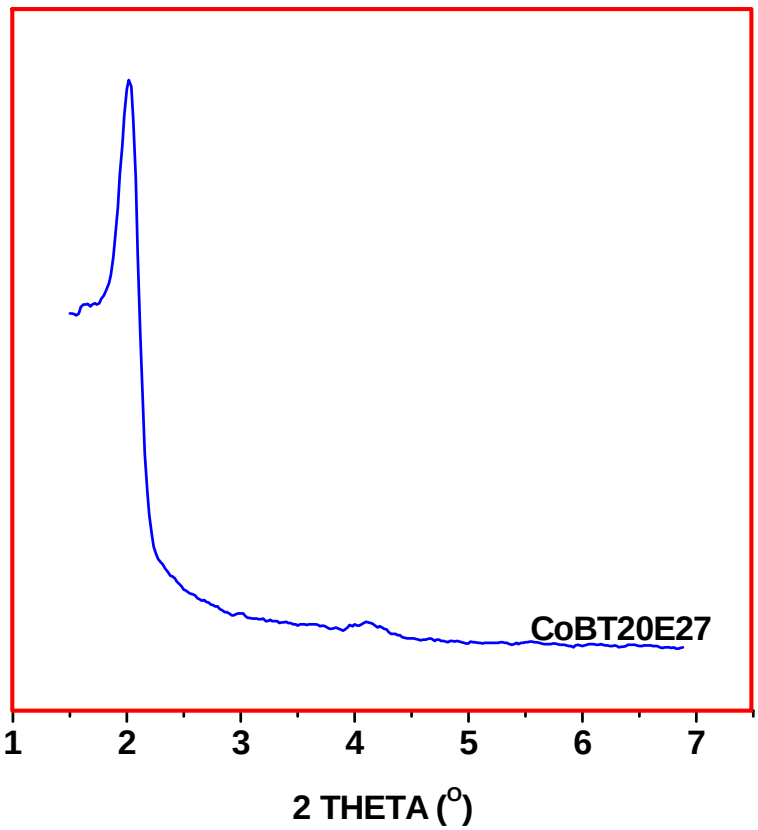

Figure 6.8 Powder XRD pattern of an extracted cobalt incorporated ethanesilica material synthesized from BTME and TEOS (CoBT20E27) and aged at room temperature.

6.3.5 Nitrogen adsorption

6.3.5.1 Influence of the BTME:TEOS ratio and cobalt incorporation. To test if the amount of the silica source had any significant effect on surface area or pore size, the ratio of BTME to TEOS was varied by increasing the amount of TEOS while keeping the amount of BTME constant.

Ethanesilica Nitrogen adsorption-desorption isotherms for extracted mesoporous organosilica materials prepared by co-condensation of TEOS and BTME using CTAB as the structure-directing template are shown in Figures 6.9 and 6.10. The structural properties (surface area, pore volume and pore diameter) of these materials are listed in Tables 6.3 and 6.4. The type of isotherm observed for BT20E80 (Figure 6.9) is commonly observed in materials with predominantly macroporous pores [27]. The material has a low surface area (27 m^2/g), which surprisingly, is lower than the values of surface areas of materials synthesized using either BTME or TEOS alone.

Sample BT67E80 exhibit a Type IV isotherm with a Type H3 hysteresis loop according to the IUPAC classification, which is typical of mesoporous materials [27]. The Type H3 hysteresis loop is observed with aggregates of plate-like particles giving rise to slit-shaped pores. The material has a surface area, pore volume and average pore diameter of 428 m^2/g, 0.66 cm^3/g and 6.17 nm respectively. The BJH pore size distribution [28] obtained from the adsorption isotherm is narrow (Figure 6.10) whereas that observed from the desorption isotherm is bimodal.

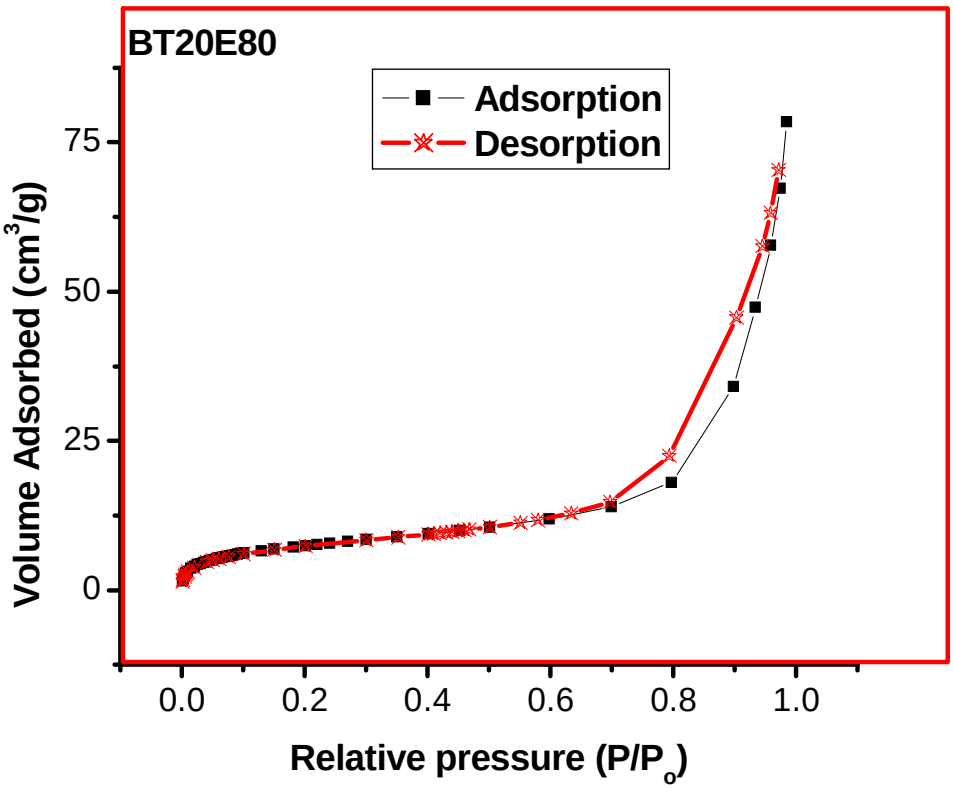

Figure 6.9 Nitrogen adsorption isotherm of an ethanesilica material containing 20 % TEOS (BT20E80).

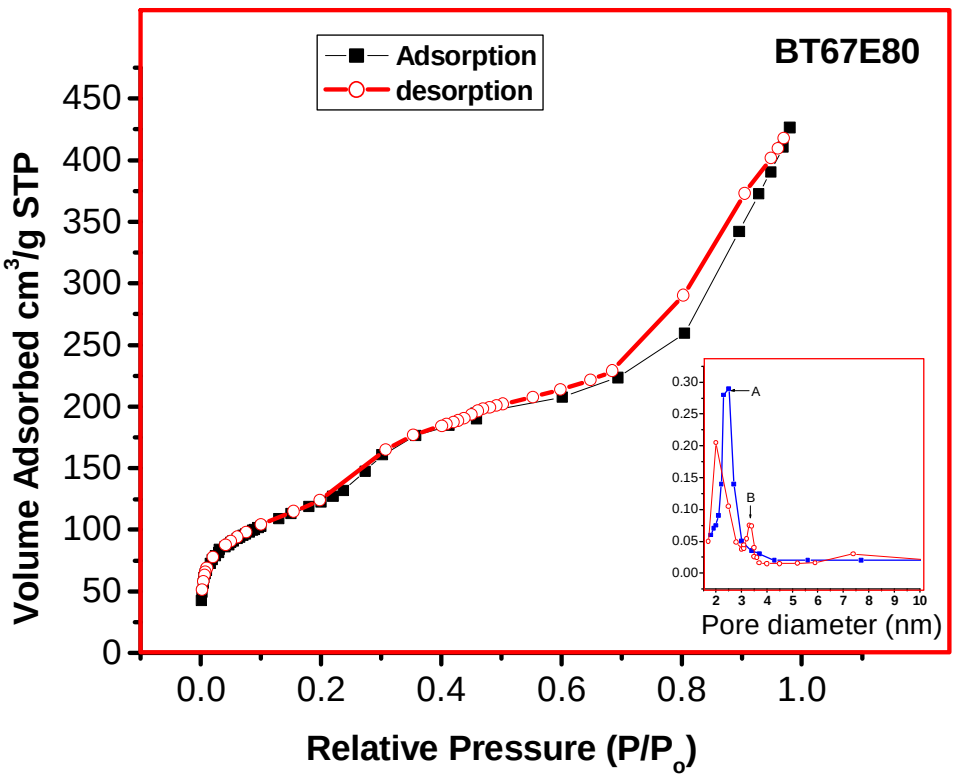

Figure 6.10 Nitrogen adsorption isotherm (main) and adsorption (A) and desorption (B) pore size distributions (insert) of an ethanesilica material containing 67 % TEOS (BT67E80).

Cobalt-incorporated ethanesilica. Nitrogen adsorption-desorption isotherms and BJH adsorption pore size distributions for extracted cobalt incorporated ethanesilica materials synthesized by co-condensation of BTME with TEOS using CTAB as the structure-directing template are shown in Figures 6.11 and 6.12. The PMO materials were aged at room temperature (27 ^{o}C) , 55 ^{o}C and 80 ^{o}C. The structural properties (surface area, pore volume and pore diameter) of these materials are listed in Tables 6.3 and 6.4. The PMO materials exhibit Type IV isotherms and narrow BJH adsorption pore size distributions characteristic of mesoporous materials [27]. A sharp inflection, indicating capillary condensation within uniform mesophases, is observed between relative pressure P/P_o = 0.25 and 0.4. The isotherms have hysteresis loops which become less pronounced as the ageing temperature is lowered.

For samples prepared at a given temperature, the surface area was found to increase with increasing amounts of TEOS added (Table 6.3 and Figure 6.11). The BET surface area increased from 636 to 858 m^2/g (for samples prepared from 20 and 67 % TEOS and aged at room temperature (i.e. CoBT20E27 and CoBT67E27, respectively), and from 359 to 483 m^2/g for the corresponding samples aged at 80 ^{o}C (i.e. CoBT20E80 and CoBT67E80, respectively). This trend was also observed for ethanesilica materials prepared from BTME (Chapter 4).

The average pore diameters for samples prepared from 20 and 67 % TEOS and aged at room temperature (CoBT20E27 and CoBT67E27) are almost equal (3.40 and 3.30 nm, respectively). However, substantially different values (6.48 and 4.40 nm for CoBT20E80 and CoBT67E80, respectively) are obtained for the corresponding materials aged at 80 ^{o}C.

Figure 6.12 shows pore size distributions (PSDs) of the organosilicas aged at 80 ^{o}C. The pore diameters derived from the desorption and adsorption isotherms are listed in Table 6.4. PSDs derived from adsorption isotherms are very narrow, whereas those derived from the desorption isotherms exhibit secondary porosity, which may be due to their small size and the presence of some disordered domains within the materials [29]. Narrow PSDs are an indication of excellent textural uniformity of a material [27]. BJH PSDs derived from the desorption

isotherms for CoBT67E80 and CoBT50E80 have two peaks each in the mesopore region. The PSD of CoBT20E80 has an additional broad peak centred at 7.2 nm. Results from density functional theory (DFT) (Figure 6.13 and Table 6.4), discussed in detail in the following paragraphs, also show the formation of a second mesopore for samples containing 50 and 67% TEOS. The pore diameters derived from the adsorption isotherm are lower than the corresponding values obtained from the desorption isotherm.

The BJH pore diameter derived from the adsorption isotherm decreases slightly when the ageing temperature is reduced from 80 ^{o}C to room temperature. BJH adsorption pore diameters of 2.4 and 2.3 nm were obtained for CoBT67E80 and CoBT67E27, respectively. The values obtained for the corresponding materials synthesized from 20 % TEOS (CoBT20E80 and CoBT20E27) are 2.7 and 2.5 nm, respectively. The BJH pore diameter derived from the adsorption isotherm increases slightly from 2.4 to 2.7 nm (for CoBT67E80 and CoBT20E80) when the amount of TEOS in the reaction mixture is changed from 67 to 20 %. The values obtained for the corresponding materials aged at room temperature (CoBT67E27 and CoBT20E27) are 2.3 and 2.5 nm, respectively. This observation also corresponds to the decrease in d-values as the amount of the inorganic silica precursor increases (Figure 6.6). It is proposed that replacement of –O– by $–CH_2CH_2-$, which is a larger moiety than the oxygen atom in the mesopore wall results in materials with larger d values and pore diameters.

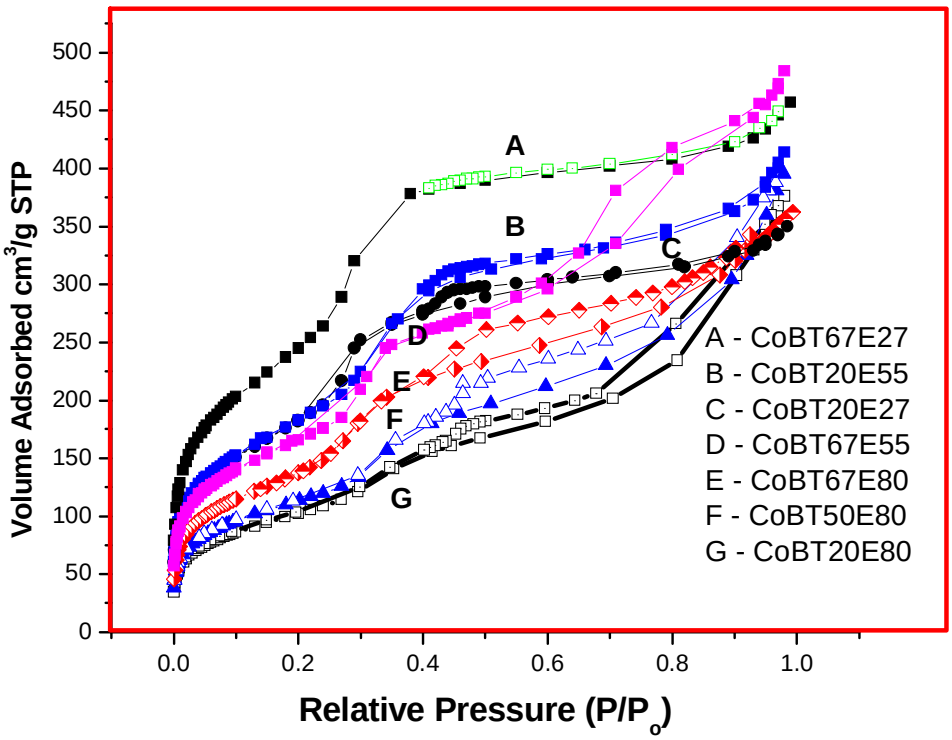

Figure 6.11 Nitrogen adsorption-desorption isotherms for extracted cobalt-incorporated mesoporous ethanesilica materials containing variable amounts of TEOS and aged at various temperatures.

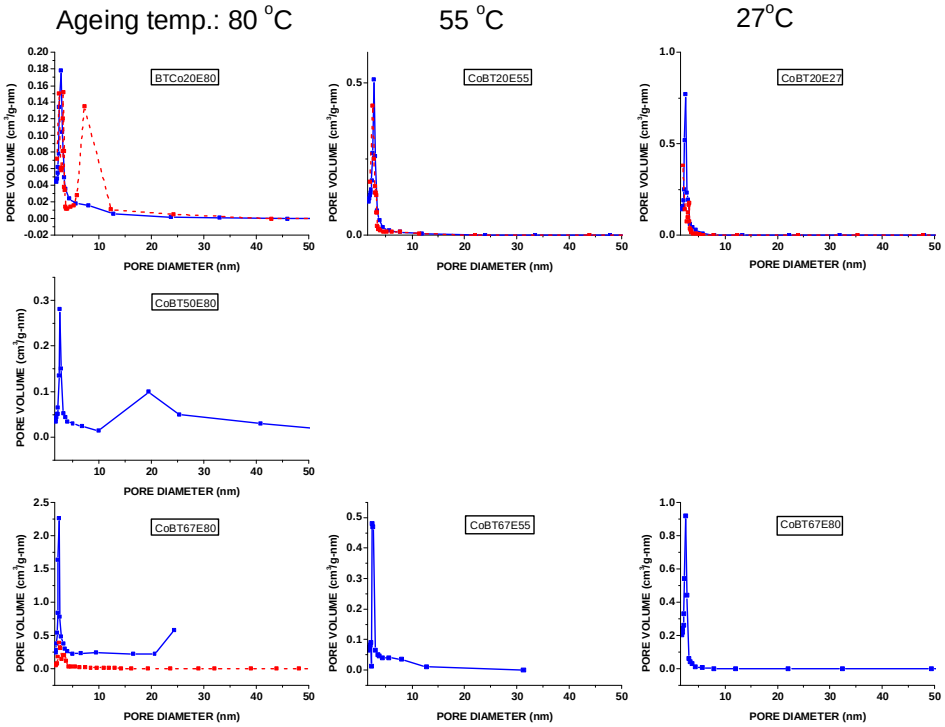

Figure 6.12 BJH Pore size distributions derived from adsorption (bold lines and square points) and desorption (dotted lines and open circular points) isotherms for extracted cobalt-incorporated mesoporous ethanesilica materials containing variable amounts of TEOS and aged at various temperatures.

6.3.6 Pore size distributions obtained from non-local density functional theory (DFT)

DFT [30] plots of cumulative pore volume versus pore width of cobalt incorporated samples containing 20, 50 and 67% TEOS in the reaction mixture and aged at 80 ^{o}C are shown in Figure 6.13. The DFT plot for the material containing 67% TEOS has two capillary condensation steps, showing the presence of two pore types. The corresponding DFT pore size distribution (plot of incremental pore volume versus pore diameter) shows two peaks with maxima at 1.3 and 2.9 nm. The first peak is in the micropore range whereas the second one is in the mesopore range. In contrast, the isotherm of the material containing 20% TEOS has three well resolved capillary condensation steps, showing the presence of three pore types. The DFT pore size distribution peaks have maxima at 1.3, 3.2 and 9.3 nm. The isotherm of the material containing equal percentages of BTME and TEOS is intermediate between those discussed above. From this observation it is clear that the presence of a certain amount of organic groups (BTME) results in two different pore types in the mesopore range. The intensity of the second mesopore increases with increasing amounts of the organofunctional silica source. In agreement with the trend obtained from BJH results, the pore diameter decreases from 3.2 (for CoBT20E80) to 2.9 nm (for CoBT67E80). It is worth mentioning that exactly the same values are obtained from the second mesopore peak of PSDs derived from BJH desorption isotherms. The above results show that DFT analysis is an invaluable method for pore size determination in organosilica materials.

CoBT20E80

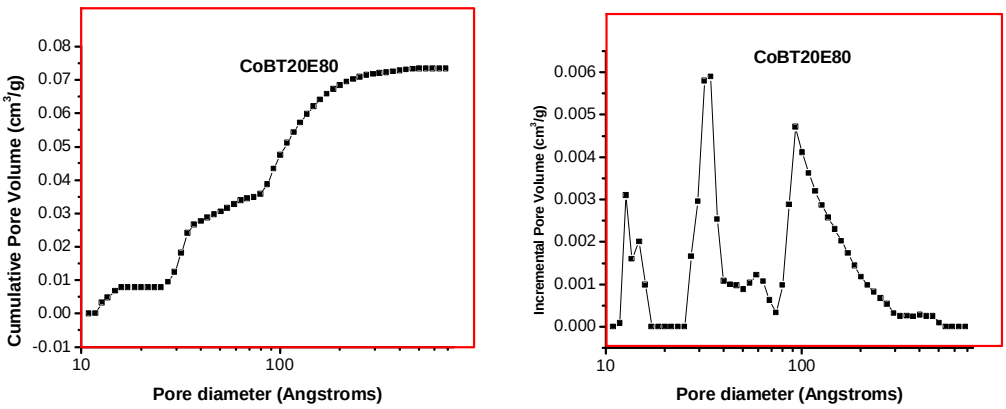

CoBT50E80

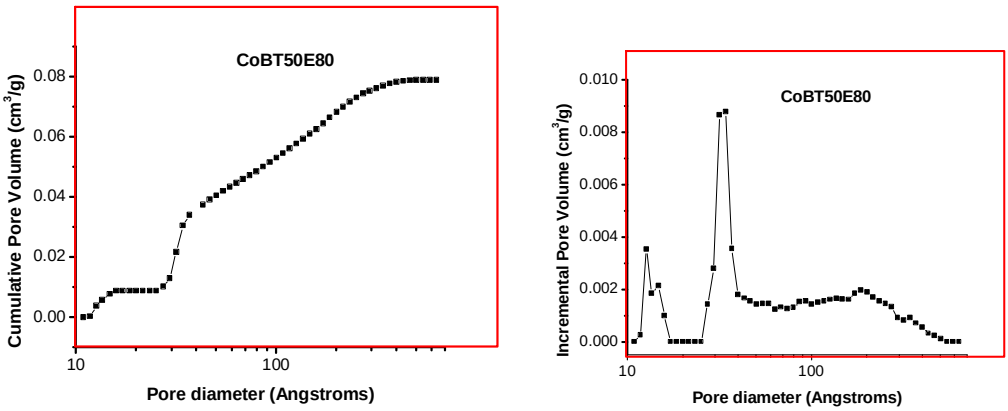

CoBT67E80

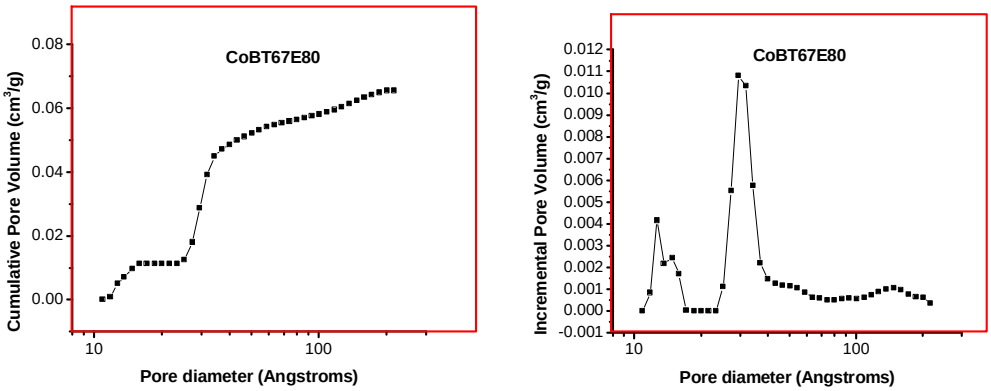

Figure 6.13 DFT plots for cobalt incorporated ethanesilica materials aged at 80 ^{o}C.

6.4 Conclusions

Periodic mesoporous ethanesilica materials were synthesized by co-condensation of BTME and TEOS. Powder XRD and nitrogen adsorption data indicated that the mesophase and textural properties of the materials are dependent on the ageing temperature, the ratio of silica precursors (BTME and TEOS) and cobalt incorporation. Cubic and hexagonal mesophases were identified using powder X-ray diffraction. Increasing the amount of TEOS in the co-condensation sol-gel reaction of BTME and TEOS favoured the formation of a hexagonal mesophase whereas materials containing no TEOS or low amounts of TEOS (i.e. more BTME) favoured the formation of a cubic mesophase. Cobalt inclusion resulted in larger XRD lattice parameters. The surface area was found to increase with increasing amount of TEOS added. The observed Type IV isotherms had hysteresis loops which became less pronounced as the ageing temperature was lowered.

6.5 References

1. R. K. Iler, The Chemistry of Silica, John Wiley & Sons, New York (1979).

2. C. J. Brinkner, and G. W. Scherer, Sol-Gel Science. The Physics and Chemistry of Sol-Gel Processing, Academic Press, San Diego (1990).

3. P. Gomez-Romero, and C. Sanchez, Eds., Functional Hybrid Materials, Wiley-VCH, Weinheim (2004).

4. D. Kumar, K. Schumacher, C. du Fresne von Hohenesche, M. Grun, and K. K. Unger, Colloids and Surfaces A : Physicochem. Eng. Aspects **187–188**, 109 (2001).

5. U. Ciesla, and F. Schüth. Micropor. Mesopor. Mater. **27**, 131 (1999).

6. T. Asefa, M. J. MacLachlan, H. Grondey, N. Coombs, and G. A. Ozin, Angew. Chem. Int. Ed. **39**, 1808 (2000).

7. S. Inagaki, S. Guan, Y. Fukushima, T. Ohsuna, and O. Terasaki, J. Am. Chem. Soc. **121**, 9611 (1999).

8. T. Asefa, M. J MacLachlan, N. Coombs, and G. A. Ozin, Nature **402**, 867 (1999).

9. B. J. Melde, B. T. Holland, C. F. Blanford, and A. Stein, Chem. Mater. **11**, 3302 (1999).

10. M. Freemantle, C&EN **Jan 24**, 33 (2000).

11. C. Yoshina-Ishii, T. Asefa, N. Coombs, M. J. MacLachlan, and G. A. Ozin, Chem. Commun. 2539 (1999).

12. T. Asefa, C. Yoshina-Ishii, M. J. MacLachlan, and G. A. Ozin, J. Mater. Chem. **10**, 1751 (2000).

13. G. A. Ozin, Chem. Commun. 419 (2000).

14. Q. Yang, M. P. Kapoor, and S. Inagaki, J. Am. Chem. Soc. **124**, 9694 (2002).

15. M. C. Burleigh, S. Dai, and E. W. Hagaman, Chem. Mater. **13**, 2537 (2001).

16. A. Fukuoka, Y. Sakamoto, S. Guan, S. Inagaki, N. Sugimoto, Y. Fukushima, K. Hirahara, S. Iijima, and M. Ichikawa, J. Am. Chem. Soc. **123**, 3373 (2001).

17. M. Kruk, M. Jaroniec, S. Guan, and S. Inagaki, J. Phys. Chem. B **105**, 681 (2001).

18. T. Asefa, M. J. MacLachlan, H. Grondey, N. Coombs, and G. A. Ozin, Angew. Chem. Int. Ed. **39**, 1808 (2000).

19. E-B. Cho, K-W. Kwon, and K. Char; Chem Mater. **13**, 3837 (2001).

20. V. Rebbin, M. Jakubowski, S. Potz, and M. Froba, Micropor. Mesopor. Mater. **72**, 99 (2004).

21. O. Dag, and G. A. Ozin, Adv. Mater. **13**, 1182 (2001).

22. N. B. Colthup, L. H. Daly, and S. E. Wiberley, Introduction to Infrared and Raman Spectroscopy, Academic Press (3rd Ed.) (1997).

23. J. S. Beck, J. C. Vartuli, W. J. Roth, M. E. Leonowicz, C. T. Kresge, K. D. Schmitt, C. T-W. Chu, D. H. Olson, E. W. Sheppard, S. McCullen, J. B. Higgins, and J. L. Schlenker, J. Am. Chem. Soc. **114**,10834 (1992).

24. C. T. Kresge, M. E. Leonowicz, W. J. Roth, J. C. Vartuli, and J. S. Beck, Nature **359**, 710 (1992).

25. D. Zhao, B. F. Chmelka, and G. D. Stucky, J. Am. Chem. Soc. **120**, 6024 (1998).

26. S. Guan, S. Inagaki, T. Ohsuna, and O. Terasaki, J. Am. Chem. Soc. **122**, 5660 (2000).

27. S. J. Gregg, and K. S. W. Sing, Adsorption, Surface Area and Porosity, Academic Press, London (1982).

28. E. P. Barrett, L. G. Joyner, and P. P. Halenda, J. Am. Chem. Soc. **73**, 373 (1951).

29. T. Asefa, M. Kruk, M . J. MacLachlan, N. Coombs, H. Grondey, M. Jaroniec, and G. A. Ozin, J. Am. Chem. Soc. **123**, 8520 (2001).

30. A. V. Neimark, and P.I. Ravikovitch. Micropor. Mesopor. Mater. **44–45**, 697 (2001).

CHAPTER SEVEN

Cobalt ion incorporation into periodic mesoporous organosilica materials synthesized by co-condensation of 1,2-bistrimethoxysilylethane with 3-glycidoxypropyltriethoxysilane[1]

7.1 Introduction

Porous materials based on silica are widely used as supports for monolayer-type catalysts in the field of heterogeneous catalysis. Loading a catalyst on an inert but high surface area silica support, by impregnation with an aqueous catalyst precursor, by vapour deposition [1] or by solid/solid wetting [2], improves the accessibility of the active phase [1]. In recent years highly ordered mesoporous silicas, such as MCM41, have shown excellent performance as a support for metal catalysts, resulting in several cases in significant improvement when compared to conventional and commercial catalysts [3, 4]. This improvement has been attributed to the high surface areas and the superior dispersion of the active metals on the support.

Periodic mesoporous organosilicas (PMOs) synthesized from organosilanes, $(R'O)_3Si\text{-}R\text{-}Si(R'O)_3$ (where R and R' are alkyl groups), via the surfactant-templated sol-gel method have gained much attention because various organic functionalities can be integrated within the stable inorganic framework [5]. PMOs possess structural properties of ordered mesoporous materials with the chemical properties of both the silica and the organic bridging group. Based on their similarity to ordered mesoporous silicas, PMOs are also expected to be good catalyst supports. Amongst the PMO materials, periodic mesoporous ethanesilica

[1] Published. A. M. Tshavhungwe, M. Layh and N. J. Coville, Journal of Sol-Gel Science and Technology 29, 167–177, 2004

has been widely studied [5 – 25]. It has been synthesized from 1,2-bistrialkoxysilylethane precursors (alkoxy = ethoxy or methoxy) in the presence of long alkylammonium [6 – 17], triblock [13,14, 18 – 22], non-ionic polymeric, and non-ionic oligomeric [12 – 14, 23 – 25] surfactants.

Further functionalization of the ethanesilica has been achieved by co-condensation of 1,2-bistrialkoxysilylethane precursors with various trialkoxyorganosilanes [26 – 30]. Inorganic-organic hybrid bifunctional PMOs containing both bridging organic functional moieties in the framework and terminal organic functional groups protruding into the channel pores were first reported by Ozin et. al. [26]. The materials were synthesized by using bistriethoxysilylethylene as the source of the bridging group and triethoxyvinylsilane as the source of the terminal organic group. It was also mentioned in the report that bifunctional PMOs incorporating ethylene/methyl and methylene/vinyl, as well as trifunctional PMOs incorporating ethylene/methylene/methyl organic functional groups were also synthesized. According to the report, bifunctional samples prepared with cetylpyridinium chloride surfactant also resulted in structurally well ordered materials. Burleigh and co-workers [27 – 30] described the preparation of a porous organosilica by co-condensation of bistriethoxysilylethane and N-(2-aminoethyl)-3-aminopropyltrimethoxysilane or N-[3-(trimethoxysilyl)propyl] ethylenediamine under acidic and basic conditions.

Herein we report on the synthesis and characterization of organosilica materials synthesized by co-condensation of 1,2-bistrimethoxysilylethane (BTME) with 3-glycidoxypropyltrimethoxysilane (GPTS) in the presence of hexadecyltrimethylammonium bromide (cetyltrimethylammonium bromide, CTAB) as the surfactant both in the presence and absence of cobalt ions. The molecular structures of these silica precursors and the surfactant are shown in Scheme 7.1. GPTS is an attractive candidate for further functionalization of organosilica materials because the epoxy ring can be opened using amines (e.g. 3-aminopropyltriethoxysilane) [31, 32] to afford other functional groups. Further, the epoxide ring of GPTS can react with water in acidic conditions and with

methanol (a solvent used to dissolve GPTS) to form diols or methyl ether terminal groups [33, 34]**.** The terminal OH and OR groups may be beneficial for binding metals and this is one of the aspects of GPTS which we wish to explore in this study.

Cobalt ion was added to the formed silicas to generate Co supported catalysts for use in Fischer-Tropsch (F-T) catalyst synthesis [35 – 39]. This work, a continuation of our studies on Co supported catalysts [40, 41], will be reported elsewhere. To the best of our knowledge, this is the first report on both the synthesis of GPTS-modified ethane silica and cobalt ion incorporated GPTS-modified ethane silica.

It is to be noted that 3-glycidoxypropyltrimethoxysilane has been used as a coupling agent in transparent abrasion-resistant hybrid coatings for polymers [42] and metals [43] and for gas separation membranes [44].

7.2 Experimental Section

7.2.1 Chemicals

1,2-Bistrimethoxysilylethane (BTME), hexadecyltrimethylammonium bromide (CTAB) and cobalt nitrate hexahydrate were obtained from Aldrich; 3-glycidoxypropyltrimethoxysilane (GPTS) was obtained from ABCR (Germany); ammonium hydroxide was obtained from Fluka. All chemicals were used as received.

7.2.2 Synthesis

7.2.2.1 GPTS-functionalized ethanesilica and cobalt ion incorporated GPTS-functionalized ethanesilica. PMOs were prepared using a modified method based on that reported by Ozin and co-workers [26]. A series of GPTS-modified ethanesilica materials were prepared starting with a mole ratio of BTME:GPTS:CTAB:NH_4OH:H_2O = 1: x : 0.293: 8: 244 (where x = 0, 0.266, 0.559, 0.866, and 1.146). A material containing only GPTS as the silica source (i.e. without BTME) was also prepared. Cobalt ion incorporated GPTS-modified ethanesilica materials were synthesized by adding cobalt nitrate to the reaction mixture so that the initial mole ratio was BTME:GPTS:CTAB:NH_4OH:H_2O:$Co(NO_3)_3$ = 1: x : 0.293: 8: 244 : 0.054 (where x = 0, 0.266, 0.559, 0.866, and 1.146). In a typical synthesis, CTAB (0.68 g; 1.86 mmol) was dissolved in a solution consisting of water (28 ml) and 28 % ammonium hydroxide (8 ml; 0.058 mol). The mixture was stirred for 15 minutes. The pH of the solution was estimated by pH paper to be approximately 10. A mixture of BTME (1.6 ml) and GPTS (varying amounts: 1.72 g; 1.30 g; 0.84 g and 0.40 g) was added dropwise to the stirred mixture. Stirring was continued for a further 30 minutes, followed by ageing at 80^oC for 4 days. The solid was suction filtered in a Büchner funnel and washed with an excess of water. The solid was dried in air overnight. Yields of between 1 and 2 g of product were obtained.

7.2.2.2 Surfactant extraction. A portion of the as synthesized sample (0.5 g) was stirred in a solution of concentrated HCl (5 ml) in methanol (200 ml) at 50 ^oC for 2 days. The solid was suction filtered in a Büchner funnel, washed with water and finally with methanol (200 ml) and then dried in air. Mass losses of between 20 and 40 % were observed after surfactant extraction.

7.2.2.3 Nomenclature. The amounts of BTME and GPTS as well as the percentage of GPTS in the reaction mixture are presented in Table 7.1. The percentage GPTS indicates the mole percentage of GPTS expressed per mole of

silicon atoms in the BTME and GPTS organosilica precursors {% GPTS = [100 x (moles Si in GPTS)/(moles Si in BTME + moles Si in GPTS)] = [100 x (moles GPTS)/(2 x moles BTME + moles GPTS)]}. The moles of BTME are multiplied by 2 because each BTME molecule supplies two moles of Si whereas a GPTS molecule supplies one. The notation used to identify the samples is as follows: G = GPTS, B = BTME, Co = cobalt. Numerical figures refer to the % GPTS in the reaction mixture, A = as synthesized and E = extracted. For example, GBCo53E refers to an extracted (*E*) sample synthesized from GPTS (*G*) and BTME (*B*) in the presence of cobalt nitrate (*Co*). The amount of GPTS in the reaction mixture is 53% by moles of Si atoms.

Table 7.1 Amounts of silica sources used in the reaction mixture

Sample	**BTME / mmol**	**GPTS / mmol**	**GPTS / %**
GB100	0	7.28	100
GB53 and GBCo53	6.35	7.28	53.4
GB46 and GBCo46	6.35	5.50	46.4
GB36 and GBCo36	6.35	3.55	35.9
GB21 and GBCo21	6.35	1.69	21.0
GB0 and GBCo0	6.35	0	0

7.2.3 Characterization

Characterization of the samples was carried out by powder X-ray diffraction (XRD), nitrogen adsorption, Raman spectroscopy, proton nuclear magnetic resonance (^{1}H NMR) spectroscopy, thermogravimetric analysis (TGA) and differential thermal analysis (DTA) as described in Chapter 3.

7.3 Results and Discussion

7.3.1 Synthesis

Addition of a mixture of BTME and GPTS to a basic solution of CTAB formed white solid materials. A gel formed immediately for samples containing larger amount of GPTS. Addition of GPTS alone (without BTME) to a basic CTAB solution formed a clear gel, which dried to a hard material. For all materials, precipitation started within 30 minutes after addition of the silica precursor. Addition of cobalt nitrate to the mixture yielded dark brown/black crystals for GBCo21 and GBCo36, which necessitated crushing before analysis. Cobalt ion incorporated materials containing more GPTS (GBCo53 and GBCo46) formed light brown powders. The base catalysed surfactant templated formation of periodic mesoporous GPTS-ethane silica is proposed to form from micelles [45] as illustrated in Scheme 7.1.

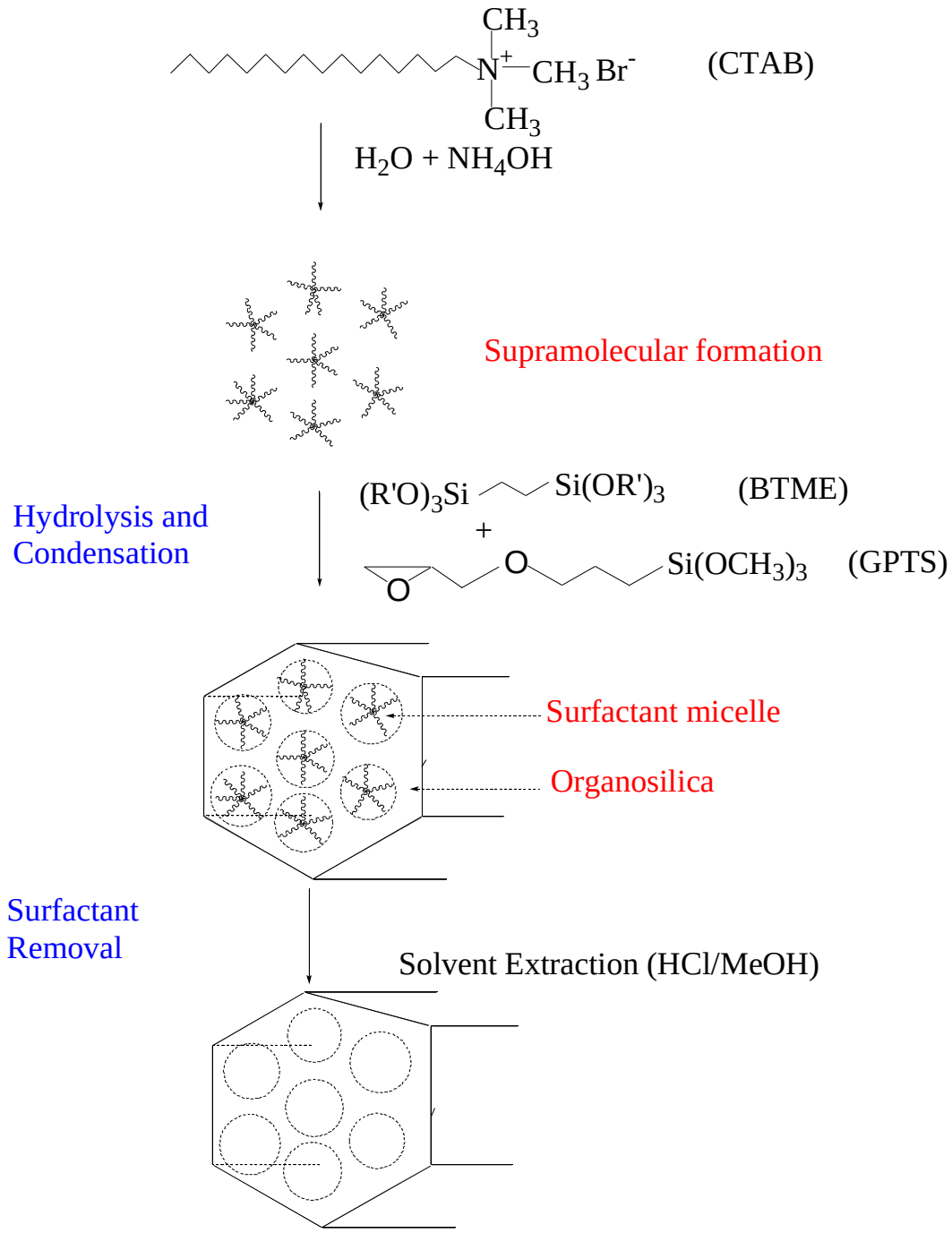

.

Scheme 7.1 Reaction scheme showing the formation of periodic mesoporous glycidoxypropyl-modified ethane silica. Note that the framework is made of units $(CH_2OCH_2)CH_2OCH_2CH_2CH_2SiO_3$ and $O_3SiCH_2CH_2SiO_3$.

7.3.2 Powder X-ray Diffraction

7.3.2.1 GPTS modified ethane silica. The periodicity of mesoporous materials was probed using powder XRD. Periodic mesoporous materials display a very high intensity peak at around $2\theta = 2^o$, together with low intensity peaks in the 2θ range $3 - 8^oC$ [45, 46]. The prominent low angle peak at approximately $2\theta = 2^o$ indicates the presence of uniformly sized pores for ordered materials. XRD patterns (Figures 7.1 and 7.2) show relatively broad low angle peaks compared to that of hexagonal MCM41 materials. The materials were assumed to be hexagonally ordered. The values of the d (100) peak and the corresponding positions of as synthesized and solvent extracted samples are given in Table 7.2. The effect of (i) solvent extraction, and (ii) amount of GPTS added on the value of the lattice parameter, d (100), is graphically shown in Figure 7.3. Higher d (100) values are obtained after solvent extraction. As expected for organic-functionalized silicas synthesized via co-condensation [26, 47], the position of the d (100) peak shifts to higher angles as the amount of GPTS added increased. This shift corresponds to the reduction in the interplanar spacing from about 4.9 to 4.2 nm.

7.3.2.2 Cobalt ion incorporated GPTS-modified ethanesilica. For materials synthesized in the presence of 0.1 g cobalt nitrate, the main peak was only observed for the as synthesized cobalt ion incorporated material containing 46% GPTS. However, the peak disappeared after solvent extraction, showing a collapse in the periodicity of the material. Cobalt ion incorporation was confirmed by scanning an ethane silica sample prepared in the presence of 0.1 g cobalt nitrate from 1.5 to 70^o. Diffraction peaks observed at 38^o and 65^o can be assigned to Co_3O_4 [48].

Table 7.2 d_{100} Spacings and their positions

	As synthesized		**Extracted**	
Sample	2 θ (^{o})	d_{100} (Å)	2 θ (^{o})	d_{100} (Å)
GB53	2.23	39.7	2.10	42.1
GB46	2.13	41.4	2.09	42.3
GB36	2.11	41.9	amorphous	
GB21	2.04	43.4	1.81	48.8
GB0	1.99	44.2	1.88	47.2

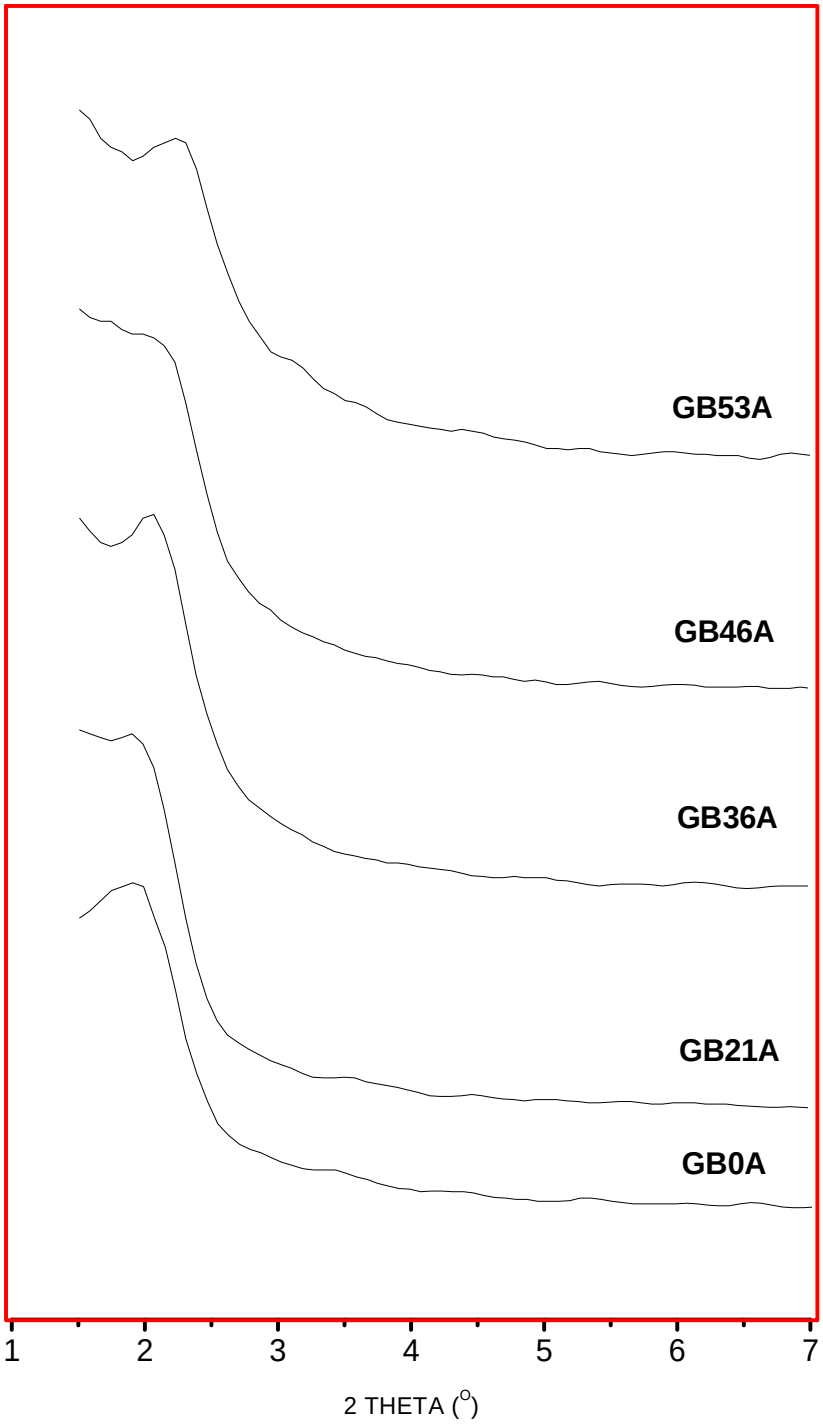

Figure 7.1 XRD patterns for solvent extracted glycidoxypropyl-functionalized ethane silicas

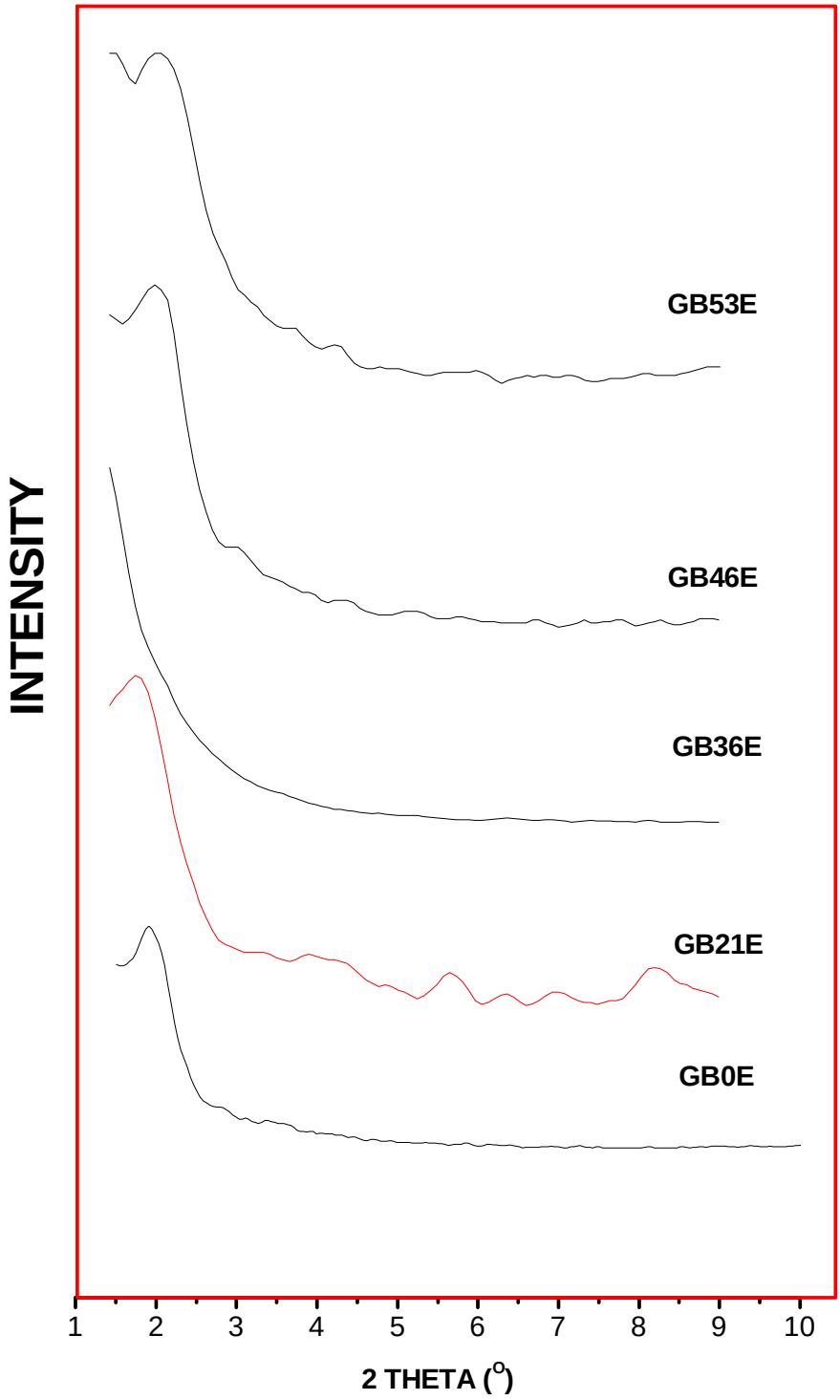

Figure 7.2 XRD patterns for solvent extracted glycidoxypropyl-functionalized ethane silicas

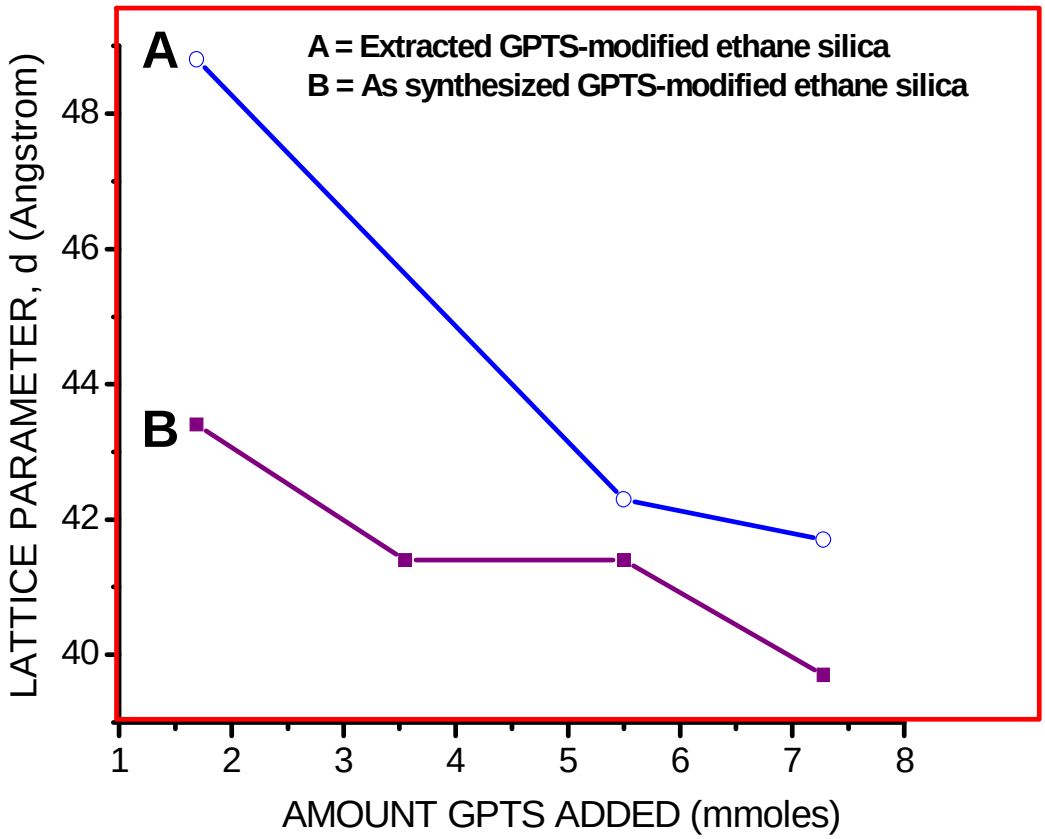

Figure 7.3 Variation of lattice parameter (d) with amount of GPTS for extracted (A) and as synthesized (B) GPTS-modified ethane silica materials.

7.3.3 Nitrogen sorption

7.3.3.1 GPTS modified ethane silica. Nitrogen adsorption-desorption isotherms and the corresponding BJH pore size distributions derived from adsorption and desorption isotherms for extracted gylcidoxypropyl-modified ethanesilica samples with the GPTS loading levels of 0, 21 and 53% in the synthesis gels are shown in Figure 7.4. The structural properties (BET surface area, pore volume and average pore diameter) of these materials are listed in Table 7.3.

All the materials exhibit Type IV isotherms according to the IUPAC classification, which is typical of mesoporous materials [49]. The hysteresis loops change from Type H3 to Type H4 with increasing amounts of GPTS in the reaction mixture. The Type H3 hysteresis loops obtained for GB0E and GB21E do not exhibit any limiting adsorption at high pressures. Type H3 hysteresis loops are observed with aggregates of plate-like particles giving rise to slit-shaped pores. GB53E has a Type H4 hysteresis loop, which is often associated with narrow slit like pores. The BJH pore diameters derived from the desorption and adsorption isotherms are listed in Table 7.3. The pore volumes derived from the adsorption isotherm are lower than the corresponding values obtained from the desorption isotherm by about 1 nm. The materials exhibit size distributions of primary pores with maxima shifting from about 3.3 nm for the sample without GPTS to 3.1 nm for the sample with 53 % GPTS. The corresponding maximum values obtained from the adsorption pore size distributions are 2.2 and 1.7 nm, respectively. The latter observation shows that addition of GPTS leads to formation of microporous materials [47]. The materials also exhibit secondary porosity, which may be due to their small size and the presence of some disordered domains within the materials [26]. The pore size distribution derived from the desorption isotherm of GB21E has two types of mesopores with maxima at 3.1 and 3.6 nm.

From the above data it can be seen that the % GPTS has an effect on the pore structure of the silica material. It is assumed that the major effect arises from an

interaction of CTAB micelle with the GPTS that modifies the micelle structure, leading to the loss of long range order. However, further work on this and other related systems will need to be performed to confirm this suggestion.

Table 7.3. Structural properties of the organosilica materials.

Sample	**BET Surface Area (m^2/g)**	**Total Pore Volume (cm^3/g)**	**Average Pore Diameter (nm)**	**BJH Adsorption Pore Diameter (nm)**	**BJH Desorption Pore Diameter (nm)**
GB0E	598	1.06	7.12	2.2 – 2.1 (2.2)	3.3 – 3.2 (3.3)
GB21E	572	0.86	6.00	1.9 – 1.8 (1.9)	3.2 – 3.2 (3.2)
					3.6 – 3.6 (3.6)
GB53E	392	0.40	4.05	1.8 – 1.7 (1.7)	3.1 – 3.0 (3.1)
GBCo0E	534	0.78	5.83	2.5 – 2.4 (2.4)	3.2 – 3.1 (3.1)
GBCo21E	331	0.38	4.62		3.7 – 3.7 (3.7)
GBCo36E	250	0.20	3.15		3.1 – 3.0 (3.0)
GBCo53E	50.5	0.09	7.11		3.0 – 2.9 (3.0)

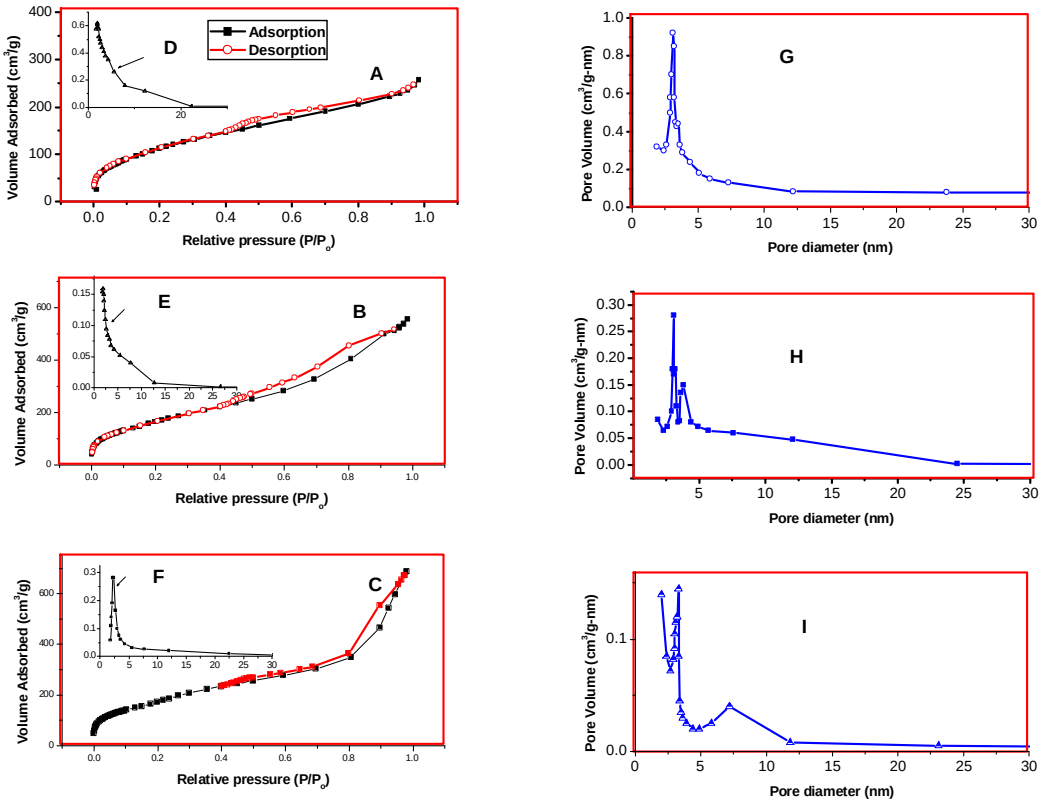

Figure 7.4 N_2 adsorption isotherms and BJH pore size distributions derived from adsorption and desorption isotherms for GPTS-modified ethane silica materials: A, B and C are isotherms of GB53E, GB21E and GB0E, respectively; D, E and F are BJH adsorption pore size distributions of GB53E, GB21E and GB0E, respectively; G, H and I are BJH desorption pore size distributions of GB53E, GB21E and GB0E, respectively.

7.3.3.2 Cobalt ion incorporated GPTS-modified ethanesilica. Nitrogen adsorption-desorption isotherms and the corresponding desorption BJH pore size distributions for extracted cobalt ion-incorporated gylcidoxypropyl-modified ethanesilica samples with the organosilica loading levels of 0, 21, 36 and 53% in the synthesis gels are shown in Figure 7.5. As the amount of GPTS added is increased the isotherms of cobalt ion incorporated GPTS-modified materials changes from Type IV to Type I (characteristic of microprous materials) and the shape of the hysteresis loop also changes. The following types of hysteresis loops were observed: Type H2 for GBCo21E, characteristic of "ink-bottle" pores; Type H4 for GBCo36E (narrow slit-like pores); and Type H3 for GBCo53E (aggregates of plate-like particles giving rise to slit-shaped pores).

From Figure 7.5, it is clear that the lower the amount of GPTS, the narrower the pore size distribution. Whereas samples GBCo36E and GBCo53E have BJH pore diameters of 3.0 nm each, the BJH pore diameter obtained for GBCo21E is 3.7 nm. The latter coincides with the value of the second mesopore peak in the corresponding material synthesized without cobalt ion (i.e. GB21E).

The effect of (i) GPTS loading on ethanesilica, and (ii) cobalt ion-incorporation on GPTS-modified ethane silica is summarized in Figure 7.6. A distinct decrease in the surface area, total pore volume and average pore diameter is observed as the amount of GPTS increases. Cobalt ion incorporated materials also have a lower surface area, total pore volume and average pore diameter than the corresponding materials without cobalt ion (Table 7.3 and Figure 7.6).

.

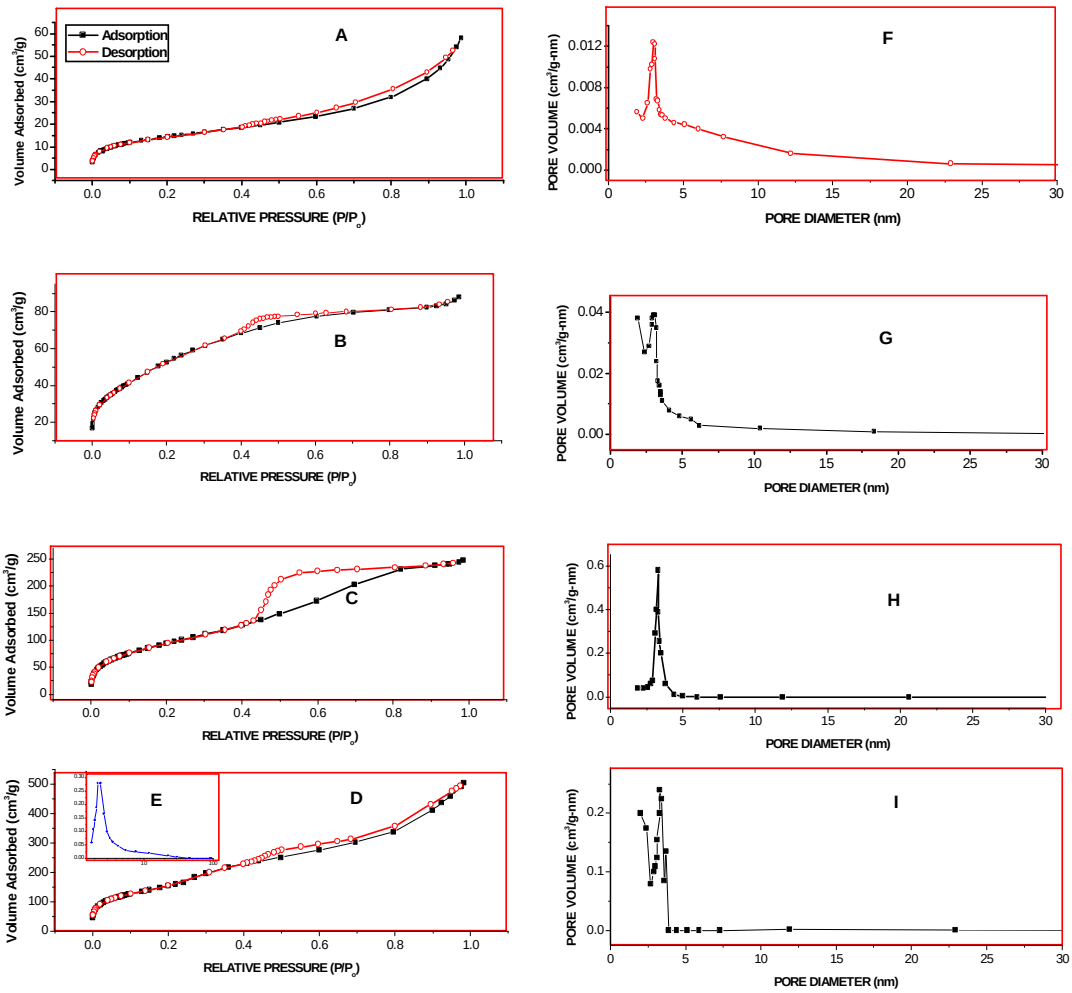

Figure 7.5 N_2 adsorption isotherms and BJH pore size distributions derived from adsorption and desorption isotherms for cobalt ion incorporated GPTS-modified ethane silica materials: A, B C and D are isotherms for GBCo53E, GBCo36E, GBCo21E and GB0E, respectively; E is the BJH adsorption pore size distribution of GB0E; F, G, H and I are BJH desorption pore size distributions of GBCo53E, GBCo36E, GBCo21E and GB0E, respectively.

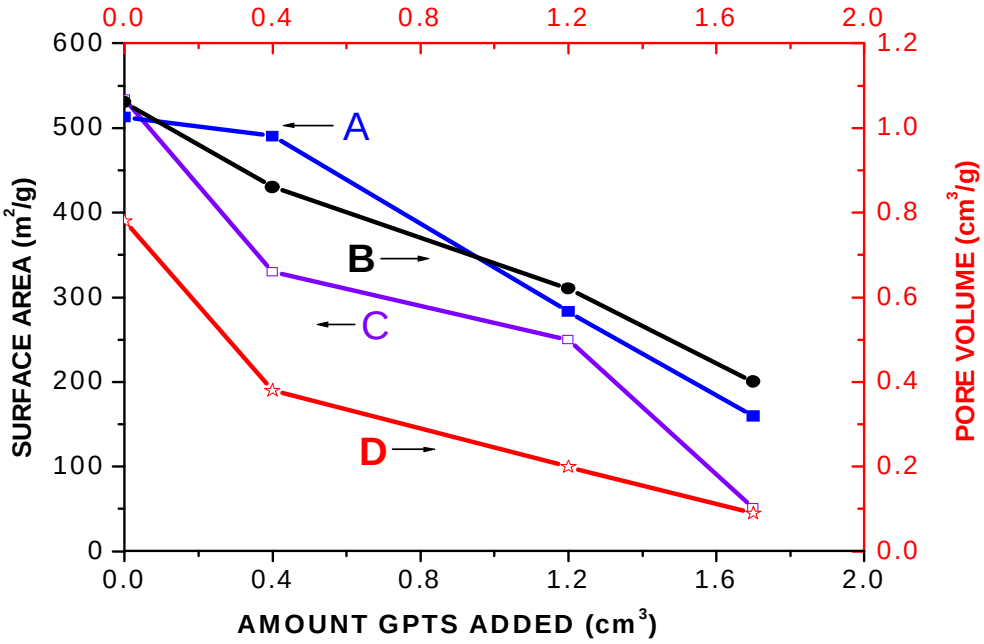

Figure 7.6 Variation of surface area and pore volume with amount of GPTS. A = Surface area vs Amount GPTS for GPTS-modified ethane silica; B = Pore volume versus Amount of GPTS for GPTS-modified ethane silica; C = Surface area vs Amount GPTS for cobalt ion incorporated GPTS-modified ethane silica; D = Pore volume versus Amount of GPTS for cobalt ion incorporated GPTS-modified ethane silica.

7.3.4 Thermal analysis

7.3.4.1 GPTS-modified ethanesilica. Samples were analysed before and after solvent extraction using thermogravimetric analysis(TGA) and differential thermal analysis (DTA). Analysis was conducted from room temperature to 800 ^{o}C or 1000 ^{o}C. The TGA and DTA curves of as-synthesized and solvent extracted ethane silica material are shown in Figure 7.7. The thermogravimetric curves for as-synthesized and solvent extracted GPTS-modified ethane silica materials (not shown) were also obtained. The profiles indicate that the organosilica materials have similar thermal stability, with distinct mass losses, as a consequence of loss of the organic groups in the materials. The samples lose physically adsorbed water at low temperatures (< 110 ^{o}C). The surfactant is then lost. The onset of organic group decompostion is observed at around 300 ^{o}C.

Typical thermograms of the as synthesized PMO and the surfactant extracted PMO prepared from BTME (GB0A and GB0E) are shown in Figures 7.7B and 7.7A, respectively. The corresponding DTA curves are presented in Figures 7.7D and 7.7C. Table 7.4 summarises the data obtained from the thermograms. The TGA curve of the as synthesized BTME sample exhibits a weight loss of about 5 % below 110 ^{o}C, accompanied by an endothermic DTA peak, attributed to the desorption of methanol and water. This is followed by a weight loss of approximately 20 % over the temperature range 108 – 262 ^{o}C with an endothermic DTA peak due to desorption of the surfactant. A 10 % mass loss attributed to matrix decomposition occurs in the range 440 – 727 ^{o}C. This mass loss appears as an exothermic DTA peak at 578 ^{o}C.

The thermogram of the solvent extracted BTME PMO shows a decrease in mass of about 2 % below 57 ^{o}C due to the loss of methanol. There is no weight loss in the region where the surfactant is desorbed (108 – 262 ^{o}C) indicating that the surfactant was totally removed by solvent extraction. A 2 % mass loss, attributed to desorption of water formed from condensation of internal hydroxyl groups, occurs in the range between 313 and 472 ^{o}C.

The thermal analysis curve for the as synthesized material prepared using GPTS as the only silica source (GB100A) is shown in Figure 7.8. The thermogram exhibits a weight loss of about 3 % below 110 ^{o}C. This is attributed to the desorption of water and methanol. A weight loss of about 14 %, due to loss of surfactant, is observed over the temperature range 110 ^{o}C – 265 ^{o}C. This is followed by a 50% mass loss in the temperature range 265 – 600 ^{o}C assigned to decomposition of 3-glycidoxypropyl groups. This mass loss is characterized by three overlapping peaks in the derivative of the thermogram.

For samples prepared in the presence of both GPTS and BTME, there is a gradual increase in the total mass loss as the amount of GPTS increases. The total mass loss for each sample, corrected for desorption of physisorbed water, is tabulated in Table 7.5.

7.3.4.2 Cobalt ion incorporated GPTS-modified ethanesilica. At temperatures up to 1000 ^{o}C, the thermal decomposition followed by cobalt ion incorporated GPTS-modified ethane silica materials is similar to that of ethane silica materials without cobalt ion. For example, the percent masses of the residues obtained for as synthesized and solvent extracted cobalt ion incorporated materials containing 21 % GPTS (GBCo21A and GBCo21E, respectively) are approximately 68 and 56 %, respectively. The residue of the extracted sample, as expected, has a lower mass than the corresponding as synthesized material.

Table 7.4. TGA results of a PMO material prepared from BTME

Temperature range (^{o}C)	**% Mass loss of as synthesized material**	**% Mass loss of Solvent extracted material**	**Source of mass loss**
25 – 110	5 %	2 %	Desorption of methanol and water
110 – 265	30 %	-	Surfactant decomposition
310 – 440	17%	2 %	Surfactant decomposition and water from condensation of internal hydroxyls
440 – 780	10 %	10 %	Matrix decomposition

Table 7.5. Total mass losses obtained by TGA for GPTS-modified ethane silica materials.

	GPTS-modified ethane silica	
% GPTS	**Total mass loss[a] of as synthesized sample**	**Total mass loss of extracted sample**
21	17	20
36	24	38
46	30	
53	38	41

[a]Total mass loss = Mass loss at 800^{o}C – Mass loss at 100^{o}C.

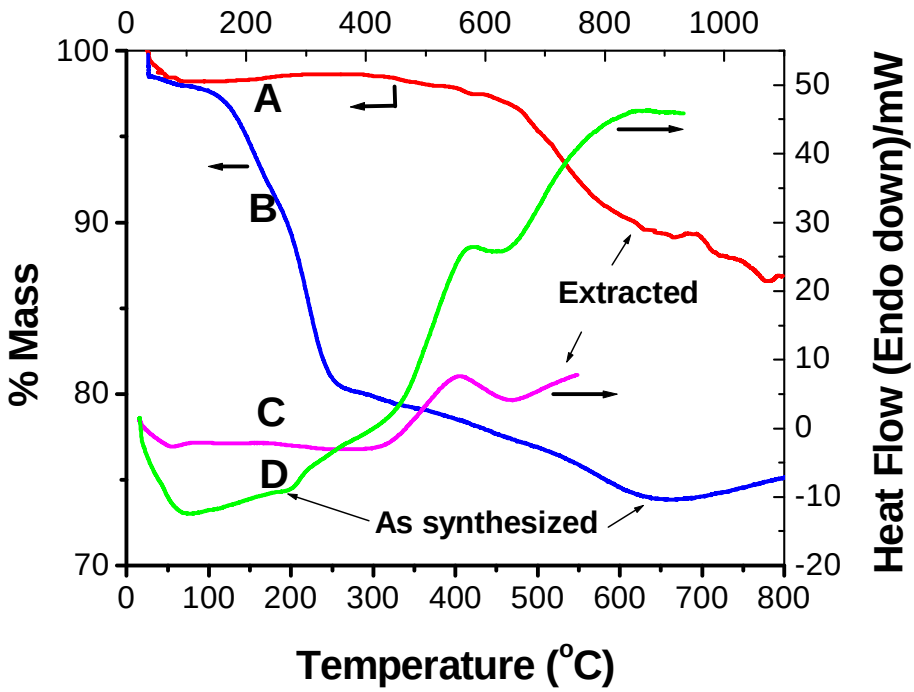

Figure 7.7 TGA and DTA curves of an as synthesized (GB0A) and extracted (GB0E) periodic ethane silica material. A = TGA, extracted; B = TGA, as-synthesized; C = DTA, extracted; D = DTA, as-synthesized.

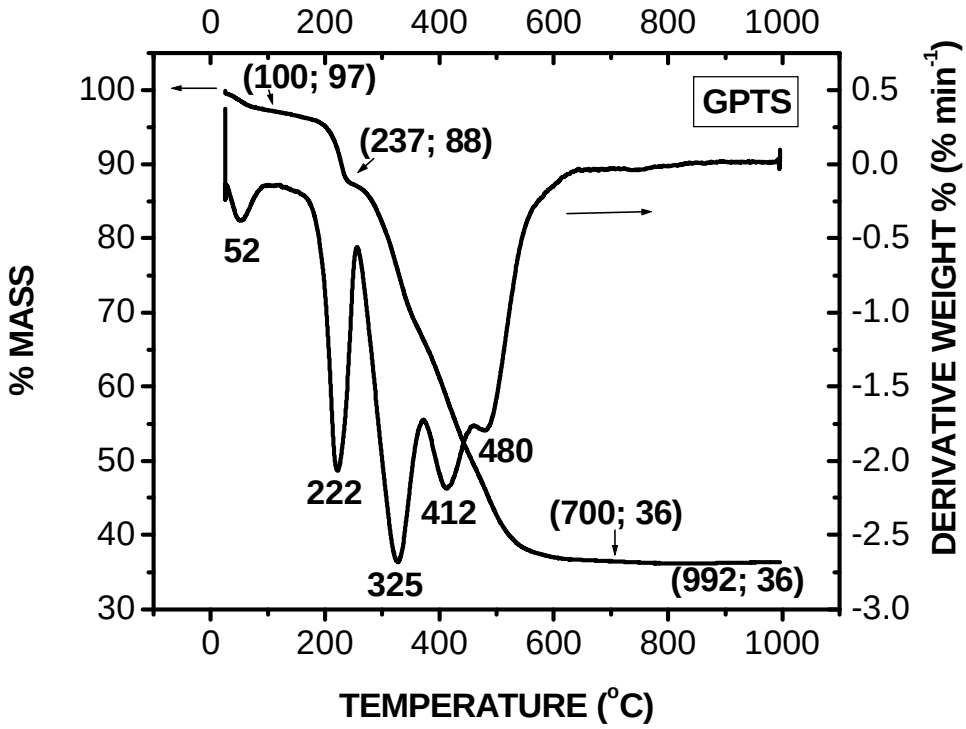

Figure 7.8 TGA curve of as synthesized GPTS silica (GB100).

7.3.5 Raman spectroscopy

7.3.5.1 GPTS-modified ethanesilica. Raman spectra of solvent extracted ethanesilica (GB0) and GPTS-modified ethanesilicas (GB21E and GB36E) are shown in Figure 7.9. The GPTS molecule has characteristic peaks at 1256 cm^{-1}, due to the breathing mode of the epoxy ring, and in the range 600 – 700 cm^{-1} (doublet) and 400 – 500 cm^{-1}, corresponding to SiO_3 vibrations and Si-O-Si network presence [34, 35]. The absence of peaks between 600 and 700 cm^{-1} indicates considerable hydrolysis and condensation of the methoxy group. Whereas a single peak is observed in the range 1400 – 1600 cm^{-1} in the spectrum of GB0E, a double peak appears in the spectra of GPTS-modified ethane silica materials. The intensity of the Raman peak at 1459 cm^{-1} increases with an increasing amount of GPTS in the reaction mixture. This peak appears to correlate with the GPTS that is incorporated into the BTME silica. Data obtained from Raman spectroscopy show that there are residual epoxy rings associated with the structure that were not opened during the sol-gel reaction. Opening of these residual epoxy ring can provide sites (OH and OR) for binding cobalt (by formation of -C -O-Co-O-C- units) by post-reaction impregnation of hybrid silica materials.

Further, ^1H NMR spectroscopy confirms the presence of the unopened epoxy rings. The ^1H NMR spectrum of GPTS was recorded and the epoxy peaks can readily be identified at 3.08 [-CHO-], 2.52 and 2.71 [-OCH_2-] [34]. These peaks are still observed in the NMR spectrum after adding aqueous base (NH_4OH) to a solution of GPTS.

7.3.5.2 Cobalt ion incorporated GPTS-modified ethanesilica. Raman spectroscopy confirms XRD results that Co_3O_4 was present in the materials in which cobalt ion was incorporated in situ into ethanesilica materials. The intense peak at 686 cm^{-1} and the peak at 480 cm^{-1} in the Raman spectrum (not shown) of a cobalt ion incorporating ethanesilica material prepared in the presence of 0.1 g cobalt nitrate can be assigned to Co_3O_4 [48, 50].

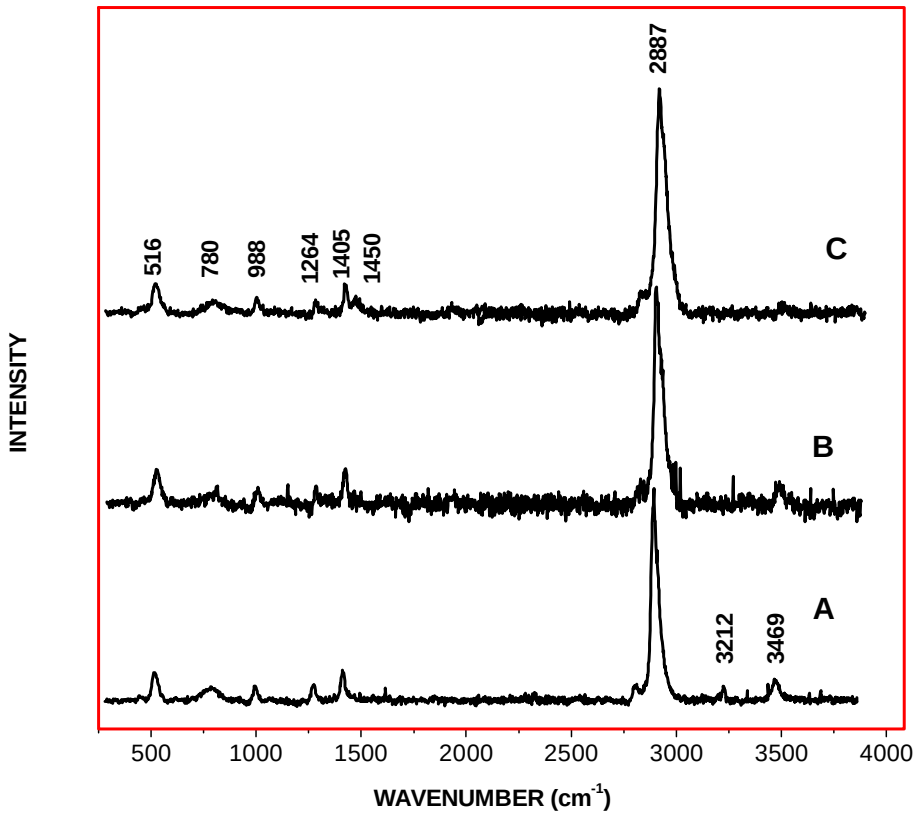

Figure 7.9 Raman spectra for solvent extracted ethane silica (A) and GPTS modified ethane silica prepared with 21 and 36 % GPTS (B and C, respectively).

7.4 Conclusions

Bifunctional periodic mesoporous organosilica materials consisting of ethane groups in the framework and glycidoxypropyl groups in the channels were synthesized. Cobalt ion incorporated GPTS-modified ethanesilica materials were synthesized by adding cobalt nitrate to the reaction mixture. Cobalt ion incorporation leads to a collapse in the periodicity of the materials, as shown by the disappearance of the XRD peak observed at $2\theta = 2^{o}$. Cobalt ion incorporation and the amount of GPTS affects pore size, surface area and pore volume as well as shapes of the isotherms and hysteresis loops.

7.5 References

1. G. J. K. Acres, A. J. Bird, J. W. Jenkins, F. King, in: Preparation of Catalysts II, edited by B. Delmon, P. A. Jacobs, and G. Poncelet, Elsevier, Amsterdam, 1 (1979).
2. H. Knozinger, Mater. Sci. Forum **25 – 26**, 233 (1988).
3. C. Song, and K. M. Reddy, Appl. Catal. *A* **176**, 1 (1999).
4. F. Schuth, A. Wingen, and J. Sauer, Micropor. Mesopor. Mater. **44 – 45**, 465 (2001).
5. A. Sayari, and S. Hamoudi, Chem. Mater. **13**, 3151 (2001).
6. B. J. Melde, B. T. Holland, C. F. Blanford, and A. Stein, Chem. Mater. **11**, 3302 (1999).
7. A. Sayari, S. Hamoudi, Y. Yang, I. Moudrakovski, and J. R. Ripmeester, Chem. Mater. **12**, 3857 (2000).
8. S. Guan, S. Inagaki, T. Ohsuna, and O. Terasaki, J. Am. Chem. Soc. **122**, 5660 (2000).
9. S. Inagaki, S. Guan, Y. Fukushima, T. Ohsuna, and O. Terasaki, J. Am. Chem. Soc. **121**, 9611 (1999).
10. S. Guan, S. Inagaki, T. Ohsuna, and O. Terasaki, Micropor. Mesopor. Mater. **44 – 45**, 165 (2001).

11. M. Kruk, M. Jaroniec, S. Guan, and S. Inagaki, J. Phys. Chem. B **105**, 681 (2001).
12. H. Fan, S. Reed, I. Baer, R. Schunk, G. P. López, and C. J. Brinker, Micropor. Mesopor. Mater. **44 – 45**, 625 (2001).
13. Y. Lu, H. Fan, N. Doke, D. A. Loy, R. A. Assink, D. A. LaVan, and C. J. Brinker, J. Am. Chem. Soc. **122**, 5258 (2000).
14. H. Fan, Y. Lu, A. Stump, S. T. Reed, T. Baer, R. Schunk, V. Perez-Luna, G. P. López, and C. J. Brinker, Nature **405**, 56 (2000).
15. S. S. Park, C. H. Lee, J. H. Cheon, and D. H. Park, J. Mater. Chem. **11**, 3397 (2001).
16. S. S. Park, C. H. Lee, J. H. Cheon, S. J. Choe, and D. H. Park, Bull. Korean Chem. Soc. **22**, 948 (2001).
17. C. H. Lee, S. S. Park, S. J. Choe, and D. H. Park, Micropor. Mesopor. Mater. **46**, 257 (2002).
18. O. Muth, C. Schellbach, and M. Froba, Chem. Commun. 2032 (2001).
19. E-B. Cho, K-W. Kwon, and K. Char, Chem. Mater. **13**, 3837 (2001).
20. H. Zhu, D. J. Jones, J. Zajac, J. Rozière, and R. Dutartre, Chem. Commun. 2568 (2001).
21. M. C. Burleigh, M. A. Markowitz, E. M. Wong, J-S. Lin, and B. P. Gaber, Chem. Mater. **13**, 4411 (2001).
22. J. R. Matos, M. Kruk, L. P. Mercuri, M. Jaroniec, T. Asefa, N. Coombs, G. A. Ozin, T. Kamiyama, and O. Terasaki, Chem. Mater. **14**, 1903 (2002).
23. T. Ren, X. Zhang, and J. Suo, Micropor. Mesopor. Mater. **54**, 130 (2002).
24. A. Sayari, and Y. Yang, Chem. Commun. **21**, 2582 (2002).
25. S. Hamoudi, and S. Kaliaguine, Chem. Comm. 2118 (2002).
26. T. Asefa, M. Kruk, M . J. MacLachlan, N. Coombs, H. Grondey, M. Jaroniec, and G. A. Ozin, J. Am. Chem. Soc. **123**, 8520 (2001).
27. M. C. Burleigh, M. A. Markowitz, M. S. Spector, and B. P. Gaber, Langmuir **17**, 7923 (2001).
28. M C. Burleigh, M. A. Markowitz, M. S. Spector, and B. P. Gaber, Chem. Mater. **13**, 4760 (2001).

29. M. C. Burleigh, M. A. Markowitz, M. S. Spector, and B. P. Gaber, J. Phys. Chem. B **105**, 9935 (2001).
30. M. C. Burleigh, S. Dai, and E. W. Hagaman, Chem. Mater. **13**, 2537 (2001).
31. S. R. Davis, A. R. Brough, and A. Atkinson, J. Non-Crystalline Solids **315**, 197 (2003).
32. P. Cardiano, S. Sergi, M. Lazzari, and P. Piraino, Polymer **43**, 6635 (2002).
33. M. Templin, U. Wiesner, and H. W. Spiess, Adv. Mater. **9**, 814 (1997).
34. P. Innocenzi, A. Sassi, G. Brusatin, M. Guglielmi, D. Favretto, R. Bertani, A. Venzo, and F. Babonneau, Chem. Mater. **13**, 3635 (2001).
35. R. S. Young, *Cobalt:* Its Chemistry, Metallurgy and Uses, American Chemical Society, Reinhold, New York (1960).
36. H. P. Withers, Jr., K. F. Eliezer, and J. W. Mitchell, Ind. Eng. Chem. Res. **29**, 1807 (1990).
37. E. Iglesia, Appl. Catal. A **161**, 59 (1997).
38. R. C. Brady, and R. J. Pettit, J. Am. Chem. Soc. **103**, 1287 (1981).
39. J. G. Goodwin, Jr., Prep. ACS Div. Pet. Chem. **36**, 156 (1991).
40. J. Li, and N. J. Coville, Appl. Catal. A **208**, 177 (2001).
41. N. N. Madikizela, and N. J. Coville, J. Molec. Catal. A: General **181**, 129 (2002).
42. C. A. Glotfelter, and R. P. Ryan, US Patent 5120811 (1992).
43. H. Schmidt, B. Seiferling, G. Phillip, and K. Deichmann, in Processing of Advanced Ceramics, Wiley, New York, 651 (1988).
44. M. Pilz, and H. Romich, J. Sol-Gel Sci. Technol. **8**, 1071 (1997).
45. J. S. Beck, J. C. Vartuli, W. J. Roth, M. E. Leonowicz, C. T. Kresge, K. D. Schmitt, C. T-W. Chu, D. H. Olson, E. W. Sheppard, S. McCullen, J. B. Higgins, and J. L. Schlenker, J. Am. Chem. Soc. **114**, 10834 (1992).
46. C. T. Kresge, M. E. Leonowicz, W. J. Roth, J. C. Vartuli, and J. S. Beck, Nature **359**, 710 (1992).
47. A. Stein, B. J. Melde, and R. C. Schroden, Adv. Mater. **12**, 1403 (2000).

48. J. Panpranot, J. G. Goodwin, Jr., and A. Sayari, Catal. Today **77**, 269 (2002).

49. S. J. Gregg, and K. S. W. Sing, Adsorption, Surface Area and Porosity, Academic Press, London (1982).

50. J. Li., and N. J. Coville, Appl. Catal. A **181**, 201 (1999).

CHAPTER EIGHT

In situ and post reaction cobalt-incorporation into aminopropyl-modified periodic mesoporous ethanesilica materials

8.1 Introduction

The sol-gel method is widely used to synthesise periodic mesoporous organosilica (PMO) materials containing both bridging organic functional moieties in the framework and terminal organic functional groups protruding into the channel pores [1 – 20]. The large ordered pore sizes of PMOs make these materials very attractive for applications such as catalyst supports, sensors and adsorbents for heavy metal ions. Periodic ethanesilica, by far the most widely studied PMO, has been modified by co-condensation of 1,2-bistrialkoxysilylethane precursors with various trialkoxyorganosilanes in the presence of surfactants [21 – 32]. Organosilane precursors co-condensed with bistrialkoxysilylethane include 3-glycidoxypropyltrimethoxysilane [21], 3-cyanopropyltriethoxysilane [22], N-(2-aminoethyl)-3-aminopropyltrimethoxysilane [H_2N-$(CH_2)_2$-$NH(CH_2)_3$] [26], N-[3-(trimethoxysilyl)propyl]ethylenediamine [27] and mercaptopropyltrimethoxysilane [HS-$(CH_2)_3$-] [26, 31, 32].

PMO materials containing "nitrogen-bearing" functional groups (e.g. cyano- (CN) [22], amines (NH) [24 – 27, 33], etc) have also received some attention. Asefa et. al. prepared periodic mesoporous aminosilicas (PMAs) that contain amine functional groups in the framework of a mesoporous network via thermal ammonolysis of periodic mesoporous organosilicas (PMOs) under a flow of ammonia gas [33]. Burleigh and co-workers described the preparation of a porous organosilica by co-condensation of bistriethoxysilylethane and N-(2-aminoethyl)-3-aminopropyltrimethoxysilane, N-[3-(trimethoxysilyl)propyl] ethylenediamine or

Cu(II)-complexed N,N'-bis[3-(trimethoxysilyl)propyl]ethylenediamine under acidic and basic conditions [24 – 27].

For catalytic applications, aminopropyl-functionalised amorphous and ordered mesoporous silicas have been the most widely studied organic-inorganic hybrid solids [34]. These organic-inorganic hybrids have been used as catalysts for the Knoevenagel condensation of various aldehydes and ketones with ethyl cyanoacetate [35 – 37] as well as for base-catalysed reactions such as the nitroaldol condensation and Michael addition reactions [38, 39].

Although, unfunctionalized silica materials, including ordered mesoporous silicas (MCM 41) have been used as supports for cobalt-based catalysts in the FT synthesis [40 – 42], there are very few reports in the literature on cobalt incorporation into periodic mesoporous organosilica materials. Further, amine functionalised silicas have not been used in the Fischer Tropsch (FT) reaction.

Herein we report on the synthesis and characterization of organosilica materials synthesized by co-condensation of 1,2-bistrimethoxysilylethane (BTME) with 3-aminopropyltriethoxysilane (APTS) in the presence of hexadecyltrimethylammonium bromide (cetyltrimethylammonium bromide, CTAB) as the surfactant both in the presence and absence of cobalt ions. The molecular structures of these silica precursors and the surfactant are shown in Scheme 8.1. Cobalt ion was added to the formed silicas to generate Co supported catalysts for use in Fischer-Tropsch (FT) catalyst synthesis [43 – 48]. 3-Aminopropyltriethoxysilane (APTS) has a terminal amine group which may be beneficial for binding metals and this is one of the aspects of APTS which we wish to explore in this study.

The FT studies are a continuation of our studies on Co supported catalysts [49]. To the best of our knowledge, this is the first report on the synthesis of cobalt ion incorporated APTS-modified ethane silica.

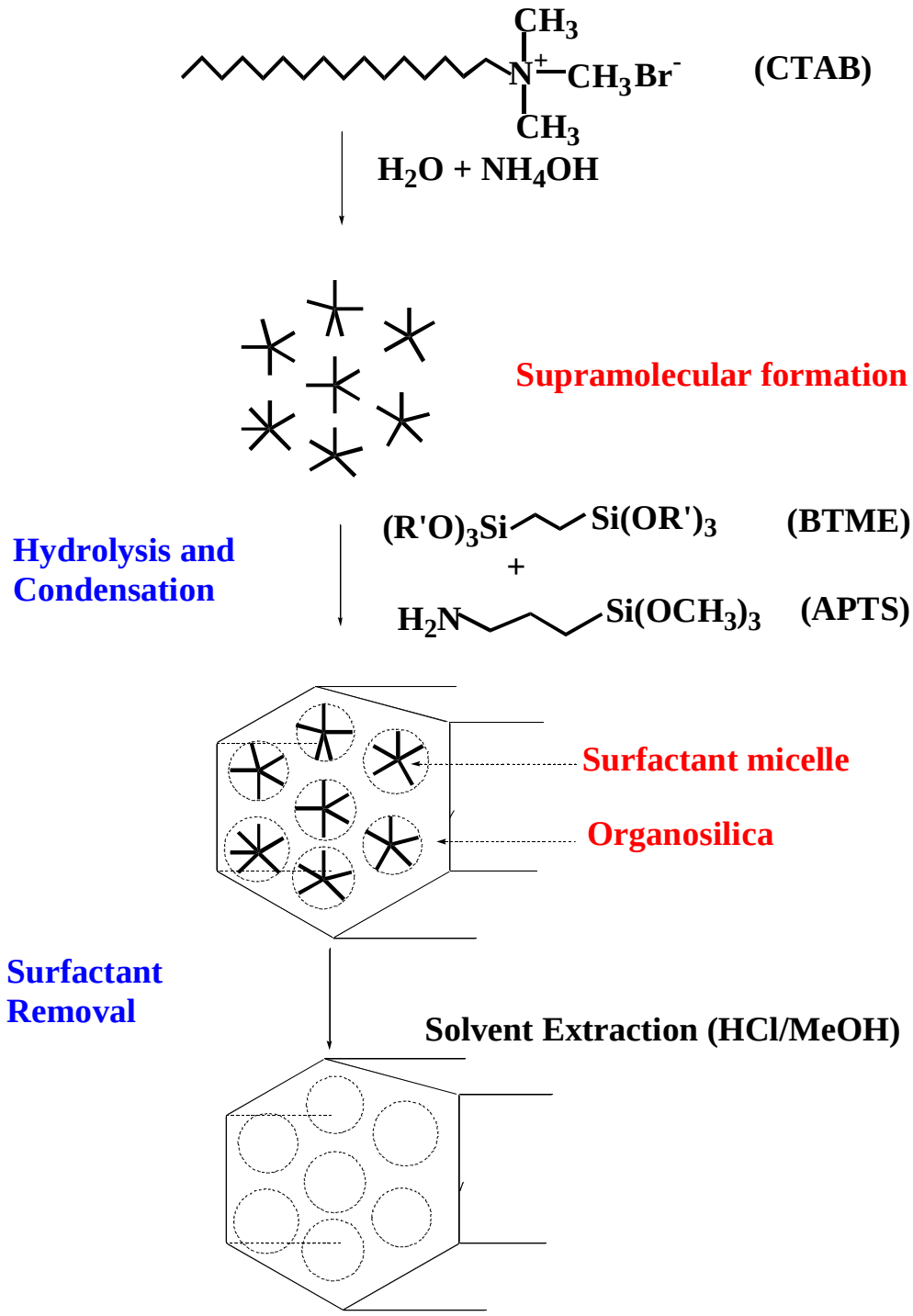

Scheme 8.1. Reaction scheme showing the formation of periodic mesoporous aminopropyl-modified ethane silica. Note that the framework is made up of units of $H_2NCH_2CH_2CH_2SiO_3$ and $O_3SiCH_2CH_2SiO_3$.

8.2 Experimental Section

8.2.1 Chemicals

1,2-bistrimethoxysilylethane (BTME), hexadecyltrimethylammonium bromide (CTAB) and cobalt nitrate hexahydrate were obtained from Aldrich; 3-aminopropyltriethoxysilane (APTS) was obtained from ABCR (Germany); ammonium hydroxide was obtained from Fluka. All chemicals were used as received.

8.2.2 Synthesis

8.2.2.1 APTS-functionalized ethanesilica. PMOs were prepared using a modified method based on that reported by Ozin and co-workers [23]. A series of APTS-modified ethanesilica materials were prepared starting with a mole ratio of BTME:APTS:CTAB:NH_4OH:H_2O = 1: x : 0.275: 16: 218 (where x = 0, 0.476, 0.714, and 0.952). In a typical synthesis, CTAB (0.36 g; 0.98 mmol) was dissolved in a solution consisting of water (14 ml) and 28 % ammonium hydroxide (8 ml; 0.058 mol). The mixture was stirred for 45 minutes. The pH of the solution was estimated by pH paper to be approximately 10. A mixture of BTME (0.9 ml, 3.57 mmol) and APTS [varying amounts: 0.8 ml (3.40 mmol), 0.6 ml (2.55 mmol) and 0.4 ml (1.70 mmol)] was added dropwise to the stirred mixture. These materials are denoted as BAA(1:1), BAA(1:0.7) and BAA(1:0.5), respectively (See section 8.2.2.5 for a description of notation used).
Stirring was continued for a further 1 hour, followed by ageing at 80 ^oC for 4 days. The solid was suction filtered in a Büchner funnel and washed with an excess of water. The solid was dried in air overnight to give the required material (between 1 and 2 g).

8.2.2.2 Surfactant extraction. A portion of the as synthesized sample (0.5 g) was stirred in a solution of concentrated HCl (5 ml) in methanol (200 ml) at 50 ^oC for 2 days. The solid was suction filtered in a Büchner funnel, washed with

water and finally with methanol (200 ml) and then dried in air. Mass losses of between 20 and 40 % were observed after surfactant extraction. Extracted materials are denoted as BAE(1:1), BAE(1:0.7) and BAE(1:0.5), respectively.

8.2.2.3 *In situ* cobalt incorporated APTS-functionalized ethanesilica. Cobalt incorporated APTS-modified ethanesilica materials were synthesized by adding cobalt nitrate [0.1 g (0.34 mmol)] to a reaction mixture of CTAB (0.36 g; 0.98 mmol), water (28 ml) and 28 % ammonium hydroxide (8 ml; 0.229 mol). A mixture of BTME and APTS (BTME:APTS = 1:1 or 1:0.5) was then added dropwise to the mixture. The procedure, including solvent extraction, was continued as described above for the synthesis of APTS-modified ethanesilicas. The APTS-modified ethanesilica materials synthesized in this manner are denoted as 6.7CoBAE(1:1)-*in situ* and 6.7CoBAE(1:0.5)-*in situ* . The corresponding ethanesilica (not modified) is denoted as 6.7CoBE-*in situ.*

8.2.2.4 Post reaction cobalt incorporated APTS-functionalized ethanesilica. Cobalt incorporated aminopropyl-modified ethanesilica was prepared using the incipient wetness impregnation method. An aminopropyl-modified ethanesilica [BAE(1:1)] having a BET surface area, pore volume and desorption BJH pore diameter of 389 m^2/g, 0.27 cm^3/g and 3.0 nm, respectively was used as the support. Different amounts of cobalt nitrate, $Co(NO_3)_2.6H_2O$, (0.1 g and 0.2g) were dissolved in deionised water and impregnated into the support (0.3 g) using incipient wetness to give materials with 6.7 % and 13.5 % cobalt. Materials were dried at 120 ^oC for 12 hours. Materials synthesized in this manner are denoted as 6.7CoBAE(1:1)-*imp* and 13.5CoBAE(1:1)-*imp.*

8.2.2.5 Nomenclature. The percentage APTS indicates the percentage of APTS expressed per mole of silicon atoms in the BTME and APTS organosilica precursors {% APTS = [100 x (mol Si in APTS)/(2 x moles Si in BTME + mol Si in APTS)]}. The moles of BTME are multiplied by 2 because each BTME molecule supplies two moles of Si whereas an APTS molecule supplies one. The notation used to identify the samples is as follows: A = APTS, B = BTME, Co =

cobalt, A = as synthesized, and E = extracted. The mole ratio of BTME to APTS in the reaction mixture is given in parenthesis. Numerical figures preceding Co refer to the percentage of cobalt in the sample in cobalt incorporated samples. The method used to incorporate cobalt is identified by *imp* (impregnated) or *in situ* after the name. For example, BAE(1:0.5) refers to an extracted (*E*) sample synthesized from APTS (*A*) and BTME (*B*) in which the ratio of BTME to APTS is 1:0.5. 6.7CoBAE (1:1) – *imp*, refers to a cobalt incorporated (6.7 % *Co*), extracted (*E*) material synthesized from APTS (*A*) and BTME (*B*) in a 1:1 ratio in which cobalt was supported by impregnation (*imp*).

8.2.3 Characterization

Characterization of the samples was carried out by powder X-ray diffraction (XRD), nitrogen adsorption, Raman spectroscopy, thermogravimetric analysis (TGA), Scanning electron microscopy (SEM) and UV-vis diffuse reflectance spectroscopy as described in Chapter 3.

8.3 Results and Discussion

8.3.1 Synthesis

Addition of a mixture of BTME and APTS to a basic solution of CTAB formed white solid materials. A gel formed immediately for samples containing large amounts of APTS. For all mixtures, precipitation started within 30 minutes after addition of the silica precursor. Addition of cobalt nitrate to the mixture yielded dark brown/black materials for CoBAE(1:0.5)-*in situ* and CoBAE(1:1)-*in situ*. The base catalysed surfactant templated formation of periodic mesoporous APTS-ethane silica is proposed to form from micelles [50] as illustrated in Scheme 8.1.

8.3.2 Powder X-ray Diffraction

8.3.2.1 APTS-modified ethanesilica. Powder XRD was used to probe the periodicity of the mesoporous materials. Periodic mesoporous materials display a very high intensity peak at around $2\theta = 2^o$, together with low intensity peaks in the 2θ range $3 – 8^o$ [50, 51]. The prominent low angle peak at approximately $2\theta = 2^o$ indicates the presence of uniformly sized pores for ordered materials. XRD patterns (shown in Figure 8.1) show relatively broad low angle peaks compared to that of hexagonal MCM41 materials. The absence of higher angle reflections suggests the lack of long range order. The most intense peak was arbitrarily assigned as the d (100) peak. Powder XRD patterns of the as synthesized and the solvent extracted APTS-modified ethane silica samples in which the BTME:APTS mole ratio is 1:1 are shown in Figure 8.1 (D and C, respectively; d values of 3.9 and 4.1 nm, respectively). Corresponding values obtained for a related amine-functionalised material synthesized by Burleigh et. al. [26] are 4.3 nm and 4.4 nm, respectively, and suggests equivalent structures.

As expected for organic-functionalized silicas synthesized via co-condensation [23, 52], the position of the d (100) peak shifts to higher angles (implying lower d values) as the amount of APTS added increased (Figure 8.1). This shift corresponds to the reduction in the interplanar spacing from about 4.9 to 3.9 nm for BAE(0.5) and BAE(1:1), respectively. The same behaviour was observed for BTME silica modified by co-condensation with various organosilanes including 3-glycidoxypropyltrimethoxysilane [21] and 3-cyanopropyltriethoxysilane [22].

From the above data it can be seen that the amount of APTS has an effect on the pore structure of the silica material. It is assumed that the major effect arises from an interaction of the CTAB micelle with the APTS that modifies the micelle structure, leading to the loss of long range order. Increasing the amount of APTS may cause an increase in the number of electrostatic interactions between the aminofunctional group of APTS and the quartenary ammonium head group of the surfactant, which can result in a change in the density of silanol groups in the

surfactant silicate interface, thereby requiring fewer surfactant molecules for charge balance. This situation leads to contraction of the micelle size in hybrid mesoporous materials with higher concentrations of APTS [22, 53]. However, further work on this and other related systems will need to be performed to confirm this suggestion.

It was also observed that when the ratio of surfactant to silica precursors was changed, by increasing the amount of surfactant while keeping the amount of silica precursors constant, the d_{100} peak observed in the surfactant-containing material (with a reduced intensity) disappeared after solvent extraction.

8.3.2.2 Co-incorporated APTS-modified ethanesilica. The XRD pattern of a solvent-extracted material synthesized in the presence of cobalt nitrate (0.1 g) using a BTME:APTS mole ratio of 1:0.5, CoBAE(1:0.5)-*in situ*, displays an intense diffraction peak with a lattice spacing, d_{100}, of 4.78 nm at 1.85^{o} (Figure 8.1B) . This value is slightly higher than that of BAE(1:05) (Figure 8.1A), by ~0.1 nm. As shown in Figure 8.1 (insert), the material obtained by impregnating 0.3 g of the material prepared from a BTME:APTS mole ratio of 1:1 with 0.1 g cobalt nitrate [6.7CoBAE(1:1)] does not show any low angle diffraction peaks, suggesting loss of mesophase for this sample. Similar results were reported for other Co-impregnated ethane silica materials [54].

Table 8.1. Structural properties of organosilica materials .

Sample and % APTS[a]	**SA**[b] **(m^2/g)**	**PV**[c] **(cm^3/g)**	**APD**[d] **(nm)**	**D_{ad}**[e] **(nm)**	**D_{des}**[f] **(nm)**	**d_{100}**[g] **(nm)**
BAE(1:1) [32 %]	389	0.27	2.78	2.1 – 2.2 (2.0)	3.0 – 2.9 (3.0)	3.92 (4.11)
BAE(1:0.7) [26 %]	426	0.30	2.83	1.7 – 1.7 (1.7)	2.6 – 2.1 (2.3) [h]	4.38
BAE(1:0.5) [19 %]	470	0.45	3.82	2.8 – 2.6 (2.7)[h]	3.2 – 3.1 (3.2)	4.93
BE	672	0.71	4.24	2.2 – 2.1 (2.2)	3.3 – 3.2 (3.3)	4.75 (4.42)
13.5CoBA(1:1) – *imp*	181	0.14	2.53	2.0 – 1.8 (1.9)	3.1 – 3.0 (3.1)	
6.7CoBAE(1:1)-*imp.*	250	0.17	2.76	1.9 – 1.8 (1.8)	3.2 – 3.1 (3.1)	
6.7CoBAE(1:1)-*in situ*	308	0.19	2.52	-[i]	-	4.34
6.7CoBE - *in situ*	438	0.48	4.34	2.5 – 2.4 (2.4)	3.2 – 3.1 (3.1)	4.45

[a] Values in square brackets are % APTS = [100 x (mol Si in APTS)/(2 x moles Si in BTME + mol Si in APTS, [b] SA = BET Surface Area, [c] PV = Total Pore volume (cm^3/g), [d] APD = Average Pore Diameter, [e] D_{ad} = BJH Adsorption Pore Diameter, [f] D_{des} = BJH Desorption Pore Diameter, [g] d_{100} = XRD lattice parameter of extracted samples. The value of the corresponding as synthesized sample is given in parenthesis. [h] broad PSD 'mesopore' peak. [i] Not determined, 5-point BET method was used to determine surface area.

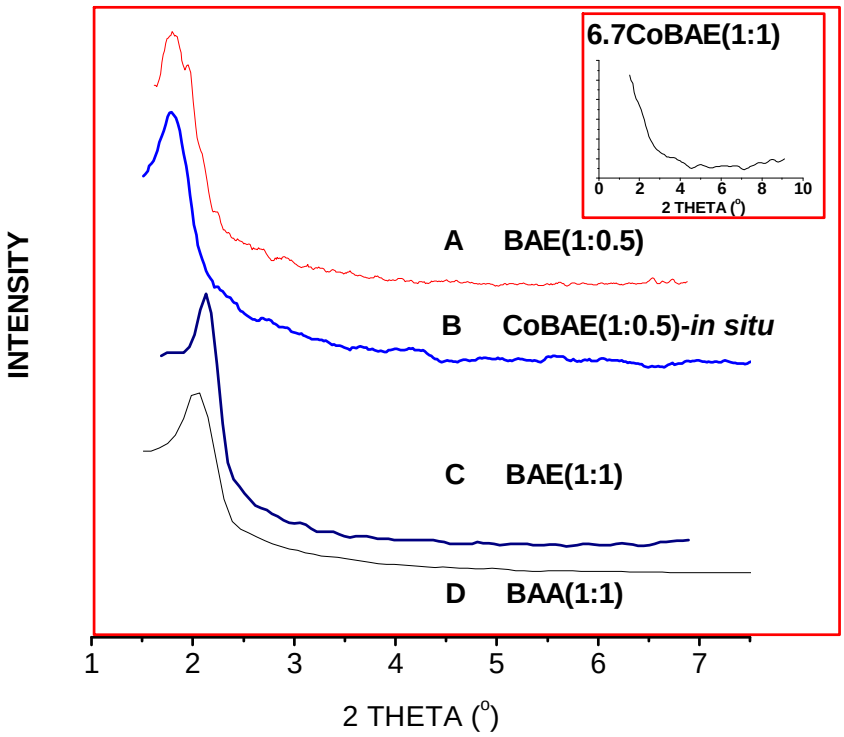

Figure 8.1. XRD patterns for aminopropyl-functionalized ethanesilicas. A = extracted APTS-modified ethane silica (BTME:APTS = 1:0.5); B = extracted APTS-modified ethane silica (BTME:APTS = 1:0.5) prepared in the presence of 0.1 g cobalt nitrate; C and D = extracted and as-synthesised APTS-modified ethane (BTME:APTS = 1:1), respectively. Insert: APTS-modified ethane silica (BTME:APTS = 1:1) impregnated with 0.1 g cobalt nitrate.

8.3.3 Nitrogen sorption

8.3.3.1 APTS-modified ethanesilica. Nitrogen adsorption-desorption isotherms for extracted aminopropyl-modified ethanesilica samples with BTME:APTS mole ratios of 1:0.5, 1:0.7 and 1:1 in the synthesis gels are shown in Figure 8.2 (A, B and C, respectively). All the materials exhibit Type IV isotherms with a narrow pore size distribution according to the IUPAC classification, which is typical for mesoporous materials [55]. The shape of the hysteresis loop (Type H4) observed for BAE(1:1) and BAE(1:0.7) is consistent with the presence of 'ink-bottle' pores having a narrow entrance and wide interior.

The structural properties (BET surface area, average pore diameter, pore volume and lattice parameter) of these materials are listed in Table 8.1. BJH desorption PSDs with maxima ranging between 3.3 (for the unmodified ethanesilica material) and 3.0 nm (for the material with BTME:APTS =1:1) are obtained. (Table 8.1, Figure 8.2). The corresponding pore diameters obtained from the adsorption isotherm are 2.2 and 2.0 nm, respectively. The pore volumes derived from the adsorption isotherm are lower than the corresponding values obtained from the desorption isotherm by about 1 nm (Table 8.1). The surface area and total pore volume decrease significantly after co-condensation with increasing amount of APTS (Figure 8.3). The same behaviour was observed for ethanesilica modified by co-condensation of BTME with 3-glycidoxypropyltrimethoxysilane [21].

8.3.3.2 Co-incorporated APTS-modified ethanesilica. Shown in Figure 8.4 (A and B) are isotherms of the materials prepared by impregnating 0.3 g samples of an APTS-modified ethanesilica [(BAE(1:1), BET surface area = 389 m^2 g^{-1}, and pore volume = 0.27 cm^3 g^{-1}] with 0.1 and 0.2 g of cobalt nitrate, yielding materials with 6.7% [6.7CoBAE(1:1)] and 13.5 % [13.5CoBAE(1:1)] cobalt, respectively. The effect of incorporating cobalt nitrate onto amine-functionalized materials on the surface area is clearly observed from the isotherms. The shape of the isotherm is not affected by post reaction cobalt incorporation. As shown in Figure 8.5, the surface area and total pore volume decreased significantly after cobalt incorporation. The decrease in surface area and pore volume as the amount

of Co loading increases suggests that Co particles were deposited in the pores of the organosilica materials [56].

The surface areas and pore volumes of the materials prepared by the impregnation method are lower than the corresponding values of the materials prepared by the *in situ* procedure (see Table 8.1). For example, the cobalt incorporated APTS-modified ethanesilica material synthesized in the presence of 0.1 g cobalt nitrate [6.7CoBAE(1:1) - *in situ*] has a higher surface area (308 m^2/g) compared to the material impregnated with an equivalent amount of cobalt nitrate (250 m^2/g for 6.7CoBAE(1:1) - *imp*). This arises since in the impregnation method all the Co nitrate fills the pores while in the *in situ* method some of the Co is incorporated in the framework to form Co-O-Si bonds and hence the Co does not block the pores as effectively.

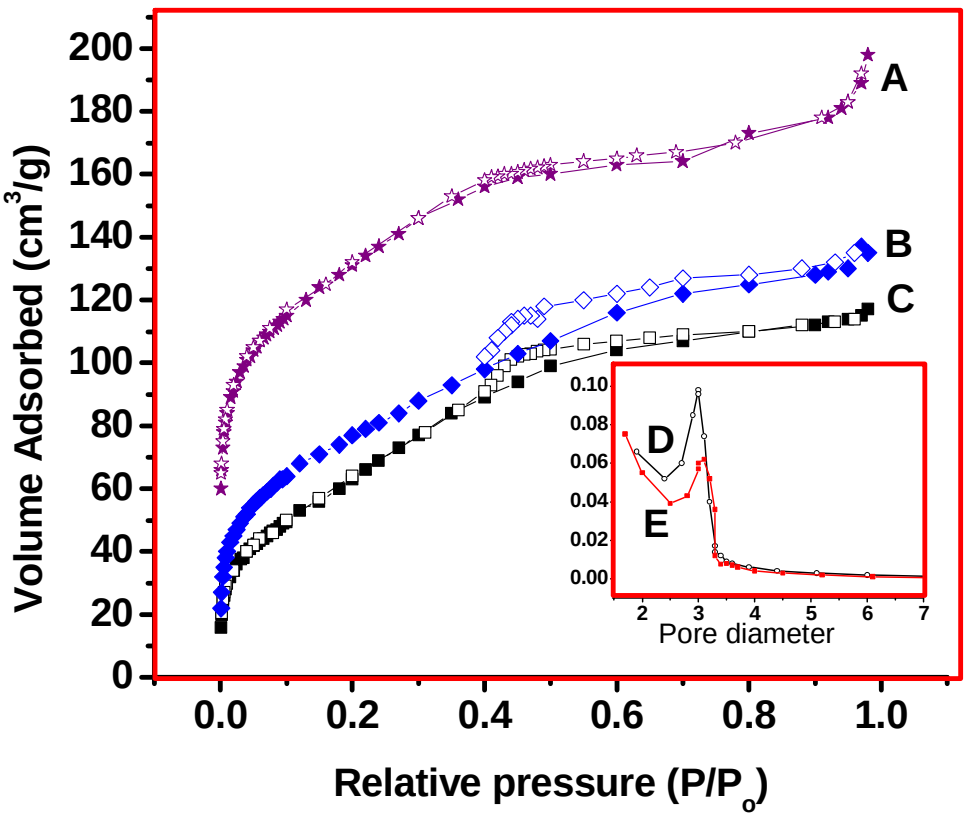

Figure 8.2. N_2 adsorption desorption isotherms and BJH pore size distributions derived from desorption isotherms for APTS-modified ethane silica and Co-incorporated APTS-modified ethane silica materials. A, B and C are isotherms of APTS-modified ethane silica with BTME:APTS mole ratios of 1:0.5, 1:0.7, and 1:1, respectively. D and E are BJH desorption PSDs for BAE1:1 and BAE(1:0.5), respectively.

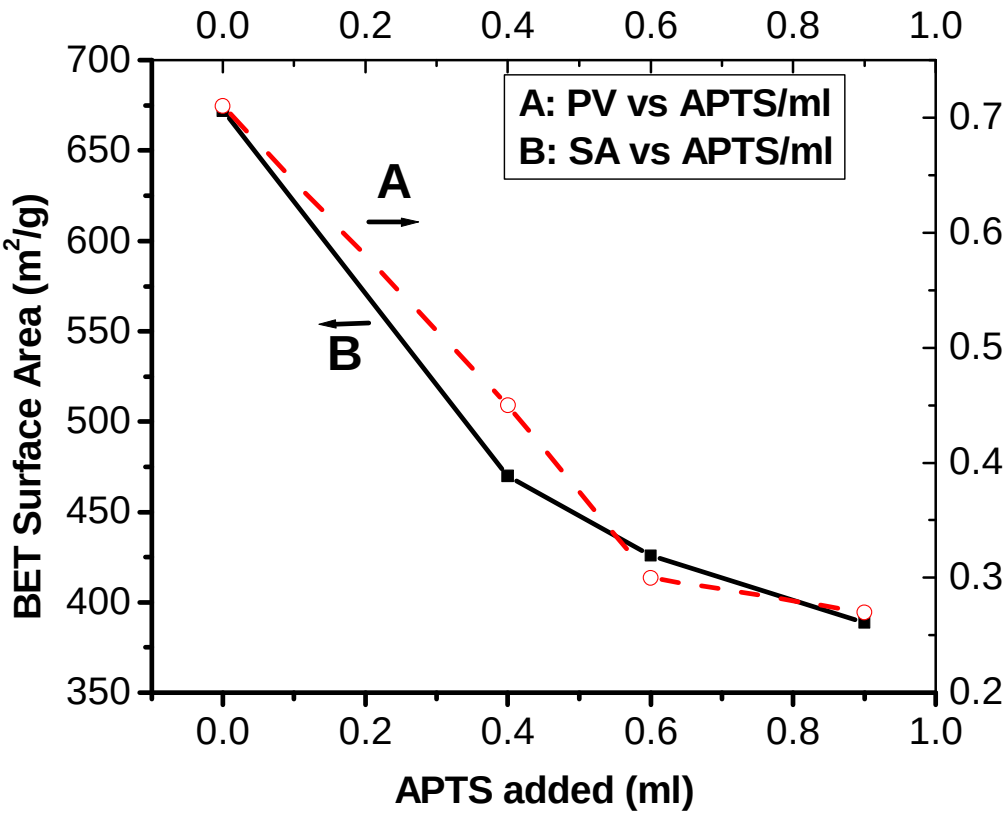

Figure 8.3. Variation of surface area (SA) and pore volume (PV) with amount of APTS loading for APTS-modified ethane silicas. (A = PV vs volume APTS; B = SA vs volume APTS).

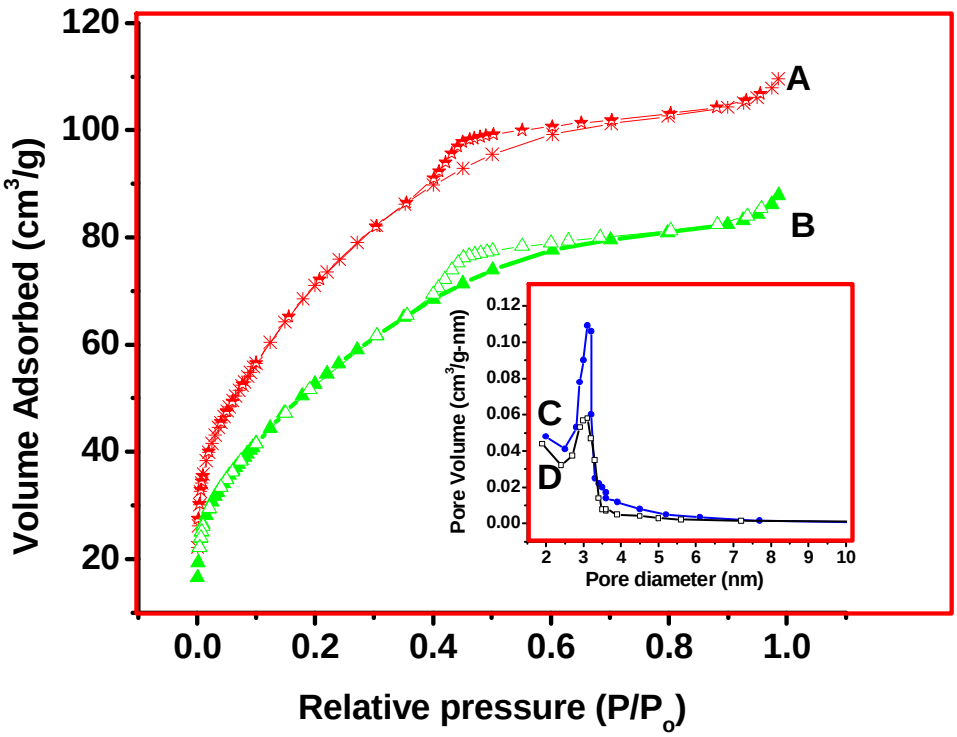

Figure 8.4. N_2 adsorption desorption isotherms and BJH pore size distributions derived from desorption isotherms for Co-incorporated APTS-modified ethane silica materials. A and B are isotherms of APTS-modified ethane silica with BTME:APTS mole ratio of 1:1 impregnated with 6.7 % and 13.5 % cobalt, respectively. C and D are BJH desorption PSDs for 6.7CoBAE(1:1)-*imp* and 13.5CoBAE(1:1)-*imp*, respectively.

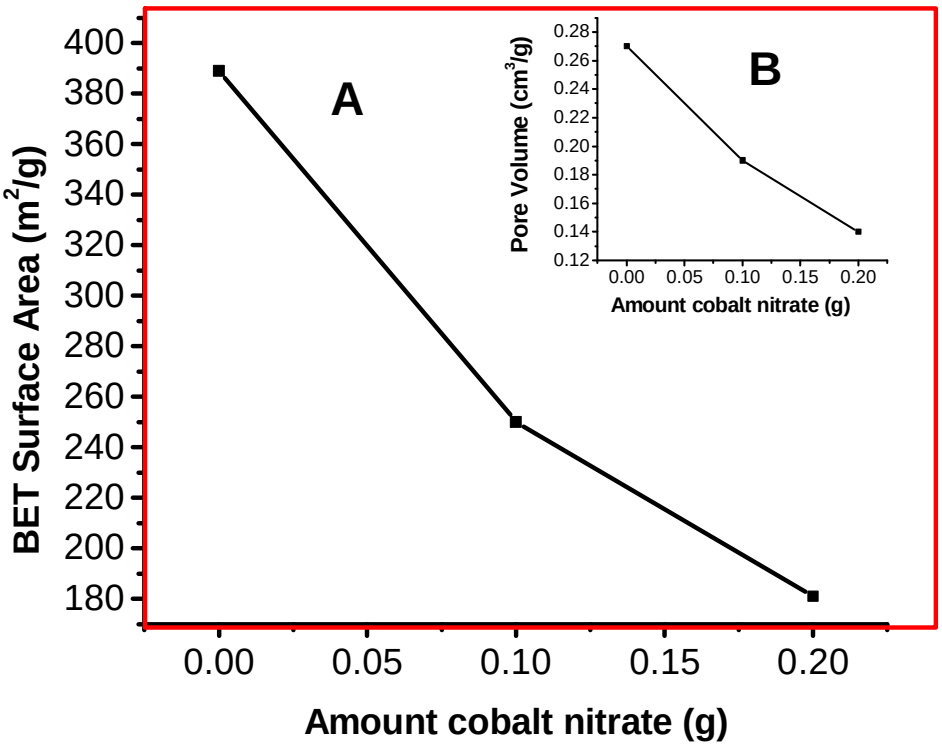

Figure 8.5. Variation of surface area and pore volume (insert) with amount of cobalt loading for APTS-modified ethane silicas obtained using the impregnation method.

8.3.4 Thermogravimetric analysis

8.3.4.1 APTS-modified ethanesilica. TGA (under N_2) was used to monitor the decomposition characteristics of the APTS-modified ethanesilica materials before and after solvent extraction. Analysis was conducted from room temperature to 1000 ^oC. Thermograms and derivative thermograms of samples prepared from a mixture of APTS and BTME are shown in Figure 8.6. The results for as-synthesized and solvent extracted APTS-modified ethanesilica materials prepared from a mixture with BTME:APTS = 1:1 are summarised in Table 8.2. The profiles indicate that the organosilica materials all have similar thermal stability, with distinct mass losses, associated with the organic groups in the materials. Whereas the extracted ethane silica loses no weight in the range 262 – 370 ^oC [21], the solvent extracted APTS-modified ethanesilica materials lose mass in this region (Figure 8.6). The mass loss in this region decreases with decreasing amount of APTS used during synthesis and is consequently attributed to loss of the aminopropyl functional group. The onset of aminopropyl group decomposition overlaps with the decomposition of surfactant molecules in as-synthesized materials. The mass losses obtained in the temperature range 100 – 400 ^oC for materials with BTME:APTS mole ratios of 1:1 and 1:0.5 [BAE(1:1) and BAE(1:0.5)] are 17 and 24 %, respectively. All extracted APTS/BTME samples lose between 10 and 12 % of their masses due to framework ethane group decompostion at temperatures between 400 and 800 ^oC. Another observation is that APTS/BTME samples lose more weight (due to methanol and ethanol desorption) below 100 ^oC compared to BTME samples. This is expected as the material formed from co-condensation of APTS and BTME is more hydrophilic than that prepared from BTME alone [26].

8.3.4.2 Co-incorporated APTS-modified ethanesilica. TGA curves of cobalt incorporated ethanesilica materials prepared by impregnation of 0.3 g ethanesilica samples with 0.1 and 0.2 g cobalt nitrate are shown in Figure 8.7. The mass loss at temperatures between 100 and 300 ^oC observed in materials obtained by impregnation is due to loss of products associated with the decomposition of the

nitrate ions and water. Sample 6.7CoBAE(1:1) loses half (16 %) the mass lost by 13.5CoBAE(1:1) (30%) in agreement with the ratio of cobalt nitrate used for the impregnation. The other mass losses observed are similar to those associated with the hybrid support.

Table 8.2. TGA results of as-synthesized and solvent-extracted APTS-modified ethanesilica materials prepared from a mixture with BTME:APTS = 1:1.

Temperature range (^{o}C)	**% Mass loss of as synthesized material**	**% Mass loss of solvent extracted material**	**Source of mass loss**
25 – 175	5 %	10 %	Desorption of water, ethanol and methanol
175 – 250	50 %	2 %	Surfactant decomposition
250 – 370	17 %	13 %	Decomposition of surfactant and aminopropyl functional group
370 – 600	5.5 %	12 %	Decomposition of ethane groups from the ethane silica network

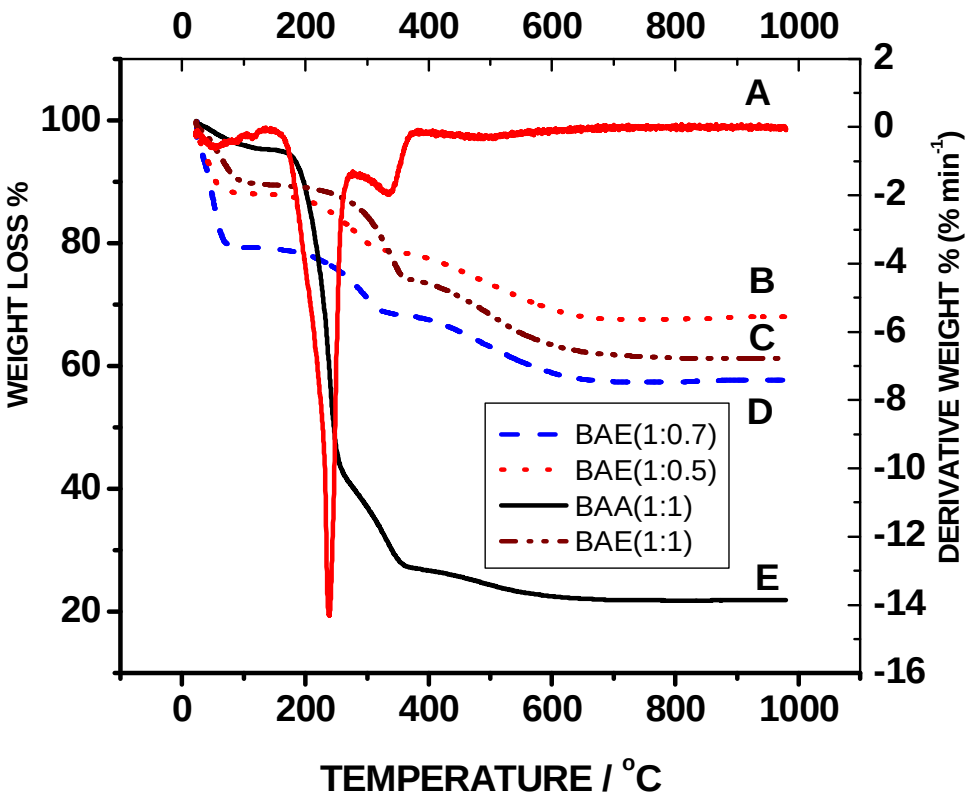

Figure 8.6. TGA curves and derivative thermograms for APTS-modified ethanesilica materials. A = derivative TGA curve of BAE(1:1); B, C, D and E are TGA curves of BAE(1:0.5), BAE(1:1), BAE(1:0.7) and BAA(1:1), respectively.

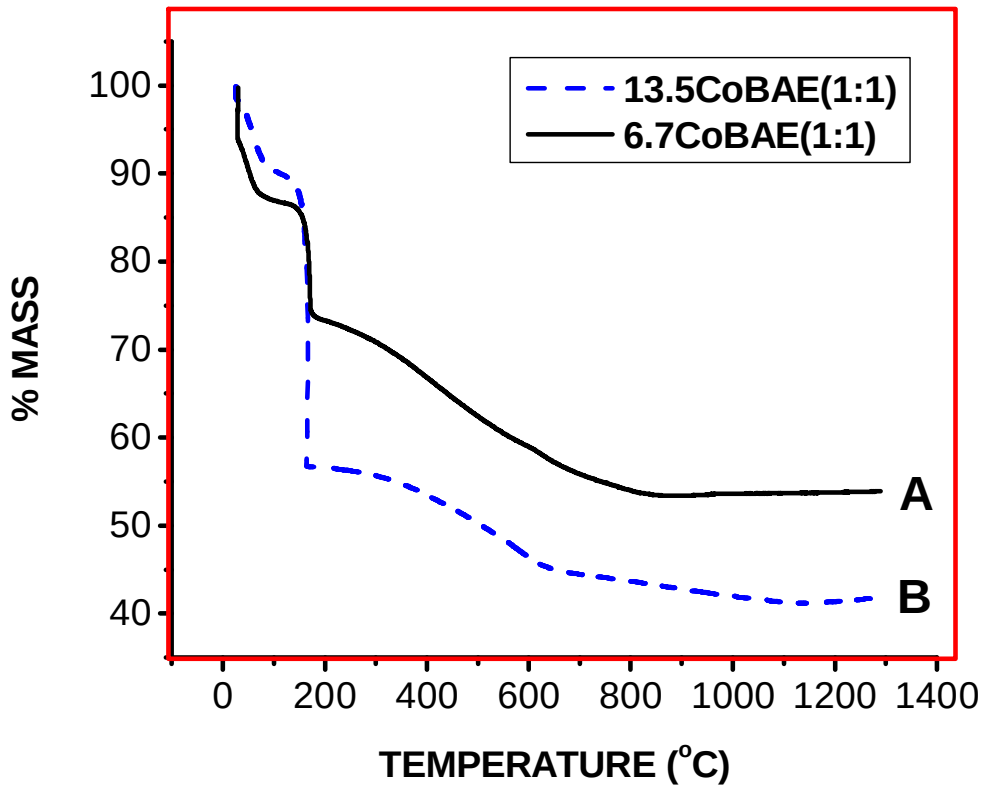

Figure 8.7. TGA curves for solvent extracted APTS-modified ethanesilica materials impregnated with cobalt nitrate. A = 6.7CoBAE(1:1) and B = 13.5CoBAE(1:1).

8.3.5 Raman spectroscopy

8.3.5.1 APTS-modified ethanesilica. Raman spectroscopy was used to identify functional groups associated with the new materials. Raman spectra of solvent extracted APTS-modified ethanesilica [BAE(1:0.5)] as well as solvent extracted ethanesilica (BE) are shown in Figure 8.8. Band assignments for fundamental Raman bands of the APTS-modified ethanesilica are listed in Table 8.3 [58, 59]. After solvent extraction the peaks associated with CTAB had disappeared while those due to the C-H vibrations of the BTME and APTS ethane groups (2885 cm^{-1}) are still to be seen (Figure 8.8). The intensity of the Raman peaks indicative of the amine functional group, observed between 3250 and 3500 cm^{-1}, increases with an increasing amount of APTS in the reaction mixture. The absence of peaks between 600 and 700 cm^{-1} (which are observed in the spectra of silicon precursors) indicates considerable hydrolysis and condensation of the methoxy and ethoxy groups of the silicon precursors. Whereas single peaks are observed in the range 1200 – 1300 (due to symmetric CH vibrations of Si–CH_2– groups) and 1400 – 1600 cm^{-1} (due to asymmetric CH vibrations of Si–CH_2– groups) in the spectrum of ethanesilica, doublets appear in the spectra of APTS-modified ethanesilica materials, indicating that the methylene groups in the framework and those due to the aminopropyl group are not equivalent (Figure 8.8).

Table 8.3. Raman band locations and assignments for APTS-modified ethane silica.

Band location /cm^{-1}	**Mode**	**Structural unit**
3473	υ (O-H)	SiO-H
3407	υ (NH)	Aminopropyl N-H
3313	υ (NH)	Aminopropyl N-H
2887	υ (CH)	Methylene C-H
1460	δ (N-CH_2) or δ(C-CH_2)	Aminopropyl C-H
1418	δ (Si-CH_2)	BTME framework C-H
1307	CH_2 in plane twist	Aminopyl C-H
1260	C-H_2 wag	BTME framework C-H
1147	υ asymmetric Si-O	Longitudinal Optical (LO) mode
1078	υ asymmetric Si-O	Transverse Optical (TO) mode
956	υ asymmetric Si-O	Si-OH
798	υ symmetric Si-O	Si-O-Si

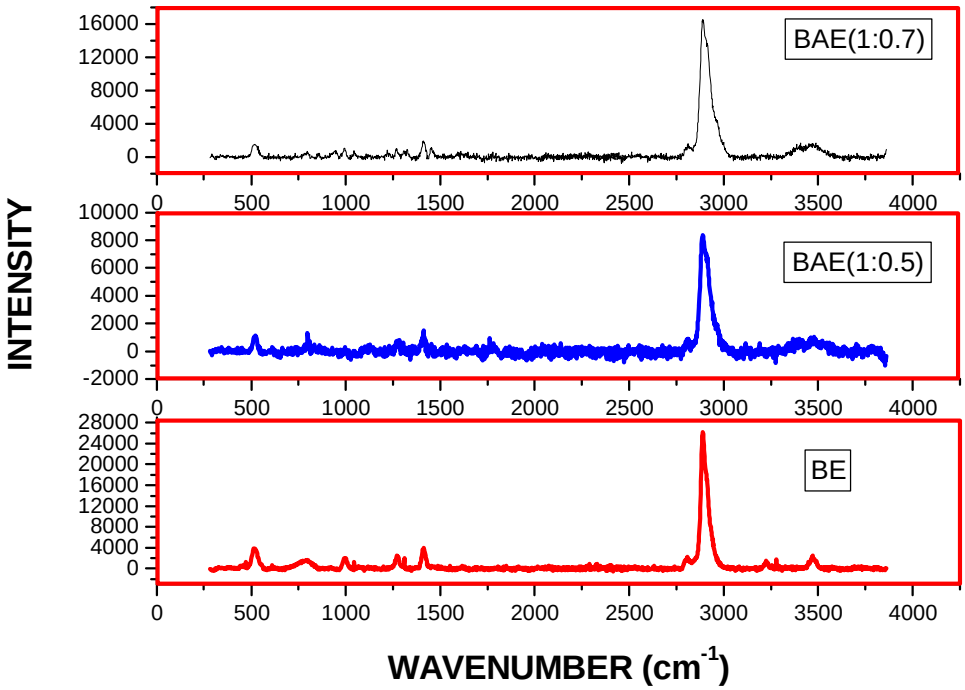

Figure 8.8. Raman spectra for solvent extracted ethanesilca (BE) and APTS-modified ethanesilica [BAE(1:0.5) and BAE(1:0.7) materials.

8.3.5.2 Co-incorporated APTS-modified ethanesilica. Incorporation of Co to ethanesilica and APTS-modified ethanesilica yielded a material that has peaks at 686 cm^{-1} and at 480 cm^{-1}, indicative of Co_3O_4 [56, 57]. However, no evidence for the presence of Si-O-Co-O-Si species was evident.

8.3.6 UV-Vis diffuse reflectance spectroscopy

8.3.6.1 Co-incorporated APTS-modified ethanesilica. UV-Vis diffuse reflectance spectra of aminopropyl-modified ethane silica materials impregnated with cobalt nitrate (0.1 and 0.2 g cobalt precursor per 0.3 g organosilica) as well as that of unsupported cobalt nitrate hexahydrate are presented in Figure 8.9. The absorption band at 428 nm is due to the formation of Co_3O_4, where a migration of Co to octahedral sites has occurred [60]. The UV-vis diffuse reflectance spectroscopy thus confirms the presence of Co_3O_4.

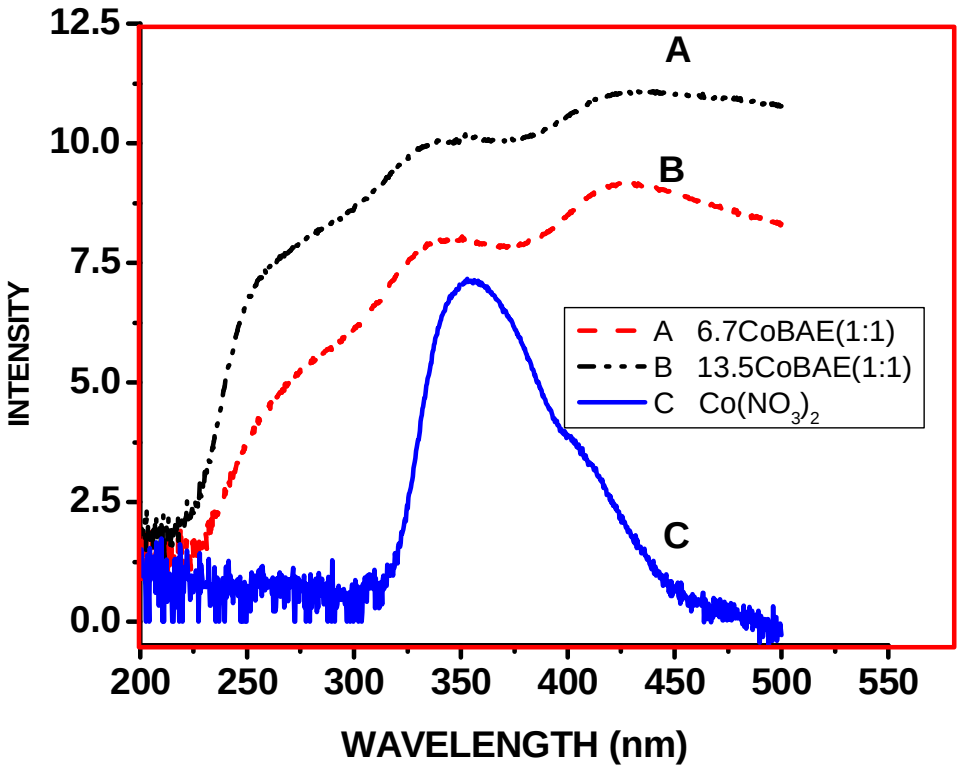

Figure 8.9. UV-Vis diffuse reflectance spectra of unsupported cobalt nitrate and supported cobalt nitrate.

8.3.7 Scanning Electron Microscopy (SEM)

8.3.7.1 APTS-modified ethanesilica. Typical scanning electron microscopy (SEM) images of ethanesilica, APTS-modified ethanesilica and cobalt incorporated APTS-modified ethanesilica materials are shown in Figure 8.10. The SEM image of an ethanesilica sample displays predominantly spherical particles with diameters in the range 11.1 to 21.8 μm. Smaller particles, with diameters ranging between 1.67 and 3.89 μm, dominate after modifying ethanesilica with APTS.

8.3.7.2 Co-incorporated APTS-modified ethanesilica. Cobalt impregnated materials, 6.7CoBAE(1:1) and 13.5CoBAE(1:1), show spherical particles with diameters in the 1.67 – 5.56 μm and 0.6 – 4.7 μm range, respectively. Particles with "shell-like" morphology are also observed for cobalt impregnated materials.

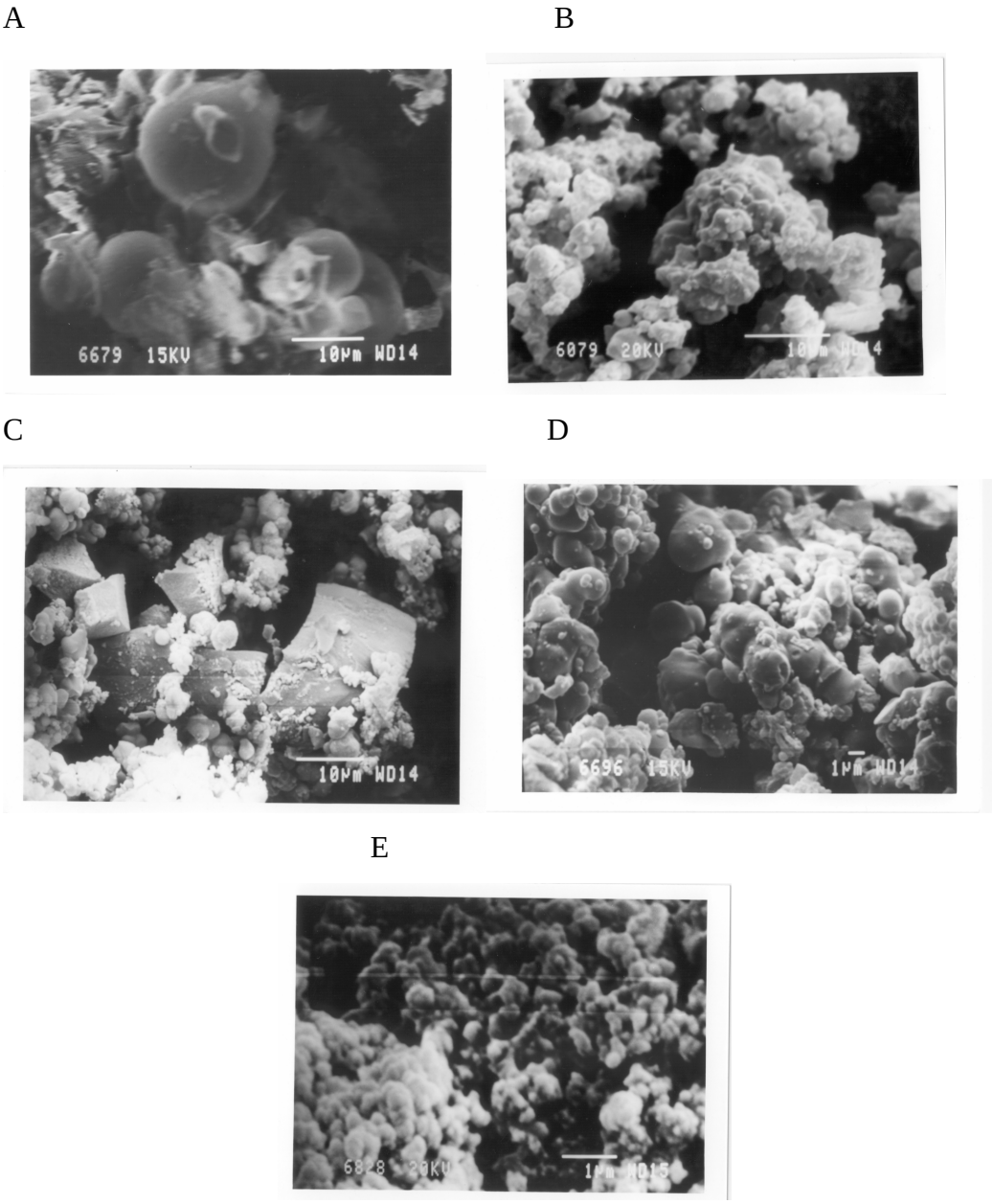

Figure 8.10. SEM micrographs of ethanesilica, APTS-modified ethanesilica and cobalt incorporated APTS-modified ethanesilica materials. A = ethanesilica (BE), B = In situ Co incorporated ethanesilica [6.7CoBAE(1:1)- *in situ*], C = APTS-modified ethanesilica [BAE(1:0.7)], D = cobalt impregnated APTS-modified silica [6.7CoBAE(1:1) - *imp*], and E = Cobalt impregnated APTS-modified ethanesilica [13.4CoBAE(1:1) - *imp*].

8.4 Conclusions

Bifunctional periodic mesoporous organosilica materials consisting of ethane groups (in the framework) and aminopropyl groups in the channels were synthesized. Cobalt incorporated APTS-modified ethanesilica materials were synthesized *in situ* by adding cobalt nitrate to the reaction mixture. Cobalt was also supported on APTS-modified materials by using the incipient wetness impregnation method. Cobalt incorporation leads to a collapse in the periodicity of the materials, as shown by the disappearance of the XRD peak observed at $2\theta = 2^{o}$. Cobalt ion incorporation was confirmed by Raman spectroscopy and UV-vis diffuse reflectance spectroscopy. The amount of APTS and cobalt incorporation determined the pore size, surface area and pore volume of the new material in a predictable manner.

8.5 References

1. A. Sayari, and S. Hamoudi, Chem. Mater. **13**, 3151 (2001).

2. B. J. Melde, B. T. Holland, C. F. Blanford, and A. Stein, Chem. Mater. **11**, (1999) 3302.

3. A. Sayari, S. Hamoudi, Y. Yang, I. Moudrakovski, and J. R. Ripmeester, Chem. Mater. **12**, 3857 (2000).

4. S. Guan, S. Inagaki, T. Ohsuna, and O. Terasaki, J. Am. Chem. Soc. **122**, 5660 (2000).

5. S. Inagaki, S. Guan, Y. Fukushima, T. Ohsuna, and O. Terasaki, J. Am. Chem. Soc. **121**, 9611(1999).

6. S. Guan, S. Inagaki, T. Ohsuna, and O. Terasaki, Micropor. Mesopor. Mater. 44 – **45**, 165 (2001).

7. M. Kruk, M. Jaroniec, S. Guan, and S. Inagaki, J. Phys. Chem. B **105**, 681 (2001).

8. H. Fan, S. Reed, I. Baer, R. Schunk, G. P. López, and C. J. Brinker, Micropor. Mesopor. Mater. **44 – 45**, 625 (2001).

9. Y. Lu, H. Fan, N. Doke, D. A. Loy, R. A. Assink, D. A. LaVan, and C. J. Brinker, J. Am. Chem. Soc. **122**, 5258 (2000).

10. H. Fan, Y. Lu, A. Stump, S. T. Reed, T. Baer, R. Schunk, V. Perez-Luna, G. P. López, and C. J. Brinker, Nature **405**, 56 (2000).

11. S. S. Park, C. H. Lee, J. H. Cheon, S. J. Choe, and D. H. Park, Bull. Korean Chem. Soc. **22**, 948 (2001).

12. C. H. Lee, S. S. Park, S. J. Choe, and D. H. Park, Micropor. Mesopor. Mater. **46**, 257 (2002).

13. O. Muth, C. Schellbach, and M. Froba, Chem. Commun. 2032 (2001).

14. E-B. Cho, K-W. Kwon, and K. Char, Chem. Mater. **13**, 3837 (2001).

15. H. Zhu, D. J. Jones, J. Zajac, J. Rozière, and R. Dutartre, Chem. Commun. 2568 (2001).

16. M. C. Burleigh, M. A. Markowitz, E. M. Wong, J-S. Lin, and B. P. Gaber, Chem. Mater. **13**, 4411 (2001).

17. J. R. Matos, M. Kruk, L. P. Mercuri, M. Jaroniec, T. Asefa, N. Coombs, G. A. Ozin, T. Kamiyama, and O. Terasaki, Chem. Mater. **14**, 1903 (2002).

18. T. Ren, X. Zhang, and J. Suo, Micropor. Mesopor. Mater. **54**, 139 (2002).

19. A. Sayari, and Y. Yang, Chem. Commun. **21**, 2582 (2002).

20. S. Hamoudi, and S. Kaliaguine, Chem. Comm. 2118 (2002).

21. A. M. Tshavhungwe, M. Layh, and N. J. Coville, J. Sol-Gel Science and Technology **29**, 167 (2004).

22. M. A. Wahab, I. Kim, and C. Ha, Micropor. Mesopor. Mater. **69**, 19 (2004).

23. T. Asefa, M. Kruk, M . J. MacLachlan, N. Coombs, H. Grondey, M. Jaroniec, and G. A. Ozin, J. Am. Chem. Soc. **123**, 8520 (2001).

24. M. C. Burleigh, M. A. Markowitz, M. S. Spector, and B. P. Gaber, Langmuir **17**, 7923 (2001).

25. M C. Burleigh, M. A. Markowitz, M. S. Spector, and B. P. Gaber, Chem. Mater. **13,** 4760 (2001).

26. M. C. Burleigh, M. A. Markowitz, M. S. Spector, and B. P. Gaber, J. Phys. Chem. B **105**, 9935 (2001).

27. M. C. Burleigh, S. Dai, and E. W. Hagaman, Chem. Mater. **13**, 2537 (2001).

28. S. Hamoudi, and S. Kaliaguine, Micropor. and Mesopor. Mater. **59**, 195 (2003).

29. S. Hamoudi, and S. Kaliaguine, Stud. Surf. Sci. Catal. **146**, 473 (2003).

30. H. Zhu, D. Jones, J. Zajac, R. Dutartre, M. Rhomari, and J. Roziere, Chem. Mater. **14**, 4886 (2002).

31. X. Yuan, H. I. Lee, J. W. Kim, J. E. Yie, and J. M. Kim, Stud. Surf. Sci. Catal. **146**, 477 (2003).

32. X. Yuan, H. I. Lee, J. W. Kim, J. E. Yie, and J. M. Kim, Chem. Lett. **32**, 650 (2003).

33. T. Asefa, M. Kruk, N. Coombs, H. Grondey, M. J. MacLachlan, M. Jaroniec, and G. A. Ozin, J. Am. Chem. Soc. **125**, 11662 (2003).

34. A. P. Wight, M. E. Davis, Chem. Rev. **102,** 3589 (2002).

35. D. J. Macquarrie, J. H. Clark, A. Lambert, and J. E. G. Mdoe, A. Priest, React. Funct. Polm. **35**, 153 (1997).

36. E. Angeletti, C. Canepa, C. Martinetti, and P. Venturello, Tetrahedron Lett. **29** 2261 (1988).

37. M. Lasperas, T. Llorett, L. Chaves, I. Rodriguez, A. Cauvel, and D. Brunel, Stud. Surf. Sci. Catal. **108**, 75 (1997).

38. F. Bigi, S. Carloni, R. Maggi, A. Mazzacani, and G. Sartori, Stud. Surf. Sci. Catal. **130**, 3501 (2000).

39. D. Demicheli, R. Maggi, A. Mazzacani, P. Righi, G. Sartori, and F. Bigi, Tetrahedron Lett. **42**, 2401 (2001).

40. Y. Ohtsuka, T. Arai, S. Takasaki, and N. Tsubouchi, Energy and Fuels **17**, 804 (2003).

41. J. Panpranot, J. G. Goodwin Jr., and A. Sayari, J. Catal. **211**, 530 (2002).

42. G. Bian, T. Machizuki, N. Fujishita, H. Namoto, and M. Yamada, Energy and Fuels **17**, 8799 (2003).

43. P. Cardiano, S. Sergi, M. Lazzari, and P. Piraino, Polymer **43**, 6635 (2002).

44. R. S. Young, Cobalt: Its Chemistry, Metallurgy and Uses, American Chemical Society, Reinhold, NY, 1960.

45. H. P. Withers, Jr., K. F. Eliezer, and J. W. Mitchell, Ind. Eng. Chem. Res. **29**, 1807 (1990).

46. E. Iglesia, Appl. Catal. A **161**, 59 (1997).

47. R. C. Brady, and R. J. Pettit, J. Am. Chem. Soc. **103**, 1287 (1981).

48. J. G. Goodwin, Jr., Prep. ACS Div. Pet. Chem. **36**, 156 (1991).

49. J. Li, and N. J. Coville, Appl. Catal. A **208**, 177 (2001).

50. J. S. Beck, J. C. Vartuli, W. J. Roth, M. E. Leonowicz, C. T. Kresge, K. D. Schmitt, C. T-W. Chu, D. H. Olson, E. W. Sheppard, S. McCullen, J. B. Higgins, and J. L. Schlenker, J. Am. Chem. Soc. **114**, 10834 (1992).

51. C. T. Kresge, M. E. Leonowicz, W. J. Roth, J. C. Vartuli, and J. S. Beck, Nature **359**, 710 (1992).

52. A. Stein, B. J. Melde, and R. C. Schroden, Adv. Mater. **12**, 1403 (2000).

53. M. H. Lim, and C. F. Blanford, A. Stein, Chem. Mater. **11**, 3285 (1999).

54. A. M. Tshavhungwe, and N. J. Coville, J. Sol-Gel Science and Technol. **31**, 161 (2004).

55. S. J. Gregg, and K. S. W. Sing, Adsorption, Surface Area and Porosity, Academic Press, London (1982).

56. J. Panpranot, J. Goodwin Jr., and A. Sayari; Catalysis Today **77**, 269 (2002).

57. J. Li, and N. J. Coville, Appl. Catal. A **181**, 201 (1999).

58. L. Bois, A. Bonhommé, A. Ribes, B. Pais, G. Raffin, and F. Tessier, Colloids and Surfaces A: Physicochem. Eng. Aspects **221**, 221 (2003).

59. N. B. Colthup, L. H. Daly, and S. E. Wiberley, Introduction to Infrared and Raman Spectroscopy. Academic Press (3rd Ed.) (1997).

60. G. A. H. Mekhemer, H. M. M. Abd-Allah, and S. A. A. Mansour, Colloids and Surfaces A: Physicochem. Eng. Aspects **160**, 251 (1999).

CHAPTER NINE

Concluding Remarks and Suggested Future Work

9.1 Conclusion

The surfactant-templated sol-gel method was used to synthesise periodic mesoporous organosilica materials (consisting of ethane groups in the framework) and bifunctional periodic mesoporous organosilica (consisting of ethane groups in the framework and either glycidoxypropyl groups or aminopropyl groups in the channels). Cobalt ion incorporated ethanesilica and modified ethanesilica materials were synthesized *in situ* by adding cobalt nitrate to the reaction mixture. Cobalt was also supported on ethanesilica materials and APTS-modified materials by using the incipient wetness impregnation method.

Solvent extraction yielded materials with high surface areas and pore sizes in the mesopore region. The pore sizes ranged between 2 and 4 nm. The amount of the silicon precursor(s), the ratio of the silicon precursors (BTME:TEOS, BTME:GPTS or BTME: APTS), reaction pH, ageing conditions and cobalt ion incorporation affected the lattice parameter, mesophase formed, pore size, surface area and pore volume as well as shapes of the isotherms and hysteresis loops.

Most of the materials had a periodic structure as indicated by the presence of low angle diffraction peaks, typical of periodic mesoporous silica materials, in powder X-ray diffraction patterns. Cubic and hexagonal mesophases were identified using powder X-ray diffraction. The XRD and pore volume data indicated that while the cobalt modified the BTME containing materials the essential mesoporous structure was maintained at the Co loadings studied (5% co-

impregnated; 10% incipient wetness). Most significant was the finding that the ethane portion of the material only decomposed at temperatures > 400 ^{o}C. The periodicity of the materials only disappeared at higher cobalt loadings. All the above data indicate that the new materials have potential in the Fischer Tropsch reaction.

Type IV isotherms, typical of mesoporous materials, were obtained for ethanesilica and modified ethanesilica materials prepared without cobalt. Isotherms of cobalt incorporated organosilica materials changed from Type IV to Type I with increasing APTS or GPTS content. Pore sizes tended to change from mesopore to micropore when the amount of GPTS was increased. The surface area, pore volume and pore diameter decreased with increasing loading of GPTS or APTS as well as after cobalt ion incorporation. These results show that the textural properties of ordered mesoporous silica can be tailored by choosing reaction conditions.

9.2 Suggested Future Work

Hybrid silica materials offer a prospect of promising applications in separations, catalysis, optics, sensors, and dielectric coatings. For catalytic applications, cobalt incorporated periodic ethanesilica materials described in this thesis can be tested as catalysts for the Fischer Tropsch reaction, whereas aminopropyl-functionalised ethanesilica materials can be tested as catalysts for the Knoevenagel condensation and Michael addition reactions as well as adsorbents for metals. Other functional groups can be introduced in materials functionalised with glycidoxypropyl and aminopropyl groups by chemical reactions of these functional groups. The PMO materials could also be incorporated with other metals, affording new potential catalysts. New PMO materials could be synthesized by co-condensation of other alkoxysilanes with BTME using CTAB and other structure directing molecules. Variation of reaction conditions would result in materials with new properties. The use of PMO materials as pre-ceramic precursors is another field that still needs to be researched. Another challenge is the formulation of experiments

aimed at understanding and controlling the polymerization reaction of organosilanes. The synthetic procedure developed in this study can be extended to a broader range of compositions.